



## Article

# Light and CO<sub>2</sub> Modulate the Accumulation and Localization of Phenolic Compounds in Barley Leaves

Lena Hunt <sup>1</sup>, Karel Klem <sup>2</sup>, Zuzana Lhotáková <sup>1</sup>, Stanislav Vosolsobě <sup>1</sup>, Michal Oravec <sup>2</sup>, Otmar Urban <sup>2</sup>, Vladimír Špunda <sup>2,3</sup> and Jana Albrechtová <sup>1,\*</sup>

<sup>1</sup> Department of Experimental Plant Biology, Faculty of Science, Charles University, Viničná 5, 12844 Praha, Czech Republic; huntl@natur.cuni.cz (L.H.); zuzana.lhotakova@natur.cuni.cz (Z.L.); vosolsob@natur.cuni.cz (S.V.)

<sup>2</sup> Global Change Research Institute, Czech Academy of Sciences, Bělidla 4a, 60300 Brno, Czech Republic; klem.k@czechglobe.cz (K.K.); oravec.m@czechglobe.cz (M.O.); urban.o@czechglobe.cz (O.U.); Vladimír.Spunda@osu.cz (V.Š.)

<sup>3</sup> Department of Physics, Faculty of Science, University of Ostrava, Dvořákova 7, 70103 Ostrava, Czech Republic

\* Correspondence: albrecht@natur.cuni.cz

**Abstract:** Barley (*Hordeum vulgare*) accumulates phenolic compounds (PhCs), which play a key role in plant defense against environmental stressors as antioxidants or UV screening compounds. The influence of light and atmospheric CO<sub>2</sub> concentration ([CO<sub>2</sub>]) on the accumulation and localization of PhCs in barley leaves was examined for two varieties with different tolerances to oxidative stress. PhC localization was visualized in vivo using fluorescence microscopy. Close relationships were found between fluorescence-determined localization of PhCs in barley leaves and PhC content estimated using liquid chromatography coupled with mass spectroscopy detection. Light intensity had the strongest effect on the accumulation of PhCs, but the total PhC content was similar at elevated [CO<sub>2</sub>], minimizing the differences between high and low light. PhCs localized preferentially near the surfaces of leaves, but under low light, an increasing allocation of PhCs in deeper mesophyll layers was observed. The PhC profile was significantly different between barley varieties. The relatively tolerant variety accumulated significantly more hydroxycinnamic acids, indicating that these PhCs may play a more prominent role in oxidative stress prevention. Our research presents novel evidence that [CO<sub>2</sub>] modulates the accumulation of PhCs in barley leaves. Mesophyll cells, rather than epidermal cells, were most responsive to environmental stimuli in terms of PhC accumulation.



**Citation:** Hunt, L.; Klem, K.; Lhotáková, Z.; Vosolsobě, S.; Oravec, M.; Urban, O.; Špunda, V.; Albrechtová, J. Light and CO<sub>2</sub> Modulate the Accumulation and Localization of Phenolic Compounds in Barley Leaves. *Antioxidants* **2021**, *10*, 385. <https://doi.org/10.3390/antiox10030385>

Academic Editor: Alfredo Aires

Received: 1 February 2021

Accepted: 1 March 2021

Published: 5 March 2021

**Publisher's Note:** MDPI stays neutral with regard to jurisdictional claims in published maps and institutional affiliations.



**Copyright:** © 2021 by the authors. Licensee MDPI, Basel, Switzerland. This article is an open access article distributed under the terms and conditions of the Creative Commons Attribution (CC BY) license (<https://creativecommons.org/licenses/by/4.0/>).

**Keywords:** phenolic compounds; histochemical localization; elevated CO<sub>2</sub>; image analysis; irradiance; plant stress; hydroxycinnamic acids; hydroxybenzoic acids; flavonoids; barley

## 1. Introduction

Barley (*Hordeum vulgare*) is one of the most widely cultivated and economically important crops. It is considered a founder crop in agriculture, with archaeological evidence placing its domestication back 10,000 years ago [1]. Today, it is the fourth most produced grain in the world, behind only corn, wheat, and rice [2]. The primary use of barley has been as livestock feed, and in the production of beer and whiskey. However, high levels of antioxidants, vitamins, minerals, and essential amino acids in young barley leaves, as well as beta-glucans in barley grains, have led to the profitable marketing of barley as a health food as well [3,4]. It is estimated that by 2050, barley production will need to increase 54% over levels in the year 2000 to keep up with the demand of a rising global population [5]. Due to its global economic importance, there is much interest in how the production of barley will fare with ongoing climate change. Areas of the world seeing increased frequencies of droughts and heatwaves will experience significant drops in barley yield [6]. The Mediterranean basin may see yield decreases up to 25% [6], while Central

Europe can expect greater variability between harvests [7]. Despite these projections, barley maintains a reputation for being resilient to environmental stress and is expected to be less impacted than other crops, such as corn or potatoes [7].

The tolerance to abiotic stressors is considerably influenced by plant secondary metabolites. Barley is rich in phenolic compounds (PhCs), a large family of compounds including phenolic acids, flavonoids, lignins, and tannins, which provide protective functions in planta [8]. PhCs have been documented to increase barley tolerance to oxidative stress—a state of excess reactive oxygen species (ROS) induced by a range of environmental stressors. ROS play a dual role: functioning as signaling molecules that regulate cellular metabolism and defense response systems in low concentrations—but causing detrimental oxidation of proteins, lipids, and nucleic acids, leading to cell damage or death when they occur in excess [9,10]. Irradiance induces ROS accumulation in plants, both directly and indirectly; directly, excess irradiance can result in an over-reduced NADP<sup>+</sup> pool, leading to the reduction of molecular oxygen and, thus, the formation of ROS during photosynthesis. Indirectly, abiotic stress typically reduces photosynthetic capacity—previously optimum light conditions can become excessive and induce photooxidation [11]. PhCs have shown a protective role in barley against a number of oxidative stress inducing factors, including excessive irradiation [12], drought and salinity [13], pathogens [14], air pollution [15], and heavy metal exposure [16].

The protective function of PhCs is a result of their UV (ultraviolet) screening and antioxidant activity [17,18]. PhCs that attenuate UV irradiation prevent the direct generation of ROS and subsequent oxidative stress, while PhCs with antioxidant activity scavenge ROS. Chemical structure plays a role in PhC function [19,20]. For instance, compounds, such as hydroxycinnamic acids, are more effective at UV screening, while flavonoids with a dihydroxylated B-ring possess higher antioxidant activity [21]. There is some debate about the role of flavonoids as antioxidants in planta [22], however, the exclusive role of PhCs in UV screening seems unlikely since UV is not necessary to induce their accumulation, and the synthesis of antioxidant flavonoids increases at the expense of hydroxycinnamic acids that are more efficient in UV screening [23]. Antioxidative PhC biosynthesis is more likely tied to ROS signals alongside the over-reduction of the photosynthetic electron transport chain [24], which would explain their accompaniment to various sources of environmental stress. PhCs accumulating in epidermal cell walls and vacuoles may play a more significant role as UV screeners in photoprotection [25,26]. However, PhCs, particularly with a dihydroxylated B-ring that possess high antioxidant activity, have been shown to accumulate deeper in the leaf—in mesophyll vacuoles and chloroplasts [22,27,28]. A third and somewhat underrated function of PhCs (specifically flavonoids) is their possible role as an energy escape valve, utilizing ATP and NADPH and promoting phosphate cycling between the cytosol and chloroplast [22]. This function may be especially relevant in elevated [CO<sub>2</sub>] conditions, where an abundance of CO<sub>2</sub> results in an increase in non-structural carbohydrate biosynthesis [29]. Although PhC accumulation is known to be affected by a plant's environment, few methods exist to visually measure the localization of phenolic compounds within leaf tissue, which is an important prerequisite for understanding their function in planta.

This study investigates the combined effects of [CO<sub>2</sub>] and light intensity on the accumulation and localization of PhCs in two varieties of barley with different tolerances to oxidative stress. We expected that the variety Bojos would accumulate more PhCs with antioxidant activity in mesophyll cells, in contrast to the oxidative-stress sensitive variety Barke. We hypothesized that: (1) both elevated [CO<sub>2</sub>] and high light intensity would increase the total accumulation of PhCs, and that light intensity especially would change the distribution of PhCs within leaf cross-sections to comply with UV screening and antioxidant roles; and (2) relative tolerance or sensitivity of barley cultivars could be connected to differences in PhC accumulation, composition, and/or localization. Histochemistry, fluorescence microscopy, and image analysis were combined to provide a

unique method for analyzing PhCs visually, alongside targeted high-performance liquid chromatography/high-resolution mass spectrometry (HPLC-HRMS) analysis.

## 2. Materials and Methods

### 2.1. Plant Material and Growth Conditions

The two barley varieties investigated in this study were selected for their widespread cultivation in Europe and their different tolerances to oxidative stress. The Barke variety is reportedly sensitive to photooxidative stress: it is known to develop necrotic physiological leaf spots when exposed to excess light [30] and show pronounced reductions in photosynthetic activity when exposed to excess UV [31]. By contrast, Bojos is one of the most widely grown barley varieties in the Czech Republic [32,33] and rarely shows even mild symptoms of photooxidative stress, according to the multi-annual testing of Central Inspection and Testing Institute of Agriculture for the Czech Republic [34]. We refer to these varieties as oxidative stress sensitive (Barke) and ‘relatively tolerant’ (Bojos).

Barley plants of Barke and Bojos varieties were grown in six growth chambers (FS-SI-3400, Photon System Instruments, Drásov, CZ). Cultivation occurred over four weeks under three different [CO<sub>2</sub>] treatments: low [CO<sub>2</sub>]—200 ppm (LC), ambient [CO<sub>2</sub>]—400 ppm (AC), and elevated [CO<sub>2</sub>]—700 ppm (EC) and two light regimes: low light (LL) with photosynthetically active radiations (PAR) and UV-A maxima of 400  $\mu\text{mol m}^{-2} \text{s}^{-1}$  and 0.75  $\text{W m}^{-2}$ , respectively and high light (HL) with PAR and UV-A maxima 1500  $\mu\text{mol m}^{-2} \text{s}^{-1}$  and 4  $\text{W m}^{-2}$ , respectively (UV-A lamps LT 30W T8/010UV with maximum emission at 370 nm, Narva Lichtquellen, Brand-Erbisdorf, Germany). The light intensity, temperature, and air humidity changed gradually from night values to a daytime maximum between 5:00 and 10:00, then remained constant between 10:00 and 15:00, and finally changed again to nighttime values between 15:00 and 20:00 to simulate natural rhythms with 15 h day and 9 h night (see Figure S1). Daily integrals for PAR were 14.4 and 54  $\text{mol m}^{-2} \text{day}^{-1}$  and for UV-A 27 and 144  $\text{J m}^{-2} \text{day}^{-1}$  under LL and HL, respectively. The air temperature varied between 15–25 °C and relative air humidity between 90–60%, for night and day respectively (see Figure S1). Light treatments were selected to mimic realistic Central European light conditions in spring for cloudy-day field conditions (LL) and sunny conditions slightly exceeding the light saturation point for barley (HL) [35].

Five plants were grown in each pot of size 11 × 11 × 12 cm filled with fertilized peat substrate TS2 (Klasmann-Deilmann, Geeste, Germany). Each combination of variety, [CO<sub>2</sub>], and light intensity was replicated 6 times (6 pots containing 5 plants each). To avoid potential artefacts from individual growth chamber, the pots were transferred every seven days between growth chambers maintaining the same [CO<sub>2</sub>] and light treatment. Positions of pots within growth chambers were also randomized. At the end of four weeks, when the plants reached the growth stage of 6 leaves (DC 16), samples for histochemical analysis, HPLC-HRMS, and measurements of chlorophyll index and UV screening of chlorophyll fluorescence (UV screening index) were taken.

### 2.2. Histochemical Detection of Phenolic Compounds

For all histochemical analyses, leaf cross-sections and transverse-sections were made from the third leaf from the top, representing the youngest completely developed leaf, in the middle of the leaf. Cross-sections were made at approximately 85  $\mu\text{m}$  thickness using a hand microtome (Leica RM 2255, Wetzlar, Germany). Paradermal images were created by slicing a whole leaf into 1 mm squares before treatment with reagents (Figure S2), which allowed better infiltration of reagents into epidermal cells via adjacent mesophyll cells while keeping the epidermal cells intact.

Initially, several histochemical tests were performed to confirm the presence of various PhCs. With light microscopy, phloroglucinol-HCl was used to detect the presence of lignin [36], and Vanillin-HCl was used to detect condensed tannins [37]. With fluorescence microscopy, Naturstoff reagent A was used to detect flavonoids [38]. Naturstoff reagent A was determined to provide the most data about induced PhC accumulation, and so we

selected it for continued use with experimental samples. The samples prepared for use with Naturstoff reagent A were mounted in a 100 mM KPi pH 6.8, 1% NaCl (*w/v*) buffer solution [24]. A few drops of 0.1% (*w/v*) Naturstoff reagent A were transferred under the coverslip using filter paper approximately five minutes before using the microscope. Naturstoff reagent A forms chelates with characteristic fluorescence depending on the hydroxyl group substitutions on the B and C rings [38]. For this study, we processed three samples treated with Naturstoff reagent A from different leaves per replication. To process and photograph samples in a short enough period to not introduce additional error factors, such as sample drying or loss of fluorescent signal, we selected to use standard fluorescence microscopy. This also enabled us to readily compare images of leaf cross-sections under white light, blue light, and UV radiation (see Microscope image acquisition for specifications). This is beneficial as the autofluorescence of certain PhCs change depending on the wavelength of light they are excited by. For example, flavonoids fluoresce yellow under both UV and blue light excitation, caffeic esters fluoresce blue-white under UV radiation and yellow under blue light excitation, and ferulic acid fluoresces blue under UV radiation, but has no fluorescence under blue light excitation [39,40].

### 2.2.1. Microscopic Image Acquisition

The samples prepared for histochemical detection tests were photographed using the microscope AX70 (Olympus, Hamburg, Germany) at 40× magnification (to capture the whole leaf) and 100× magnification (to capture details on tissue and cellular localization) under bright field for phloroglucinol-HCl and Vanillin-HCl, and using fluorescence microscopy under both UV and blue light excitation with Naturstoff reagent A. Excitation was achieved using epi-fluorescent filter cubes: wide UV (U-MWU, excitation 330–385 nm, dichroic cut-off 400 nm, emissions > 420 nm) and wide blue (U-MWB, excitation 450–480 nm, dichroic cut-off 500 nm, emission > 515 nm) (Olympus, Hamburg, Germany). Image analysis for quantitative analysis on histochemical localization was performed on images of cross-sections treated with Naturstoff reagent A and excited with blue light.

### 2.2.2. Quantitative Analysis of Phenolic Compounds Using Image Analysis

The reaction with Naturstoff reagent A was mainly detected in mesophyll cells and displayed a gradient across internal cell depths. To obtain a relative measure of PhC fluorescence localization, the chlorophyll autofluorescence was digitally removed using a macro in Adobe Photoshop and applied to all photographs as a batch. The macro selected all yellow color and moved it to a new layer in Photoshop, showing only the PhC fluorescence. The PhC fluorescence-only images were opened in ImageJ. The plug-in LinSys Cycloides was used to randomly generate equally spaced vertical lines to provide unbiased systematic random sampling to achieve unbiased estimations of histochemical localization across a gradient in the mesophyll [41] while not intersecting vascular tissues. The distance between these lines was adjusted so that each leaf was vertically intersected in five equally-spaced locations—the first being near the midrib and the fifth being near to the edge of the leaf. The straight-line tool and Plot Profile function provided intensity data for each pixel intersected by the sampling line (Figure 1). The data from the five intersections through the mesophyll tissue along the width of the leaf were further divided by mesophyll depth: adaxial mesophyll layer (AD), upper mesophyll (UM), middle mesophyll (MM), lower mesophyll (LM), and abaxial mesophyll layer (AB). The data from three samples per replication and five locations within leaf width were averaged and used for subsequent statistical analyses.

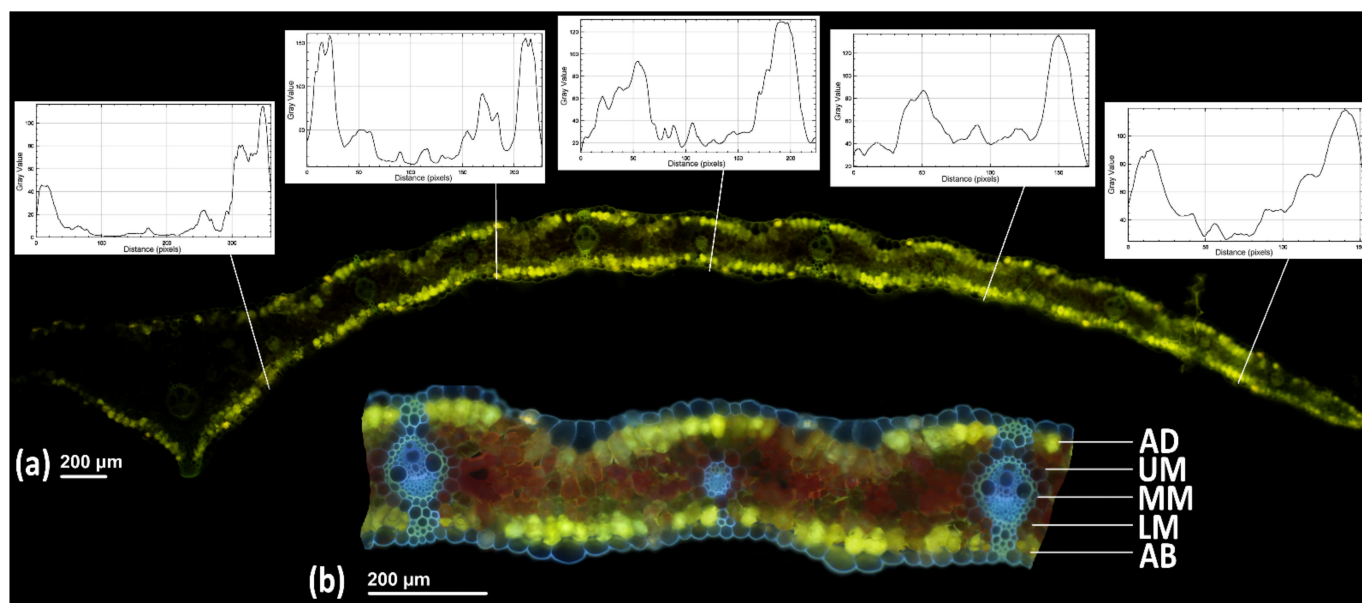


**Figure 1.** Method for quantitative measurements of relative intensities of PhC fluorescence throughout the mesophyll tissue inside half of a *Hordeum vulgare* leaf lamina using LinSys Cycloides and Plot Profile function in ImageJ. The plugin LinSys Cycloides automatically generates equally spaced lines over the image to provide systematic random sampling sites. (a) Straight line and Plot Profile tools are used to measure the intensity of pixel brightness at the sampling sites throughout the image of leaf PhC fluorescence (5 white graphs). (b) Pixel values of sample lines are divided into 5 segmental sections corresponding to 5 mesophyll depths: adaxial layer of mesophyll adjacent adaxial epidermis (AD), upper mesophyll (UM), middle mesophyll (MM), lower mesophyll (LM), abaxial layer of mesophyll adjacent to abaxial epidermis (AB).

### 2.3. Targeted HPLC-HRMS Analysis of Contents of Phenolic Compounds

The third leaf from the top from each replication was sampled between 11:00 and 14:00 (Central European Time) and immediately after scanning for leaf area frozen in liquid nitrogen for target high-performance liquid chromatography analyses (i.e., the leaves from the same position on the plant were sampled for HPLC and histochemical analyses). The samples were homogenized using a mortar and pestle with liquid nitrogen and then extracted using methanol:chloroform: H<sub>2</sub>O solution (v:v:v, 1:2:2). An aliquot of the upper (polar) phase was used to analyze metabolites using an UltiMate 3000 high-performance liquid chromatography (HPLC) (Thermo Fisher Scientific, US/Dionex RSLC, Dionex, Waltham, MA, USA) coupled with an LTQ Orbitrap XL high-resolution mass spectrometer (HRMS) (Thermo Fisher Scientific, Waltham, MA, USA) that was equipped with a heated electrospray ionization source. All samples were analyzed in the positive and negative polarity of Orbitrap, operated in full-scan mode over a range of m/z 50 to 1000 (positive mode) and 65 to 1000 (negative mode). For details see [12].

### 2.4. Chlorophyll and UV Screening Indices

A Dualex optical sensor was used to measure chlorophyll and UV screening indices (Dualex Flav, Force A, Orsay, FR). Measurements are in Dualex units based on light transmittance and UV screening of chlorophyll fluorescence excitation. The UV screening index measurement is mainly related to the content of ortho-dihydroxylated flavonoids, which have absorption maxima around 375 nm (the excitation wavelength of the Dualex instrument) [42]. The UV screening is often referred to as “epidermal”, however the screening functions can come also from the layer below the epidermis. For more information on Dualex, see [43]. Three measurements in the central part of the same leaf (third leaf from the top) used for targeted HPLC-HRMS and histochemical analyses were performed. The means from one leaf were used for statistical analyses (6 replicates).

### 2.5. Statistical Analysis

Data were analyzed using a four- or three-way fixed-effect ANOVA model using Statistica 12 software (StatSoft, Tulsa, OK, USA). Fishers' LSD post hoc test ( $p = 0.05$ ) was used to identify significant differences between means. The bar graphs with indicated standard errors and the multiple scatter graphs with linear regressions were created in the program SigmaPlot 11.0 (Systat Software, San Jose, CA, USA). The redundancy analysis (RDA) and biplot of RDA results were set up in the software CANOCO 5 [44].

## 3. Results

### 3.1. Localization of Phenolic Compounds within Leaf Cross-Sections

After treatment with Naturstoff reagent A, three colors of fluorescence were observed when leaves were excited by UV radiation: Red from chlorophyll, blue from autofluorescent PhCs, and yellow from flavonoids reacting with the reagent. Red chlorophyll autofluorescence was detected throughout the mesophyll but was absent in the epidermal pavement cells. Significant blue autofluorescence was observed in vascular bundles, external epidermal cell walls, and sclerenchyma cells associated with the midrib of the leaf (Figure 2d), as well as in stomatal guard cells and epidermal trichomes (Figure 2f). The presence of lignin was confirmed in the vascular bundles via phloroglucinol HCl histochemical detection, however, it was not detected in the epidermis or sclerenchyma cells (Figure 2b). Epidermal pavement cells exhibited blue-fluorescing cell-wall bound PhCs, particularly on the external surface, but lacked any autofluorescence from vacuoles or other organelles. Leaves were examined for presence of the yellow flavonoid fluorescence in the epidermal cells both in cross-section (Figures 2d and 3) and paradermally on leaf segments (Figures 2f,g and S2). The paradermal view on a leaf segment allows epidermal cells to be observed in their intact state while allowing histochemical reagent to penetrate epidermal cells (Figure S2). As with the cross-sections, a faint blue autofluorescence was detected from cell walls of epidermal pavement cells but not from their organelles or central vacuole. The epidermal pavement cells themselves were transparent enough to transmit the yellow flavonoid fluorescence of the mesophyll layers below them (Figures 2d,f,g and S2). The exception was in stomata subsidiary cells, which showed yellow flavonoid fluorescence in vacuoles and cell walls (Figure 2f,g). Subsidiary and guard cells were the only source of flavonoid fluorescence observed from the epidermis. Since epidermal PhCs did not show any changes in localization or intensity of blue autofluorescence across treatments during the pilot screening, only mesophyll PhC accumulation across five leaf depths will be further discussed in results. In the mesophyll cells, PhC fluorescence was detected from cell walls, vacuoles, and chloroplasts (not always simultaneously) (Figure 3).

As the results of ANOVA show, location within the leaf, together with light intensity, was the most significant factor determining the accumulation of PhCs ( $p < 0.001$ , Table 1). HL leaves accumulated visibly more PhCs than their LL counterparts (Figure 4). One general pattern was observed for leaves cultivated in either HL or EC conditions: fluorescence intensity from the accumulation of PhCs was generally high in AD mesophyll layer of the leaves, slightly lower in AB mesophyll layer, and a decreasing intensity was observed through both UM and LM with the lowest values found in MM (Figure 5). On the contrary, leaves cultivated in LL and either LC or AC conditions had the highest accumulation of PhCs in the LM rather than the AD mesophyll (although leaves cultivated in LL, but EC followed the same pattern as the HL leaves; Figures 4 and 5).

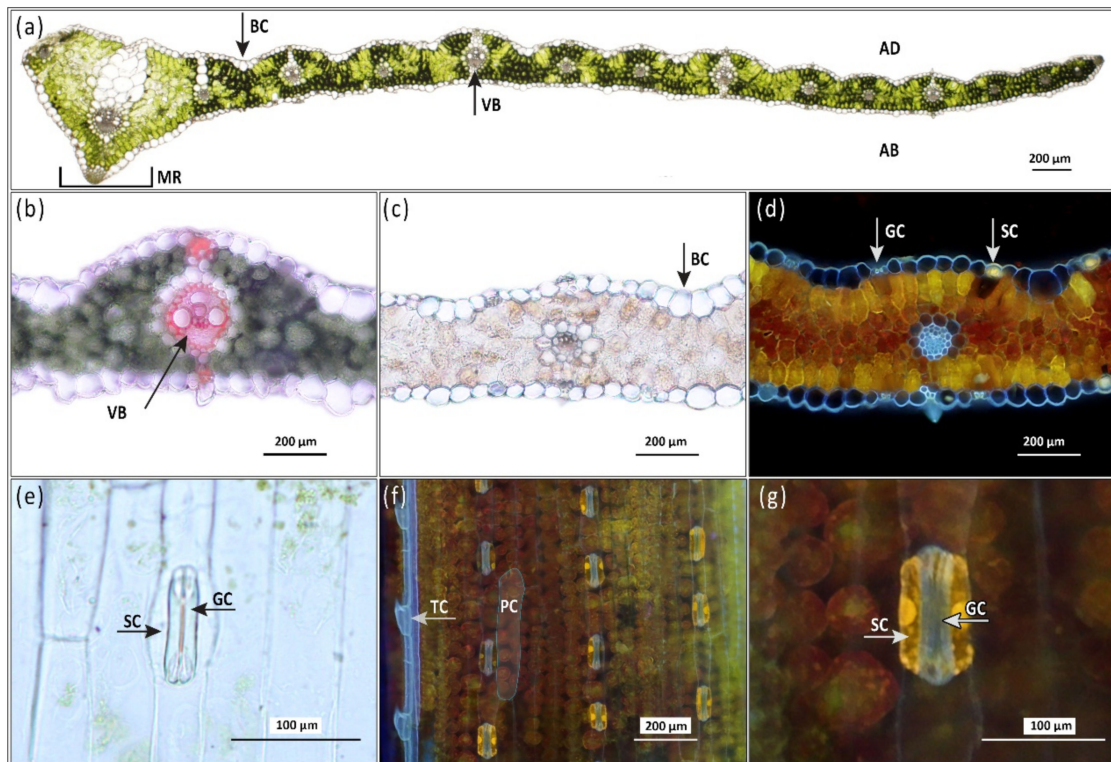


**Figure 2.** Examples of histochemical analyses of barley (*Hordeum vulgare*) leaves. (a) Partial barley leaf cross section from one half of the lamina including midrib (MR) on left, bulliform cells (BC) of the abaxial epidermis, adaxial side (AD), and abaxial side (AB). Fresh hand section not treated histochemically, imaged at 40× magnification, bright field. (b) Phloroglucinol-HCl test for lignins (pink-red color) in vascular bundle (VB) and sclerenchymatous extensions of bundle sheath leading to epidermal cells, 100×, bright field. (c) Vanillin HCl test for condensed tannins (bright red) not detected in mesophyll, 100×, bright field. (d) Naturstoff reagent A test (yellow fluorescence) for flavonoids, detected in the mesophyll but absent in the epidermis except for stomatal subsidiary cells, arrows point to stomatal guard cells (GC) and subsidiary cells (SC), 100×, UV fluorescence. (e) Barley stomata from an epidermal peel showing guard cells (GC) and subsidiary cells (SC), 200×, bright field. (f) The paradermal view on a segment of a barley leaf treated with Naturstoff reagent A showing vacuolar flavonoids (yellow fluorescence). Leaf segments were of 1 mm<sup>2</sup> size so the reagent could penetrate the intact epidermal cells via mesophyll cells. Flavonoids are present only in SC and GC and in the mesophyll cells below the transparent epidermal pavement cells. Trichome cells (TC) along leaf vein show blue autofluorescence and pavement cells (PC) (highlighted to indicate size and position) lack fluorescence except a faint blue color along cell walls, 100×, UV fluorescence. (g) Zoomed in view of stomatal guard cells (GC) and subsidiary cells (SC) treated with Naturstoff reagent A showing intracellular fluorescence of phenolic compounds. Adjacent epidermal pavement cells do not show flavonoid fluorescence and their transparency enables the viewing of flavonoid fluorescence in the mesophyll layer below, 100×, UV fluorescence.

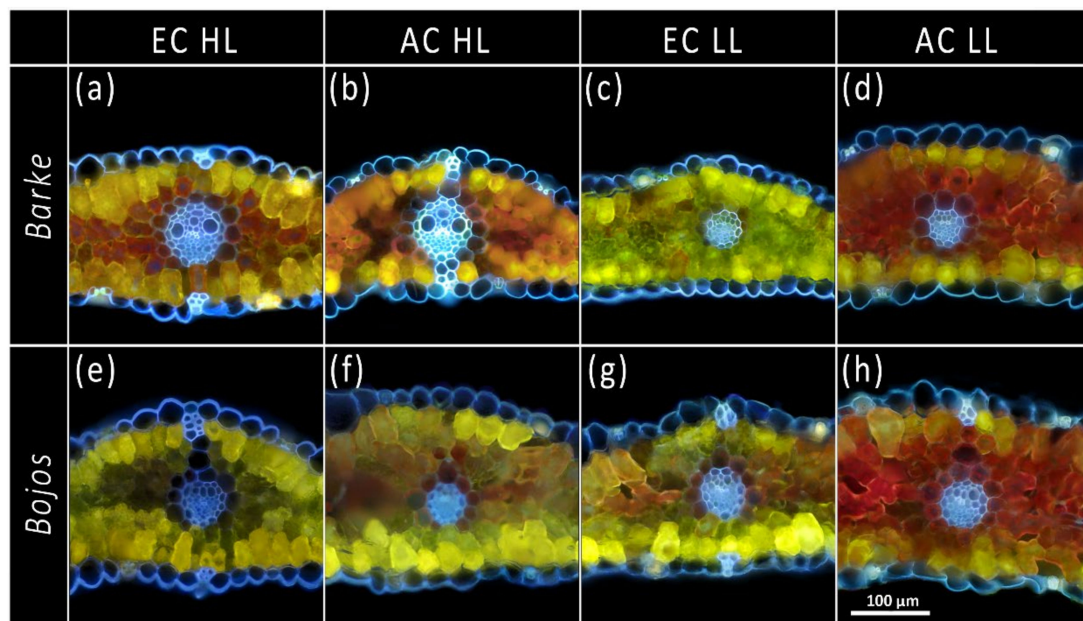


**Figure 3.** Cross-sections of barley (*Hordeum vulgare*) leaves showing the strong presence of flavonoids in the mesophyll, especially close to leaf surfaces, and the absence of flavonoids in the epidermal pavement cells, 100× magnification, treated with Naturstoff reagent A and acquired under UV light. Epidermal pavement cells exhibit blue fluorescence mainly from outer cell walls, but not from intracellular compartments. Strong yellow fluorescence indicates the presence of flavonoids in mesophyll layers adjacent to both epidermises, with reduced intensity towards the internal leaf tissue. The effect of elevated [CO<sub>2</sub>] on flavonoid accumulation even in the absence of high light is illustrated in (c,g). Barke (a) AC-LL; (b) EC-LL; (c) AC-HL; (d) EC-HL. Bojos (e) AC-LL; (f) EC-LL; (g) AC-HL; (h) EC-HL. (Abbreviations are AC-ambient [CO<sub>2</sub>], EC-elevated [CO<sub>2</sub>], HL-high light, LL-low light.).

**Table 1.** Results of four-way ANOVA on the effects of barley variety (Var), CO<sub>2</sub> concentration ([CO<sub>2</sub>]), light intensity (Light), and tissue localization (Loc) in leaf cross-sections, and their mutual interactions (×) on fluorescence intensity emitted by phenolic compounds enhanced with Naturstoff reagent A showing localization of within leaf cross-sections. Degrees of freedom (df), F and p values shown for each factor and interaction. Significant effects ( $p < 0.05$ ) are indicated in bold.

	df	F	p
Var	1	10.09	<b>0.002</b>
[CO <sub>2</sub> ]	2	7.85	<b>&lt;0.001</b>
Light	1	266.23	<b>&lt;0.001</b>
Loc	4	147.23	<b>&lt;0.001</b>
Var × [CO <sub>2</sub> ]	2	8.82	<b>&lt;0.001</b>
Var × Light	1	2.01	0.157
[CO <sub>2</sub> ] × Light	2	15.15	<b>&lt;0.001</b>
Var × Loc	4	3.00	<b>0.019</b>
[CO <sub>2</sub> ] × Loc	8	5.92	<b>&lt;0.001</b>
Light × Loc	4	44.58	<b>&lt;0.001</b>
Var × [CO <sub>2</sub> ] × Light	2	1.67	0.189
Var × [CO <sub>2</sub> ] × Loc	8	2.33	<b>0.019</b>
Var × Light × Loc	4	0.17	0.955
[CO <sub>2</sub> ] × Light × Loc	8	2.12	<b>0.034</b>
Var × [CO <sub>2</sub> ] × Light × Loc	8	0.24	0.982



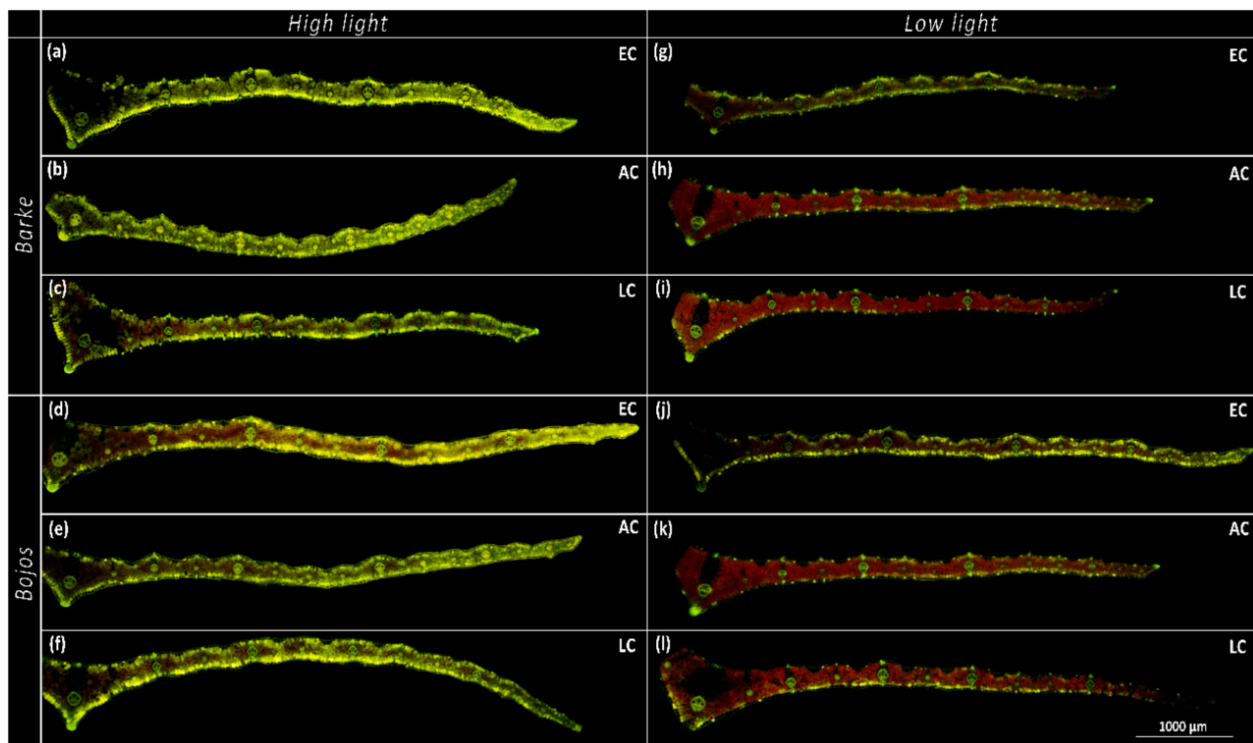


**Figure 4.** Cross-sections of barley (*Hordeum vulgare*) leaves for each treatment, showing the clear effect of high light intensity, and elevated  $[\text{CO}_2]$ , on leaf phenolic compounds, 40 $\times$  magnification, treated with Naturstoff reagent A and excited under blue light—half leaf lamina shown from midrib (left) to leaf margin (right). Left column of images shows high light (HL) treatment, right column shows low light (LL) treatment.  $[\text{CO}_2]$  is denoted in frame on right as elevated (EC), ambient (AC), or low (LC). Barke (a) EC-LL; (b) AC-LL; (c) LC-LL; (g) EC-HL; (h) AC-HL; (i) LC-HL. Bojos (d) EC-LL; (e) AC-LL; (f) LC-LL; (j) EC-HL; (k) AC-HL; (l) LC-HL.

The effect of light intensity on PhCs accumulation, estimated by image analysis of fluorescence intensity, was highly significant ( $p < 0.001$ , Table 1) such that plants grown under HL conditions had on average a 46% greater accumulation of PhCs. Specifically, the effect of HL on the accumulation of PhCs was highest and statistically significant in both AD and AB mesophyll layers. Interestingly, for LL cultivation conditions, equal or slightly higher accumulation was found in LM (with the exception of EC leaves) (Figure 5). The differences in PhCs content between LL and HL cultivation conditions decreased in the inner mesophyll layers of the leaves and were statistically insignificant for internal leaf mesophyll positions MM and UM. The differences between HL and LL conditions notably converged with rising  $[\text{CO}_2]$ . This interaction between light intensity and  $[\text{CO}_2]$  was highly significant, as confirmed by ANOVA ( $p < 0.001$ , Table 1). Also, highly significant were the interactions between light intensity and  $[\text{CO}_2]$  and localization of PhCs within the mesophyll.

The variety showed a significant effect on fluorescence emitted by phenolic compounds on in EC (Figure 5) with Bojos exhibiting higher overall accumulation of PhCs than Barke. On the other hand, the differences between varieties and interactive effects with variety were less significant or insignificant. The only highly significant interaction, including variety, was the interaction with  $[\text{CO}_2]$ . This was mainly evident under HL conditions and in AB and AD mesophyll layers. In variety Bojos, EC cultivation increased accumulation of PhCs in AD but not in AB, however, in variety Barke, EC decreased accumulation in AB mesophyll layer (Figure 5).

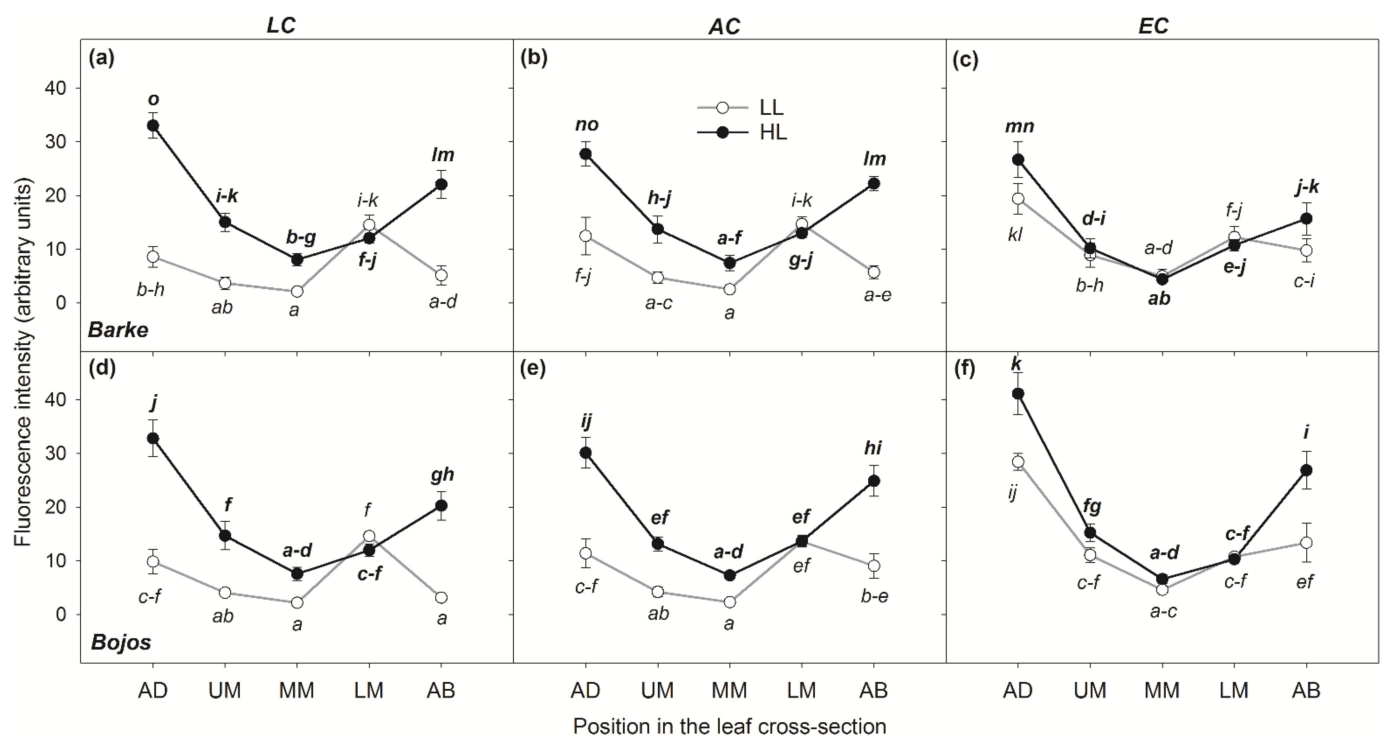


**Figure 5.** Localization of PhCs in mesophyll tissue of barley (*Hordeum vulgare*) leaf cross section measured by image analysis of fluorescence microscopy. The fluorescence intensity was measured as pixel brightness analyzed in ImageJ software, see Material and Methods. The means (points) and standard errors (error bars) are presented (n = 6). Empty points and grey lines represent low light conditions (LL), black points and black lines represent high light conditions (HL). The graphs in the same line show results for variety Barke (upper, a–c) and Bojos (lower, d–f). The graphs in the same column show data for the same growth [CO<sub>2</sub>]: low (LC); ambient (AC); elevated (EC). The following abbreviations are used for localization in mesophyll depth across leaf cross-section: AD–adaxial mesophyll layer, UM–upper mesophyll, MM–middle mesophyll, LM–lower mesophyll and AB–abaxial mesophyll layer. Letters indicate statistically significant differences between means tested by Fishers LSD post hoc test ( $p = 0.05$ ) tested within each variety separately.

### 3.2. Target Analysis of Phenolic Compounds by HPLC-HRMS

Specific flavones and phenolic acids were determined by HPLC-HRMS. The phenolic acids are categorized in two groups: hydroxybenzoic acids and hydroxycinnamic acids. The identified compounds were: (1) hydroxybenzoic acids, including 3-hydroxybenzoic acid, protocatechuic acid, vanillic acid, and syringic acid; (2) hydroxycinnamic acids, including 3-coumaric acid, ferulic acid, chlorogenic acid, caffeic acid, and sinapic acid, and (3) flavones, including apigenin, luteolin, isovitexin, homoorientin, and saponarin. Here we discuss mainly the 3 groups, as the microscopic localization of PhCs does not allow discrimination between individual PhCs. However, individual PhC amounts can be found in Table S1.

Among hydroxybenzoic acids, syringic acid in particular was significantly affected by variety, and was increased in both HL and EC leaves. Among hydroxycinnamic acids, a major effect was observed in ferulic, sinapic, and chlorogenic acids. All three were affected by variety (in the opposite way as hydroxybenzoic acids, greater amounts in Bojos), and accumulated more in HL and EC leaves. Among flavones, the dominant effect of treatment was found in saponarin, isovitexin, and homoorientin: higher accumulation under the combination of HL and EC, with almost no differences between varieties.

All three groups of PhCs were significantly affected by the light environment ( $p < 0.001$ , Table 2). While the accumulation of hydroxycinnamic acids and flavones were significantly increased by HL cultivation irrespective of [CO<sub>2</sub>] treatment and variety, for hydroxybenzoic acids, a significant effect of HL found only in the oxidative-stress sensitive variety Barke in AC or EC conditions (Figure 6). This indicates highly significant (variety  $\times$  [CO<sub>2</sub>], variety

× light, and variety × [CO<sub>2</sub>] × light) or significant ([CO<sub>2</sub>] × light) interactive effects on the content of hydroxycinnamic acids, while for hydroxycinnamic acids the significant interaction was found only in case interaction variety × light. In the case of flavones, significant interactive effects were found for [CO<sub>2</sub>] × light and variety × light (Table 2).

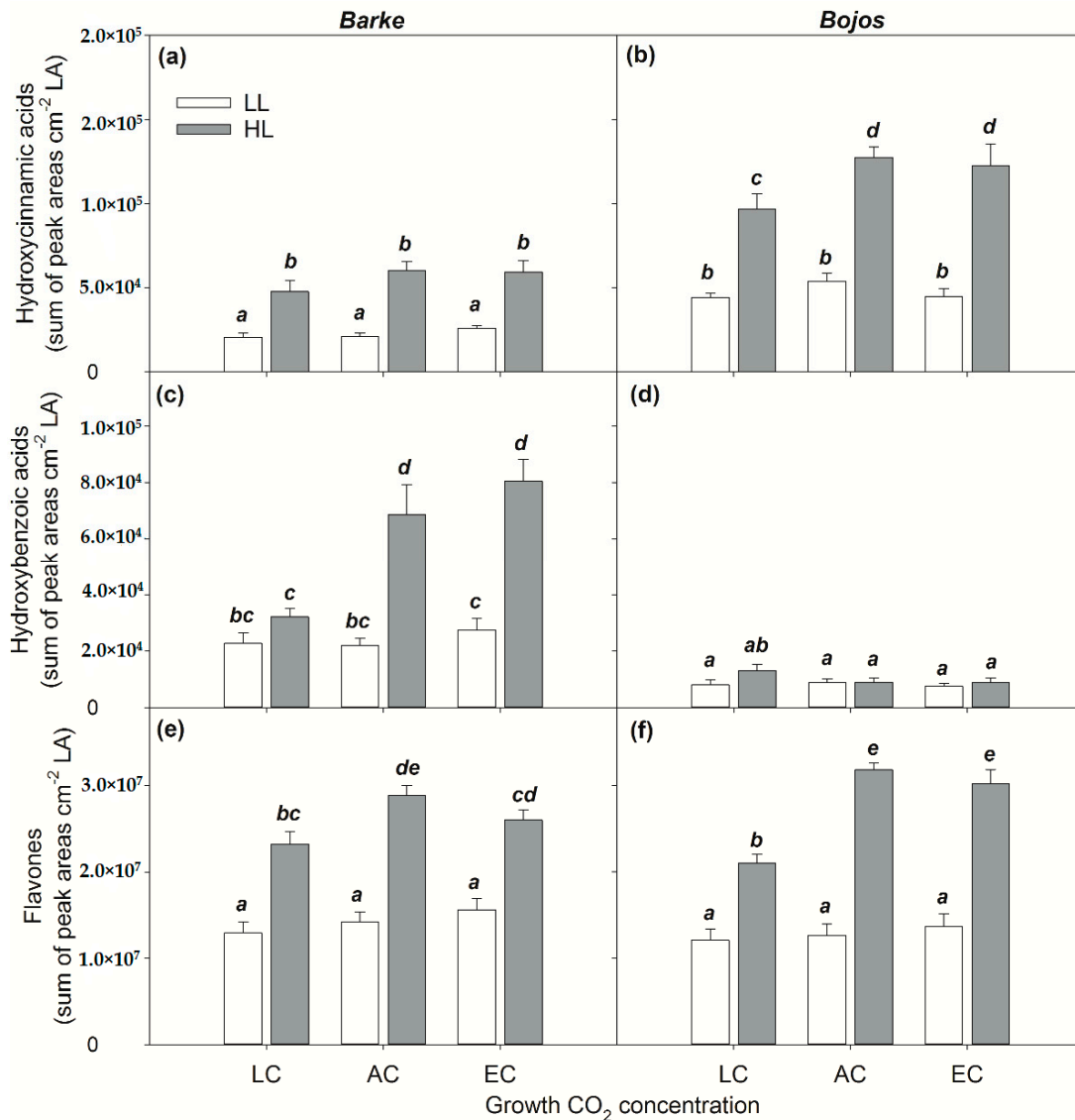


**Figure 6.** The effect of barley (*Hordeum vulgare*) variety on the accumulation of different groups of PhCs per unit leaf area (LA) under experimental treatment measured by HPLC-HRMS. (a,c,e) relatively tolerant Bojos (b,d,f) oxidative-stress sensitive Barke; Light intensity: white columns–low light (LL); grey columns–high light (HL); and CO<sub>2</sub> concentration: low (LC), ambient (AC) and elevated (EC) on total amount of (a,b) hydroxycinnamic acids, (c,d) hydroxybenzoic acids, and (e,f) flavones. The means (columns) and standard errors (error bars) are presented (n = 6). Different letters above columns indicate statistically significant differences between means tested by Fisher's LSD post hoc test ( $p = 0.05$ ) across both varieties.

**Table 2.** Results of three-way ANOVA on the effects of barley (*Hordeum vulgare*) variety (Var), CO<sub>2</sub> concentration ([CO<sub>2</sub>]), light intensity (Light), and their mutual interactions on total hydroxybenzoic acids, hydroxycinnamic acids, and flavones determined by HPLC-HRMS and on chlorophyll and UV screening index measured in vivo using the instrument Dualex. Degrees of freedom (*df*), *F* and *p* values are denoted for each factor or interaction. Significant effects (*p* < 0.05) are indicated in bold.

	<i>df</i>	Hydroxybenzoic Acids		Hydroxycinnamic Acids		Flavones		Chlorophyll Index		UV Screening Index	
		<i>F</i>	<i>p</i>	<i>F</i>	<i>p</i>	<i>F</i>	<i>p</i>	<i>F</i>	<i>p</i>	<i>F</i>	<i>p</i>
Var	1	167.03	<0.001	140.09	<0.001	0.02	0.895	44.94	<0.001	223.92	<0.001
[CO <sub>2</sub> ]	2	7.73	0.001	5.21	0.008	15.28	<0.001	73.39	<0.001	62.87	<0.001
Light	1	56.98	<0.001	198.83	<0.001	325.94	<0.001	160.55	<0.001	1517.14	<0.001
Var × [CO <sub>2</sub> ]	2	11.15	<0.001	1.21	0.305	1.22	0.302	0.43	0.653	6.72	0.002
Var × Light	1	44.61	<0.001	23.16	<0.001	4.43	0.040	0.74	0.394	14.83	<0.001
[CO <sub>2</sub> ] × Light	2	5.72	0.005	2.22	0.117	8.05	<0.001	1.49	0.234	16.13	<0.001
Var × [CO <sub>2</sub> ] × Light	2	8.67	<0.001	0.58	0.562	2.35	0.104	2.40	0.099	0.53	0.592

Barley variety showed highly significant effects on hydroxycinnamic acid and hydroxybenzoic acid accumulation, but no significant effect on flavones (Table 2). Hydroxycinnamic acids generally accumulated in higher amounts in the relatively tolerant variety Bojos, while hydroxybenzoic acids were higher in oxidative-stress sensitive variety Barke. Specifically, Barke plants accumulated syringic acid (Table S1), which Bojos plants did not accumulate at all. Flavones accumulated slightly more in variety Bojos, but in comparison of treatment means, the differences between varieties were generally low and mostly insignificant (Figure 6). Significant differences in flavones between varieties were found only under EC and HL conditions.

The effect of [CO<sub>2</sub>] on accumulation of all three groups of PhCs, (Table 2; Figure 6) was statistically significant (*p* < 0.05) only under HL conditions. The major differences were found between LC/AC and EC, however, the responses to [CO<sub>2</sub>] were variety specific. While higher effect of [CO<sub>2</sub>] on hydroxycinnamic acids and flavones was found in variety Bojos, variety Barke showed an increase of hydroxybenzoic acids in response to [CO<sub>2</sub>] (Figure 6). In general, the differences between AC and EC in accumulation of all three groups of PhCs were small and statistically insignificant. The interactive effects of light intensity and [CO<sub>2</sub>] show that both LL and LC plants accumulated less PhCs, irrespective of barley variety (Figure 6).

### 3.3. Chlorophyll and UV Screening Indices

Both chlorophyll index and UV screening index were significantly affected by barley variety, [CO<sub>2</sub>], and light intensity (Table 2). However, statistically significant interactions were found only for the UV screening index. These were highly significant (*p* < 0.01) for interactions variety × light, [CO<sub>2</sub>] × light and variety × [CO<sub>2</sub>] (Table 2).

HL significantly increased both chlorophyll index and UV screening index across all treatments independently on variety (Figure 7). The effect of light on the UV screening index slightly increased with increasing [CO<sub>2</sub>]. The oxidative-stress sensitive variety Barke showed generally higher chlorophyll index and particularly UV screening index comparing to relatively tolerant Bojos. The differences between varieties were significant for UV screening index in all [CO<sub>2</sub>] and light treatments, while the differences in chlorophyll index between varieties were less evident and only statistically significant under EC (both HL and LL), AC (only LL), LC (only HL). Increasing [CO<sub>2</sub>] generally increased both the chlorophyll index and UV screening index. While this effect was evident for the chlorophyll index under both light intensities, the effect of [CO<sub>2</sub>] was more pronounced for the UV screening index under HL.

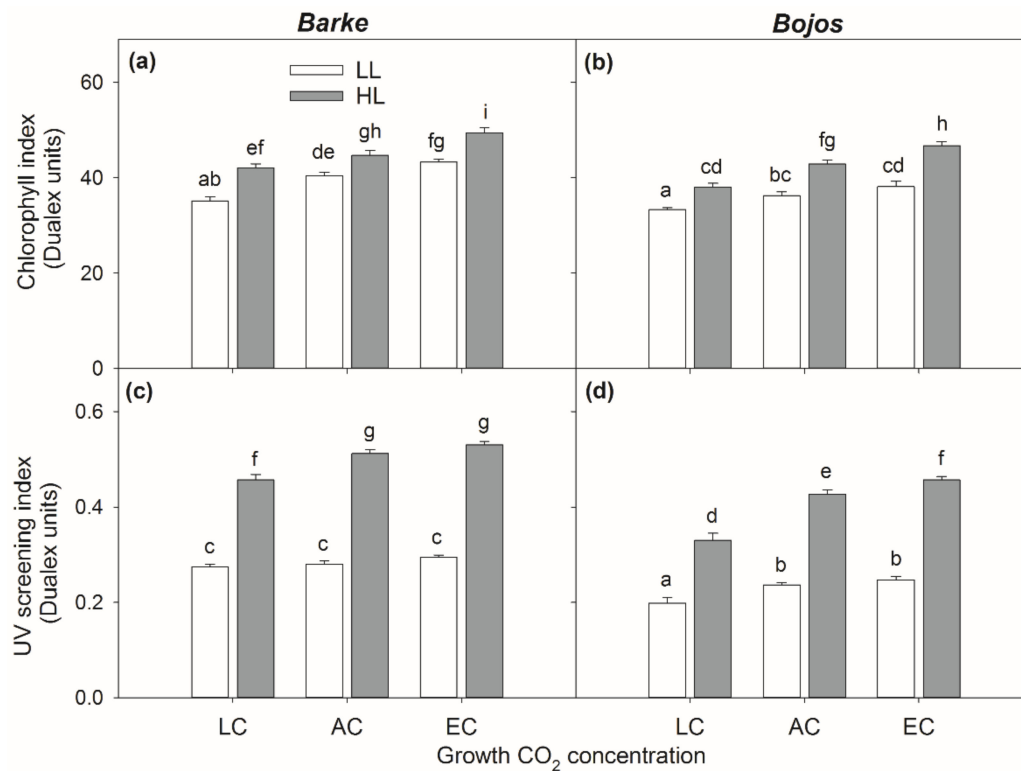


**Figure 7.** The effect of barley (*Hordeum vulgare*) variety on chlorophyll index and UV screening index under different experimental treatments. (a,c) Barke, (b,d) Bojos, light intensity (white columns–low light (LL); grey columns–high light, (HL) and CO<sub>2</sub> concentration [CO<sub>2</sub>]: low (LC), ambient (AC), elevated (EC) on chlorophyll index (a,b) and UV screening index (c,d) determined in vivo using instrument Dualex. The means (columns) and standard errors (error bars) are presented (n = 6). Different letters above columns indicate statistically significant differences between means tested by Fishers LSD post hoc test ( $p = 0.05$ ) across both varieties.

### 3.4. Relationships between Localization and Accumulation of PhCs in Leaves

The associations between environmental drivers ([CO<sub>2</sub>], light intensity) and accumulation of PhCs, either expressed as total amounts of individual groups of PhCs expressed per unit leaf area or their accumulation within leaf cross-sections assessed by Naturstoff reagent A fluorescence, were tested using redundancy analysis (RDA, Figure 8). Most parameters related to the accumulation of PhCs were affected primarily by light intensity during cultivation. As an exception, the effect of light was lower for hydroxybenzoic acid accumulation and reversed for PhC accumulation in the LM compared to other locations in leaf cross-section or total content of other groups of PhCs. Accumulation in the lower mesophyll was also inversely related to [CO<sub>2</sub>]. Increasing [CO<sub>2</sub>] also positively affected the chlorophyll index (alongside the positive effect of light intensity).

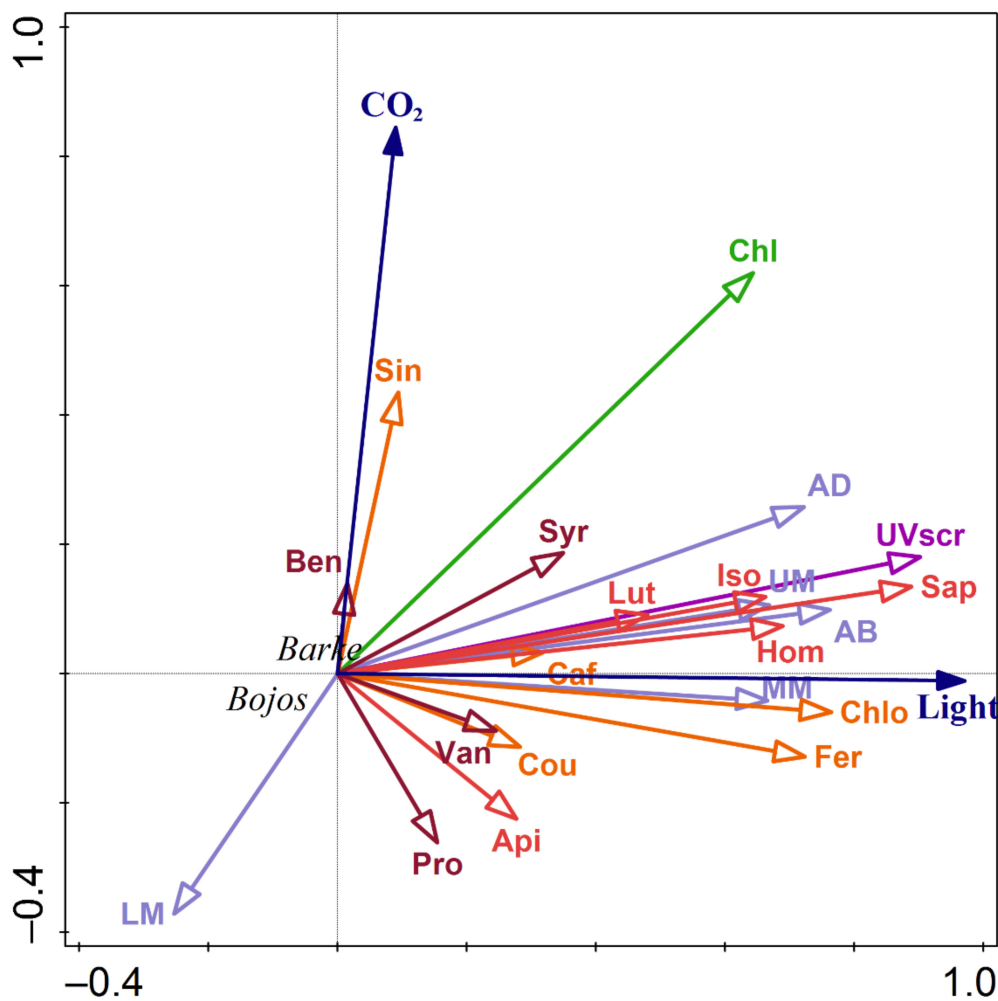


**Figure 8.** Biplot diagram representing results of redundancy analysis (RDA) on the effects of light intensity (Light), CO<sub>2</sub> concentration (CO<sub>2</sub>), barley variety (Barke, Bojos) on the localization of PhCs within leaf cross-section (light purple; AD—adaxial mesophyll layer, UM—upper mesophyll, MM—middle mesophyll, LM—lower mesophyll and AB—abaxial mesophyll layer), content of hydroxycinnamic acids (orange; Cou—3-coumaric acid, Caf—caffeic acid, Fer—ferulic acid, Sin—sinapic acid, Chlo—chlorogenic acid), hydroxybenzoic acids (brown; Ben—3-hydroxybenzoic acid, Pro—protocatechuic acid, Van—vanillic acid, Syr—syringic acid), flavones (red; Api—apigenin, Lut—luteolin, Iso—isovitexin, Hom—homoorientin, Sap—saponarin), chlorophyll index (Chl) and UV screening of chlorophyll fluorescence (UVscr). Explained variation by axis 1 = 82.8% and cumulative explained variation by both axis = 91.6% (Pseudo-F = 25.9,  $p = 0.002$ ).

Close relationships between PhC localization in adaxial leaf surface and accumulation of individual groups of PhCs confirmed the results of RDA, however, variety had an important effect (Figure 9). For the same fluorescence intensity in AD, variety Barke accumulated more hydroxybenzoic acids and flavones, and less hydroxycinnamic acids. Barke also showed a higher UV screening index for the same fluorescence intensity in AD compared to variety Bojos. The varieties show fundamentally different relationships for hydroxybenzoic acids. While almost no relationship was found for Bojos, in Barke the relationship between fluorescence intensity in AD mesophyll and hydroxybenzoic acids was much steeper, although not statistically significant.

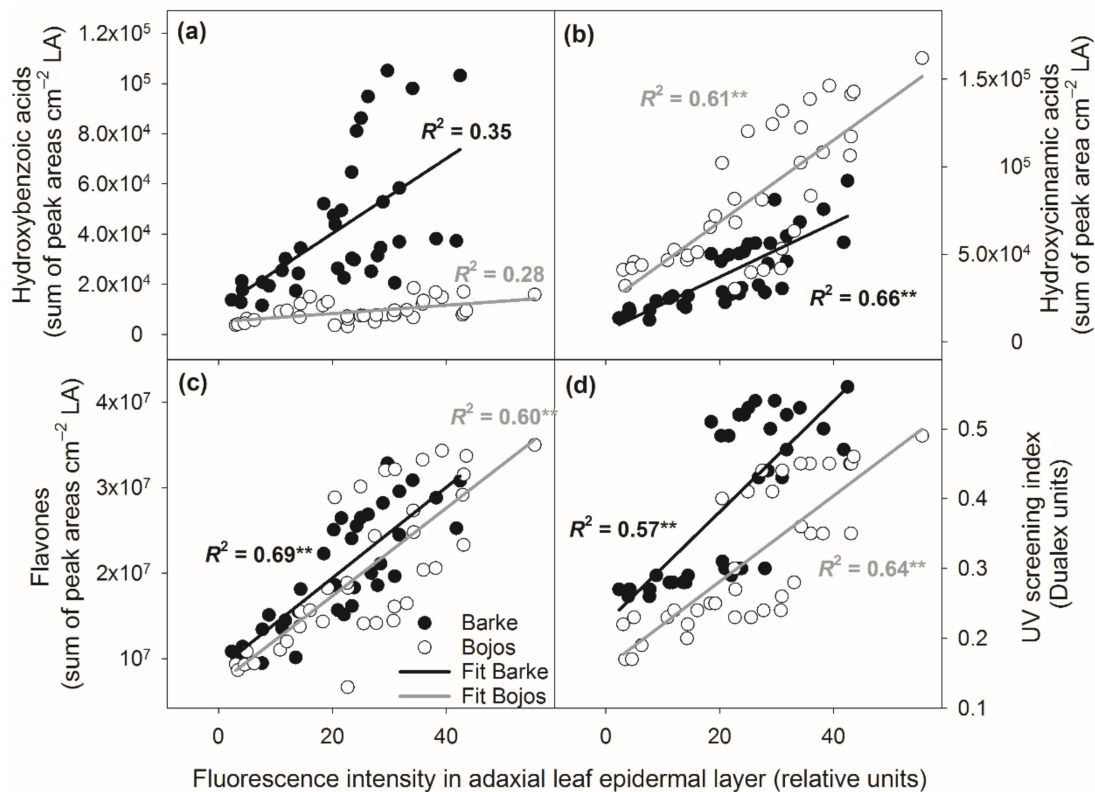


**Figure 9.** Linear relationships between accumulation of different groups of PhCs in adaxial leaf epidermal layer measured as fluorescence intensity under blue light excitation and total amount of (a) hydroxybenzoic acids, (b) hydroxycinnamic acids, (c) flavones, and (d) UV screening index. Amounts of hydroxybenzoic acids, hydroxycinnamic acids, and flavones are expressed per unit leaf area (LA). Relationships are separated by barley (*Hordeum vulgare*) variety: Barke—black points and black lines, Bojos—empty points and grey lines. The index of determination ( $R^2$ ) and significance of Pearson's correlation coefficient (\*\* significant at  $p = 0.01$ ).

#### 4. Discussion

PhCs are known to play a role in many biotic and abiotic stress responses, particularly by functioning as antioxidants to scavenge ROS and screen UV radiation [18,23,26,28]. Visualizing changes in PhC localization and accumulation is the next step for understanding how leaves respond to environmental conditions. This paper presents an original method for measuring the relative accumulation of PhCs throughout leaf tissue layers (Figure 1). We are aware that due to heterogeneity in excitation wavelength penetration into the leaf tissues [45] (also known as a sieve effect [42,46,47]) our proposed approach cannot replace quantification of PhCs, such as fluorescence spectroscopy or HPLC-HRMS, which were also used in the present study. However, the presented method can add another dimension for analysis of PhCs in leaf tissues, while localization may contribute to the understanding of their functional role in the plant defense mechanisms.

PhC detection in leaf cross-sections brought us to the surprising conclusion that PhC accumulation in response to environmental inputs, represented by [CO<sub>2</sub>] and light intensities, occurred primarily in the mesophyll of barley instead of the epidermis (Figures 2d,f,g, 3 and S2). This finding is contrary to the idea that PhCs localize primarily in the vacuoles of epidermal cells for UV screening, as has been commonly shown for other species, such as *Ginkgo biloba* [48] and *Kalanchoë daigremontiana* [49]. By contrast, our results show only cell-wall bound PhCs along the outer epidermis and in thorn-like extensions, and no visible signal from epidermal pavement cell vacuoles (Figures 2d,f,g and 3).

PhCs are primarily synthesized via a multi-enzyme complex localized in the cytoplasmic surface of the endoplasmic reticulum and then transported either to the vacuole or to the cell wall [50]. Cell wall PhCs play a role in tolerance to pathogens [51], and screening

UV radiation [12,52], while vacuolar PhCs provide a reservoir for antioxidant functions—although physically separated from the source of ROS production in chloroplasts [21]. In the chloroplast,  $O_2^-$  is quickly converted to  $H_2O_2$ , a diffusible oxidant which can then diffuse into the vacuole and be scavenged by PhCs [53]. The transport of PhCs to the vacuole is a key prerequisite for their ongoing biosynthesis as it creates a sink for assimilated carbon [54]. Differing fluorescence patterns under UV excitation indicate that different groups of PhCs accumulate in the epidermal pavement cell walls (blue fluorescence characteristic of cell-wall bound hydroxycinnamic acid derivatives) compared to the mesophyll cell walls, vacuoles, and chloroplasts (yellow fluorescence characteristic of flavonoids) (Figures 2d and 3). This is supported by the claim that hydroxycinnamic acid derivatives and flavonoids may have different roles in responding to high-intensity light, i.e., that HCA derivatives are better at UV screening (and localize close to the leaf surface-epidermis) but that flavonoids serve as free radical scavengers induced by excess light (and therefore localize around cells with active photosynthesis, i.e., in the mesophyll) [55].

According to Hutzler et al. [25], UV screening is mainly achieved by hydroxycinnamic acids and flavonoids in the epidermis, primarily in the cuticle, cell walls, or vacuole. However, studies in herbaceous plants show that UV-B still penetrated the anticlinal cell walls of the epidermis and reached the mesophyll [45], implying the need for protective PhCs even below the epidermis. A study by Liu et al. [56] showed that at least 50% of barley flavonoids occurred in the lower mesophyll rather than in the epidermis. This study used HPLC analysis on epidermal peels and isolated mesophyll tissue—although the presence of flavonoids in barley mesophyll was confirmed, the gradient from outer mesophyll (epidermis-adjacent) to middle mesophyll was not described. Studies in rye (*Secale cereale*) showed both epidermal hydroxycinnamic acids and mesophyll flavonoids were constitutive, while epidermal flavonoids increased with age and light intensity [57]. This is contrary to our finding that hydroxycinnamic acids were increased by high light intensity (Figure 6) and that flavonoids were mostly absent from the epidermis (except in stomata) while flavonoids in the mesophyll had a strong light-responsive and  $[CO_2]$ -responsive presence (Figures 2d and 3). This discrepancy could indicate a greater variety in how PhC-mediated stress response occurs in leaves of different species. For instance, dicotyledonous soybeans (*Glycine max*) are known to accumulate flavonoids only in the epidermis, while monocotyledonous oats (*Avena sativa*) accumulate flavonoids also in the mesophyll [56,58]. Another study, also using Naturstoff reagent A, found varying PhC localization even between closely related species of *Vaccinium*: notably, one species allocated the majority of PhCs to the outer surface of the epidermis, while another species only had PhCs associated with stomatal guard cells, but a greater localization in the palisade mesophyll layer [59]. This study further noted that while total phenolic compositions varied, the blue fluorescent signal from cell-wall bound PhCs in the epidermis remained constant (also observed by Lichtenhaler and Schweiger [40]). The most prevalent cell-wall bound PhCs are hydroxycinnamic acids [40,60] and specifically ferulic acid in Poaceae [61]. The observed primary presence of PhCs in the mesophyll, rather than in the epidermis, of barley leaves is a relatively unique result which suggests that leaves of different species and phenological stages present varied PhC-modulated leaf protective responses. In fact, later in the ontogeny of Bojos variety plants, occasional presence of flavonoids in some epidermal pavement cells was observed after exposure to stressors, such as drought and high temperature (results not shown). Clearly, flavonoids can occur in barley epidermal pavement cells, although they were not detected under the conditions of the present experiment.

Our results showed that light intensity is the major factor in terms of accumulation and localization of total PhCs (Figure 4, Table 1), with higher light intensity resulting in higher accumulation of PhCs in the mesophyll, particularly in cells adjacent to the epidermis (Figures 3 and 5). Leaves grown in low light showed accumulation of PhCs deeper in the mesophyll at low and ambient  $CO_2$  (Figure 5), but fewer PhCs overall (Figures 4 and 6). EC reduced the differences between HL and LL treatments and promoted an accumulation pattern similar to HL (Figures 3–5). The flavones (luteolin, isovitexin,



homoorientin and saponarin) were strongly associated with UV screening index (Figure 8). The UV screening index indicates that the accumulation and localization, especially of ortho-dihydroxylated flavonoids, increases with increasing  $[\text{CO}_2]$  at HL (Figure 7), a result noted in other plants, such as *Betula pendula* [62]. Strong antioxidant flavones, luteolin, and homoorientin, were accumulated much more in HL leaves, but not to the same degree in EC leaves (Table S1). Similarly, HL induced the increase of selected flavonoids in other barley varieties [63]. Our results show that high light increased both flavones and hydroxycinnamic acids similarly (Figure 6), although certain compounds with poor antioxidant qualities (coumaric acid, apigenin) showed a weaker association with light intensity than other compounds (Figure 8). As reported by Kowalczewski et al. [63], the high-light induced increase of hydroxycinnamic acids in barley was slightly more pronounced than the increase for flavones. Several studies report that high light + UV increases the ratio of flavonoids to hydroxycinnamic acids, which is interesting as hydroxycinnamic acids and their derivatives are more effective in UV-B screening, while flavonoids are more effective antioxidants [23,55,64]. It has been proposed that the accumulation of flavonoids may effectively protect sensitive tissues from photooxidative damage via intercellular scavenging of ROS [65]. Another highly attractive, and not mutually exclusive hypothesis, is that the biosynthesis of flavonoids serves as an alternative use for excess photosynthetic energy under conditions of high light or high C:N ratios. PhC biosynthesis may sustain photosynthesis under stress by consuming reducing power and excess carbon intermediates [22]. In this case, PhCs could theoretically be evenly distributed throughout the mesophyll, however, EC leaves still accumulated the greatest amount of PhCs near to leaf surfaces.

This study investigated barley leaves cultivated in various levels of atmospheric  $[\text{CO}_2]$ . Plant responses to EC are interesting in terms of how future plants will fare, while LC cultivation addresses mechanisms of carbon limitation, as well as questions of past eco-physiological function—200 ppm is representative of the low levels of atmospheric  $[\text{CO}_2]$  experienced by land plants during the last glacial period [66,67]. Extending the range of  $[\text{CO}_2]$  allows for a better understanding of its role in plant secondary metabolism. The effect of carbon limitation may not be seen at AC or EC, especially if other factors such as low light intensity or low nitrogen availability are reducing photosynthetic capacity [68,69]. The role of  $[\text{CO}_2]$  on secondary metabolism is not fully clarified yet and shows compound-specific responses and dependence on other environmental conditions such as light intensity [70]. Moreover, the plant response to  $[\text{CO}_2]$  regarding carbon allocation to PhCs may be different for annual plants such as barley versus woody species. A study on Norway spruce [71] showed that trees grown under elevated  $[\text{CO}_2]$  invested the extra carbon rather to stem and shoot growth than to accumulation of PhCs in needles. Our findings show that barley plants grown in EC benefit from the excess available  $[\text{CO}_2]$  to synthesize PhCs to a higher degree than plants grown in equivalent light conditions in AC and particularly in LC (Figures 3 and 5). This effect is more evident under LL conditions, so it seems that elevated  $[\text{CO}_2]$  is partly able to replace the role of HL in the accumulation of PhCs. The result is a convergence of differences between LL and HL conditions with increasing  $[\text{CO}_2]$ . The positive effect of elevated  $[\text{CO}_2]$  on PhC metabolism was already proven in recent studies by Ibrahim et al. and Peñuelas et al. [29,72].

Although the mechanisms remain unclear, Ibrahim et al. [29] showed tight relationships between photosynthetic rate and accumulation of PhCs. Carbon-rich PhCs form a substantial carbon sink for photosynthetic assimilates and may reduce the occurrence of feedback down-regulation of photosynthesis under elevated  $[\text{CO}_2]$  [72]. What is curious about the localization data for EC barley leaves grown in LL versus HL is that both groups accumulate PhCs near to the surface, rather than in the lower mesophyll as seen for other LL treatments. Such a pattern of PhC localization can be attributed to increasing chlorophyll content per area unit due to increasing  $[\text{CO}_2]$  and high light (Figure 7) and by an increase in leaf thickness mainly due to high light. Both factors can reduce the light transmittance to the middle mesophyll and thus results in higher gradients within

leaf cross-section. Positive effect of both light intensity and [CO<sub>2</sub>] on leaf thickness was documented by meta-analysis across several species [73]. An increasing chlorophyll content under both high [CO<sub>2</sub>] and light intensity was also documented in wheat by Yi et al. [74].

Overall, the PhC content was significantly influenced by barley variety, especially for hydroxycinnamic acids and hydroxybenzoic acids (Table 2). Previous studies already demonstrated lower constitutive PhCs (under UV exclusion and low light conditions) in Barke variety compared to another tolerant genotype (Bonus) [75]. However, high light led to an accumulation of PhCs exceeding the constitutive contents several fold. In our study, the Bojos variety showed a higher accumulation of hydroxycinnamic acids, while the Barke variety had a higher accumulation of hydroxybenzoic acids (Figure 6), particularly syringic acid, which was absent in the Bojos variety (Table S1). In other studies, PhCs profile was shown to be variety dependent and among environmental factors, timing of water scarcity had stronger effect on PhCs than light intensity [63]. Syringic acid levels, in particular, can be a distinguishing trait among barley varieties [76]. Between the two groups of phenolic acids, the hydroxycinnamic acids are usually cited as being stronger antioxidants than hydroxybenzoic acids [20]. While hydroxycinnamic acids play a role in UV screening, hydroxybenzoic acids may promote resistance to biotic stressor. Barley leaves treated with vanillic, isovanillic, or syringic acid showed a reduction in mildew by more than 80% [77]. The higher accumulation of hydroxybenzoic acids in the Barke variety may explain its purported tolerance to common biotic stressors [78], including leaf rust, leaf scald, net blotch, and mildew, while maintaining its status as oxidative-stress sensitive. Barke also showed higher accumulation of ortho-dihydroxylated flavonoids, as indicated by the UV screening index (Figure 7) which is associated mainly to the accumulation of ortho-dihydroxylated flavonoids [42]. The accumulation of antioxidant PhCs in stress-sensitive plants may be the result of less efficient initial defenses to ROS production, and thus exposure to more severe states of oxidative stress [23]. Meanwhile, the high level of hydroxycinnamic acids in leaves of Bojos plants provide better protection from high light and a possible lower stress load on the plant. Additionally, the Bojos variety accumulated more PhCs in epidermal-adjacent mesophyll cell layers, especially under EC conditions (Figure 5). These data could lead to a hypothesis that certain groups of PhCs (i.e., hydroxycinnamic acids) and certain mesophyll localizations (i.e., adjacent to epidermal leaf surfaces) provide increased protection from direct photooxidative stress as a product of high light.

In conclusion, our findings show that high light intensity enhanced the accumulation of nearly all PhCs detected by HPLC-HRMS and promoted their localization in the epidermal-adjacent mesophyll layers (Figures 4 and 5). Elevated [CO<sub>2</sub>] also increased PhC accumulation, even in the absence of high intensity light (Figures 3 and 5). Additionally, barley varieties with varying tolerance to oxidative stress showed differences in their respective levels of hydroxycinnamic acids and hydroxybenzoic acids. Oxidative-stress sensitive variety Barke accumulated more flavones and hydroxybenzoic acids, particularly syringic acid, which was absent in Bojos (Table S1), while the variety Bojos accumulated more hydroxycinnamic acids (Figure 6). We hypothesize that the greater antioxidative efficiency provided by the CH=CH-COOH group in hydroxycinnamic acids compared to the COOH group in hydroxybenzoic acids may be responsible for the higher tolerance of oxidative stress in the Bojos variety.

In addition, we believe that our study brings an original multidisciplinary aspect to the study of PhC accumulation and localization. The combination of histochemical detection on leaf cross sections with image analysis in tissue layers allows for a more complex, more detailed evaluation of the localization of detected compound in gradients across organs and tissues. This approach could be valuable not only in plant histochemistry but in animal and human studies as well.

**Supplementary Materials:** The following are available online at <https://www.mdpi.com/2076-3921/10/3/385/s1> Figure S1: Diurnal courses of air temperature, relative air humidity, photosynthetically active and UV-A radiation inside the growth chambers during the experiment. Figure S2:

Paradermal images of barley (*Hordeum vulgare*) leaf segments demonstrating the absence of PhCs detected by Naturstoff reagent A in the epidermal pavement cells. Table S1: Levels of specific PhCs levels measured using HPLC-HRMS.

**Author Contributions:** J.A. conceived the study with the contribution of L.H., K.K., and V.Š., K.K. and O.U. performed the chamber experiment in the facilities of the Global Change Research Institute. L.H. performed histochemical analyses and their image analysis processing. M.O. performed HPLC analyses and Dualex measurements. Subsequent data analysis was performed mainly by L.H., statistical analysis by L.H., K.K. and S.V. and data were interpreted mainly by L.H. L.H. drafted the manuscript under supervision of J.A. and acted as the leading author throughout manuscript preparation. K.K. provided chief contributions to the manuscript draft. L.H., J.A., and K.K. performed final manuscript writing with contributions of Z.L., O.U., V.Š. who reviewed the manuscript. All authors have read and agreed to the published version of the manuscript.

**Funding:** This research was funded by the Czech Science Foundation (GAČR 18-23702S). Participation of K.K., M.O., V.Š. and O.U. was also supported by the project “SustES-Adaptation strategies for sustainable ecosystem services and food security under adverse environmental conditions” (CZ.02.1.01/0.0/0.0/16\_019/0000797).

**Institutional Review Board Statement:** Not Applicable.

**Informed Consent Statement:** Not Applicable.

**Data Availability Statement:** Data available upon request.

**Acknowledgments:** We thank Miroslav Barták for his technical help in laboratory analyses, microscopy, and image processing. We also thank to students helping in sampling and sample processing during harvest campaign.

**Conflicts of Interest:** The authors declare no conflict of interest.

## References

- Zohary, D.; Hopf, M. *Domestication of Plants in the Old World*; Oxford University Press: Oxford, UK, 2000; ISBN 0198503563.
- FAOSTAT. *Crops/Regions/World List/Production Quantity for Barley*; UN Food and Agriculture Organization Corporate Statistical Database: Rome, Italy, 2019.
- Kamiyama, M.; Shibamoto, T. Flavonoids with potent antioxidant activity found in young green barley leaves. *J. Agric. Food Chem.* **2021**, *60*, 6260–6267. [[CrossRef](#)] [[PubMed](#)]
- Baik, B.K.; Ullrich, S.E. Barley for food: Characteristics, improvement, and renewed interest. *J. Cereal Sci.* **2008**, *48*, 233–242. [[CrossRef](#)]
- Kruse, J. *Estimating Demand for Agricultural Commodities to 2050*; Report No. 3-16-10; Global Harvest Initiative: Washington, DC, USA, 2011.
- Cammarano, D.; Ceccarelli, S.; Grando, S.; Romagosa, I.; Benbelkacem, A.; Akar, T.; Al-Yassin, A.; Pecchioni, N.; Francia, E.; Ronga, D. The impact of climate change on barley yield in the Mediterranean basin. *Eur. J. Agron.* **2019**, *106*, 1–11. [[CrossRef](#)]
- Xie, W.; Xiong, W.; Pan, J.; Ali, T.; Cui, Q.; Guan, D.; Meng, J.; Mueller, N.D.; Lin, E.; Davis, S.J. Decreases in global beer supply due to extreme drought and heat. *Nat. Plants* **2018**, *4*, 964–973. [[CrossRef](#)]
- Jansen, M.A.; Hectors, K.; O'Brien, N.M.; Guisez, Y.; Potters, G. Plant stress and human health: Do human consumers benefit from UV-B acclimated crops? *Plant Sci.* **2008**, *175*, 449–485. [[CrossRef](#)]
- De Gara, L.; Locato, V.; Dipierro, S.; de Pinto, M.C. Redox homeostasis in plants. The challenge of living with endogenous oxygen production. *Respir. Physiol. Neurobiol.* **2010**, *173*, S13–S19. [[CrossRef](#)] [[PubMed](#)]
- Foyer, C.; Noctor, G. Redox homeostasis and antioxidant signaling: A metabolic interface between stress perception and physiological responses. *Plant Cell* **2005**, *17*, 1866–1875. [[CrossRef](#)]
- Foyer, C.H.; Lelandais, M.; Kunert, K.J. Photooxidative stress in plants. *Physiol. Plant.* **1994**, *92*, 696–717. [[CrossRef](#)]
- Klem, K.; Gargallo-Garriga, A.; Rattanapichai, W.; Oravec, M.; Holub, P.; Veselá, B.; Sardans, J.; Peñuelas, J.; Urban, O. Distinct morphological, physiological, and biochemical responses to light quality in barley leaves and roots. *Front. Plant Sci.* **2019**, *10*, 1026. [[CrossRef](#)] [[PubMed](#)]
- Fayez, K.A.; Bazaid, S.A. Improving drought and salinity tolerance in barley by application of salicylic acid and potassium nitrate. *J. Saudi Soc. Agric. Sci.* **2014**, *13*, 45–55. [[CrossRef](#)]
- Corcuera, L.J. Biochemical basis for the resistance of barley to aphids. *Phytochemistry* **1993**, *33*, 741–747. [[CrossRef](#)]
- Pfanz, H.; Oppmann, B.; Wolf, P.; Lomsky, B. Detoxification of air pollutants in the presence of apoplastic phenols. *Ishs Acta Hort.* **1994**, *381*, 360–366. [[CrossRef](#)]
- Michalak, A. Phenolic compounds and their antioxidant activity in plants growing under heavy metal stress. *Pol. J. Environ. Stud.* **2006**, *15*, 523–530.






17. Caldwell, M.M.; Robberecht, R.; Flint, S.D. Internal filters: Prospects for UV-acclimation in higher plants. *Physiol. Plant.* **1983**, *58*, 445–450. [[CrossRef](#)]
18. Rice-Evans, C.; Miller, N.; Paganga, G. Antioxidant properties of phenolic compounds. *Trends Plant Sci.* **1997**, *2*, 152–159. [[CrossRef](#)]
19. Chen, J.W.; Zhu, Z.Q.; Hu, T.X.; Zhu, D.Y. Structure-activity relationship of natural flavonoids in hydroxyl radical-scavenging effects. *Acta Pharmacol. Sin.* **2002**, *23*, 667–672.
20. Cuvelier, M.E.; Richard, H.; Berset, C. Comparison of the antioxidative activity of some acid-phenols: Structure-activity relationship. *Biosci. Biotechnol. Biochem.* **1992**, *56*, 324–325. [[CrossRef](#)]
21. Agati, G.; Brunetti, C.; Di Ferdinando, M.; Ferrini, F.; Pollastri, S.; Tattini, M. Functional roles of flavonoids in photoprotection: New evidence, lessons from the past. *Plant Physiol. Biochem.* **2013**, *72*, 35–45. [[CrossRef](#)]
22. Hernández, I.; Alegre, L.; Van Breusegem, F.; Munné-Bosch, S. How relevant are flavonoids as antioxidants in plants? *Trends Plant Sci.* **2009**, *14*, 125–132. [[CrossRef](#)] [[PubMed](#)]
23. Agati, G.; Azzarello, E.; Pollastri, S.; Tattini, M. Flavonoids as antioxidants in plants: Location and functional significance. *Plant Sci.* **2012**, *196*, 67–76. [[CrossRef](#)] [[PubMed](#)]
24. Akhtar, T.A.; Lees, H.A.; Lampi, M.A.; Enstone, D.; Brain, R.A.; Greenberg, B.M. Photosynthetic redox imbalance influences flavonoid biosynthesis in *Lemma gibba*. *Plant Cell Environ.* **2010**, *33*, 1205–1219. [[PubMed](#)]
25. Hutzler, P.; Fischbach, R.; Heller, W.; Jungblut, T.P.; Reuber, S.; Schmitz, R.; Veit, M.; Weissenböck, G.; Schnitzler, J.P. Tissue localization of phenolic compounds in plants by confocal laser scanning microscopy. *J. Exp. Bot.* **1998**, *49*, 953–965. [[CrossRef](#)]
26. Burchard, P.; Bilger, W.; Weissenböck, G. Contribution of hydroxycinnamates and flavonoids to epidermal shielding of UV-A and UV-B radiation in developing rye primary leaves as assessed by ultraviolet-induced chlorophyll fluorescence measurements. *Plant Cell Environ.* **2000**, *23*, 1373–1380. [[CrossRef](#)]
27. Csepregi, K.; Neugart, S.; Schreiner, M.; Hideg, É. Comparative evaluation of total antioxidant capacities of plant polyphenols. *Molecules* **2016**, *21*, 208. [[CrossRef](#)] [[PubMed](#)]
28. Agati, G.; Brunetti, C.; Fini, A.; Gori, A.; Guidi, L.; Landi, M.; Sebastiani, F.; Tattini, M. Are flavonoids effective antioxidants in plants? Twenty years of our investigation. *Antioxidants* **2020**, *9*, 1098. [[CrossRef](#)] [[PubMed](#)]
29. Ibrahim, M.H.; Jaafar, H.Z.; Rahmat, A.; Rahman, Z.A. The relationship between phenolics and flavonoids production with total non structural carbohydrate and photosynthetic rate in *Labisia pumila* Benth. under high CO<sub>2</sub> and nitrogen fertilization. *Molecules* **2011**, *16*, 162–174. [[CrossRef](#)] [[PubMed](#)]
30. Wu, Y.X.; Tiedemann, A.V. Light-dependent oxidative stress determines physiological leaf spot formation in barley. *Phytopathology* **2004**, *94*, 584–592. [[CrossRef](#)] [[PubMed](#)]
31. Klem, K.; Ač, A.; Holub, P.; Kováč, D.; Špunda, V.; Robson, T.M.; Urban, O. Interactive effects of PAR and UV radiation on the physiology, morphology and leaf optical properties of two barley varieties. *Environ. Exp. Bot.* **2012**, *75*, 52–64. [[CrossRef](#)]
32. Hartman, I. Quality of malting barley grain in the Czech Republic, crop 2017. *Kvasny Prumysl.* **2018**, *64*, 64–69. [[CrossRef](#)]
33. Kofroň, P.; Skoblík, R.; Enge, J.; Sekora, M. Testing of malting barley—Variety bojós. *Kvasny Prumysl.* **2006**, *52*, 179–184. [[CrossRef](#)]
34. Agrární Komora České Republiky. Ústřední Kontrolní a Zkušební Ústav Zemědělský; *Obilniny 2018*; Národní odrůvový úřad: Brno, Czech Republic, 2018; ISBN 9788074011610.
35. Arenas-Corraliza, M.G.; Rolo, V.; López-Díaz, M.L.; Moreno, G. Wheat and barley can increase grain yield in shade through acclimation of physiological and morphological traits in Mediterranean conditions. *Sci. Rep.* **2019**, *9*, 9547. [[CrossRef](#)] [[PubMed](#)]
36. Phillips, M. *The Chemistry of Lignin*; Waverly Press: New York, NY, USA, 1934.
37. Gardner, R. Vanillin-hydrochloric acid as a histochemical test for tannin. *Stain Technol.* **1975**, *50*, 315–317. [[CrossRef](#)] [[PubMed](#)]
38. Neu, R. Chelates of diarylboric acids with aliphatic oxyalkylamines as reagents for the detection of oxyphenyl-benzo- $\gamma$ -pyrones. *Die Nat.* **1957**, *44*, 181–182. [[CrossRef](#)]
39. Valette, C.; Andary, C.; Geiger, J.P.; Sarah, J.L.; Nicole, M. Histochemical and cytochemical investigations of phenols in roots of banana infected by the burrowing nematode *Radopholus similis*. *Phytopathology* **1998**, *88*, 1141–1148. [[CrossRef](#)] [[PubMed](#)]
40. Lichtenthaler, H.K.; Schweiger, J. Cell wall bound ferulic acid, the major substance of the blue-green fluorescence emission of plants. *J. Plant Physiol.* **1998**, *152*, 272–282. [[CrossRef](#)]
41. Albrechtová, J.; Kubínová, Z.; Soukup, A.; Janáček, J. Image analysis: Basic procedures for description of plant structures. *Methods Mol. Biol.* **2014**, *1080*, 67–76. [[PubMed](#)]
42. Agati, G.; Cerovic, Z.G.; Pinelli, P.; Tattini, M. Light-induced accumulation of ortho-dihydroxylated flavonoids as non-destructively monitored by chlorophyll fluorescence excitation techniques. *Environ. Exp. Bot.* **2011**, *73*, 3–9. [[CrossRef](#)]
43. Goulas, Y.; Cerovic, Z.G.; Cartelat, A.; Moya, I. Dualex: A new instrument for field measurements of epidermal ultraviolet absorbance by chlorophyll fluorescence. *Appl. Opt.* **2004**, *43*, 4488–4496. [[CrossRef](#)] [[PubMed](#)]
44. Smilauer, P.; Lepš, J. *Multivariate Analysis of Ecological Data Using Canoco 5*, 2nd ed.; Cambridge University Press: Cambridge, UK, 2014.
45. Day, T.A.; Martin, G.; Vogelmann, T.C. Penetration of UV-B radiation in foliage: Evidence that the epidermis behaves as a non-uniform filter. *Plant Cell Environ.* **1993**, *16*, 735–741. [[CrossRef](#)]
46. McClendon, J.H.; Fukshanksky, L. On the interpretation of absorption spectra of leaves—II. The non-absorbed ray of the sieve effect and the mean optical pathlength in the remainder of the leaf. *Photochem. Photobiol.* **1990**, *51*, 211–216. [[CrossRef](#)]

47. Kolb, C.A.; Pfündel, E.E. Origins of non-linear and dissimilar relationships between epidermal UV absorbance and UV absorbance of extracted phenolics in leaves of grapevine and barley. *Plant Cell Environ.* **2005**, *25*, 580–590. [[CrossRef](#)]
48. Li, B.; Neumann, E.K.; Ge, J.; Gao, W.; Yang, H.; Li, P.; Sweedler, J.V. Interrogation of spatial metabolome of *Ginkgo biloba* with high-resolution matrix-assisted laser desorption/ionization and laser desorption/ionization mass spectrometry imaging. *Plant Cell Environ.* **2018**, *41*, 2693–2703. [[CrossRef](#)] [[PubMed](#)]
49. Bogucka-Kocka, A.; Zidorn, C.; Kasprzycka, M.; Zyna Szymczak, G.; Szewczyk, K. Phenolic acid content, antioxidant and cytotoxic activities of four *Kalanchoë* species. *Saudi J. Biol. Sci.* **2016**, *25*, 622–630. [[CrossRef](#)] [[PubMed](#)]
50. Hrazdina, G.; Wagner, G. Metabolic pathways as enzyme complexes: Evidence for the synthesis of phenylpropanoids and flavonoids on membrane associated enzyme complexes. *Arch. Biochem. Biophys.* **1985**, *237*, 88–100. [[CrossRef](#)]
51. McNally, D.J.; Wurms, K.V.; Labbé, C.; Bélanger, R.R. Synthesis of C-glycosyl flavonoid phytoalexins as a site-specific response to fungal penetration in cucumber. *Physiol. Mol. Plant Pathol.* **2003**, *63*, 293–303. [[CrossRef](#)]
52. Schmitz-Hoerner, R.; Weissenböck, G. Contribution of phenolic compounds to the UV-B screening capacity of developing barley primary leaves in relation to DNA damage and repair under elevated UV-B levels. *Phytochemistry* **2003**, *64*, 243–255. [[CrossRef](#)]
53. Mubarakshina, M.M.; Ivanov, B.N.; Naydov, I.A.; Hillier, W.; Badger, M.R.; Krieger-Liszka, A. Production and diffusion of chloroplastic H<sub>2</sub>O<sub>2</sub> and its implication to signalling. *J. Exp. Bot.* **2010**, *61*, 3577–3587. [[CrossRef](#)]
54. Zhao, J.; Dixon, R.A. MATE transporters facilitate vacuolar uptake of epicatechin 3-O-glucoside for proanthocyanidin biosynthesis in *medicago truncatula* and *Arabidopsis*. *Plant Cell* **2009**, *21*, 2323–2340. [[CrossRef](#)] [[PubMed](#)]
55. Tattini, M.; Galardi, C.; Pinelli, P.; Massai, R.; Remorini, D.; Agati, G. Differential accumulation of flavonoids and hydroxycinnamates in leaves of *Ligustrum vulgare* under excess light and drought stress. *New Phytol.* **2004**, *163*, 547–561. [[CrossRef](#)]
56. Liu, L.; Gitz, D.C.; McClure, J.W. Effects of UV-B on flavonoids, ferulic acid, growth and photosynthesis in barley primary leaves. *Physiol. Plant.* **1995**, *93*, 725–733. [[CrossRef](#)]
57. Reuber, S.; Bornman, J.F.; Weissenböck, G. Phenylpropanoid compounds in primary leaf tissues of rye (*Secale cereale*). Light response of their metabolism and the possible role in UV-B protection. *Physiol. Plant.* **1996**, *97*, 160–168. [[CrossRef](#)]
58. Knogge, W.; Weissenböck, G. Tissue-distribution of secondary phenolic biosynthesis in developing primary leaves of *Avena sativa* L. *Planta* **1986**, *167*, 196–205. [[CrossRef](#)]
59. Semerdjieva, S.I.; Sheffield, E.; Phoenix, G.K.; Gwynn-Jones, D.; Callaghan, T.V.; Johnson, G.N. Contrasting strategies for UV-B screening in sub-Arctic dwarf shrubs. *Plant Cell Environ.* **2003**, *26*, 957–964. [[CrossRef](#)] [[PubMed](#)]
60. Donaldson, L. Autofluorescence in plants. *Molecules* **2020**, *25*, 2393. [[CrossRef](#)] [[PubMed](#)]
61. Harris, P.J.; Hartley, R.D. Phenolic constituents of the cell walls of monocotyledons. *Biochem. Syst. Ecol.* **1980**, *8*, 153–160. [[CrossRef](#)]
62. Peltonen, P.A.; Vapaavuori, E.; Julkunen-Tiitto, R. Accumulation of phenolic compounds in birch leaves is changed by elevated carbon dioxide and ozone. *Glob. Chang. Biol.* **2005**, *11*, 1305–1324. [[CrossRef](#)]
63. Kowalczewski, P.L.; Radzikowska, D.; Ivanišová, E.; Szwengel, A.; Kačániová, M.; Sawinska, Z. Influence of abiotic stress factors on the antioxidant properties and polyphenols profile composition of green barley (*Hordeum vulgare* L.). *Int. J. Mol. Sci.* **2020**, *21*, 397. [[CrossRef](#)]
64. Tattini, M.; Guidi, L.; Morassi-Bonzi, L.; Pinelli, P.; Remorini, D.; Degl'Innocenti, E.; Giordano, C.; Massai, R.; Agati, G. On the role of flavonoids in the integrated mechanisms of response of *Ligustrum vulgare* and *Phillyrea latifolia* to high solar radiation. *New Phytol.* **2005**, *167*, 457–470. [[CrossRef](#)]
65. Grace, S.G.; Logan, B.A. Energy dissipation and radical scavenging by the plant phenylpropanoid pathway. *Philos. Trans. R. Soc. B* **2000**, *355*, 1499–1510. [[CrossRef](#)] [[PubMed](#)]
66. Delmas, R.J.; Ascencio, J.M.; Legrand, M. Polar ice evidence that atmospheric CO<sub>2</sub> 20,000 yr BP was 50% of present. *Nature* **1980**, *284*, 155–157. [[CrossRef](#)]
67. Ehleringer, J.R.; Cerling, T.E. Atmospheric CO<sub>2</sub> and the ratio of intercellular to ambient CO<sub>2</sub> concentrations in plants. *Tree Physiol.* **1995**, *15*, 105–111. [[CrossRef](#)]
68. Fatichi, S.; Leuzinger, S.; Körner, C. Moving beyond photosynthesis: From carbon source to sink-driven vegetation modeling. *New Phytol.* **2014**, *201*, 1086–1095. [[CrossRef](#)] [[PubMed](#)]
69. Palacio, S.; Hoch, G.; Sala, A.; Körner, C.; Millard, P. Does carbon storage limit tree growth? *New Phytol.* **2014**, *201*, 1096–1100. [[CrossRef](#)] [[PubMed](#)]
70. Jaafar, H.Z.; Ibrahim, M.H.; Karimi, E. Phenolics and flavonoids compounds, phenylalanine ammonia lyase and antioxidant activity responses to elevated CO<sub>2</sub> in *Labisia pumila* (Myrsinaceae). *Molecules* **2012**, *17*, 6331–6347. [[CrossRef](#)] [[PubMed](#)]
71. Lhotáková, Z.; Urban, O.; Dubánková, M.; Cvíková, M.; Tomášková, I.; Kubínová, L.; Zvára, K.; Marek, M.V.; Albrechtová, J. The impact of long-term CO<sub>2</sub> enrichment on sun and shade needles of Norway spruce (*Picea abies*): Photosynthetic performance, needle anatomy and phenolics accumulation. *Plant Sci.* **2012**, *188–189*, 60–70.
72. Peñuelas, J.; Estiarte, M.; Kimball, B.A.; Idso, S.B.; Pinter, P.J.; Wall, G.W.; Garcia, R.L.; Hansaker, D.J.; LaMorte, R.L.; Hendrix, D.L. Variety of responses of plant phenolic concentration to CO<sub>2</sub> enrichment. *J. Exp. Bot.* **1996**, *47*, 1463–1467.
73. Poorter, H.; Niinemets, Ü.; Poorter, L.; Wright, I.J.; Villar, R. Causes and consequences of variation in leaf mass per area (LMA): A meta-analysis. *New Phytol.* **2009**, *182*, 565–588. [[CrossRef](#)] [[PubMed](#)]

74. Yi, Z.; Cui, J.; Fu, Y.; Liu, H. Effect of different light intensity on physiology, antioxidant capacity and photosynthetic characteristics on wheat seedlings under high CO<sub>2</sub> concentration in a closed artificial ecosystem. *Photosynth. Res.* **2020**, *144*, 23–34. [[CrossRef](#)] [[PubMed](#)]
75. Holub, P.; Nezval, J.; Štroch, M.; Špunda, V.; Urban, O.; Jansen, M.A.; Klem, K. Induction of phenolic compounds by UV and PAR is modulated by leaf ontogeny and barley genotype. *Plant Physiol. Biochem.* **2019**, *134*, 81–93. [[CrossRef](#)] [[PubMed](#)]
76. Klepacka, J.; Gujska, E.; Michalak, J. Phenolic compounds as cultivar- and variety-distinguishing factors in some plant products. *Plant Foods Hum. Nutr.* **2011**, *66*, 64–69. [[CrossRef](#)] [[PubMed](#)]
77. Walters, D.; Mitchella, A.; Hampson, J.; McPherson, A. The induction of systemic resistance in barley to powdery mildew infection using salicylates and various phenolic acids. *Ann. Appl. Biol.* **1993**, *122*, 451–456. [[CrossRef](#)]
78. Oliver, G. (Ed.) *The Oxford Companion to Beer*; Oxford University Press: Oxford, UK, 2011; ISBN 0195367138.

## Article

# Barley Genotypes Vary in Stomatal Responsiveness to Light and CO<sub>2</sub> Conditions

Lena Hunt <sup>1</sup>, Michal Fuksa <sup>1</sup>, Karel Klem <sup>2</sup>, Zuzana Lhotáková <sup>1</sup>, Michal Oravec <sup>2</sup>, Otmar Urban <sup>2</sup>  
and Jana Albrechtová <sup>1,\*</sup>

<sup>1</sup> Department of Experimental Plant Biology, Faculty of Science, Charles University, Viničná 5, 12844 Praha, Czech Republic; huntl@natur.cuni.cz (L.H.); Michal.Fuksa@gmail.com (M.F.); zuzana.lhotakova@natur.cuni.cz (Z.L.)

<sup>2</sup> Global Change Research Institute, Czech Academy of Sciences, Bělidla 4a, 60300 Brno, Czech Republic; klem.k@czechglobe.cz (K.K.); oravec.m@czechglobe.cz (M.O.); urban.o@czechglobe.cz (O.U.)

\* Correspondence: albrecht@natur.cuni.cz; Tel.: +420-221-95-1959

**Abstract:** Changes in stomatal conductance and density allow plants to acclimate to changing environmental conditions. In the present paper, the influence of atmospheric CO<sub>2</sub> concentration and light intensity on stomata were investigated for two barley genotypes—Barke and Bojos, differing in their sensitivity to oxidative stress and phenolic acid profiles. A novel approach for stomatal density analysis was used—a pair of convolution neural networks were developed to automatically identify and count stomata on epidermal micrographs. Stomatal density in barley was influenced by genotype, as well as by light and CO<sub>2</sub> conditions. Low CO<sub>2</sub> conditions resulted in increased stomatal density, although differences between ambient and elevated CO<sub>2</sub> were not significant. High light intensity increased stomatal density compared to low light intensity in both barley varieties and all CO<sub>2</sub> treatments. Changes in stomatal conductance were also measured alongside the accumulation of pentoses, hexoses, disaccharides, and abscisic acid detected by liquid chromatography coupled with mass spectrometry. High light increased the accumulation of all sugars and reduced abscisic acid levels. Abscisic acid was influenced by all factors—light, CO<sub>2</sub>, and genotype—in combination. Differences were discovered between the two barley varieties: oxidative stress sensitive Barke demonstrated higher stomatal density, but lower conductance and better water use efficiency (WUE) than oxidative stress resistant Bojos at saturating light intensity. Barke also showed greater variability between treatments in measurements of stomatal density, sugar accumulation, and abscisic levels, implying that it may be more responsive to environmental drivers influencing water relations in the plant.

**Keywords:** stomata; stomatal density; stomatal conductance; stomatal regulation; barley; CO<sub>2</sub>; light; ABA; neural network; phenolics



**Citation:** Hunt, L.; Fuksa, M.; Klem, K.; Lhotáková, Z.; Oravec, M.; Urban, O.; Albrechtová, J. Barley Genotypes Vary in Stomatal Responsiveness to Light and CO<sub>2</sub> Conditions. *Plants* **2021**, *10*, 2533. <https://doi.org/10.3390/plants10112533>

Academic Editors: Angela Augusti, Maria Cristina Monteverdi and Andrea Scartazza

Received: 29 October 2021

Accepted: 18 November 2021

Published: 21 November 2021

**Publisher's Note:** MDPI stays neutral with regard to jurisdictional claims in published maps and institutional affiliations.



**Copyright:** © 2021 by the authors. Licensee MDPI, Basel, Switzerland. This article is an open access article distributed under the terms and conditions of the Creative Commons Attribution (CC BY) license (<https://creativecommons.org/licenses/by/4.0/>).

## 1. Introduction

Stomata are made up of paired guard cells which regulate the aperture of a pore through changes in their turgor, allowing controlled gas exchange between the atmosphere and internal air spaces of a plant. Guard cells are flanked by subsidiary cells, which act as reservoirs of water and osmolytes that can facilitate guard cell movement [1]. Open stomata allow for gas exchange mediated by concentration gradients resulting in an influx of CO<sub>2</sub>, the substrate of photosynthesis, and efflux of O<sub>2</sub> and H<sub>2</sub>O, the latter providing transpirational cooling of the plant. Closed stomata conserve water inside the plant necessary for physiological functions and act as a barrier to pollutants and pathogens. They serve a key role in plant productivity by balancing the photosynthetic CO<sub>2</sub>-demand with maintaining a suitable temperature and water status for the plant. Although stomata occupy only 0.3–5% of leaf epidermal surface, they account for up to 95% of all gas exchange between the plant and atmosphere [2], while cuticular transpiration makes up the remainder. The

recent advances in research on the plasticity of stomatal development and regulation make stomata a key feature in eco-physiological investigations of plant adaptation and a target for increasing agricultural productivity under the limiting environmental conditions of ongoing climate change.

The number of stomata on leaves may increase or decrease according to environmental cues. Mature leaves sense environmental cues and transmit signals to determine the frequency of stomata on developing leaves [3]. Allocation of epidermal space to stomata is constrained by the cost of developing and operating stomata [4] and both an inadequate and an excessive number of stomata present significant trade-offs in plant productivity and survival [5]. The stomatal responses to light and atmospheric CO<sub>2</sub> concentration ([CO<sub>2</sub>]) oppose each other—increasing light tends to increase stomatal density, while increasing [CO<sub>2</sub>] tends to decrease stomatal density [6], although exceptions exist [7,8]. Changes in atmospheric [CO<sub>2</sub>] have led to observable decreases in stomatal density in modern plants compared to pre-industrial herbarium samples [9] and fossilized plants [10]. However, work by Zhang et al. [11] suggests that the determination of stomatal density is species-specific, with some species influenced mainly by genetics, and others more responsive to environmental drivers. It is, therefore, useful to examine the influence of environmental cues on both the density and function of stomata among genotypes within a single species.

In the short term, gas exchange is regulated by the aperture of the stomatal pore, a phenomenon that occurs via changes in guard cell turgor pressure mediated by complex signaling cascades. Accumulation of potassium ions, chloride, and organic ions (such as malate and sucrose) in guard cells causes water uptake from the apoplast, resulting in high turgor and stomatal opening [12]. Stomatal closure occurs when ions and solutes are released, inducing a loss of turgor as water moves out of the guard cells. Stomatal conductance ( $G_s$ ), a measure of the simultaneous influx of CO<sub>2</sub> and efflux of water vapor occurring through stomatal pores, is an integral of stomatal density and stomatal opening.  $G_s$  is driven by photosynthesis and is thus dependent on light and [CO<sub>2</sub>] conditions, as well as water availability, and mediated through signaling from the phytohormone abscisic acid (ABA) and the generation of reactive oxygen species (ROS) [13,14]. The influence of light on stomatal conductance varies by intensity and spectral quality: Low intensity blue-light initiates stomatal opening by activating a plasma membrane ATPase [15], while red light drives stomatal response via photosynthetic CO<sub>2</sub> consumption [16]. CO<sub>2</sub> also affects  $G_s$ : Elevated [CO<sub>2</sub>] suppresses inward K<sup>+</sup> channels and enhances outward K<sup>+</sup> channels, depolarizing the guard cell membrane resulting in loss of turgor and stomatal closure [17]. Changes in stomatal aperture in response to [CO<sub>2</sub>] occur in response to intercellular [CO<sub>2</sub>] (C<sub>i</sub>) rather than atmospheric [CO<sub>2</sub>] [18]. C<sub>i</sub> can oscillate between over 600 ppm in the dark to less than 200 ppm in the light [19]. Stomatal response to elevated [CO<sub>2</sub>] is mediated through ABA, with ABA increasing sensitivity to [CO<sub>2</sub>] [14]. For plants with a C3 photosynthetic pathway, elevated [CO<sub>2</sub>] means greater water use efficiency (WUE): more efficient photosynthesis and less water lost through transpiration (at least in the short term) [15]. Photosynthetic CO<sub>2</sub> consumption is important, but the end products of photosynthesis, soluble sugars, also influence stomatal regulation.

The role of sugars in stomatal regulation is still under investigation. It was initially thought that sugar functioned as an osmolyte in stomatal movements, however, experiments with mannitol as an osmotic control showed that sucrose regulation of stomatal aperture was not an osmotic process [16] and sucrose actually induces stomatal closure at higher concentrations [17]. Sucrose accumulates in guard cells through photosynthesis, starch degradation, or apoplastic import from the mesophyll [18,19]. When biosynthesis of sucrose occurs in excess, sucrose is broken down into hexoses (glucose and fructose) by the sugar phosphorylating enzyme, hexokinase (HXK), which in turn initiates ABA-mediated stomatal closure [16]. This creates a natural feedback mechanism to limit transpiration when photosynthetic CO<sub>2</sub> fixation is occurring in excess, causing an accumulation of sugars. HXK is also involved in the downregulation of photosynthesis under elevated [CO<sub>2</sub>] when plants lack sufficient sinks for the products of photosynthesis [15].



This study looks at how experimentally manipulated [CO<sub>2</sub>] and light conditions modulate both the stomatal density and stomatal conductance alongside physiological processes in two barley varieties differing in sensitivity to oxidative stress and phenolic compound profiles [20]—oxidative stress sensitive Barke and oxidative stress resistant Bojos. To measure stomatal density, we used a novel automated approach—a convolution neural network (CNN). The CNN was trained to recognize and count stomata on barley epidermal imprints. Here we also describe the process of training a CNN to count stomata on our dataset of micrographs. To better understand the biochemical and physiological background of stomatal regulation under changing light and [CO<sub>2</sub>] conditions we measured gas exchange parameters as well as the accumulation of sugars and ABA by biochemical assays.

Barley, as an economically important crop around the world, is increasingly exposed to conditions of limited water availability. Understanding of stomatal regulation under future CO<sub>2</sub> conditions is thus vital to understanding and improving water use in barley. We hypothesized that low [CO<sub>2</sub>] and high light would increase stomatal density and WUE. We further hypothesized that the two barley varieties differing in their sensitivity to oxidative stress would show differences in their responsiveness to environmental driver in terms of stomatal density and conductance. Finally, we hypothesized that levels of hexose and ABA would provide insight into the regulation of stomatal conductance and contribute to our understanding of how stomata function as a key trait in plant response to environmental conditions. We provide a summary of how barley stomata are affected by light and [CO<sub>2</sub>] conditions and examine how pentoses, hexoses, disaccharides and ABA drive physiological changes in stomatal conductance.

## 2. Results

### 2.1. Changes in Stomatal Density

Stomatal densities varied significantly ( $p < 0.001$ ) according to light treatment, [CO<sub>2</sub>] treatment, and barley genotype (Table 1). Low light (LL) conditions were set at 400  $\mu\text{mol m}^{-2}\text{s}^{-1}$  photosynthetically active radiation (PAR) with 0.75  $\text{W m}^{-2}$  UV-A maxima and high light (HL) conditions were set at 1500  $\mu\text{mol m}^{-2}\text{s}^{-1}$  PAR with 4  $\text{W m}^{-2}$  UV-A maxima. Low [CO<sub>2</sub>] (LC) conditions were set at 200 ppm, ambient [CO<sub>2</sub>] (AC) at 400 ppm, and elevated [CO<sub>2</sub>] (EC) at 700 ppm. For more details, see Material and Methods (Section 4.1). Stomatal density was measured on both the leaf abaxial and adaxial sides, however, no significant difference was found between sides in any treatments and so results show the average of stomata counted on both sides. Barley leaves grown in HL had significantly ( $p < 0.001$ ) higher stomatal density than those grown in LL conditions (Table 2). Among the three [CO<sub>2</sub>] treatments, plants grown in LC had significantly ( $p < 0.001$ ) higher stomatal densities than plants grown in either AC or EC, while there was not a significant difference between AC and EC leaves (Table 2).

**Table 1.** Results of a three-way ANOVA test showing interaction between experimental factors. Statistical significance is denoted by bold font. Significance was established at  $p \leq 0.05$ . Abbreviations are defined as  $E_{max}$  (maximum transpiration rate),  $A_{max}$  (maximum photosynthesis rate),  $G_{Smax}$  (maximum stomatal conductance),  $WUE_{max}$  (maximum water use efficiency), and ABA (abscisic acid).

Treatment	Stomatal Density	$E_{max}$	$A_{max}$	$G_{Smax}$	$WUE_{max}$	Pentoses	Hexoses	Disaccharides	ABA
Genotype (G)	<0.001	<0.001	<0.001	0.002	<0.001	0.005	0.003	0.054	0.002
CO <sub>2</sub>	<0.001	0.046	<0.001	<0.001	<0.001	0.268	<0.001	0.007	<0.001
Light (L)	<0.001	<0.001	<0.001	<0.001	0.013	<0.001	<0.001	<0.001	<0.001
G × CO <sub>2</sub>	0.068	0.869	0.073	0.018	<0.001	0.550	0.060	0.474	0.272
G × L	0.084	0.004	0.472	0.010	0.253	0.041	0.004	0.715	<0.001
CO <sub>2</sub> × L	0.119	0.059	<0.001	<0.001	0.171	<0.001	<0.001	0.037	0.017
G × CO <sub>2</sub> × L	0.273	0.464	0.166	0.120	0.802	0.576	0.091	0.980	0.021

**Table 2.** Average stomatal density  $\text{mm}^{-2}$  for two barley genotypes, Barke and Bojos, in various experimental groups  $\pm$  standard deviation. LC = low  $[\text{CO}_2]$ , AC = ambient  $[\text{CO}_2]$ , EC = elevated  $[\text{CO}_2]$ ; HL = high light, LL = low light.

Stomata Density (Pores $\text{mm}^{-2}$ )					
All Genotypes		Barke		Bojos	
Average	$35 \pm 7$	Average	$37 \pm 8$	Average	$33 \pm 7$
HL	$37 \pm 8$	HL	$40 \pm 8$	HL	$35 \pm 7$
LL	$33 \pm 7$	LL	$35 \pm 7$	LL	$32 \pm 6$
LC	$37 \pm 8$	LC	$40 \pm 8$	LC	$35 \pm 6$
AC	$34 \pm 7$	AC	$35 \pm 7$	AC	$33 \pm 7$
EC	$35 \pm 7$	EC	$37 \pm 7$	EC	$33 \pm 6$

Between the two barley genotypes, Barke plants had significantly ( $p < 0.001$ ) higher stomatal densities than Bojos (Tables 1 and 2). Both Barke and Bojos had significantly higher stomatal densities in high light conditions, however, this effect was more pronounced in Barke ( $p < 0.001$ ) than it was for Bojos ( $p = 0.004$ ) (Figure 1). The average HL density for Bojos was the same as the average LL density for Barke—35 per  $\text{mm}^2$  (Table 2).  $[\text{CO}_2]$  significantly influenced stomatal density for Barke ( $p < 0.001$ ) but not for Bojos ( $p = 0.088$ ) (Figure 1).

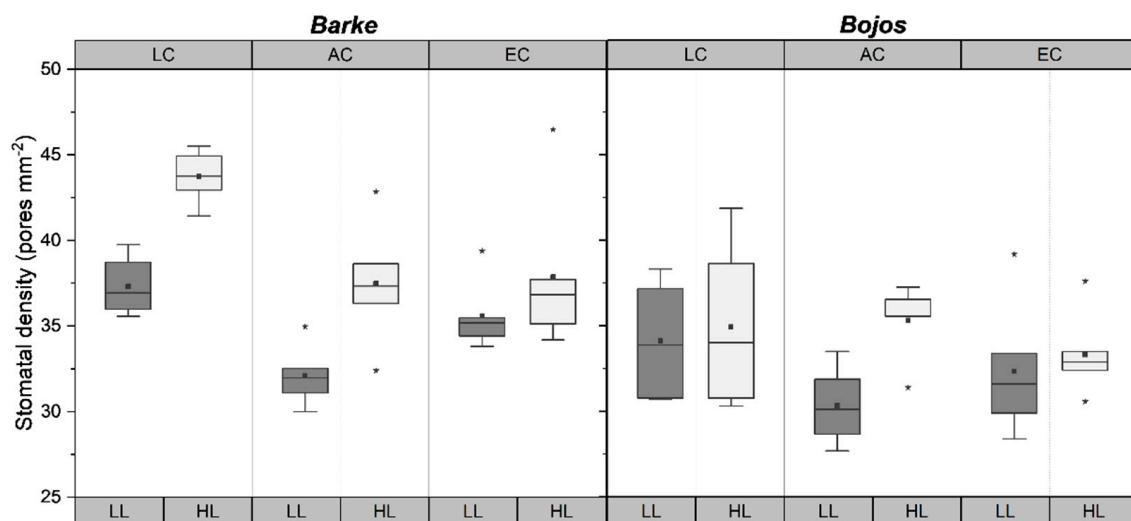


**Figure 1.** Boxplots showing differences in stomatal density  $\text{mm}^{-2}$  for barley genotypes, Barke (left) and Bojos (right). LC = low  $[\text{CO}_2]$ , AC = ambient  $[\text{CO}_2]$ , EC = elevated  $[\text{CO}_2]$ ; LL = low light (dark grey boxes), HL = high light (light grey boxes). Medians (central line), means (black squares), 25 and 75 percentiles (boxes), 1.5 interquartile range (error bars) and outliers (stars) are presented ( $n = 20$ ).

## 2.2. Stomatal Function

Light,  $[\text{CO}_2]$ , and barley genotype all significantly ( $p \leq 0.05$ ) influenced transpiration ( $E_{\text{max}}$ ), photosynthesis ( $A_{\text{max}}$ ), stomatal conductance ( $G_{S\text{max}}$ ), and  $\text{WUE}_{\text{max}}$ , when measured at saturating light intensity (Table 1). HL plants had significantly ( $p < 0.001$ ) higher levels of  $E_{\text{max}}$ ,  $A_{\text{max}}$ , and  $G_{S\text{max}}$ , and higher  $\text{WUE}_{\text{max}}$  ( $p = 0.013$ ) (Figure 2). LC plants had higher  $E_{\text{max}}$  and  $G_{S\text{max}}$  and lower  $A_{\text{max}}$  compared to AC and EC plants (Figure 2). In all cases, the highest rate of  $G_{S\text{max}}$  occurred for LC/HL plants, considerably higher than any other treatment combination (Figure 2). HL  $G_{S\text{max}}$  values were higher than under LL in all cases and decreased with increasing  $[\text{CO}_2]$ . The differences between LL and HL  $G_{S\text{max}}$  also decreased with increasing  $[\text{CO}_2]$  (Figure 2).  $\text{WUE}_{\text{max}}$  was significantly ( $p < 0.001$ ) different between all three  $[\text{CO}_2]$  treatments, with LC plants exhibiting the lowest  $\text{WUE}_{\text{max}}$  and EC plants exhibiting the highest  $\text{WUE}_{\text{max}}$  (Figure 2).

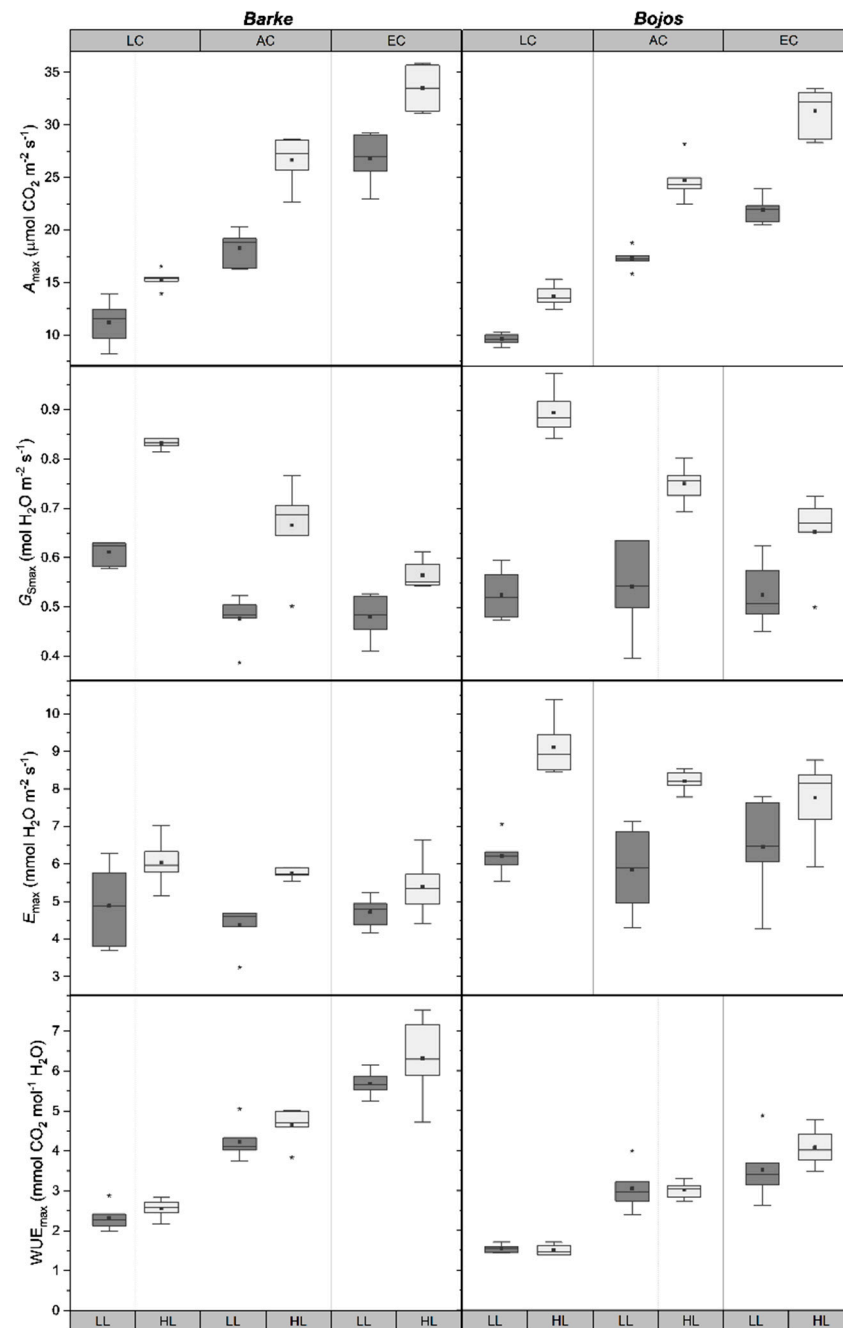


**Figure 2.** Boxplots showing differences gas exchange parameters for barley genotypes Barke (left) and Bojos (right). LC = low [CO<sub>2</sub>], AC = ambient [CO<sub>2</sub>], EC = elevated [CO<sub>2</sub>]; LL = low light (dark grey boxes), HL = high light (light grey boxes). Medians (central line), means (black squares), 25 and 75 percentiles (boxes), 1.5 interquartile range (error bars) and outliers (stars) are presented ( $n = 6$ ).

Differences between the stomatal behavior of the two barley genotypes were apparent. Bojos plants had significantly higher ( $p < 0.002$ ) rates of  $G_{Smax}$  and  $E_{max}$ , and a lower  $WUE_{max}$  than Barke plants (Table 1, Figure 2). Not only did Barke show reduced transpiration compared to Bojos, but  $E_{max}$  levels under LL for Bojos exceeded HL levels in Barke, and Bojos showed greater changes in  $E_{max}$  between light treatments compared to Barke (Figure 2).  $WUE_{max}$  was significantly ( $p < 0.001$ ) higher in Barke (Table 1), and the increase in  $WUE_{max}$  between each [CO<sub>2</sub>] treatment was greater between Barke plants compared to Bojos (Figure 2).

### 2.3. Sugar Metabolites

Accumulation of sugars—pentoses, hexoses, and disaccharides—were all found to be significantly ( $p < 0.001$ ) influenced by light conditions (Table 1). All HL plants had a greater accumulation of all sugars compared to LL plants, except for hexoses in LC, which did not show a difference between HL and LL (Figure 3). Genotype significantly influenced pentose ( $p = 0.005$ ) and hexose ( $p = 0.003$ ) levels, with Barke having higher levels of accumulation of both, and a greater increase at HL compared to Bojos (Figure 3). Hexose levels peaked for AC-HL and EC-HL plants for both genotypes (Figure 3).  $[CO_2]$  significantly influenced hexose ( $p < 0.001$ ) and disaccharides ( $p = 0.007$ ) (Table 1). Disaccharides show an increasing trend alongside increasing  $[CO_2]$  in HL but were relatively stable across  $[CO_2]$  treatments in LL (Figure 3). Pentose was significantly influenced by a combination of genotype and light ( $p = 0.041$ ) and  $[CO_2]$  and light ( $p < 0.001$ ): In both Barke and Bojos, levels of pentoses showed a slightly increasing trend with increasing  $[CO_2]$  under HL, but a decreasing trend with increasing  $[CO_2]$  under LL. The increase of pentoses under HL was more prominent for Barke, while the low light decrease was more prominent for Bojos (Figure 3).

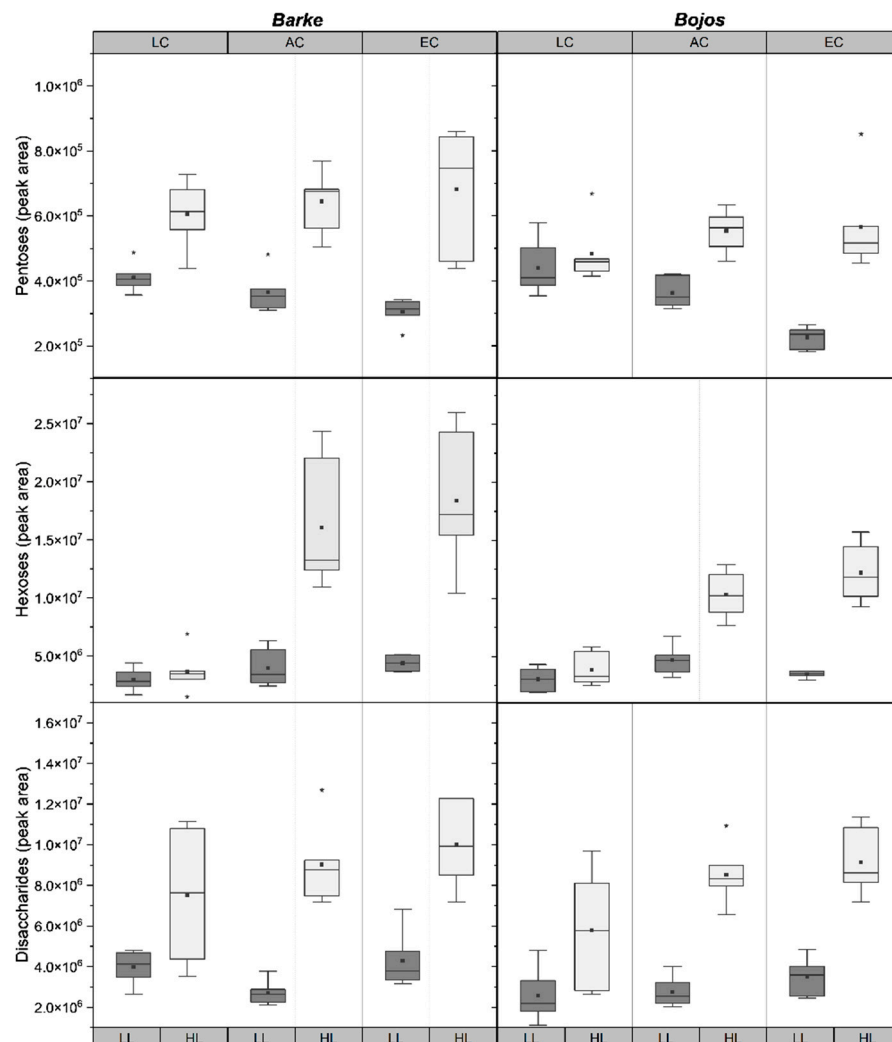


**Figure 3.** Boxplots showing differences in peak area sugars measured in barley genotypes, Barke (left) and Bojos (right). LC = low  $[CO_2]$ , AC = ambient  $[CO_2]$ , EC = elevated  $[CO_2]$ ; LL = low light (dark grey boxes), HL = high light (light grey boxes). Medians (central line), means (black squares), 25 and 75 percentiles (boxes), 1.5 interquartile range (error bars) and outliers (stars) are presented ( $n = 6$ ).

#### 2.4. Abscisic Acid

Peak area of ABA was influenced by almost all tested environmental factors and was the only measured parameter to show significant differences driven by the interactions of genotype, [CO<sub>2</sub>], and light in combination (Table 1). Generally, ABA decreased in EC and HL. LC-LL plants had the highest ABA levels, while EC-HL plants had the lowest ABA levels (Figure 4). Barke plants showed higher variability between HL and LL, as well as higher variability among [CO<sub>2</sub>] treatments compared to Bojos genotype (Figure 4).

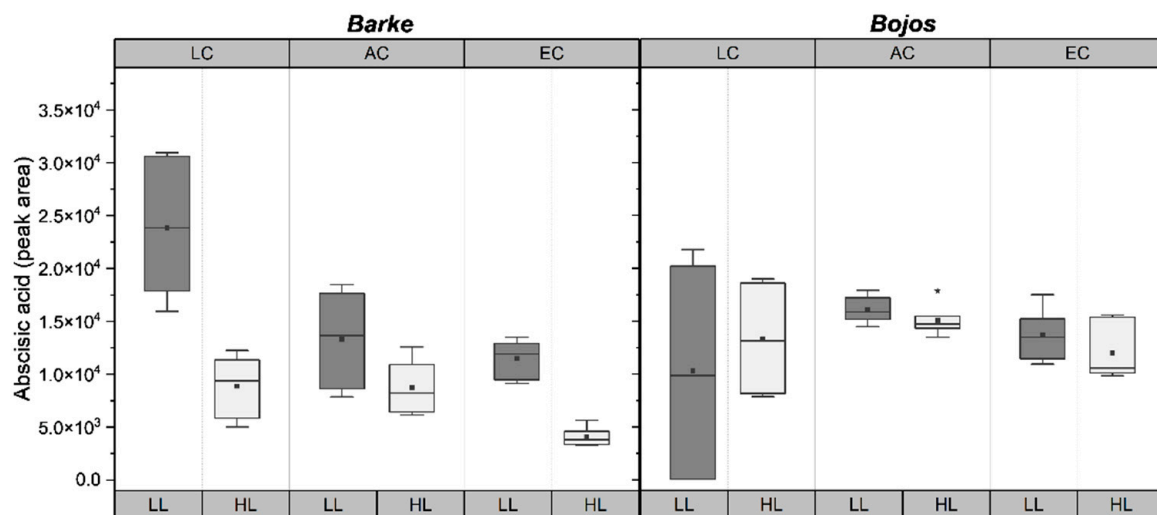


**Figure 4.** Boxplots showing differences in peak area abscisic acid measured in barley genotypes, Barke (left) and Bojos (right). LC = low [CO<sub>2</sub>], AC = ambient [CO<sub>2</sub>], EC = elevated [CO<sub>2</sub>]; LL = low light (dark grey boxes), HL = high light (light grey boxes). Medians (central line), means (black squares), 25 and 75 percentiles (boxes), 1.5 interquartile range (error bars), and outliers (stars) are presented ( $n = 6$ ).

#### 2.5. Redundancy Analysis

Associations between environmental drivers (light intensity, [CO<sub>2</sub>]), genotype (Barke, Bojos) and anatomical, physiological, and biochemical parameters related to stomatal function were tested using redundancy analysis (RDA). The explained cumulative variation by components 1 and 2 was 83.23%, pseudo-F = 34.2,  $p = 0.002$ . [CO<sub>2</sub>] was most positively correlated with WUE and  $A_{max}$  (Figure 5). Accumulation of sugars, especially disaccharides and pentoses, positively associated more closely with light, although hexoses were nearly split between the influence of light and the influence of [CO<sub>2</sub>] (Figure 5).  $G_{Smax}$  and stomatal density correlated positively, but stomatal density did not explain the full extent of  $G_{Smax}$ , which was additionally negatively related to ABA (Figure 5). The interactive effect of [CO<sub>2</sub>] and light was most pronounced positively on  $A_{max}$  and accumulation of hexoses, and negatively on accumulation of ABA. This resulted in negative associations between ABA and  $A_{max}$ , and between ABA and hexoses. Pentose levels and  $E_{max}$  also correlated (Figure 5).  $WUE_{max}$ ,  $A_{max}$ , and the effect of [CO<sub>2</sub>] were more associated with Barke than Bojos, while ABA and  $G_{Smax}$  levels were more associated with the Bojos genotype, however, the effect of barley genotype was rather small (Figure 5).

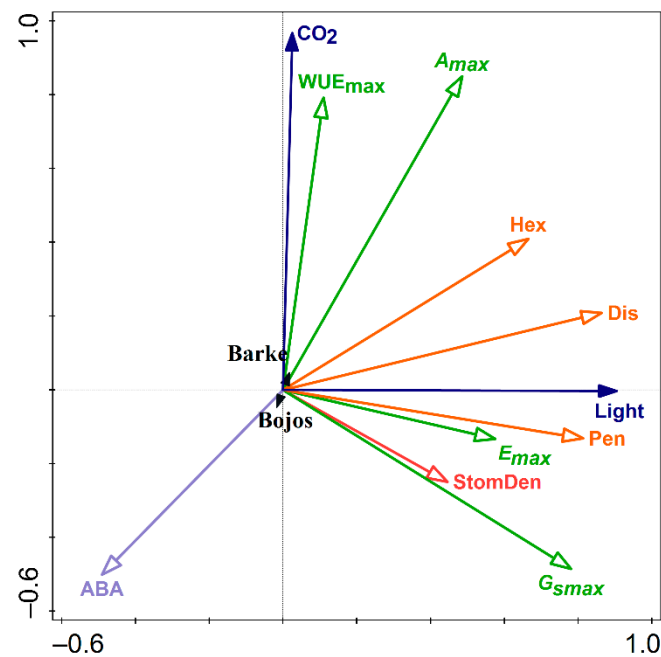


**Figure 5.** Biplot diagram representing the results of redundancy analysis (RDA) on the effects of light intensity (Light), CO<sub>2</sub> concentration (CO<sub>2</sub>), and genotype (Barke and Bojos) on stomatal density (StomDen), accumulation of pentose (Pen), disaccharides (Dis), hexose (Hex), and abscisic acid (ABA), and parameters of stomatal function: Photosynthesis ( $A_{max}$ ), Transpiration ( $E_{max}$ ), stomatal conductance ( $G_{Smax}$ ), and water use efficiency ( $WUE_{max}$ ).

### 3. Discussion

Considerable attention has been given to stomata as a target for improving the resilience of crops to reduced water availability in the face of ongoing climate change. Changes in stomatal density have implications for crop productivity. For instance, manipulation of the EPF (epidermal patterning factor) family of signaling peptides to reduce stomatal density in barley may improve drought tolerance [21,22]. However, a reduction in stomatal density may lead to more residual transpiration and potential decreases in tolerance to stress factors, such as salinity [23]. Changes in stomatal density affect WUE [24] and this trait can be used to improve WUE through genetic manipulation [25]. Thus, stomatal density plays a role in determining plant productivity, especially in the context of environmental stress, particularly drought.

Manual counting of stomatal cells can be a tedious and time-consuming task, especially when large datasets are involved. The idea of using computer algorithms to count stomata has received some attention in recent years. Recently a CNN was developed to recognize stomata across species and was made publicly available [26]. However, we found that a CNN created specifically for our data set worked faster and more reliably. Moreover, our case-tailored CNN could be trained to ignore human-generated defects in the images, such as air bubbles captured on slides. By using a CNN trained on our dataset, we were able to achieve results comparable to human counting and maintain the ability to reuse and even retrain our CNN to fit future research questions (Figure 6).

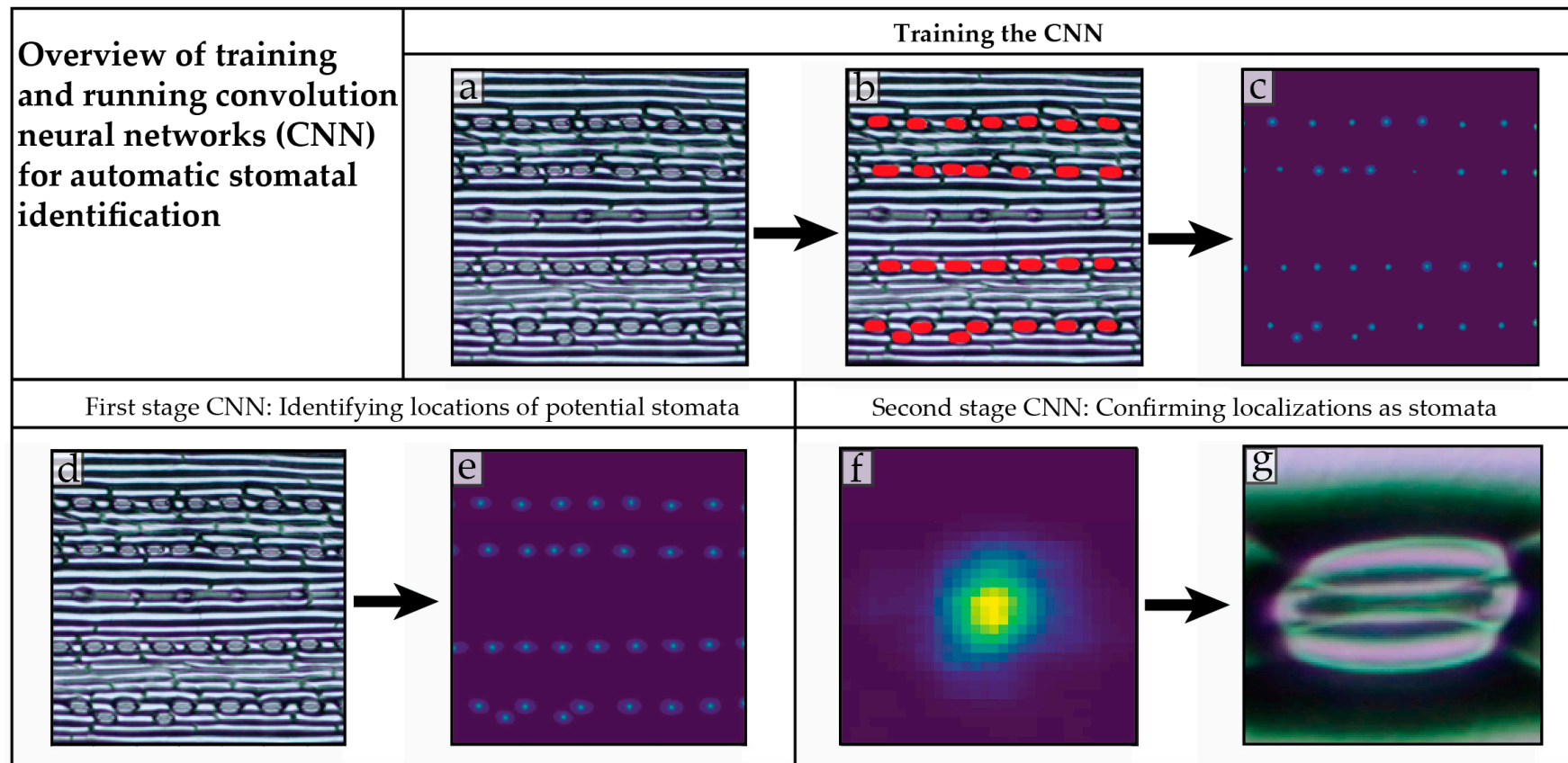


**Figure 6.** Basic outline of how the convolution neural network (CNN) was trained, and how it functioned in two stages to determine stomatal density. To train the CNN, first unmarked micrographs (a) were manually labelled, highlighting stomata in red (b) to indicate to the CNN what feature to search for. The output of the training was a label image generated by the CNN (c). The label image consisted of Gaussian peaks centered on stomata which enabled the network to extract relevant 2D features for the following two stages. Once the CNN was trained, the first stage CNN scanned an unmarked epidermal micrograph (d) for possible stomatal complexes and output a heatmap of potential locations (e). The second stage CNN was centered on windows around each heatmap reaction point from the previous CNN (f) and determined if the visual object is a stomatal complex or not (g).

Although the effects of elevated  $[\text{CO}_2]$  and light intensity on stomatal density and stomatal conductance have been previously described separately [7,27], the interactive effects of  $[\text{CO}_2]$  and light on stomata regulation are not yet sufficiently understood. Research on *Arabidopsis* suggests that the light and  $\text{CO}_2$  signaling pathways for stomatal opening are linked [28]. To our knowledge, there are only two existing studies of how the stomatal density of barley specifically is affected by light conditions [29,30], and no data on how stomatal density is affected by  $[\text{CO}_2]$  in barley varieties not specifically genetically modified for stomatal density [21]. In this study, we aimed to improve understanding of the interwoven relationships between stomatal density, stomatal conductance, sugar metabolism, and ABA in relation to changing  $[\text{CO}_2]$  and light intensity and the possible impacts on WUE. Additional graphs representing the effect of light and  $[\text{CO}_2]$  on barley for all measured parameters independent of genotype can be found in the supplementary material (Figure S1).

High light intensity is known to increase stomatal density [31,32]. The molecular background for the increase in stomatal density under HL conditions has been identified as signaling peptide known as STOMAGEN or EPFL9, which encodes an epidermal patterning factor that positively influences stomatal density and index on both sides of the leaf [33,34]. A previous study on the effect of light on stomatal density in barley showed no significant difference between leaves grown in LL versus HL environments [30], however that study used significantly lower levels of light intensity even for HL environment ( $200 \mu\text{mol m}^{-2}\text{s}^{-1}$ ), which is half of the intensity of our LL conditions. Our high light treatment conditions coincided with the average light saturation point for barley ( $1500 \mu\text{mol m}^{-2}\text{s}^{-1}$ ) [35] and shows a strong positive effect on stomatal density (Table 1, Figure 1). This suggests that light can increase the stomatal density at high intensities, however, perhaps stomatal density will not be decreased by progressively dimmer light below a certain point.

While specific data regarding the effect of  $[\text{CO}_2]$  on stomata in barley are missing, there are several studies on the effect of altered  $[\text{CO}_2]$  on stomata in wheat, *Triticum aestivum* [8,36,37]. A study on the influence of  $[\text{CO}_2]$  in wheat found that stomatal density decreased significantly with increasing  $[\text{CO}_2]$  [38]. Studies on *Arabidopsis* have identified the HIC (high carbon dioxide) gene, which encodes an enzyme involved in the negative regulation of stomatal development in elevated  $[\text{CO}_2]$  [39]. Our results show that barley had a higher stomatal density at LC, but differences between AC and EC were not pronounced (Figure 1). This discrepancy may be because the study on wheat [38] used a  $[\text{CO}_2]$  range between 400 and 1200 ppm, so perhaps the difference between 400 and 700 ppm in this study was not great enough to elicit a strong significant response in terms of stomatal density. However, in the context of climate change, 700 ppm is a potential natural atmospheric  $[\text{CO}_2]$  for the end of the 21st century [40], while values above that are unlikely to be encountered by crop plants. Furthermore, an older study on wheat also did not find significant differences between stomatal density at ambient (370 ppm) vs. elevated (550 ppm), indicating that EC increase in stomatal density occurs only at sufficiently higher atmospheric  $[\text{CO}_2]$  (i.e., above 700 ppm). Investigation of the low  $[\text{CO}_2]$  response was included in this study to address past ecophysiological function. The 200-ppm value used for LC plants is representative of atmospheric  $\text{CO}_2$  levels experienced by plants during the last glacial period [41,42]. The influence of both low and elevated  $[\text{CO}_2]$  was more pronounced for Barke than for Bojos (Figure 1), which is not surprising as barley displays great genetic diversity and a recent report on wheat showed significant genetic variation in terms of stomatal response [43].

Past studies have generally found a positive relationship between stomatal density and  $G_{Smax}$  [23,24,44]. *Arabidopsis* mutants with reduced stomatal densities have lower  $G_{Smax}$  and increase WUE by up to 20% [25]. Our results did show higher stomatal densities (Figure 1) corresponded with higher  $G_{Smax}$  (Figure 2) between individual treatments. RDA analysis shows that stomatal density and  $G_{Smax}$  did positively correlate, however that stomatal density did not fully explain the full extent of the measured  $G_{Smax}$  (Figure 5).



Our results also showed that the genotype with a greater stomatal density, Barke, had a greater  $WUE_{max}$  than the genotype with a lower stomatal density, Bojos (Figure 2). This indicates the possibility of compensating mechanisms, such as more sensitive stomatal aperture regulation, as being a greater driver of  $WUE_{max}$  than stomatal density among barley genotypes. In fact, the RDA graph suggests a slight correlation of  $G_{Smax}$  with ABA (Figure 5). The compensation of altered stomatal density by regulating stomatal aperture was previously described in *Arabidopsis* stomatal mutants and the mechanism appeared to be light-dependent [45]. Other studies on crop grass species have noted a decoupling of stomatal density with  $G_{Smax}$ . For instance, one study on wheat cultivars found significant differences between stomatal densities, as well as  $A_{max}$ ,  $E_{max}$ , and  $WUE_{max}$ , despite no significant differences in  $G_{Smax}$  levels [46]. In another study, overexpression of the maize gene SHORTROOT1 (*ZmSHR1*) in rice led to increased stomatal density, but no corresponding change  $G_{Smax}$  [47]. Previous studies also indicate interactions between light intensity and  $[CO_2]$  play a role in  $G_{Smax}$  regulation. Studies on *Fagus sylvatica* showed the stomata of EC plants remained closed at light intensity up to  $500 \mu mol m^{-2} s^{-1}$ , suggesting that plants grown in EC may require a higher activation energy to trigger stomatal opening [48]. Low intensity light may lack sufficient energy to activate the biochemical processes for stomatal opening when  $[CO_2]$  is high. Our results show a positive effect of  $[CO_2]$  on  $WUE_{max}$ , which is typical of stomatal closure under EC conditions (Figure 5).

Differences in accumulation of metabolites may account for the differences in stomatal behavior between genotypes [49,50]. The energy required to drive stomatal regulation exceeds the synthetic capacity of guard cells, meaning mesophyll cell support guard cell by providing metabolites and ATP [51,52]. Hexoses enter the guard cells and induce stomatal closure via a hexokinase mediated mechanism mediated by ABA [16]. Barke did show higher hexose levels—although mainly for AC-HL and EC-HL (Figure 3). Hexoses were negatively correlated with ABA in the RDA graph (Figure 5). Moreover, the genotypes Barke and Bojos were previously characterized in our recent work on the accumulation of phenolic compounds in barley [20]. We found that Barke, considered an oxidative stress sensitive genotype, accumulated more hydroxybenzoic acids, while Bojos, an oxidative stress resistant genotype, accumulated more hydroxycinnamic acids. For both species, soluble phenolics were not identified in the epidermis, except in stomatal guard cells. The accumulation of phenolic compounds in guard cells but not pavement cells has also been documented for *Arabidopsis*, where their presence in the guard cells was hypothesized to play a role in ABA signaling and stomatal aperture due to their antioxidative properties [53]. ABA acts in stomata regulation with the help of reactive oxygen species (ROS). ROS (hydrogen peroxide,  $H_2O_2$ ; superoxide,  $O_2^-$ ; hydroxyl radical,  $OH^-$ ; and singlet oxygen,  $^1O_2$ ) are known to cause oxidative damage to lipid membranes, proteins, and DNA, but  $H_2O_2$  in particular plays an integral role as secondary messengers in signal transduction pathways [54]. ABA triggers the production of  $H_2O_2$  by activating respiratory burst oxidase homolog enzymes on the plasma membrane [55]. This ROS burst triggers calcium channels to increase cytosolic  $Ca^{2+}$  and activate anion efflux channels resulting in stomatal closure [56,57]. For a recent review of ABA effects in crop grasses, see Gietler et al. [58]. Our results show lower levels of ABA (except for treatment at LC-LL) (Figure 4) as well as lower transpiration and higher  $WUE_{max}$  (Figure 2) for Barke, the genotype known to accumulate fewer hydroxycinnamic acids and be more sensitive to oxidative stress. The structure of hydroxycinnamic acids makes them more efficient at scavenging ROS [59]. The comparative lack of hydroxycinnamic acids in Barke may make ABA-induced ROS signaling more efficient, thus requiring lower ABA levels to trigger stomatal closure. In fact, studies on *Arabidopsis* indicated that mutants lacking phenolic compounds in their guard cells were more sensitive to ABA-induced ROS signaling. Phenolic compounds in guard cells may be scavenging ROS to a high enough degree that they modulate ABA-signaling and stomatal aperture [53]. Although no studies have thus far been conducted on barley, a study on *Commelina communis* found that p-coumaric, caffeic, chlorogenic, salicylic, and sinapic acids inhibited stomatal opening, while ferulic acid stimulated stomatal opening [60].

Another study on *Lactuca sativa* showed a commensurate increase in  $G_{Smax}$  alongside blue-light induced accumulation of phenolic acids and flavonoids [61]. There is still a paucity of research exploring the relationship between ABA-dependent stomatal signaling and phenolic compounds, however it remains an intriguing question for future investigation.

Physiological studies have demonstrated convergent and antagonistic effect of ABA and sugars on stomatal response [62]. As sucrose accumulates in the apoplast, water moves out of guard cells osmotically, creating an inverse relationship between photosynthetic rate and transpiration [63,64]. Water soluble carbohydrates, such as sucrose, glucose, and fructose, serve as indicators of assimilate accumulation. Metabolism of sucrose into hexoses provides substrate for glycolysis and biosynthesis of other essential molecules, such as starch, cellulose, and fructan [65]. ABA influences overall plant metabolism by inducing the conversion of sucrose into hexose by cell wall invertase (CWIN) which is taken into the cytoplasm and enhances sink strength [65]. Levels of hexoses are sensed by nucleus-located hexokinase (HXK) which phosphorylates glucose, plays a role in sugar sensing, and regulates gene expression [65,66]. Our results show that sugar accumulation was higher in all HL plants (Figure 3), while ABA levels were lower in HL plants (Figure 4). Studies on rice (*Oryza sativa*) show that sugar starvation increases concentrations of ABA and ROS, inducing programmed cell death and early senescence [67]. In tomato plants overexpressing HXK, ABA concentrations spiked and induced early senescence [68]. Increased ABA levels promote  $H_2O_2$  production which, in turn, acts as a signal to reduce stomatal aperture [52]. This corresponds with our RDA, indicating a negative relationship between hexoses and ABA, and a slight influence of ABA on  $G_{Smax}$  (Figure 5).

## 4. Materials and Methods

### 4.1. Plant Material

Barley plants (*Hordeum vulgare* L.) of either Barke (sensitive to oxidative stress [69,70]), or Bojos (relatively resistant to oxidative stress [71]) varieties were grown in growth chambers (FS-SI-3400, Photon System Instruments, Drásov, CZ). Cultivation occurred over four weeks under three different  $[CO_2]$  treatments: low  $[CO_2]$ —200 ppm (LC), ambient  $[CO_2]$ —400 ppm (AC), and elevated  $[CO_2]$ —700 ppm (EC) and two light regimes: low light (LL) with photosynthetically active radiation (PAR) and UV-A maxima of  $400 \mu mol m^{-2} s^{-1}$  and  $0.75 W m^{-2}$ , respectively and high light (HL) with PAR and UV-A maxima  $1500 \mu mol m^{-2} s^{-1}$  and  $4 W m^{-2}$ , respectively. The light intensity, temperature, and air humidity changed gradually to simulate natural rhythms with 15 h:9 h, light:dark. Air temperature and relative air humidity varied between 15–25 °C and 90–60%, respectively.

After 4 weeks, the third leaf from the top was sampled. Stomatal imprints were made using clear nail varnish on the middle of a fresh leaf. The nail varnish was applied to the leaf in a thin layer, and then peeled off when sufficiently dry and taped to a microscope slide. These stomatal imprints were made on both the abaxial and adaxial sides of the leaves. Stomatal imprints were photographed at 10× magnification using an Olympus BX40 light microscope equipped with Canon EOS100D camera.

### 4.2. Training a Convolution Neural Network to Recognize Stomata

To streamline the process of counting stomata, a convolution neural network (CNN) was trained to recognize and count stomata. A CNN is a type of neural network particularly efficient at recognizing two-dimensional patterns and extracting searchable features from pixel images [72]. Our stomata counting program was written in the Python programming language. The TensorFlow framework and Keras [73] library was used to develop the CNN, and a human-in-the-loop approach helped to quickly extend the training set and maximize performance. The complete model combines two CNNs working in distinct processing phases. The first CNN takes a micrograph of barley leaf epidermis and outputs a heatmap of predicted stomatal locations. The second CNN takes cropped windows of

the predicted stomatal locations and classifies the window as either containing a stomatal complex, or not.

In the initial training phase, representative micrographs of barley epidermal imprints were labelled: Labelled images were generated by using source microscopy image and highlighting the cells with red color (#FF0000) using the brush tool in a graphics editor and leaving the rest of the epidermis unmarked. The input images were originally sized at  $3456 \times 5184$ , but due to hardware limitations, were cut into 6 tile-pairs for processing.

The red-colored areas corresponding to stomata locations in the training images were extracted as a binary matrix the size of the image: 0 for pixels that do not contain stomata and 1 for pixels that do. The labelled stomatal areas were replaced by gaussian peaks centered on the stomatal complex (a two-dimensional gaussian function). This removed the discontinuity of the label function on the edge of the cell, making it continuous, and making detection of the stomatal complex easier. This generated 1396 training image pairs and 156 testing/validation images (12 tiles for each original image, pairs consist of one original micrograph tile and one label-image tile. Of the total training image dataset, 90% of labeled image-pairs were allocated to training and 10% were used for testing.

The first CNN consisted of six convolutional layers interspersed with normalization layers (Batch normalization [74] and Dropout [75]), and two Max Pooling layers that reduced the size of the image by a factor of four. The first two convolution layers utilized ReLu activation [76], and the next four utilized sigmoid activation. To extract cell centers, images are blurred using a gaussian blur and thresholded. Afterwards, an algorithm extracted the cell complex centers.

The second stage CNN was a classifier with a binary output. Output from the first stage became input for the second stage. The training data was extracted from the training images processed by the first stage model. Input of the second stage CNN was a  $32 \times 32$ -pixel window centered on predicted cell locations from the first stage CNN heatmap output. Output of the second CNN was a single number from 0 to 1, representing the estimated probability of the window containing a stomata cell in the center. The second model is composed of 2 convolution layers with a ReLu activation function and batch normalization, and 2 fully connected layers with sigmoid activation function. See Figure 6 for a basic overview, and Supplementary Material (Figures S2 and S3) for the full model of both stages.

To ensure unbiased sampling, stereological principles were incorporated after the CNN was applied—specifically, an unbiased counting frame. The idea behind a counting frame is that, if the whole leaf blade was sampled by counting frames lying next to each other but not overlapping, each object (in this case, stomatal complex) would have the same probability to be sampled, i.e., would only be counted once, even if appearing in two counting frames [77]. This is achieved by having 2 borders (usually top and right sides) as inclusionary, meaning that stomata appearing partially on these borders are counted. Conversely, stomata appearing on the exclusionary borders (bottom and left sides) are not counted. Exclusionary borders then continue behind the borders of counting frame—left side continuing to the top and right side continuing to the bottom (see Figure S4 for visualization). All stomata that are fully inside the borders are counted [77–79]. To achieve this effect, boundaries were defined in terms of pixels from the edge of the image. Stomatal complex centers detected lying on the boundary lines were counted according to whether they fell on an inclusionary or exclusionary boundary. Stomatal frequency can be measured in terms of stomatal density (SD): the number of stomata per unit leaf area, or as stomatal index, SI: the number of stomata relative to the total number of epidermal cells [80]. We use stomatal density rather than stomatal index because the epidermal cells of grass are significantly longer than stomata and extend past the borders of our counting frame.

To test the efficacy of the CNN in correctly identifying and counting stomata, four identification scenarios had to be considered: (1) True positive ( $N_{TP}$ ), correct labeling of a stomata, (2) False positive ( $N_{FP}$ ), labeling a non-stomata as a stomata, (3) True negative ( $N_{TN}$ ), non-labelling of a non-stomata, and (4) False negative ( $N_{FN}$ ), non-labeling of a stomata. From these parameters, it was possible to assess the accuracy, precision, and

recall of the CNN. Precision ( $P$ ) was defined as:  $P = \frac{N_{TP}}{N_{TP} + N_{FP}}$ . Recall ( $R$ ) was defined as:  $R = \frac{N_{TP}}{N_{TP} + N_{FN}}$ . Accuracy ( $Ac$ ) was defined as:  $Ac = \frac{N_{TP} + N_{FN}}{N_{TP} + N_{FP} + N_{TN} + N_{FN}}$ .

The first stage CNN generated 1332 true positives, 25 false positives, and 55 false negatives, resulting a precision of 98.1% and a recall of 96% after 68 epochs. (An epoch is running all the training images through the algorithm once).

The dataset for the second stage CNN model (generated from the training set of the first model) consisted of 24,033 potential cell-location windows: 8881 of the potential cell windows contained stomata and 15,152 of the potential cell windows were merely artifacts (i.e., small bubbles, thorn cells, or imprint damages) which created a detection response (hotspot) in the heatmap. The accuracy score was 98.5%.

#### 4.3. Gas Exchange Measurements

Leaf level gas exchange measurements were performed on intact leaves of light adapted plants between 10:00–15:00 CET. Light saturated ( $1200 \mu\text{mol photons m}^{-2}\text{s}^{-1}$ )  $\text{CO}_2$  assimilation rate ( $A_{max}$ ), stomatal conductance ( $G_{Smax}$ ), transpiration rate ( $E_{max}$ ) were measured using open path gas exchange system Li-6800 (LiCOR, LI-COR Biosciences, Lincoln, NE, USA) at growth  $[\text{CO}_2]$  (200, 400, and 700 ppm for LC, AC, and EC respectively), relative air humidity of 60%, and air temperature of 25 °C. Water use efficiency (WUE) was then calculated as the ratio between  $A_{max}$  and  $E_{max}$  at saturating light intensity.

#### 4.4. Identification of Sugar Metabolites and Phytohormones

Approximately 0.3 g of leaves for metabolite analyses were sampled between 10:00 and 15:00 CET directly after gas exchange measurement, immediately placed into liquid nitrogen, and then stored at 80 °C until the time of processing. Levels of barley metabolites were measured in terms of peak area using liquid chromatography coupled with mass spectrometry according to the protocol in Večerová et al., 2019 [81]. The samples were homogenized and extracted in a methanol:chloroform:H<sub>2</sub>O solution (1:2:2). An aliquot of the upper (polar) phase was used to identify pentoses, hexoses, and disaccharides. An UltiMate 3000 high performance liquid chromatograph (HPLC) coupled with an LTQ Orbitrap XL high-resolution mass spectrometer (HRMS) (Thermo Fisher Scientific, Waltham, MA, USA) was used. A Hypersil GOLD column (150 × 2.1 mm, 3 mm; Thermo Fisher Scientific) tempered at 30 °C was used for separation. The flow rate of the mobile phase (acetonitrile and water with 0.1% acetic acid) was 0.3 mL min<sup>-1</sup>. The HRMS was equipped with a HESI II heated electrospray ionization source (Thermo Fisher Scientific, Waltham, MA, USA) and was operated at the full scan resolution of 60,000. Full scan spectra were acquired over the mass range of 50–1000 and 65–1000  $m/z$  in positive and negative polarity mode, respectively. The target compounds were assigned based on our own mass library created using standards measured in MS and MS<sup>n</sup> modes.

#### 4.5. Statistical Analysis

Three-way analysis of variance (ANOVA) was used for the analysis of barley genotype,  $[\text{CO}_2]$  and light intensity effects and their interactions. Fisher's LSD ANOVA post-hoc test ( $p = 0.05$ ) was used to analyze significant differences between means. Statistical analyses were conducted using the software STATISTICA 12 (StatSoft, Tulsa, CA, USA). The bar graphs representing means with standard errors were developed with the software SigmaPlot 11.0 (Systat Software, San Jose, CA, USA). The redundancy analysis (RDA) and biplot of RDA results were set up in the software CANOCO 5 (Microcomputer Power, Ithaca, NY, USA) [82].

## 5. Conclusions

In conclusion, although barley varieties show significant differences in stomatal density, and especially high differences in responsiveness of stomatal density to  $[\text{CO}_2]$  and light conditions, levels of  $G_{Smax}$  are similar for both genotypes, indicating some mechanisms for compensating the stomatal density differences to optimize the stomatal conductance to a

given environment. Such mechanisms could be associated with differences in accumulation of hexoses and responsiveness of ABA to [CO<sub>2</sub>] and light conditions, which were generally higher in genotype Barke. Such differences could also explain the generally higher WUE in genotype Barke, although higher WUE is often reported as trait linked with lower stomatal density (which was the case for the Bojos genotype). Barke is a genotype known to be more sensitive to oxidative stress and have fewer hydroxycinnamic acids, which may make it more sensitive to the ROS initiated ABA signaling cascades. Crop plants, such as barley, are already facing harsher and more erratic environmental conditions due to ongoing climate change. Investigations on genotype-specific responses of important grain crops expand the availability of useful information which can lead to selection or modification of more resistant crop genotypes.

**Supplementary Materials:** The following are available online at <https://www.mdpi.com/article/10.3390/plants10112533/s1>, Figure S1: Graphs of all measured parameters showing the effects of light and [CO<sub>2</sub>] without genotype, Figure S2: Model of first stage CNN, Figure S3: Model of second stage CNN, Figure S4: Stereological counting frame, Table S1: Full data set.

**Author Contributions:** Conceptualization, J.A. with L.H., M.F., K.K., Z.L. and O.U.; software, M.F.; formal analysis, L.H., M.F., K.K.; investigation, L.H., M.O., K.K.; resources, J.A., K.K.; data curation, L.H., K.K.; writing—original draft preparation, L.H.; writing—review and editing, K.K., Z.L., O.U., J.A.; visualization, L.H., K.K.; project administration, J.A.; funding acquisition, J.A., K.K. All authors have read and agreed to the published version of the manuscript.

**Funding:** This research was funded by the Czech Science Foundation (GAČR 18-23702S). K.K., M.O. and O.U. were also supported by the project “SustES—Adaptation strategies for sustainable ecosystem services and food security under adverse environmental conditions” (CZ.02.1.01/0.0/0.0/16\_019/0000797).

**Data Availability Statement:** Data is contained within the article or supplementary materials.

**Acknowledgments:** We thank Miroslav Barták for his technical help in microscopy and image processing, as well as the preparation of graphics for this paper. We also thank students from the team of prof. Jana Albrechtová for their help in preparing the epidermal peels for analysis.

**Conflicts of Interest:** The authors declare no conflict of interest.

## References

1. Gray, A.; Liu, L.; Facette, M. Flanking Support: How Subsidiary Cells Contribute to Stomatal Form and Function. *Front. Plant Sci.* **2020**, *11*, 881. [\[CrossRef\]](#)
2. Keenan, T.F.; Hollinger, D.Y.; Bohrer, G.; Dragoni, D.; Munger, J.W. Increase in forest water-use efficiency as atmospheric carbon dioxide concentrations rise. *Nature* **2013**, *499*, 324–327. [\[CrossRef\]](#)
3. Lake, J.; Quick, W.; Beerling, D.; Woodward, F. Plant development—Signals from mature to new leaves. *Nature* **2001**, *411*, 154. [\[CrossRef\]](#)
4. De Boer, H.J.; Price, C.A.; Wagner-Cremer, F.; Dekker, S.; Franks, P.; Veneklaas, E.J. Optimal allocation of leaf epidermal area for gas exchange. *New Phytol.* **2016**, *210*, 1219–1228. [\[CrossRef\]](#)
5. Vatén, A.; Bergmann, D.C. Mechanisms of stomatal development: An evolutionary view. *EvoDevo* **2012**, *3*, 11. [\[CrossRef\]](#)
6. Driesen, E.; Ende, W.V.D.; De Proft, M.; Saeys, W. Influence of Environmental Factors Light, CO<sub>2</sub>, Temperature, and Relative Humidity on Stomatal Opening and Development: A Review. *Agronomy* **2020**, *10*, 1975. [\[CrossRef\]](#)
7. Woodward, F.I.; Kelly, C.K. The influence of CO<sub>2</sub> concentration on stomatal density. *New Phytol.* **1995**, *131*, 311–327. [\[CrossRef\]](#)
8. Estiarte, M.; Peñuelas, J.; Kimball, B.; Idso, S.; Lamorte, R.; Pinter, J.P.; Wall, G.; Garcia, R. Elevated CO<sub>2</sub> effects on stomatal density of wheat and sour orange trees. *J. Exp. Bot.* **1994**, *45*, 1665–1668. [\[CrossRef\]](#)
9. Woodward, F.I. Stomatal numbers are sensitive to increases in CO<sub>2</sub> from pre-industrial levels. *Nature* **1987**, *327*, 617–618. [\[CrossRef\]](#)
10. McElwain, J.C.; Chaloner, W.G. Stomatal Density and Index of Fossil Plants Track Atmospheric Carbon Dioxide in the Palaeozoic. *Ann. Bot.* **1995**, *76*, 389–395. [\[CrossRef\]](#)
11. Zhang, L.; Niu, H.; Wang, S.; Zhu, X.; Luo, C.; Li, Y.; Zhao, X. Gene or environment? Species-specific control of stomatal density and length. *Ecol. Evol.* **2012**, *2*, 1065–1070. [\[CrossRef\]](#) [\[PubMed\]](#)
12. Blatt, M.R. Cellular Signaling and Volume Control in Stomatal Movements in Plants. *Annu. Rev. Cell Dev. Biol.* **2000**, *16*, 221–241. [\[CrossRef\]](#)
13. Shimada, T.; Sugano, S.S.; Hara-Nishimura, I. Positive and negative peptide signals control stomatal density. *Cell. Mol. Life Sci.* **2011**, *68*, 2081–2088. [\[CrossRef\]](#)

14. Chater, C.; Peng, K.; Movahedi, M.; Dunn, J.A.; Walker, H.J.; Liang, Y.-K.; McLachlan, D.H.; Casson, S.; Isner, J.-C.; Wilson, I.; et al. Elevated CO<sub>2</sub> -Induced Responses in Stomata Require ABA and ABA Signaling. *Curr. Biol.* **2015**, *25*, 2709–2716. [[CrossRef](#)]
15. Long, S.P.; Ainsworth, E.A.; Rogers, A.; Ort, D.R. Rising Atmospheric Carbon Dioxide: Plants FACE the Future. *Annu. Rev. Plant Biol.* **2004**, *55*, 591–628. [[CrossRef](#)] [[PubMed](#)]
16. Kelly, G.; Moshelion, M.; David-Schwartz, R.; Halperin, O.; Wallach, R.; Attia, Z.; Belausov, E.; Granot, D. Hexokinase mediates stomatal closure. *Plant J.* **2013**, *75*, 977–988. [[CrossRef](#)]
17. Talbott, L.D.; Zeiger, E. Central Roles for Potassium and Sucrose in Guard-Cell Osmoregulation. *Plant Physiol.* **1996**, *111*, 1051–1057. [[CrossRef](#)]
18. Gotow, K.; Taylor, S.; Zeiger, E. Photosynthetic Carbon Fixation in Guard Cell Protoplasts of *Vicia faba* L.: Evidence from Radiolabel Experiments. *Plant Physiol.* **1988**, *86*, 700–705. [[CrossRef](#)] [[PubMed](#)]
19. Taiz, L.; Zeiger, E.; Møller, I.M.; Murphy, A. *Plant Physiology and Development*; Sinauer Associates Incorporated: Sunderland, MA, USA, 2015.
20. Hunt, L.; Klem, K.; Lhotáková, Z.; Vosolsobě, S.; Oravec, M.; Urban, O.; Špunda, V.; Albrechtová, J. Light and CO<sub>2</sub> Modulate the Accumulation and Localization of Phenolic Compounds in Barley Leaves. *Antioxidants* **2021**, *10*, 385. [[CrossRef](#)]
21. Hughes, J.; Hepworth, C.; Dutton, C.; Dunn, J.A.; Hunt, L.; Stephens, J.; Waugh, R.; Cameron, D.D.; Gray, J.E. Reducing Stomatal Density in Barley Improves Drought Tolerance without Impacting on Yield. *Plant Physiol.* **2017**, *174*, 776–787. [[CrossRef](#)]
22. Dunn, J.; Hunt, L.; Afsharinafar, M.; Al Meselmani, M.; Mitchell, A.; Howells, R.; Wallington, E.; Fleming, A.J.; Gray, J.E. Reduced stomatal density in bread wheat leads to increased water-use efficiency. *J. Exp. Bot.* **2019**, *70*, 4737–4748. [[CrossRef](#)]
23. Hasanuzzaman, M.; Shabala, L.; Zhou, M.; Brodribb, T.J.; Corkrey, R.; Shabala, S. Factors determining stomatal and non-stomatal (residual) transpiration and their contribution towards salinity tolerance in contrasting barley genotypes. *Environ. Exp. Bot.* **2018**, *153*, 10–20. [[CrossRef](#)]
24. Bertolino, L.T.; Caine, R.; Gray, J.E. Impact of Stomatal Density and Morphology on Water-Use Efficiency in a Changing World. *Front. Plant Sci.* **2019**, *10*, 225. [[CrossRef](#)] [[PubMed](#)]
25. Franks, P.J.; Doheny-Adams, T.W.; Britton-Harper, Z.J.; Gray, J.E. Increasing water-use efficiency directly through genetic manipulation of stomatal density. *New Phytol.* **2015**, *207*, 188–195. [[CrossRef](#)] [[PubMed](#)]
26. Fetter, K.C.; Eberhardt, S.; Barclay, R.S.; Wing, S.; Keller, S.R. StomataCounter: A neural network for automatic stomata identification and counting. *New Phytol.* **2019**, *223*, 1671–1681. [[CrossRef](#)]
27. Jumrani, K.; Bhatia, V.S. Influence of different light intensities on specific leaf weight, stomatal density photosynthesis and seed yield in soybean. *Plant Physiol. Rep.* **2020**, *25*, 277–283. [[CrossRef](#)]
28. Takahashi, S.; Monda, K.; Negi, J.; Konishi, F.; Ishikawa, S.; Hashimoto-Sugimoto, M.; Goto, N.; Iba, K. Natural Variation in Stomatal Responses to Environmental Changes among *Arabidopsis thaliana* Ecotypes. *PLoS ONE* **2015**, *10*, e0117449. [[CrossRef](#)]
29. Miskin, E.; Rasmusson, D.C. Frequency and distribution of stomata in barley. *Crop Sci.* **1970**, *10*, 575–578. [[CrossRef](#)]
30. Kubinova, L. Stomata and Mesophyll Characteristics of Barley Leaf as Affected by Light: Stereological Analysis. *J. Exp. Bot.* **1991**, *42*, 995–1001. [[CrossRef](#)]
31. Wild, A.; Wolf, G. The Effect of Different Light Intensities on the Frequency and Size of Stomata, the Size of Cells, the Number, Size and Chlorophyll Content of Chloroplasts in the Mesophyll and the Guard Cells during the Ontogeny of Primary Leaves of *Sinapis alba*. *Z. Pflanzenphysiol.* **1980**, *97*, 325–342. [[CrossRef](#)]
32. Tichá, I. *Photosynthetic Characteristics during Ontogenesis of Leaves. VII: Stomata Density and Sizes*; Czechoslovak Academy of Science, Institute of Experimental Botany: Prague, Czech Republic, 1982.
33. Hronková, M.; Wiesnerová, D.; Šimková, M.; Skúpa, P.; Dewitte, W.; Vráblová, M.; Zažímalová, E.; Šantrůček, J. Light-induced STOMAGEN-mediated stomatal development in *Arabidopsis* leaves. *J. Exp. Bot.* **2015**, *66*, 4621–4630. [[CrossRef](#)] [[PubMed](#)]
34. Hepworth, C.; Caine, R.; Harrison, E.; Sloan, J.; Gray, J.E. Stomatal development: Focusing on the grasses. *Curr. Opin. Plant Biol.* **2018**, *41*, 1–7. [[CrossRef](#)]
35. Arenas-Corraliza, M.G.; Rolo, V.; López-Díaz, M.L.; Moreno, G. Wheat and barley can increase grain yield in shade through acclimation of physiological and morphological traits in Mediterranean conditions. *Sci. Rep.* **2019**, *9*, 9547. [[CrossRef](#)]
36. Yu, Q.; Zhang, Y.; Liu, Y.; Shi, P. Simulation of the Stomatal Conductance of Winter Wheat in Response to Light, Temperature and CO<sub>2</sub> Changes. *Ann. Bot.* **2004**, *93*, 435–441. [[CrossRef](#)]
37. Morison, J.I.L. Sensitivity of stomata and water use efficiency to high CO<sub>2</sub>. *Plant, Cell Environ.* **1985**, *8*, 467–474. [[CrossRef](#)]
38. Xu, M. The optimal atmospheric CO<sub>2</sub> concentration for the growth of winter wheat (*Triticum aestivum*). *J. Plant Physiol.* **2015**, *184*, 89–97. [[CrossRef](#)]
39. Gray, J.E.; Holroyd, G.H.; Van Der Lee, F.M.; Bahrami, A.R.; Sijmons, P.C.; Woodward, F.I.; Schuch, W.; Hetherington, A.M. The HIC signalling pathway links CO<sub>2</sub> perception to stomatal development. *Nature* **2000**, *408*, 713–716. [[CrossRef](#)]
40. Meehl, G.A.; Stocker, T.F.; Collins, W.D.; Friedlingstein, P.; Gaye, A.T.; Gregory, J.M.; Kitoh, A.; Knutti, R.; Murphy, J.M.; Noda, A.; et al. Global Climate Projections. In *Climate Change 2007: The Physical Science Basis. Contribution of Working Group I to the Fourth Assessment Report of the Intergovernmental Panel on Climate Change*; Cambridge University Press: Cambridge, UK; New York, NY, USA, 2007; pp. 747–845.
41. Delmas, R.J.; Ascencio, J.-M.; Legrand, M. Polar ice evidence that atmospheric CO<sub>2</sub> 20,000 yr BP was 50% of present. *Nature* **1980**, *284*, 155–157. [[CrossRef](#)]

42. Ehleringer, J.R.; Cerling, T.E. Atmospheric CO<sub>2</sub> and the ratio of intercellular to ambient CO<sub>2</sub> concentrations in plants. *Tree Physiol.* **1995**, *15*, 105–111. [[CrossRef](#)] [[PubMed](#)]
43. Faralli, M.; Cockram, J.; Ober, E.; Wall, S.; Galle, A.; Van Rie, J.; Raines, C.; Lawson, T. Genotypic, Developmental and Environmental Effects on the Rapidity of gs in Wheat: Impacts on Carbon Gain and Water-Use Efficiency. *Front. Plant Sci.* **2019**, *10*, 492. [[CrossRef](#)]
44. Franks, P.J.; Beerling, D. Maximum leaf conductance driven by CO<sub>2</sub> effects on stomatal size and density over geologic time. *Proc. Natl. Acad. Sci. USA* **2009**, *106*, 10343–10347. [[CrossRef](#)] [[PubMed](#)]
45. Büssis, D.; von Groll, U.; Fisahn, J.; Altman, T. Stomatal aperture can compensate altered stomatal density. *Funct. Plant Biol.* **2006**, *33*, 1037–1043. [[CrossRef](#)] [[PubMed](#)]
46. Liao, J.-X.; Chang, J.; Wang, G.-X. Stomatal density and gas exchange in six wheat cultivars. *Cereal Res. Commun.* **2005**, *33*, 719–726. [[CrossRef](#)]
47. Schuler, M.L.; Sedelnikova, O.V.; Walker, B.J.; Westhoff, P.; Langdale, J.A. Shortroot-Mediated Increase in Stomatal Density Has No Impact on Photosynthetic Efficiency. *Plant Physiol.* **2018**, *176*, 757–772. [[CrossRef](#)] [[PubMed](#)]
48. Urban, O.; Klem, K.; Holišova, P.; Šigut, L.; Šprtová, M.; Teslová-Navrátlová, P.; Zitová, M.; Špunda, V.; Marek, M.V.; Grace, J. Impact of elevated CO<sub>2</sub> concentration on dynamics of leaf photosynthesis in *Fagus sylvatica* is modulated by sky conditions. *Environ. Pollut.* **2014**, *185*, 271–280. [[CrossRef](#)]
49. Misra, B.B.; Acharya, B.R.; Granot, D.; Assmann, S.M.; Chen, S. The guard cell metabolome: Functions in stomatal movement and global food security. *Front. Plant Sci.* **2015**, *6*, 334. [[CrossRef](#)]
50. Gago, J.; De Menezes Daloso, D.; Figueroa, C.M.; Flexas, J.; Fernie, A.R.; Nikoloski, Z. Relationships of Leaf Net Photosynthesis, Stomatal Conductance, and Mesophyll Conductance to Primary Metabolism: A Multispecies Meta-Analysis Approach. *Plant Physiol.* **2016**, *171*, 265–279. [[CrossRef](#)]
51. Zeiger, E.; Talbott, L.D.; Frechilla, S.; Srivastava, A.; Zhu, J. The guard cell chloroplast: A perspective for the twenty-first century. *New Phytol.* **2002**, *153*, 415–424. [[CrossRef](#)]
52. Medeiros, D.B.; Barros, J.A.; Fernie, A.R.; Araújo, W.L. Eating Away at ROS to Regulate Stomatal Opening. *Trends Plant Sci.* **2020**, *25*, 220–223. [[CrossRef](#)]
53. Watkins, J.M.; Hechler, P.J.; Muday, G.K. Ethylene-induced flavonol accumulation in guard cells suppressed reactive oxygen species and moderates stomatal aperture. *Plant Physiol.* **2014**, *164*, 1707–1717. [[CrossRef](#)]
54. Mittler, R.; Vanderauwera, S.; Suzuki, N.; Miller, G.; Tognetti, V.B.; Vandepoele, K.; Gollery, M.; Shulaev, V.; Van Breusegem, F. ROS signaling: The new wave? *Trends Plant Sci.* **2011**, *16*, 300–309. [[CrossRef](#)]
55. Postiglione, A.E.; Muday, G.K. The Role of ROS Homeostasis in ABA-Induced Guard Cell Signaling. *Front. Plant Sci.* **2020**, *11*, 968. [[CrossRef](#)] [[PubMed](#)]
56. Chen, Z.-H.; Hills, A.; Lim, C.K.; Blatt, M.R. Dynamic regulation of guard cell anion channels by cytosolic free Ca<sup>2+</sup> concentration and protein phosphorylation. *Plant J.* **2010**, *61*, 816–825. [[CrossRef](#)] [[PubMed](#)]
57. Schroeder, J.; Hagiwara, S. Repetitive increases in cytosolic Ca<sup>2+</sup> of guard cells by abscisic acid activation of nonselective Ca<sup>2+</sup> permeable channels. *Proc. Natl. Acad. Sci. USA* **1990**, *87*, 9305–9309. [[CrossRef](#)] [[PubMed](#)]
58. Gietler, M.; Fidler, J.; Labudda, M.; Nykiel, M. Abscisic Acid—Enemy or Savior in the Response of Cereals to Abiotic and Biotic Stresses? *Int. J. Mol. Sci.* **2020**, *21*, 4607. [[CrossRef](#)]
59. Cuvelier, M.-E.; Richard, H.; Berset, C. Comparison of the Antioxidative Activity of Some Acid-phenols: Structure-Activity Relationship. *Biosci. Biotechnol. Biochem.* **2014**, *56*, 324–325. [[CrossRef](#)]
60. Plumbe, A.M.; Willmer, C.M. Phytoalexins, Water-stress and Stomata. iii. The effects of some phenolics, fatty acids and some other compounds on stomatal responses. *New Phytol.* **1986**, *103*, 17–22. [[CrossRef](#)]
61. Ouzounis, T.; Parjikelaei, B.R.; Frettä, X.; Rosenqvist, E.; Ottosen, C.-O. Predawn and high intensity application of supplemental blue light decreases the quantum yield of PSII and enhances the amount of phenolic acids, flavonoids, and pigments in *Lactuca sativa*. *Front. Plant Sci.* **2015**, *6*, 19. [[CrossRef](#)]
62. Finelstein, R.R.; Gibson, S.I. ABA and sugar interactions regulating development: Cross-talk or voices in a crowd? *Curr. Opin. Plant Biol.* **2002**, *5*, 26–32. [[CrossRef](#)]
63. Lu, P.; Outlaw, W.H., Jr.; Smith, B.G.; Freed, G.A. A New Mechanism for the Regulation of Stomatal Aperture Size in Intact Leaves (Accumulation of Mesophyll-Derived Sucrose in the Guard-Cell Wall of *Vicia faba*). *Plant Physiol.* **1997**, *114*, 109–118. [[CrossRef](#)]
64. Outlaw, W.H.; De Vlieghere-He, X. Transpiration Rate. An Important Factor Controlling the Sucrose Content of the Guard Cell Apoplast of Broad Bean. *Plant Physiol.* **2001**, *126*, 1716–1724. [[CrossRef](#)]
65. Ruan, Y.-L. Sucrose Metabolism: Gateway to Diverse Carbon Use and Sugar Signaling. *Annu. Rev. Plant Biol.* **2014**, *65*, 33–67. [[CrossRef](#)]
66. Granot, D. Potting plant hexokinases in their proper place. *Phytochemistry* **2008**, *69*, 2649–2654. [[CrossRef](#)]
67. Asad, M.A.U.; Wang, F.; Ye, Y.; Guan, X.; Zhou, L.; Han, Z.; Pan, G.; Cheng, F. Contribution of ABA metabolism and ROS generation to sugar starvation-induced senescence of rice leaves. *Plant Growth Regul.* **2021**, *95*, 241–257. [[CrossRef](#)]
68. Dai, N.; Schaffer, A.; Petreikov, M.; Shahak, Y.; Giller, Y.; Ratner, K.; Levine, A.; Granot, D. Overexpression of Arabidopsis Hexokinase in Tomato Plants Inhibits Growth, Reduces Photosynthesis, and Induces Rapid Senescence. *Plant Cell* **1999**, *11*, 1253. [[CrossRef](#)]

69. Wu, Y.; Tiedemann, A. Light-dependent oxidative stress determines physiological lead spot formation in barley. *Phytopathology* **2004**, *94*, 584–592. [[CrossRef](#)] [[PubMed](#)]
70. Klem, K.; Ač, A.; Holub, P.; Kováč, D.; Špunda, V.; Robson, T.M.; Urban, O. Interactive effects of PAR and UV radiation on the physiology, morphology and leaf optical properties of two barley varieties. *Environ. Exp. Bot.* **2012**, *75*, 52–64. [[CrossRef](#)]
71. Agrární Komora České Republiky. *Ústřední Kontrolní a Zkušební Ústav Zemědělský: Obilniny 2018*; Národní Odrůvový Úřad: Brno, Czech Republic, 2018.
72. Le Cun, Y.; Bottou, L.; Bengio, Y.; Haffner, P. Gradient-Based Learning Applied to Document Recognition. *Proc. IEEE* **1998**, *86*, 2278–2324. [[CrossRef](#)]
73. Chollet, F.E.A. Keras. 2015. Available online: <https://github.com/fchollet/keras> (accessed on 4 March 2019).
74. Ioffe, S.; Szegedy, C. Batch normalization: Accelerating deep network training by reducing internal covariate shift. *arXiv* **2015**, arXiv:1502.03167.
75. Srivastava, N.; Hinton, G.; Krizhevsky, A.; Sutskever, I.; Salakhutdinov, R. Dropout: A simple way to prevent neural networks from overfitting. *J. Mach. Learn. Res.* **2014**, *15*, 1929–1958.
76. Nair, V.; Hinton, G.E. Rectified linear units improve restricted boltzmann machines. In Proceedings of the 27th International Conference on Machine Learning (ICML-10), Haifa, Israel, 21–24 June 2010; pp. 807–814.
77. Gunderson, H.J.G. Notes on estimation of numerical density of arbitrary profiles: The edge effect. *J. Microsc.* **1997**, *111*, 219–223. [[CrossRef](#)]
78. Kubinova, L. Recent stereological methods for measuring leaf anatomical characteristics: Estimation of the number and sizes of stomata and mesophyll cells. *J. Exp. Bot.* **1994**, *45*, 119–127. [[CrossRef](#)]
79. Albrechtová, J.; Kubinova, L. Quantitative Analysis of the Structure of Etiolated Barley Leaf Using Stereological Methods. *J. Exp. Bot.* **1991**, *42*, 1311–1314. [[CrossRef](#)]
80. Kubínová, L.; Radichivá, B.; Lhotáková, Z.; Kubínová, Z.; Albrechtová, J. Stereology, an unbiased methodological approach to study plant anatomy and cytology: Past, present and future. *Image Anal. Stereol.* **2017**, *36*, 187–205. [[CrossRef](#)]
81. Večeřová, K.; Večeřa, Z.; Mikuška, P.; Coufalík, P.; Oravec, M.; Dočekal, B.; Novotná, K.; Veselá, B.; Pompeiano, A.; Urban, O. Temperature alters susceptibility of *Picea abies* seedlings to airborne pollutants: The case of CdO nanoparticles. *Environ. Pollut.* **2019**, *253*, 646–654. [[CrossRef](#)]
82. Smilauer, P.; Lepš, J. *Multivariate Analysis of Ecological Data Using Canoco 5*, 2nd ed.; Cambridge University Press: Cambridge, UK, 2014.





Article

# Regulation of Phenolic Compound Production by Light Varying in Spectral Quality and Total Irradiance

Radomír Pech <sup>1,†</sup>, Adriana Volná <sup>1,†</sup>, Lena Hunt <sup>2</sup> , Martin Bartas <sup>3</sup> , Jiří Červeň <sup>3</sup>, Petr Pečinka <sup>3</sup> , Vladimír Špunda <sup>1,4,\*</sup> and Jakub Nezval <sup>1,\*</sup>

<sup>1</sup> Department of Physics, Faculty of Science, University of Ostrava, 710 00 Ostrava, Czech Republic; radomir.pech@osu.cz (R.P.); adriana.volna@osu.cz (A.V.)

<sup>2</sup> Department of Experimental Plant Biology, Faculty of Science, Charles University, 128 00 Praha, Czech Republic; huntl@natur.cuni.cz

<sup>3</sup> Department of Biology and Ecology, Faculty of Science, University of Ostrava, 710 00 Ostrava, Czech Republic; martin.bartas@osu.cz (M.B.); jiri.cerven@osu.cz (J.Č.); petr.pecinka@osu.cz (P.P.)

<sup>4</sup> Global Change Research Institute, Czech Academy of Sciences, 603 00 Brno, Czech Republic

\* Correspondence: vladimir.spunda@osu.cz (V.Š.); jakub.nezval@osu.cz (J.N.)

† These authors contributed equally to this work.

**Abstract:** Photosynthetically active radiation (PAR) is an important environmental cue inducing the production of many secondary metabolites involved in plant oxidative stress avoidance and tolerance. To examine the complex role of PAR irradiance and specific spectral components on the accumulation of phenolic compounds (PheCs), we acclimated spring barley (*Hordeum vulgare*) to different spectral qualities (white, blue, green, red) at three irradiances (100, 200, 400  $\mu\text{mol m}^{-2} \text{s}^{-1}$ ). We confirmed that blue light irradiance is essential for the accumulation of PheCs in secondary barley leaves (in UV-lacking conditions), which underpins the importance of photoreceptor signals (especially cryptochrome). Increasing blue light irradiance most effectively induced the accumulation of B-dihydroxylated flavonoids, probably due to the significantly enhanced expression of the *F3'H* gene. These changes in PheC metabolism led to a steeper increase in antioxidant activity than epidermal UV-A shielding in leaf extracts containing PheCs. In addition, we examined the possible role of miRNAs in the complex regulation of gene expression related to PheC biosynthesis.

**Keywords:** antioxidants; flavonoids; HPLC; miRNA; photoprotection; secondary metabolism; spectral quality of light; spring barley (*Hordeum vulgare*); transcriptomics; UV tolerance



**Citation:** Pech, R.; Volná, A.; Hunt, L.; Bartas, M.; Červeň, J.; Pečinka, P.; Špunda, V.; Nezval, J. Regulation of Phenolic Compound Production by Light Varying in Spectral Quality and Total Irradiance. *Int. J. Mol. Sci.* **2022**, *23*, 6533. <https://doi.org/10.3390/ijms23126533>

Academic Editor: Daniela Trono

Received: 12 May 2022

Accepted: 2 June 2022

Published: 10 June 2022

**Publisher's Note:** MDPI stays neutral with regard to jurisdictional claims in published maps and institutional affiliations.



**Copyright:** © 2022 by the authors. Licensee MDPI, Basel, Switzerland. This article is an open access article distributed under the terms and conditions of the Creative Commons Attribution (CC BY) license (<https://creativecommons.org/licenses/by/4.0/>).

## 1. Introduction

Light is the source of energy which enables photosynthesis, but also serves as a source of environmental information influencing plant physiology, metabolism, and development. This information is derived from both spectral intensity and spectral quality, which vary depending on factors such as time of day/season [1,2], canopy position [3,4], and atmospheric conditions [5]. However, light can also be a stressor, as excessive photosynthetically active radiation (PAR) or ultraviolet (UV) irradiation leads to the overproduction of reactive oxygen species (ROS) and the subsequent state of oxidative stress. At appropriate levels, ROS also play an important role in plant physiology and development by regulating tip growth; modulating cell wall properties [6]; and acting as signaling molecules influencing stomatal activity [7], protective responses, plant stress acclimation, and programmed cell death [8–10]. At high levels, ROS interact with biomolecules, disrupting their structure and function via protein oxidation (particularly the proteins of Photosystem II [11,12]), changes in nucleic acid sequences [13], and lipid peroxidation, which can cause disturbances in the structural integrity of cellular and subcellular membranes [8,12,14]. Excessive ROS concentrations may thus cause many adverse effects, such as plant growth reduction, impaired development, or even the death of a whole plant.

Plants have developed many protective mechanisms to cope with adverse light conditions and excessive ROS production. While some mechanisms prevent ROS production (e.g., epidermal UV shielding, thermal dissipation of excess light energy, adjustment of leaf inner structure, chloroplasts movements, photosystem state transitions, etc.), others utilize compounds with antioxidative properties to scavenge already-produced ROS [12]. In non-stress conditions, the production of ROS is balanced by the scavenging activity of plant antioxidative systems. The plant antioxidant defense system, specifically the part responsible for eliminating ROS (ROS scavenging), consists of two functionally interconnected (coacting) components—enzymes with antioxidative function (superoxide dismutase—SOD, catalase—CAT, ascorbate peroxidase—APX, etc.) and low-molecular-weight antioxidants (LMWA), such as tocopherols, ascorbate, glutathione, carotenoids, and phenolic compounds (PheCs).

Antioxidative enzymes work in tightly linked systems. These enzymes are highly efficient (e.g., catalytic efficiency of SOD is approximately  $\text{kcat}/\text{KM } 7 \times 10^9 \text{ M}^{-1} \text{ s}^{-1}$ ), and their activity can be adjusted (for instance, the activity of SOD is driven by the concentration of  $\text{H}_2\text{O}_2$  and superoxide anion radicals [15]). In addition to antioxidative enzymes, other LMWAs may be modulated by incident light, including PheCs and the enzymes involved in their biosynthesis. PheCs play a role in plant defense against a wide range of stressors [16]. This large group of secondary metabolites includes photoprotective compounds, such as flavonoids and anthocyanins (important subclasses of PheCs), which absorb strong UV and PAR when localized in the epidermis [17] and parenchyma [18].

Flavonoid synthesis requires precursors from several metabolic pathways: phenylalanine (from the shikimic acid pathway), which is further transformed to 4-coumaroyl-CoA within the phenylpropanoid pathway (Figure 1). The first reaction belonging to the flavonoid pathway itself occurs when 4-coumaroyl-CoA further reacts with malonate (from the malonic acid pathway). Flavonoids contain two aromatic benzene nuclei linked through a 3-carbon oxygen-containing heterocycle (C6-C3-C6 structure). Due to the presence of aromatic rings in their structure, flavonoids are effective UV attenuators. The accumulation of flavonoids in epidermal layers thus plays important role in plant UV tolerance (and avoidance of ROS production during UV stress). The efficiency of their antioxidant activity strongly depends on the configuration and the total number of hydroxyl groups, e.g., it is known that flavonoids containing a dihydroxylated B-ring, including homoorientin derivatives (such as luteolin and quercetin derivatives), may exhibit a higher antioxidant capacity than corresponding monohydroxylated PheCs [19]. In addition to antioxidant activity, PheCs suppress the formation of reactive species due to metal chelation, which prevents the formation of hydroxyl radicals produced by the Fenton reaction and may affect ROS signaling as well [20,21].

Biosynthesis of PheCs is tightly linked with PAR irradiance and spectral quality; thus, manipulation of light conditions can lead to changes in the content of these metabolites and consequently altered states of photoprotection [22]. Perception of light is ensured by photoreceptors, which can trigger a complex signaling cascade leading to acclimation and adaptive responses, induced at the level of gene expression (GE) via specific transcription factors (TFs) and their complexes [23]. UV-B and UV-A radiation stimulate PheC synthesis via the UV Resistance Locus 8 [24]. High intensities of PAR also induce PheC accumulation [25], especially blue light, which is perceived via cryptochromes (CRYs) [26,27]. Although phytochromes (PHY) are active primarily in the red region of light spectra [28], it was recently found that phytochromes in their active state (Pfr form) absorb photons also in the blue region [29,30]; thus, a role of PHY in blue-light-dependent regulation of PheCs synthesis cannot be excluded. Moreover, PHY may participate in the regulation of PheC biosynthesis through PIFs (PHYTOCHROME INTERACTING FACTORS), which can interact directly with CRY (PIF4 and PIF5) [31] or cooperate with TFs [32].

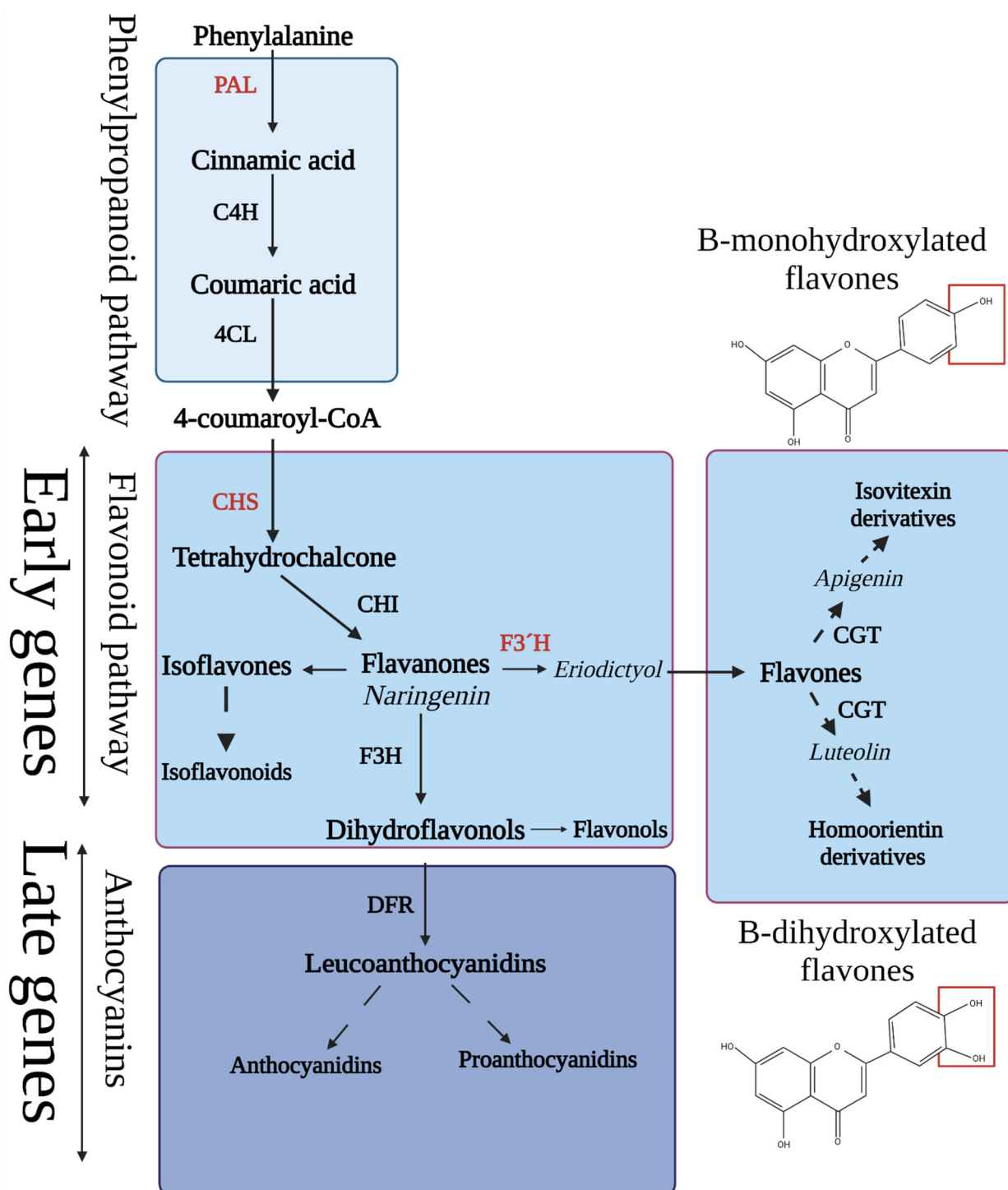


**Figure 1.** Simplified scheme of pathways responsible for phenolic compound biosynthesis with highlighted early and late gene groups encoding PheC-related enzymes. The expression of genes labeled in red was studied in this experiment. *PAL* (phenylalanine ammonia lyase; EC 4.3.1.24), *C4H* (cinnamate 4-hydroxylase; EC 1.14.13.11), *4CL* (4-coumarate CoA-ligase; EC 6.2.1.12), *CHS* (chalcone synthase; EC 2.3.1.74), *CHI* (chalcone isomerase; EC 5.5.1.6), *F3'H* (flavonoid 3'-hydroxylase; EC 1.14.14.82), *CGT* (c-glucosyltransferase; EC 2.4.1.360), *F3H* (flavanone 3-hydroxylase; EC 1.14.11.9), and *DFR* (dihydroflavonol 4-reductase; EC 1.1.1.219). Typical structures of B-monohydroxylated (apigenin) and B-dihydroxylated (luteolin) flavones (derivatives of which are present in soluble form in barley leaves) are shown and their structural difference is marked red.

All the above-mentioned photoreceptors regulate PheC production mainly through the TF HY5 (ELONGATED HYPOCOTYL 5), which was proposed as an integrator of light and temperature signals [33–35] (Figure 2), regulating the expression of approximately 3000 genes in Arabidopsis [36]. A major repressor of HY5-related photomorphogenic responses is the COP1/SPA complex (CONSTITUTIVELY PHOTOMORPHOGENIC 1, SUPPRESSOR OF PHYA-105), responsible for HY5 degradation. Light-activated photoreceptors may directly interact with COP1/SPA and prevent HY5 ubiquitination due to changes in COP1/SPA functionality [37]. Once photoreceptors prevent HY5 degradation, the whole signaling pathway leads mostly to the increased transcription of PheC-related genes, which induces PheC production. The main targets of HY5 are sequences containing G-box, but also other motifs (T/G-box, E-box, GATA-box, ACE-box, Z-box, C-box, and even hybrid C/G or C/A boxes) [36].

The TF HY5 may consequently promote the expression of genes encoding enzymes involved in the early biosynthesis of flavonoids (chalcone synthase—CHS, chalcone isomerase—CHI, flavonoid 3'-hydroxylase—F3'H) and downstream anthocyanins (late biosynthetic genes including dihydrokaempferol 4-reductase, leucoanthocyanidin oxygenase, flavonol 3-O-glucosyltransferase) (Figure 1). Additionally, the expression of regulatory genes in the large MYB family of TFs, such as MYB12, MYB111, MYBD (MYB—like protein D), MYBL2 (MYB—like protein B), and MYB75 (also known as phosphatidic acid phosphatase 1—PAP1), can be stimulated by HY5 [38–41] (Figure 2). While TFs MYB11, MYB12, and MYB111 can promote the expression of flavonoid-related genes directly, expression of anthocyanins (downstream in the biosynthetic pathway) is driven via the MBW complex consisting of three proteins—MYB75 (PAP1), bHLH (TT8), and WD40 (TTG1) [33].

Another possible mechanism involved in the regulation of PheC synthesis includes the action of microribonucleic acids (miRNAs). This level of regulation is ensured by double-stranded miRNAs, which are later degraded to single-stranded miRNAs and incorporated into the RISC complex (RNA-induced silencing complex). Once the miRNA finds a complementary messenger ribonucleic acid (mRNA), the translation may be stopped, or the mRNA strand coding for functional protein is degraded [42]. PheC-related genes are regulated by multiple miRNAs (Figure 2) from families 156, 858, 828, and others [43,44] to ensure precise modulation of GE in response to environmental factors. However, studies focused on the connecting light-signaling and miRNA-driven regulation of PheC metabolism are still limited.

Many published works studying light-driven changes of PheC metabolism in plant tissues deal with the impact of UV radiation, the spectral composition of PAR, or the total irradiance of an individual PAR region, and their combinations. However, there is a lack of experiments examining the effects of the main spectral components of PAR (B, G, R) on PheC production (including regulation mechanisms) at various irradiance levels. This type of study is important, as photoreceptor responses may differ at various irradiances. Furthermore, PheC regulation may be affected indirectly by light-induced changes in the photosynthetic process (affecting the availability of assimilates for secondary metabolism, as well as overall ROS production). Finally, the spectral composition may differently affect plant growth and development (and in turn, sink/source ratios) at various irradiances. Therefore, we decided to perform comparative analyses of PheC profiles and GE to inspect how the individual spectral regions of PAR and total irradiance affect the production of these protective compounds. We also performed a basic analysis of parameters related to plant tolerance against light-induced stress, including the determination of UV-A epidermal shielding, the total antioxidant activity (AOX) of polar LMWAs, as well as a basic assessment of antioxidant enzyme activity (based on the expression of related genes).

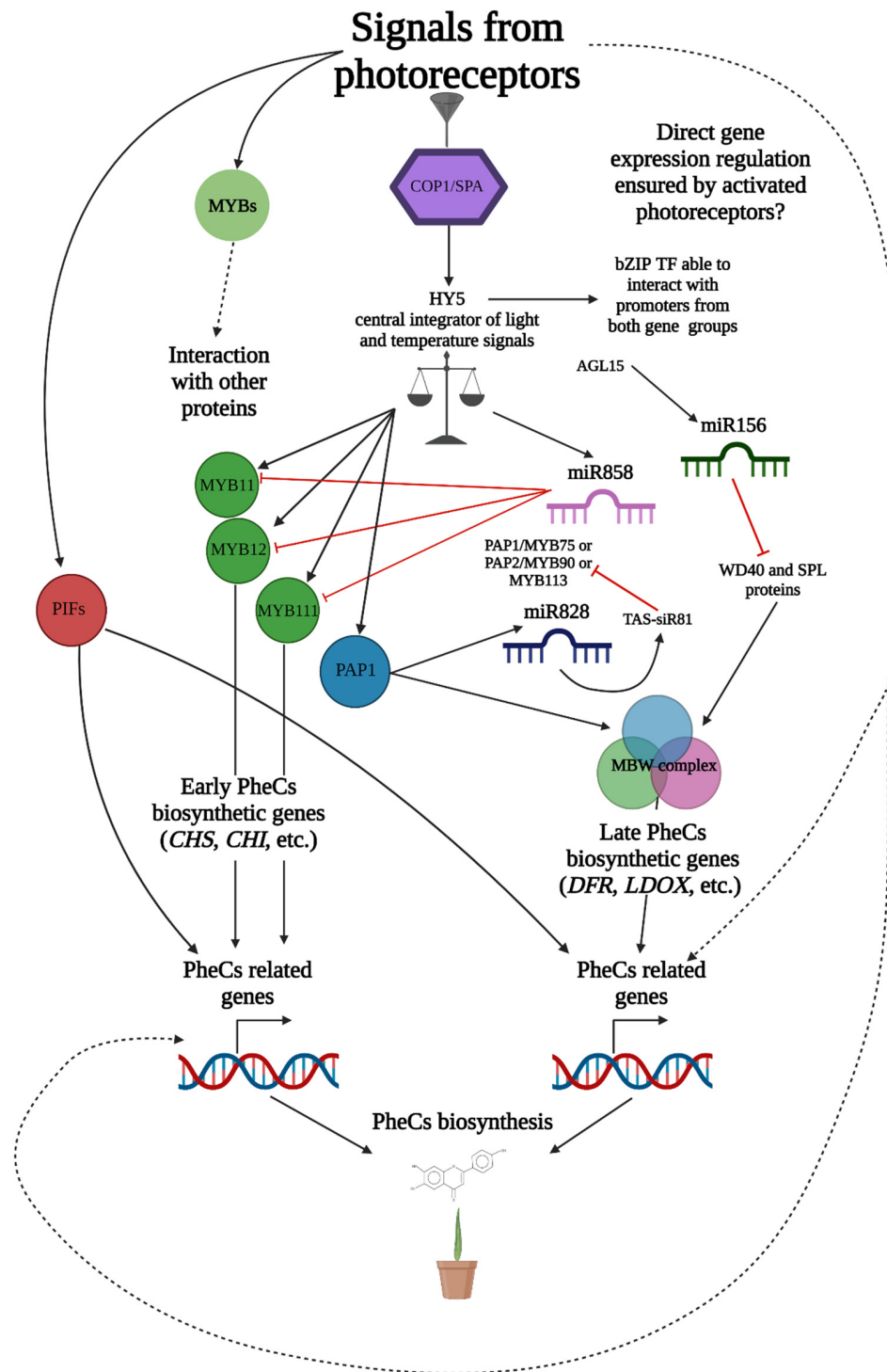


**Figure 2.** Simplified schematic representation of genes related to PheC biosynthesis and their regulation. Solid black arrows indicate known interactions, signaling, and regulatory mechanisms involved in PheC synthesis. Dashed black arrows mark other presumed regulatory pathways which are not yet confirmed. Red lines mark known downregulation or inhibitory interactions. TF (transcription factor), COP1/SPA complex (CONSTITUTIVELY PHOTOMORPHOGENIC 1, SUPPRESSOR OF PHYA-105); HY5 (ELONGATED HYPOCOTYL 5); PIFs (PHYTOCHROME INTERACTING FACTORS); miRNA (micro ribonucleic acid); MBW complex consisting of three proteins—MYB75 (PAP1), bHLH (TT8), and WD40 (TTG1); *CHS* (chalcone synthase; EC 2.3.1.74); *CHI* (chalcone isomerase, EC 5.5.1.6); *DFR* (dihydroflavonol 4-reductase; EC 1.1.1.219); and *LDOX* (leucocyanidin oxygenase; EC 1.14.11.19).

## 2. Results

### 2.1. Accumulation of Soluble PheCs Induced by Light Differing in Total Irradiance and Spectral Composition

To examine the effect of various light treatments on PheC accumulation and changes in their profile, HPLC (high performance liquid chromatography) analysis of leaf extracts was performed (Sections 4.3 and 4.4). The total content of soluble PheCs (proxied by the sum of peak areas of individual compounds detected at 314 nm) varied significantly among tested light treatments. Plants exposed to low light intensity (LI;  $100 \mu\text{mol m}^{-2} \text{s}^{-1}$ ) exhibited the lowest concentration of PheCs (Figure 3). Moreover, plants acclimated to various spectral qualities at LI conditions did not exhibit statistically significant differences in total PheC content (based on Tukey's post-hoc test multiple comparisons—TPT). Although the BL plants contained a slightly higher concentration of PheCs compared to other spectral treatments at LI, the effect of spectral quality was negligible.

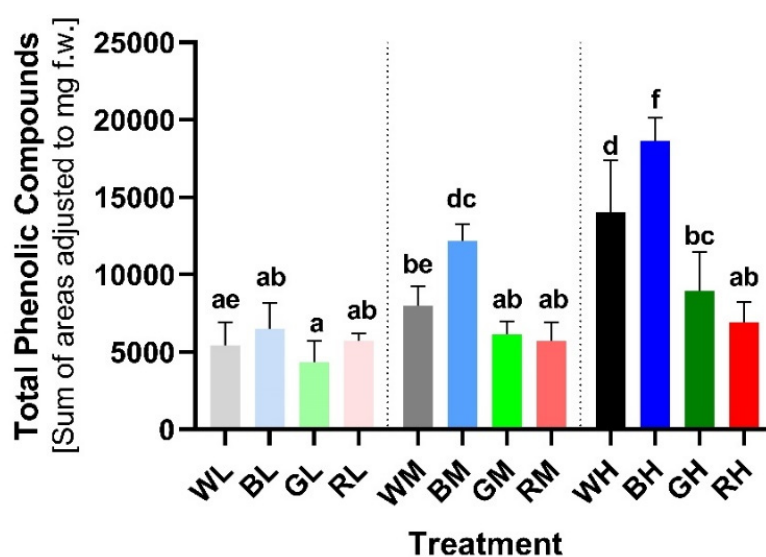


**Figure 3.** Total PheC content in secondary leaves of *Hordeum vulgare* L. cv. Bojos acclimated to light conditions varying in irradiance and spectral qualities. W (white), B (blue), R (red), G (green), L (low irradiance,  $100 \mu\text{mol m}^{-2} \text{s}^{-1}$ ), M (medium irradiance,  $200 \mu\text{mol m}^{-2} \text{s}^{-1}$ ), and H (high irradiance,  $400 \mu\text{mol m}^{-2} \text{s}^{-1}$ ),  $n = 5-6 \pm \text{SD}$ . The total content of soluble PheCs was evaluated based on HPLC-DAD data as a sum of peak areas (detected at 314 nm) and adjusted to the FW of each sample (for more details, see Section 4.4). Treatments marked above with same letters did not significantly differ based on Tukey's *post-hoc* test.

Plants exposed to medium light intensity (MI;  $200 \mu\text{mol m}^{-2} \text{s}^{-1}$ ) exhibited different levels of PheC accumulation based on spectral quality. Comparing irradiance intensity (LI vs. MI), the only significant increase in PheC content was observed for the blue spectral treatment (BM vs. BL: +87.61%, TPT  $p < 0.0001$ ). Plants grown under BM conditions exhibited the highest PheC content among plants cultivated at MI. Although plants acclimated to WM and GM treatments exhibited an increase compared to corresponding LI variants, it was not considered statistically significant (WM vs. WL: +46.26%, TPT ns; GM vs. GL: +41.34%, TPT ns). The red light MI did not cause any difference in PheC content (RM vs. RL:  $-0.82\%$ , TPT ns).

Plants acclimated to high light intensity (HI;  $400 \mu\text{mol m}^{-2} \text{s}^{-1}$ ) exhibited the highest total PheC content among all irradiance treatments (i.e., MI, LI); however, this difference was the most pronounced (and statistically significant) in conditions containing a higher proportion of blue spectral component (i.e., B, W). The highest accumulation of PheCs was observed in BH treatment (BH vs. BL: +187.66%, TPT  $p < 0.0001$ ) and subsequently WH (WH vs. WL: +157.84%, TPT  $p < 0.0001$ ). Surprisingly, a positive—yet less pronounced—effect of

green light was also observed (GH vs. GL: +106.70%, TPT  $p = 0.0018$ ). The effect of the red light was negligible regardless of the irradiance level (RH vs. RL: +20.23%, TPT ns). Based on the results of two-way ANOVA, we confirmed that both observed factors—irradiance and spectral quality—as well as their interaction had a statistically significant effect on the total soluble PheC accumulation (in all cases  $p < 0.0001$ , Supplementary Table S1).

## 2.2. Changes in the Profile of PheCs Caused by Different Light Conditions

Figure 4 shows an overview of the changes in PheC profiles induced by varying light conditions in spring barley as heatmaps, including the results of a cluster analysis. The determined PheCs were tentatively identified (Supplementary Section S1: Identification of soluble phenolic compounds) as: FQA (feruloylquinic acid), LUT (lutonarin), SAP (saponarin), ISD (isoscoparin derivative), HSG (homoorientin-7-O-[6-sinp]-glc), HFG (homoorientin-7-O-[6-fer]-glc), ISG (isovitexin-7-O-[6-sinp]-glc), and IFG (isovitexin-7-O-[6-fer]-glc). The first heatmap (Figure 4A) depicts the similarities of whole profiles among light treatments, which are divided into two main clusters. The first cluster (C1) is formed by plants grown in the spectral conditions containing higher irradiances of blue light, such as BM, WH, and BH variants, which exhibited the highest relative concentration of PheCs in the data set (Figure 4A). These plants are characterized by the presence of FQA and a higher content of homoorientin derivatives, such as LUT, HSG, and HFG, compared to other treatments.

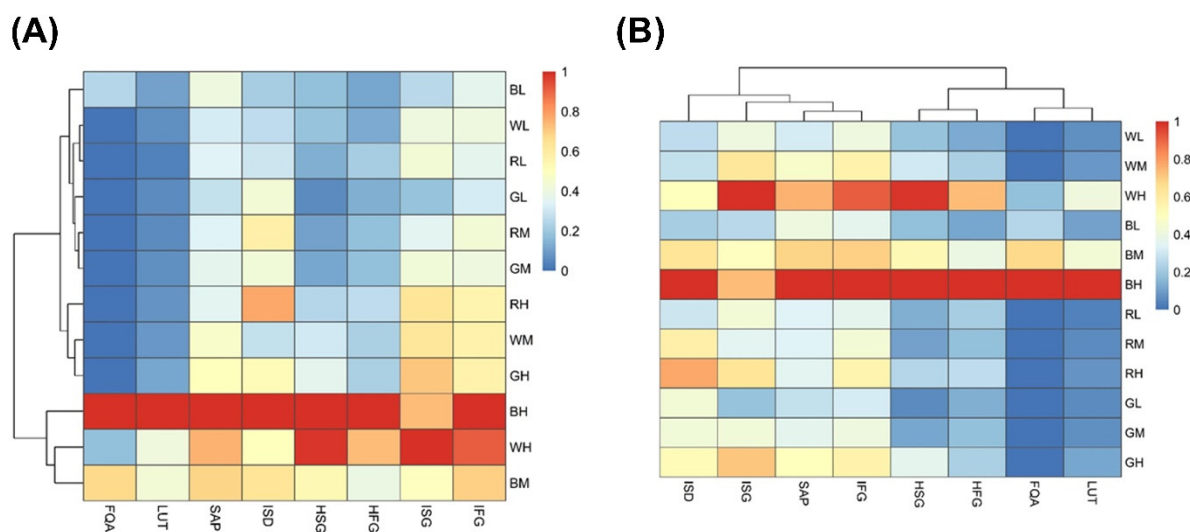


**Figure 4.** Heatmaps depicting similarities of PheC profiles among light treatments (A) as well as similarities in response of individual PheCs to the same light conditions (B). The relative contents of each PheC per treatment were averaged ( $n = 5-6$ ) and subsequently normalized to the maximum value among all light treatments. Cluster analysis was performed on normalized PheC quantitative data (distance function: Euclidean distance; linkage function: Average linkage). Specifications of light treatments: W (white), B (blue), R (red), G (green), L (low irradiance  $100 \mu\text{mol m}^{-2} \text{s}^{-1}$ ), M (medium irradiance  $200 \mu\text{mol m}^{-2} \text{s}^{-1}$ ), and H (high irradiance  $400 \mu\text{mol m}^{-2} \text{s}^{-1}$ ). Compounds of interest: FQA (feruloylquinic acid), LUT (lutonarin), SAP (saponarin), ISD (isoscoparin derivative), HSG (homoorientin-7-O-[6-sinp]-glc), HFG (homoorientin-7-O-[6-fer]-glc), ISG (isovitexin-7-O-[6-sinp]-glc), and IFG (isovitexin-7-O-[6-fer]-glc).

The second cluster (C2) is separated into two subclusters (SC). SC1 is formed by the LI and MI treatments (BL, WL, RL, GL, RM, and GM), in which low PheC content was typical regardless of spectral quality (Figure 4A). The samples belonging to BL treatment form an independent group within SC1 due to the slightly higher relative content of PheCs (mainly SAP and FQA). SC2, which consists of RH-, WM-, and GH-treated samples, exhibits low

content of homoorientin derivatives (LUT, HSG, HFG) and FQA similarly to SC1, but (contrary to SC1) high content of SAP, ISG, and IFG.

In the second heatmap (Figure 4B), individual PheCs are divided into two main clusters based on similarities in their responses to light intensity and spectral quality. The C1 consists of ISD, SAP (in the range of 63.72 to 77.87% of the total PheC content, Supplementary Table S4), and other isovitexin derivatives (ISG, ISF). The content of these compounds was less affected by the spectral quality of light and rather depends on the irradiance. Thus, LI treatments contained generally low concentrations of isovitexin derivatives compared to plants exposed to MI and HI conditions. By contrast, C2 is formed by FQA, LUT, HSG, and HFG, which exhibited a strong dependence on the proportion of blue spectral component. This is especially true of LUT and FQA, which did not occur in leaves of plants acclimated to the light without a blue component or occurred only in trace amounts.

These results are illustrated in more detail in Figure 5, which contains a comparison of isovitexin derivatives (Figure 5A,C,E) with the corresponding B-dihydroxylated counterparts (Figure 5B,D,F). The relative content of isovitexin derivatives in plants was many times higher than homoorientin derivatives under all tested conditions. However, the strong positive effect of blue light on the accumulation of homoorientin derivatives led to a decrease in the isovitexin/homoorientin ratio in plants acclimated to HI (Figure 5H; WH, BH vs. WL, BL). A similar trend is visible also for plants acclimated to green and red light, although the decrease in the ratio of isovitexin/homoorientin derivatives with increasing irradiance is statistically insignificant. It is noteworthy that detectable accumulation of FQA was observed only in plants acclimated to blue light and under WH conditions.

### 2.3. Light Regulation of Epidermal UV-A Shielding

In vivo measurement of epidermal UV-A shielding determined by Dualex (Section 4.2) reflects the PheC content in the epidermal layer of secondary leaves (flavonoids/flavonols mainly). The lowest epidermal UV-A shielding was observed in plants acclimated to LI conditions (Figure 6). The shielding index among LI plants of various spectral qualities was comparable and statistically (also biologically) insignificant. Thus, the spectral quality at the low level of irradiance had a negligible effect on the UV-A transmittance of the epidermis.

On the contrary, the effect of spectral quality on the epidermal UV-A shielding was significant in plants acclimated to MI. Whereas BM and WM caused accumulation of UV-A shielding epidermal phenolics (BM vs. BL: +48.89%, TPT  $p < 0.0001$ ; WM vs. WL: +40.01%, TPT  $p = 0.0027$ ), no significant difference was observed under GM and RM conditions (GM vs. GL: +15.56%, TPT ns; RM vs. RL: +14.95%, TPT ns). Within MI, the blue-light-acclimated plants exhibited slightly higher epidermal UV-A shielding compared to other spectral treatments (mainly to GM).

Among all variants, the most effective induction of epidermal shielding occurred in plants cultivated in HI blue light (BH vs. BL: +114.93%, TPT  $p < 0.0001$ ). The WH treatment exhibited a statistically significant positive effect on epidermal PheC induction (WH vs. WL: +81.32%, TPT  $p < 0.0001$ ), although the effect was slightly weaker than observed for blue light. HI green light slightly increased shielding (GH vs. GL: +30.76%, TPT  $p = 0.004$ ), followed by red light (RH vs. RL: +26.49%, TPT ns), the significant effect of which was not statistically confirmed. BH and WH plants revealed significantly higher epidermal UV-A shielding compared to GH- and RH-acclimated ones—such a pronounced effect of spectral quality was not observed under MI or LI.

The efficiency of UV-A epidermal shielding of secondary leaves showed a linear correlation with total soluble PheC content (measured on the same leaf segments as used for HPLC analysis, Supplementary Figure S4), and thus showed similar trends as the response to light treatments. Two-way ANOVA confirmed that spectral quality ( $p < 0.0001$ ), irradiance ( $p < 0.0001$ ), and their interaction ( $p < 0.0001$ ) all had a statistically significant effect on epidermal UV-A transmittance (Supplementary Table S1).



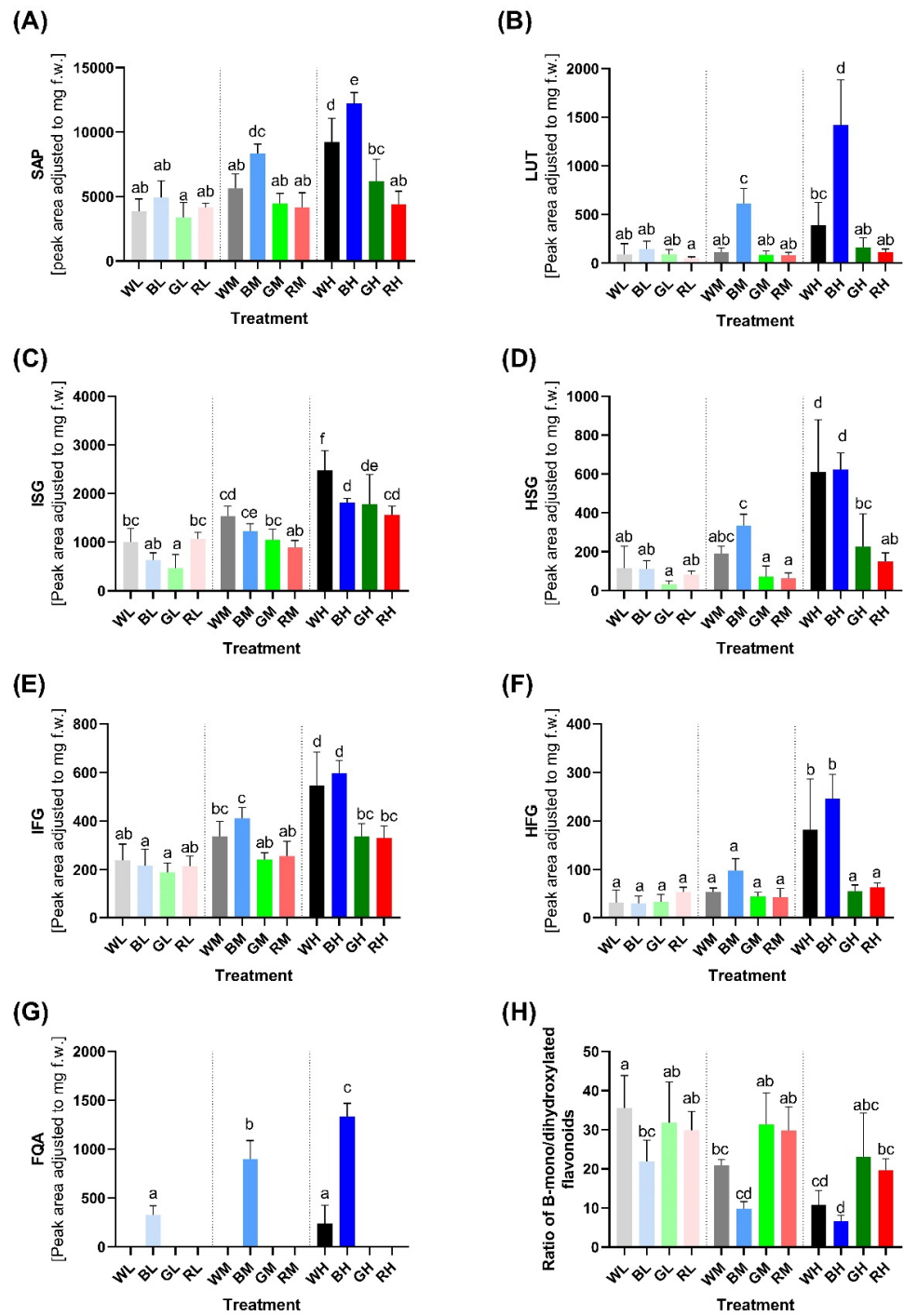


**Figure 5.** The relative content of individual PheCs in the secondary leaves of *Hordeum vulgare* L. cv. Bojos acclimated to the light conditions varying in irradiance and spectral qualities. Specifications of light treatment: W (white), B (blue), R (red), G (green), L (low irradiance,  $100 \mu\text{mol m}^{-2} \text{s}^{-1}$ ), M (medium irradiance,  $200 \mu\text{mol m}^{-2} \text{s}^{-1}$ ), and H (high irradiance,  $400 \mu\text{mol m}^{-2} \text{s}^{-1}$ );  $n = 5-6 \pm \text{SD}$ ; the relative content was determined for: (A)—SAP (saponarin), (B)—LUT (lutonarin), (C)—ISG (isovitexin-7-O-[6-sinp]-glc), (D)—HSG (homoorientin-7-O-[6-sinp]-glc), (E)—IFG (isovitexin-7-O-[6-fer]-glc), (F)—HFG (homoorientin-7-O-[6-fer]-glc), (G)—FQA (feruloylquinic acid), and (H)—Ratio of B-mono/dihydroxylated flavonoids. Treatments marked above with same letters did not significantly differ based on Tukey's *post-hoc* test.

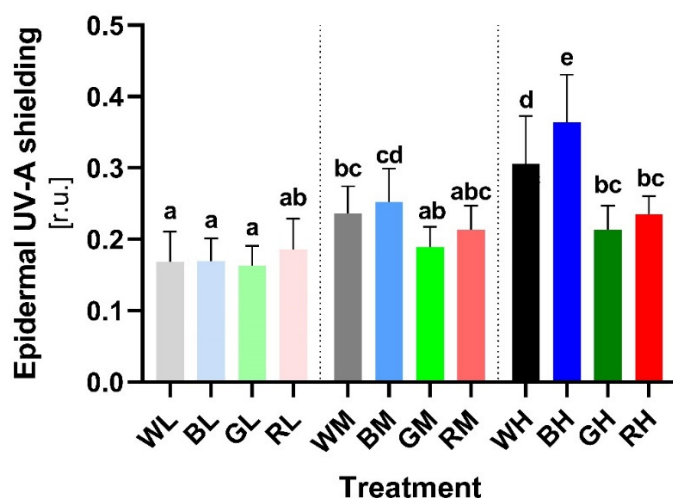


**Figure 6.** Epidermal UV-A shielding of *Hordeum vulgare* L. cv. Bojos secondary leaves acclimated to light conditions varying in irradiance and spectral qualities. Specifications of light treatments: W (white), B (blue), R (red), G (green), L (low irradiance,  $100 \mu\text{mol m}^{-2} \text{s}^{-1}$ ), M (medium irradiance,  $200 \mu\text{mol m}^{-2} \text{s}^{-1}$ ), and H (high irradiance,  $400 \mu\text{mol m}^{-2} \text{s}^{-1}$ );  $n = 10\text{--}12 \pm \text{SD}$ . Treatments marked above with same letters did not significantly differ based on Tukey's *post-hoc* test.

#### 2.4. Antioxidative Activity of Soluble PheCs

The lowest TEAC (Trolox-equivalent antioxidant capacity) measured spectrophotometrically using DPPH stable radical (Section 4.6) was observed in plants grown at LI. Although the average value was comparable within WL, RL, and GL groups, plants grown in BL exhibited a significantly higher TEAC, which suggests a positive effect of blue light on the antioxidative potential of plants, even at LI (Figure 7). This result differs from the effect of irradiance and spectral quality on total PheC content and epidermal UV-A shielding (Figures 3 and 6), where statistical differences between LI treatments were not confirmed.

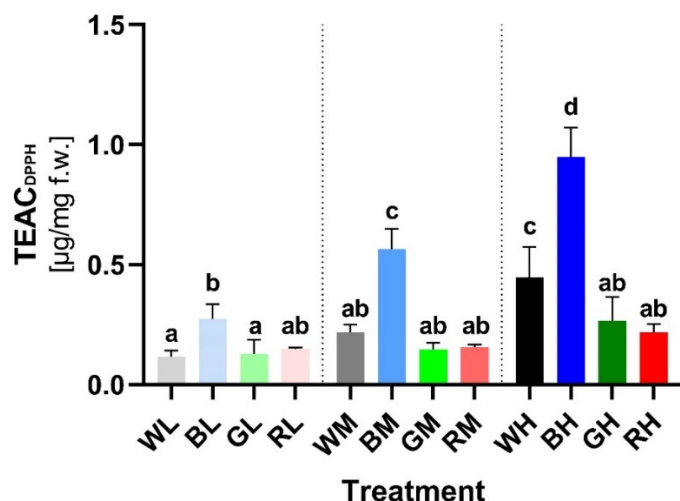


**Figure 7.** Antioxidant activity of soluble PheCs in secondary leaf extracts of *Hordeum vulgare* L. cv. Bojos acclimated to light conditions varying in irradiance and spectral qualities, expressed as a TEAC (Trolox-equivalent antioxidant capacity). Antioxidant activity was determined by colorimetric assay using 2,2-Diphenyl-1-picrylhydrazil stable radical (for details see Section 4.6). Specifications of light treatments: W (white), B (blue), R (red), G (green), L (low irradiance,  $100 \mu\text{mol m}^{-2} \text{s}^{-1}$ ), M (medium irradiance,  $200 \mu\text{mol m}^{-2} \text{s}^{-1}$ ), and H (high irradiance,  $400 \mu\text{mol m}^{-2} \text{s}^{-1}$ );  $n = 5\text{--}6 \pm \text{SD}$ . Treatments marked above with same letters did not significantly differ based on Tukey's *post-hoc* test.

MI ( $200 \mu\text{mol m}^{-2} \text{s}^{-1}$ ) led to a significant increase in TEAC in BM-treated plants (BM vs. BL: +106.38%, TPT  $p < 0.0001$ ) and contained a greater amount of PheCs compared to other MI variants (Figure 3). Negligible TEAC increases were observed in plants exposed to WL (WM vs. WL: +30.13%, TPT ns), followed by GM (GM vs. GL: +14.51%, TPT ns) and RM (RM vs. RL: +3.65%, TPT ns) conditions.

The highest TEAC was observed in plants acclimated to HI, but the TEAC values varied considerably compared to LI plants only in WH (WH vs. WL: +165.10%, TPT  $p < 0.0001$ ) and especially BH (BH vs. BL: +246.37%, TPT  $p < 0.0001$ ) treatments. These results suggest an important role of blue light in inducing the biosynthesis of PheCs with effective antioxidant properties. Exposure of plants to GH (GH vs. GL: +107.97%, TPT ns) and RH (RH vs. RL: +46.39%, TPT ns) did not lead to statistically significant differences compared to LI.

The TEAC values exhibited a linear dependence on PheC content ( $R = 0.9027$ ,  $y = 5.401 \times 10^{-5} x - 0.1467$ , Supplementary Figure S3) and thus similar trends in response to acclimation light treatments. However, increasing irradiance of blue light enhanced the antioxidant activity of soluble PheCs more than the efficiency of epidermal UV-A shielding. The importance of spectral quality and irradiance on AOX of PheCs was confirmed by two-way ANOVA ( $p < 0.0001$ ), including the interaction of these two factors ( $p < 0.0001$ ) (Supplementary Table S1).

#### 2.5. Expression Analysis of Genes Related to PheCs Biosynthesis, AOX Enzymes, and Senescence Markers

We performed RT-qPCR analysis (Sections 4.7 and 4.8) of three important genes involved in PheC biosynthesis: *PAL* (phenylalanine ammonia lyase), *CHS* (chalcone synthase), and *F3'H* (flavonoid-3'-hydroxylase) (see Figure 1 for their roles). We aimed to test whether the effects of light intensity and spectral composition on GE had the same trends as PheC accumulation. Indeed, our results showed a similar pattern to that described in Section 2.1. The highest PheC-associated GE was observed under blue light conditions, particularly under HI (Figure 8A,B). This suggests that total PheC accumulation occurs via both increased transcription after the seven-day acclimation and increased enzyme activity. This also indicates that blue light induces constitutively higher expression of PheC-related enzymes, even in the long term (Figure 8A,B). *PAL* catalyzes the synthesis of transcinnamic acid and *CHS* is responsible for the synthesis of naringenin chalcone. Upregulation of *PAL* and *CHS* was strongly dependent on spectral quality. Upregulation with increasing irradiance occurred only for plants acclimated under blue light (Figure 8). To determine how spectral quality and irradiation affect the expression of genes responsible for flavonoid hydroxylation, we also analyzed *F3'H*, which catalyzes the addition of hydroxyl groups to the flavonoid skeleton resulting in 3'-hydroxyflavonoid. The highest *F3'H* expression was observed in BH conditions, but also in GM and GH conditions. In all other conditions, *F3'H* expression was considerably weaker, but nonzero. ANOVA confirmed the statistically significant effect of spectral quality, irradiance, and their interaction for all analyzed genes (Supplementary Table S2).

To assess how spectral quality and irradiance of light influence the function of the key antioxidant enzymes, we determined gene expression of the *SOD* gene (encoding the superoxide dismutase), which converts superoxide radicals to hydrogen peroxide, and *APX* (encoding ascorbate peroxidase), which catalyzes the conversion of hydrogen peroxide to water. Increased GE of enzymes related to antioxidative defense occurs under blue light conditions as well (Figure 8). *SOD* expression was highly affected by spectral quality ( $p = 0.0003$ ), irradiance ( $p = 0.0001$ ), and their interaction ( $p < 0.0001$ ) (Supplementary Table S2). Intriguingly, the expression of both AOX-related genes exhibited a positive correlation with increasing irradiance of white, blue, and green light. However, under red spectral treatment, the response to irradiance was the opposite—increasing irradiance of red light led to decreased *SOD* expression (Figure 8D). *APX* displayed a similar expression pattern—its

expression was affected by spectral quality ( $p = 0.0216$ ), irradiance ( $p = 0.0178$ ), and the interaction of those two factors ( $p = 0.0147$ ) (Supplementary Table S2).

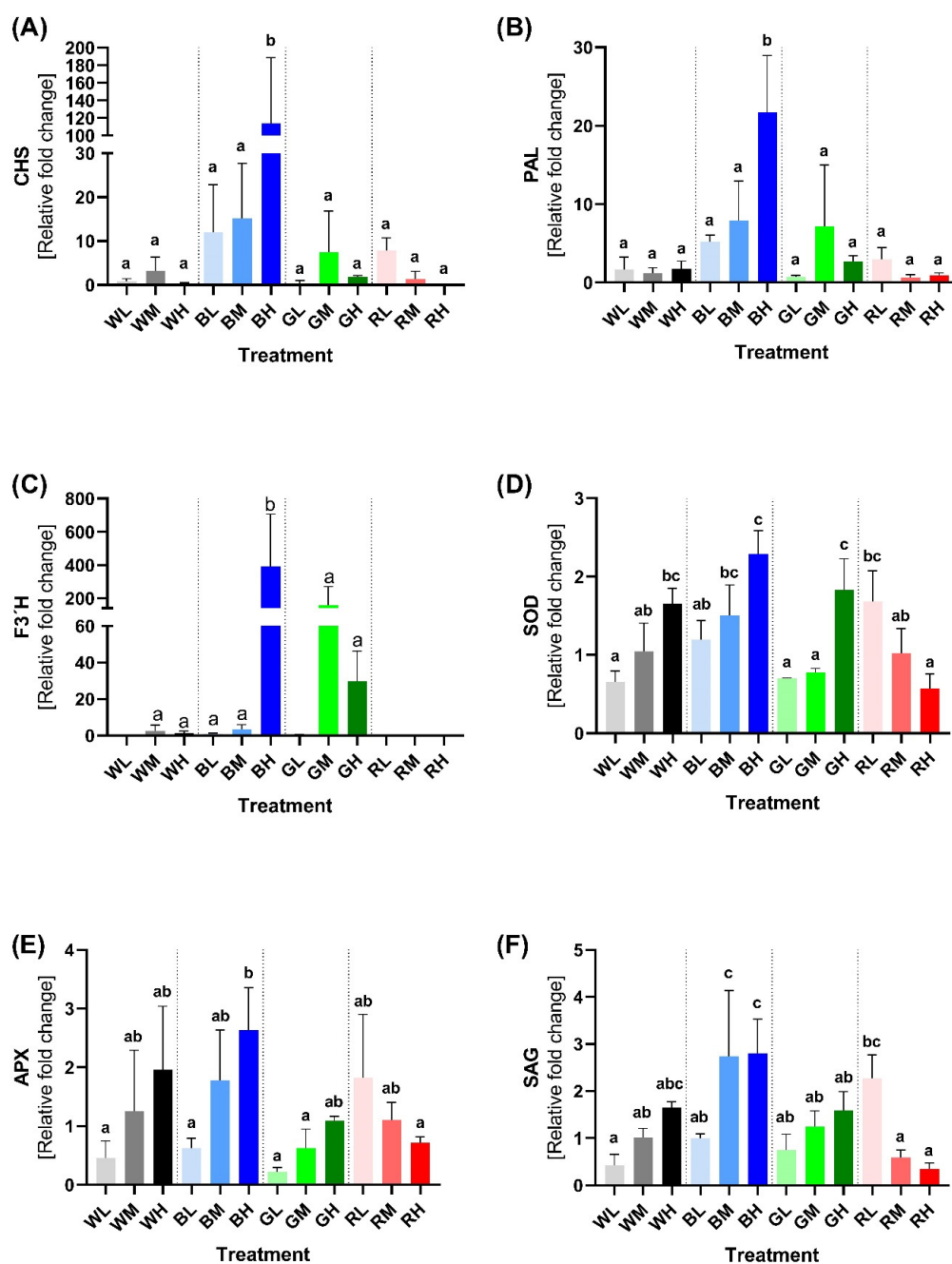


**Figure 8.** Results of RT-qPCR analysis of selected genes involved in the production of PheCs, antioxidant enzymes, and senescence in *Hordeum vulgare* L. cv. Bojos acclimated to light conditions varying in irradiance and spectral qualities. Specifications of light treatments: W (white), B (blue), R (red), G (green), L (low irradiance,  $100 \mu\text{mol m}^{-2} \text{s}^{-1}$ ), M (medium irradiance,  $200 \mu\text{mol m}^{-2} \text{s}^{-1}$ ), and H (high irradiance,  $400 \mu\text{mol m}^{-2} \text{s}^{-1}$ ); (A)—*CHS* (chalcone synthase; EC 2.3.1.74), (B)—*PAL* (phenylalanine ammonium lyase; EC 4.3.1.24), (C)—*F3'H* (flavonoid 3'-hydroxylase; EC 1.14.14.82), (D)—*SOD* (superoxide dismutase; EC 1.15.1.1), (E)—*APX* (ascorbate peroxidase; EC 1.11.1.11), and (F)—*SAG* (senescence associated gene 12). Treatments marked above with same letters did not significantly differ based on Tukey's *post-hoc* test.

It is known that light affects plant aging; therefore, we analyzed *SAG* (senescence associated gene 12), a senescence marker in Arabidopsis [45] and barley [46–48], to discover how spectral quality and irradiance influence leaf senescence. We showed that spectral quality ( $p = 0.0002$ ), and the interaction of spectral quality and irradiance ( $p = 0.0001$ ) affect the GE of *SAG*. On the other hand, the effect of total irradiance was not confirmed ( $p = 0.0897$ ), which suggests that the spectral quality of incident light plays a major role in plant senescence. It is questionable whether this relationship can be observed at irradiances higher than  $400 \mu\text{mol m}^{-2} \text{s}^{-1}$ . Interestingly, the *SAG* expression pattern is very similar to genes encoding antioxidative enzymes (Figure 8F), which highlights the importance of this poorly understood gene in plants.

## 2.6. Transcriptomic Analysis of Genes Affecting the Production of PheCs

RNA-seq analysis revealed many differentially expressed genes among plants acclimated to BH, GH, and RH—due to the scope of this article, we focused on genes related to PheC biosynthesis (Figure 9). The comparison between BH and RH conditions revealed that BH showed upregulated *DAHP* (3-deoxy-D-arabino-heptulosonic acid 7-phosphate synthase), *CS* (chorismate synthase), *ADT* (arogenate dehydratase), *PAL* (phenylalanine ammonia lyase), *CHS1* (chalcone synthase isoform 1), *CHS/SSfp* (chalcone/stilbene synthase family protein), *CH/SSfp* (chalcone/stilbene synthases family protein), *CHIfp* (chalcone-flavonone isomerase family protein), and *C/Fifp* (chalcone/flavonone family protein) compared to RH. Similarly, a comparison between BH and GH light conditions revealed that *ADT*, *DAHP*, *CS*, *ESPS* (3-phosphoshikimate 1-carboxyvinyltransferase), *PAL*, *CHS1*, *CHS*, *CHS/SSfp*, *CHIfp*, and *C/Fifp* were significantly overexpressed in BH conditions. We also compared BH to BL growth conditions to find out whether irradiation affects PheC-related GE and found that in BH acclimated plants, *DAHP*, *PAL*, *CHS1*, *CH/SSfp*, *CHS/SSfp*, *CHIfp*, and *C/Fifp* were significantly overexpressed, but the enzymes involved in later steps of PheC biosynthesis were not.

Once we summarized our RNA-seq results, we could conclude that in BH conditions, genes related to the flavonoid pathway (so-called “early genes”; *CHS1*, *CHS/SSfp*, *CH/SSfp*, *CHIfp*, and *C/Fifp*) and genes from the phenylpropanoid pathway (specifically *PAL*) were significantly overexpressed, as well as some genes from the shikimic pathway (*DAHP*, *ESPS*, *CS*, and *ADT*). The greatest differences in GE between PheC biosynthesis genes were observed between BH and RH plants; the differences between BH and GH plants were less pronounced, and the least pronounced were the differences between BH and BL plants. All together, our analyses confirmed trends observed in the RT-qPCR analysis—the expression of PheC-related genes is proportional to blue light irradiance (BH vs. BL comparison) but also depends on the spectral quality (BH vs. RH, BH vs. GH)—the higher the wavelength of incident light, the lower the expression of these genes.

We also performed an analysis of differentially expressed small RNAs, including miRNAs. Our analysis revealed a whole scale of overexpressed small RNAs. The majority of them were snoR/snoZ/SNORD (small nucleolar RNAs responsible for chemical modifications of other RNAs), tRNAs (transfer RNAs involved in proteosynthesis), and rRNAs (responsible for ribosome constitution alongside specific proteins). However, those miRNAs are unable to induce post-transcriptional gene silencing (PTGS) and so were excluded from our detailed analysis. We discovered that miR1122 family members do not act uniformly in the context of different spectral quality and irradiance—some of them are overexpressed at BH conditions, while others are under-expressed (to avoid misinterpretation, their precise PLAZA IDs will be used further, Table 1). HVU0038G1818 and HVU0040G0316 were significantly overexpressed at BH conditions compared to GH and BL plants. A similar pattern was displayed by HVU0798G0114—this miRNA was overexpressed at BH conditions compared to GH and RH conditions.

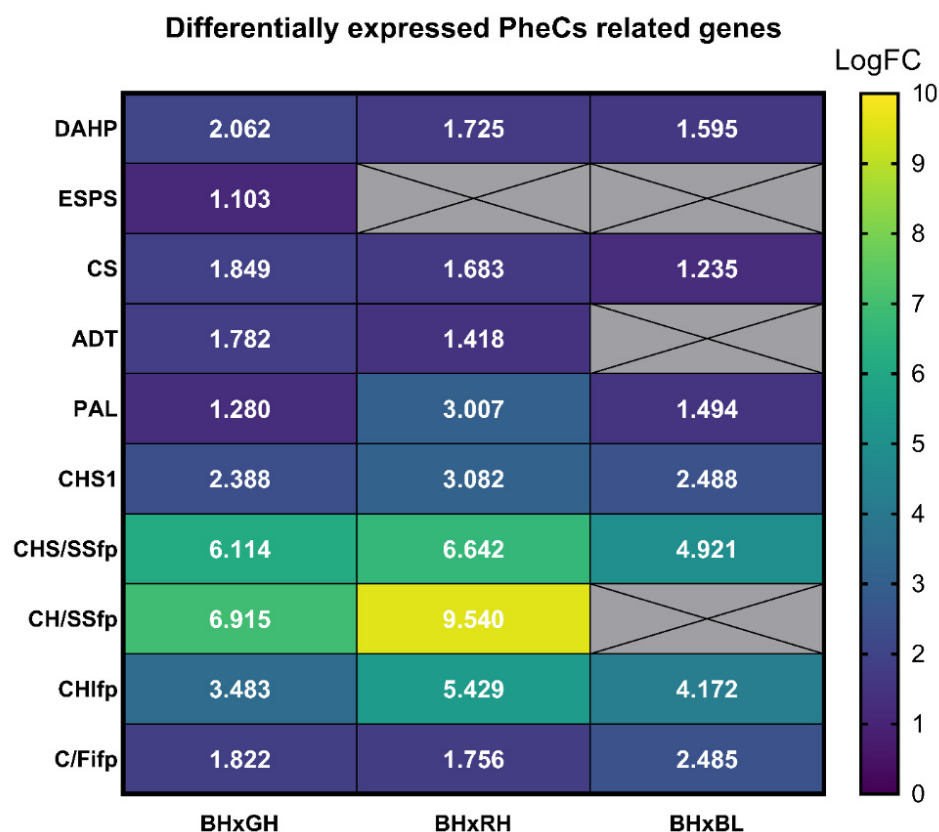


**Figure 9.** RNA sequencing analysis of PheC-related genes and genes of the shikimic pathway (which produces important substrates for PheC synthesis): Annotated genes are listed in rows from the top to the bottom in order of involvement in the biosynthetic pathways, whilst comparisons among light treatments are listed in columns (BH compared to GH, BH compared to RH, and BH compared to BL). Gray color denotes a missing value (in at least one of the datasets, the transcript was either not present or was excluded due to the parameters listed in Section 4.8). Displayed values correspond to logs of relative fold changes of gene expression (LogFC) between treatments and are also indicated by color according to the presented color scale. Specifications of light treatments: B (blue), R (red), G (green), L (low irradiance,  $100 \mu\text{mol m}^{-2} \text{s}^{-1}$ ), and H (high irradiance,  $400 \mu\text{mol m}^{-2} \text{s}^{-1}$ ). *DAHP* (3-deoxy-D-arabino-heptulosonic acid 7-phosphate synthase; MLOC\_17364.2), *ESPS* (3-phosphoshikimate 1-carboxyvinyltransferase; MLOC\_56626.1), *CS* (chorismate synthase; MLOC\_66898.1), *ADT* (arogenate dehydratase; MLOC\_65725.1), *PAL* (phenylalanine ammonia lyase; MLOC\_79728.1), *CHS1* (chalcone synthase isoform 1; MLOC\_74116.1), *CHS/SSfp* (chalcone/stilbene synthase family protein; MLOC\_7936.1), *CH/SSfp* (chalcone/stilbene synthases family protein; MLOC\_64305.2), *CHlfp* (chalcone-flavonone isomerase family protein; MLOC\_5324.1), and *C/Fifp* (chalcone/flavonone family protein; MLOC\_80571.3). MLOC IDs are unique identifiers in the STRING database (<https://string-db.org/>, accessed on 6 October 2021).

In BH conditions, HVU0038G1160 and HVU0038G1161 from the miR1122 family, and also miR396 (HVU0042G1661), were underexpressed (Table 1) compared to GH and RH. Additionally, it is noteworthy that miR156 (HVU0042G2193) was significantly downregulated in BH compared to GH. MiR169\_5 was also downregulated in BH conditions compared to RH and BL. On the other hand, two distinct isoforms (HVU0045G0592 in RH and HVU0037G2782 in BL) were preferred under those conditions. Together, our data suggest that miRNAs can also be differentially expressed at various light conditions to ensure an additional level of GE regulation and thus (indirectly) metabolic maintenance in suboptimal conditions, which is—to date (in the context of spectral quality and irradiation)—an undescribed phenomenon.

**Table 1.** Analysis of miRNAs with the potential to induce PTGS which were underexpressed under BH conditions compared to GH, RH, and BL, respectively.

Comparison	Plaza ID	miRNA
Compared to GH	HVU0042G1661	miR396
	HVU0042G2193	miR156
	HVU0038G1160	miR1122
	HVU0038G1161	miR1122
	HVU0040G1583	miR1122
	HVU0040G1584	miR1122
Compared to RH	HVU0042G1661	miR396
	HVU0045G0592	miR169_5
	HVU0038G1160	miR1122
	HVU0038G1161	miR1122
Compared to BL	HVU0037G2782	miR169_5

### 3. Discussion

#### 3.1. Photosynthetically Active Radiation as an Important Factor Inducing PheC Biosynthesis and Plant Protective Mechanisms against Adverse Environmental Influences

Beyond powering photosynthesis, PAR plays a role in regulating plant defense to (photo)oxidative stress through the biosynthesis of PheCs. However, not all wavelengths contribute equally. Changes in spectral quality result in quantitative and qualitative changes to PheC profiles and, consequently, altered states of photoprotection [22]. There is increasing evidence that blue-light-induced accumulation of PheCs is a common plant response, as it was observed not only for *Hordeum vulgare* [49], but also in several other plant species: *Lactuca sativa* [50,51], *Chrysanthemum morifolium* [52], *Pisum sativum* [53], *Stevia rebaudiana* [54], *Eruca sativa* [55], and *Cucumis sativus* [56]. A study on Arabidopsis mutants with impaired CRY1 (blue-light-sensing) function showed significantly lower resistance against UV-B radiation due to the limited accumulation of UV-shielding compounds, but also lower catalase and peroxidase enzyme activity [57].

Importantly, the final plant response to photoreceptor-induced signals always depends on the other environmental stimuli as well as their mutual interaction (coaction) [58]. It is reasonable to investigate the interaction of light intensity and spectral quality since the variations of these two factors affect photoreceptor function itself, as well as their signaling pathways and, conclusively, PheC metabolism and its role in plant tolerance against oxidative stress.

#### 3.2. PheC Production Is Effectively Enhanced by Blue Light but Not by Other Spectral Components of PAR during Acclimation of Spring Barley to Higher Irradiances

In our study, the acclimation of spring barley plants to the varying irradiance and spectral composition of PAR had a pronounced impact on soluble PheC metabolism. This involved changes in the total PheC content (Figure 3) as well as changes in the relative quantity of individual compounds (Figures 4 and 5). PheCs accumulated in response to increasing PAR irradiance, but only if the acclimation light treatment involved a substantial blue spectral component. Increasing irradiance of blue light itself, i.e., in the absence of light belonging to the other spectral regions (UV-B, UV-A, G, R, FR) was sufficient to activate the PheC pathway and led to the most pronounced accumulation of PheCs among all treatments. However, results showed that interaction/co-action of blue-light-driven regulation of PheC metabolism and different irradiance levels might have important eco-physiological implications. For example, acclimation of spring barley to blue light of low irradiance  $100 \mu\text{mol m}^{-2} \text{s}^{-1}$  did not enhance the quantity of PheCs compared to the other spectral qualities (Figure 3). Based on our results, we presume that the minimal total irradiance of blue light allowing effective accumulation of PheCs lies within  $100\text{--}200 \mu\text{mol m}^{-2} \text{s}^{-1}$  in the case of spring barley (and the experimental conditions used). This may underpin the importance of UV radiation for initiating plant protective mechanisms against oxidative

stress in forest understory or very dense canopies, where the blue light irradiance might not reach the necessary threshold level for PheC production. A minor yet non-negligible enhancement of total PheC accumulation was observed after acclimation of barley plants to HI green light (compared to GL; Figure 3). This observation was rather unexpected because blue-light-dependent PheC biosynthesis is driven to a high extent by CRYs induced signals [59]. It is known that green light can partially inactivate CRYs, presumably as a consequence of chromophore shifts to fully reduced FADH<sub>2</sub> form [60]. Thus, green light is usually considered a signal to stop or slow down responses caused by activated CRY, including stem growth rate inhibition, anthocyanin accumulation, or chloroplast GE [61], which corresponds to results reporting a negligible effect of green light on PheC accumulation [62]. One possible explanation for the slightly stimulating effect of increasing green light irradiance on PheC biosynthesis in our conditions is the spectral overlap of green LED into the blue spectral region, which could activate CRYs (green LED spectral range 480–600 nm, Supplementary Figure S6). Although the primary absorption peak of cryptochromes in *Arabidopsis* corresponds approximately to 450 nm, absorption of FAD embedded in cryptochromes reaches up to 550 nm [63]. The green light may also affect cryptochromes localized deeper in the plant tissue due to its higher transmission compared to blue light [64,65]. Thus, the overlap of green LEDs to the blue spectral region could cause a change in the equilibrium of activated and inactivated CRYs, which in turn could slightly enhance total PheC content. Several studies have demonstrated the positive effect of green light on ascorbic acid, anthocyanin, and total phenolic content in lettuce [65–67]. However, Zhang et al. (2021) [68] concluded that green light reduces stem elongation when partially replacing blue light independent of CRY signaling. These results indicate that the green light responses may be induced also via CRY-independent pathway(s), which can contribute also to the observed enhancement of PheC accumulation in barley leaves.

### 3.3. Changes of PheC Profiles under Various Light Treatments—Blue Light as the Main Component of PAR Affecting the Ratio of B-Mono and Dihydroxylated Flavonoids

Aside from the total content of soluble PheCs, PAR irradiance and its spectral quality also had a significant impact on the PheC profile (i.e., relative content of PheCs within the sample). The soluble PheCs contained in barley secondary leaves could be divided into two distinctive groups according to their response to irradiance and spectral quality (Figure 4B). Isovitexin derivatives (1st group) tended to increase with HI (and availability of assimilates), even if it did not contain a blue spectral component. Conversely, the accumulation of homoorientin derivatives and FQA (2nd group) in response to HI was much more reliant on the presence of blue light, and thus rather low amounts of these compounds were observed in RH and GH treatments (Figures 4A and 5). The most abundant soluble PheC detected in barley leaf extract was saponarin (in accordance with Kaspar (2010) [17]). Herein, saponarin represents from 63.72 to 77.87% of the total soluble PheC content in barley leaves acclimated to different irradiance and PAR spectra (one of the first studies, Seikel and Geissman (1957) [69] estimated approximately 72%), and hence, isovitexin derivatives exceeded the content of homoorientin derivatives in all tested plants. Isovitexin derivatives (SAP, ISG, IFG) are also exclusively responsible for the above-discussed increase in PheCs in GH compared to GL condition (compare Figure 5A,C,E and Figure 5B,D,F). However, the contribution of isovitexin derivatives to the total content of soluble PheCs decreased in favor of homoorientin derivatives in response to higher irradiance of blue and white light, while the changes in the ratio of isovitexin and homoorientin derivatives were statistically insignificant in barley plants acclimated to increasing irradiance of green and red light (Figure 5H). A previous study on barley showed that UV and PAR treatments had a minor effect on saponarin, whereas lutonarin was markedly enhanced by high PAR and UV irradiances, which led to comparable or even slightly higher content of lutonarin compared to saponarin in young leaves of *Hordeum vulgare* [70]. Thus, it seems that the content of isovitexin and homoorientin derivatives may gradually level out under suitable light conditions.



Importantly, under LI, the content of observed PheCs was not significantly affected by spectral treatments. Whether a certain threshold irradiance of blue light must be reached to effectively activate relevant photoreceptor (CRYs) signaling, or whether effective PheC accumulation (and metabolic profile change) was limited by insufficient availability of assimilates (e.g., saccharose signaling)—or other factors influencing plant metabolism under LI—remains unknown. In general, the accumulation pattern of glycosylated–acylated flavonoids (ISG, IFG; HSG, HFG) followed the light-induced response of their glycosylated counterparts (SAP or LUT), particularly under blue light. This indicates that these compounds may have similar functions concerning photoprotection—substitution by hydroxycinnamic acids (HCAs) could affect their AOX as well as their transport and cellular localization [71]. On the other hand, their content may rise due to the higher availability of SAP and LUT, which may serve as substrates for acylation. FQA was the most abundant representative of soluble HCA derivatives present in barley leaves. FQA content exhibited a strong dependence on the irradiance of blue light, i.e., in examined irradiance range, it was observed only in blue treatments and WH. Although some HCAs are relatively strong antioxidants and UV-B attenuators, the observed increase in soluble FQA content might not be necessarily related to the production of protective metabolites. Alternatively, it may be the consequence of reduced longitudinal growth under blue light (or stronger white light). HCAs are incorporated into the cell walls during growth [72–74], thus reducing longitudinal growth together with overall activation of the PheC synthesis pathway, including its early steps (represented by the activation of PAL; Figure 8B), especially in BH treatment, may lead to the observed steep increase in FQA content.

Our results clearly showed that higher irradiance of blue light serves as an important environmental cue negatively affecting the ratio of B-mono/-di hydroxylated flavonoids (specifically ratio of isovitexin/homoorientin based flavonoids) in barley leaf tissue (Figure 5H). The number of hydroxyl groups on the B ring is the primary determinant of flavonoid antioxidant activity [75]. Such change in favor of B-dihydroxylated compounds is often considered as the plant enhancing tolerance against (light-induced) oxidative stress and damage (as discussed below) and as part of high-light acclimation [76]. This phenomenon is at least partially controlled at the GE level since the expression of the gene related to the *F3'H* enzyme (which catalyzes the formation of catechol group at flavonoid B-cycle) remains significantly upregulated in BH condition, even at the end of the acclimation phase (Figure 8C). This indicates that homoorientin derivatives are still synthesized; therefore, their content does not reach a final stable state two weeks after the plants were exposed to BH conditions. This is contrary to WH conditions, where the content of homoorientin derivatives is also higher (compared to RH treatment) but the *F3'H* expression is very low. Thus, the *F3'H* gene exhibits striking sensitivity to co-acting facets of light—irradiance (HI) and spectral quality (B). Although its response to HI itself (e.g., in WH, RH, GH conditions) appears to be negligible after prolonged acclimation to increased irradiance. The relative fold change of *F3'H* GE induced by higher irradiance of blue light was at least 3× higher compared to *CHS* and *PAL* genes (Figure 8C vs. A,B).

In summary, our data reveal that the production of all studied PheCs is positively regulated by higher irradiance of blue light. Production of isovitexin derivatives is mildly enhanced regardless of spectral quality while homoorientin derivatives require the presence of blue light in the spectrum, probably due to the high sensitivity of *F3'H* expression to this spectral component.

Such discrepancies between activation of GE related to PheC biosynthesis and the actual content of PheCs observed in plants exposed to different PAR irradiance and spectral quality might originate from different dynamics of gene expression and PheC metabolism—while the GE usually responds immediately, the detectable PheC accumulation occurs over hours or days. Further, contrary to GE, the content of PheCs remains relatively stable once synthesized, even after the removal of the inductive environmental cue [77]. Thus, if a high PheC content is observed but the expression of involved gene(s) is

low, this could mean that we observe the final metabolic acclimation to current conditions while the initial GE signal already faded out.

#### 3.4. Light as a Factor Affecting Plant (Photo-)Tolerance through Regulation of PheC Metabolism and AOX Enzymes

In this study, we observed a clear trend of soluble PheCs accumulating with increasing blue and white irradiance. Production of B-dihydroxylated flavonoids (homoorientin derivatives) was particularly enhanced. This response was not present or was markedly reduced during acclimation of plants to HI of other spectral qualities (G, R). Since the majority of flavonoids are effective UV absorbers, it could be concluded that blue light is an important component of natural sunlight which can coact with UV or even act independently (in artificial conditions) as a positive regulator of plant UV tolerance [57,78].

Moreover, acclimation of barley plants to increased blue and white irradiance markedly enhanced the in-vitro-measured AOX of leaf extracts (Figure 7). Contrary to the epidermal UV-A shielding, a positive effect of blue light on the AOX was detected even at the lowest irradiance of blue light. In addition, increasing irradiance of blue (and to a lesser extent also white) light enhanced the AOX activity of leaf extracts more pronouncedly than the efficiency of UV-A screening (Figure 6 vs. Figure 7 and Supplementary Figure S1 vs. S4). On the other hand, increasing irradiance of red light stimulated the efficiency of UV-A shielding more than the AOX activity of soluble PheCs. This could be due to red light being a reliable signal for top-of-canopy position, making UV shielding of greater importance than antioxidative function [79]. However, we presume that the observed increase in AOX is at least partially caused by the significantly higher proportion of B-hydroxylated flavonoids (such as LUT, HFG, HSG) in extracts (Figure 5H) (AOX shows a higher correlation and dependency on the content of homoorientin derivatives, Supplementary Figure S2 vs. Figure S3) and hypothetically also due to higher content of FQA. The dominant contribution of blue light to the AOX capacity of PheCs may also be related to their localization since high PAR selectively accumulates PheCs in mesophyll cells, where they contribute to AOX rather than to UV-A shielding [18]. Nevertheless, the possible presence of other LMWA with strong antioxidant activity in extracts cannot be excluded. Interestingly, in plant organs most exposed to UV-B radiation, the synthesis of HCA derivatives declines in favor of flavonoids [80,81], even though HCAs absorb UV-B more efficiently than flavonoids [82] and accumulation of HCAs is associated with higher tolerance of oxidative stress among barley genotypes [83]. As shown in Arabidopsis, acylation of some PheCs (such as saignolins) may enhance their UV-B absorption properties, which confers a fitness advantage to plants that produce them following exposure to prolonged UV-B [84,85]. However, whether the further binding of HCAs on flavonoid molecules (HFG, HSG) substantially affects (enhances) flavonoid AOX or shielding activity and their cellular localization compared to nonacylated counterparts is yet not clear.

Enhanced AOX may not only increase the tolerance of plants against UV-B stress, which is accompanied by overproduction of ROS in the chloroplast and especially in UV-B damaged PSII [86,87], but it can also alleviate the detrimental effects of excessive PAR stress, which is more frequent in natural environments (compared to UV-B stress). As with UV-B stress, excessive PAR leads to a significant production of ROS in the chloroplast (primarily singlet oxygen), however, their quality and origin within photosynthetic apparatus are different than in the case of UV-B stress. As shown by Agati et al. (2012) [88] B-dihydroxylated flavonoids were detected in chloroplasts in the proximity of ROS production sites. Thus, B-dihydroxylated flavonoids may participate in the reduction of ROS-induced damage and influence ROS-related signaling from the chloroplast [76,82,88]. In this context, the activation of phenylpropanoid and flavonoid pathways followed by the accumulation PheCs in leaf tissues could be classified as one of the many blue-light-induced acclimation responses of plants to high/excessive PAR. Since PheCs are relatively stable in leaf tissues [77], blue light could be used as an instrument for priming the plants against photo-oxidative stress [26] and should be further studied as a factor which increases plant

tolerance against other environmental stresses interconnected with high ROS production (i.e., cross-tolerance) [89]. The importance of PheCs increases in conditions impairing the function of AOX enzymes (strong UV, high or low temperature, heavy metals) which are more sensitive to degradation/inactivation due to their protein nature.

Within this study, we also examined the regulation of the AOX enzymes *SOD* and *APX* at the level of GE, which increased proportionally to the irradiance of blue, white, and partially also green light (in the case of *SOD*; Figure 8D). Although the sensitivity of response (GE fold change) to blue light was much lower compared to GE of PheC related genes (especially *F3'H*), we can presume that enhanced *SOD* and *APX* activity may lead to reduced concentration of superoxide anion radicals and hydrogen peroxide under blue light conditions. Surprisingly, we observed the opposite trend (i.e., decrease in GE) with increasing irradiance of red light, which is in agreement with the decreased activity of *SOD* enzyme observed in *Boehmeria nivea* under red light [90]. This decrease may be due to the lack of a blue-light-induced CRY signal, which is part of high-light acclimation. Alternatively, this could indicate some sort of red-light-induced negative feedback, hypothetically involving phytochromes. The straightforward explanation of the lower production of ROS—and thus, lower demand for AOX enzymes—is not probable since the GE decreases with irradiance. A trend similar to the AOX enzymes—decreasing GE with increased red light irradiation—was observed for *SAG* (senescence associated gene 12), which is linked with natural and induced senescence in Arabidopsis [45] and barley [47,91]. This indicates that spectral quality and irradiance can affect leaf senescence, which is consistent with the current literature [92]. Together, these results indicate that blue-light-induced HI acclimatory responses—including accumulation of PheCs with antioxidant function as well as activation of enzymatic ROS scavenging machinery—are accompanied by a speeding-up of leaf ontogeny, whereas the absence of these responses at red light of the same irradiance alleviates the onset of senescence.

### 3.5. Spectral Quality Affects Expression of Genes Related to the PheCs Biosynthesis

As mentioned above, RT-qPCR analysis confirmed that barley plants acclimated to blue light had strongly upregulated GE for the production of PheC precursors (*PAL*, Figure 8A), as well as the “early genes” of PheC biosynthesis (*CHS* and *F3'H*, Figure 8B,C)—for a discussion of metabolic and physiological relevance, see Sections 3.3 and 3.4. The stimulative effect of blue light on PheC-related GE has been already reported, e.g., for *Glycine max* seedlings [62], *Fagopyrum tataricum* sprouts [93], *Cyclocarya paliurus* [94], and *Agastache rugosa* plants [95]. However, in comparison with previous publications, our analyses proved for the first time that the degree of upregulation of *PAL*, *CHS*, and particularly *F3'H* in spring barley leaves depends strongly on blue light irradiance.

RNA-seq analysis confirmed that the “early genes” related to the flavonoid pathway (*CHS1*, *CHS/SSfp*, *CH/SSfp*, *CHIfp*, *C/Fifp*) were upregulated under the BH conditions in comparison with the GH-, RH-, and BL- (*CH/SSfp* was in this comparison insignificant) acclimated seedlings. In addition, we also observed increased expression of genes linked to the shikimic pathway (*DAHP*, *ESPS*, *CS*) under BH conditions compared to GH (*DAHP*, *ESPS*, *CS*), RH (*DAHP*, *CS*), or BL (*DAHP*, *CS*) light conditions (Figure 9). To our knowledge, the impact of spectral quality on the expression of genes linked to the shikimic pathway has not been reported. Additionally, the *ADT* (arogenate dehydratase) gene (linked to the biosynthesis of aromatic amino acids) seems to be upregulated under the BH conditions compared to the GH and RH acclimated plants (but not compared to BL plants). This phenomenon has not yet been described at the level of GE in the context of spectral quality before now. Interestingly, the “early genes” displayed the greatest differences in LogFC values, while none of the “late genes” related to the PheC biosynthesis displayed statistically significant overexpression in BH conditions compared to GH, RH, and BL treatments. The question is whether this result is caused by the different regulation of “early genes” and “late genes” in PheC biosynthetic machinery, (see Figure 2) or by possible

epigenetic regulations. To address this question, direct experiments on the epigenetic regulations of the “late gene” group are needed.

### 3.6. Complex Role of miRNAs in the Regulation of PheCs Related Genes

In general, miRNAs are involved in PTGS and play an important role in regulating physiological processes, including plant development [96,97]. Three miRNAs seem to be essential (Figure 10) for PheC “late genes” regulation via MBW complex transcript degradation (PTGS). These miRNAs are: miR828, involved in the PAP1 (TF enhancing expression of PheC related genes) transcript degradation [98,99]; miR156, which induces the PTGS of the WD40 mRNA (this protein is necessary for MBW complex assembly); and miR396, which degrades the mRNA of bHLH74 in Arabidopsis [100]. However, the interaction of miRNAs with other transcripts encoding the bHLH proteins (proteins necessary for the MBW complex constitution) has not yet been reported, although such interaction could be expected—members of the same bHLH subfamily share structural similarity and expression patterns [101].

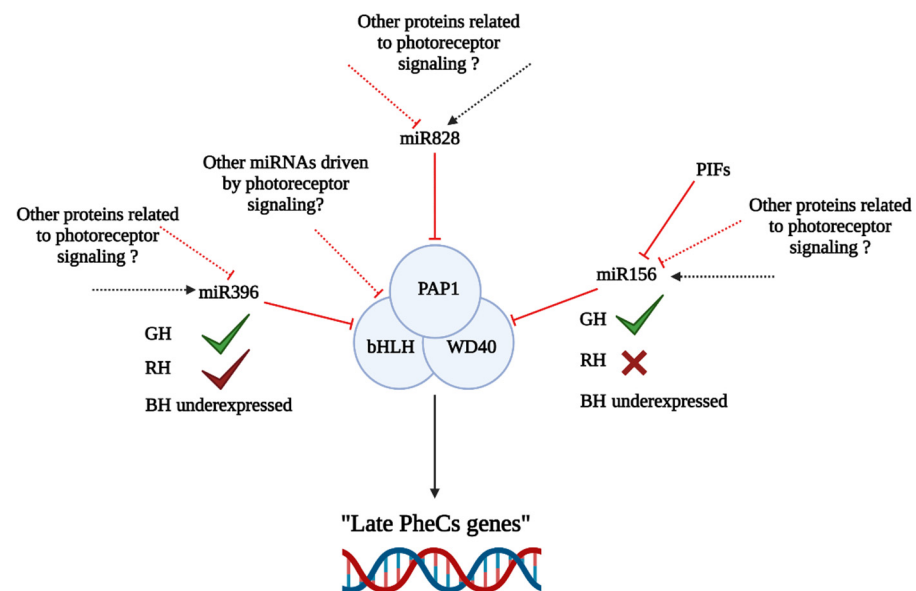


**Figure 10.** Schematic representation of possible effects of miRNAs on the MBW complex, which is responsible for the regulation of “late PheC genes”—presence (check), absence (cross), or downregulation of corresponding miRNAs under specific light conditions are indicated; full lines were validated by articles cited in the text above; dashed lines indicate possible alternative ways of regulation. Solid lines represent known interactions, whereas dashed lines indicate presumed alternative methods of regulation (not yet confirmed) (black—induction/upregulation; red—inhibition/downregulation). BH (blue), RH (red), and GH (green) light of high intensity;  $400 \mu\text{mol m}^{-2} \text{s}^{-1}$ .

Our RNA-seq analysis revealed under expressed miRNAs (Table 1) in barley seedlings acclimated to BH conditions (compared to GH or RH)—specifically miR156 (compared to GH conditions) and miR396 (compared to both GH and RH conditions), which can degrade two out of three MBW mRNA transcripts via PTGS. This could explain why the “late genes” are not expressed under RH and GH. However, this does not explain why the “late genes” leading to anthocyanin biosynthesis are not transcribed in the BH. Even low temperature conditions, which strongly stimulate anthocyanin production in Arabidopsis, hardly affect barley anthocyanin accumulation (unpublished data). The question is whether this difference is due to primary DNA structure caused by epigenetic modification (e.g., DNA methylation) or a direct result of PTGS ensured by miRNAs. Epigenetic modifications could explain the lower responsiveness of “late genes” in barley compared to Arabidopsis, while the activity of miRNAs could explain the different responsiveness between “early

genes" and "late genes" in barley under different experimental conditions. To validate such hypotheses, further study of the barley epigenome is needed.

In Arabidopsis, the connection between miR156 and R/FR (red/far-red) signaling via PhyB and PIFs has been documented [102]. Expression of miR156 seems to be linked to the R/FR signaling cascade, but experimental data focused on miR156 expression in plants acclimated to monochromatic red light conditions are missing (for blue and green monochromatic lights as well). Similarly, miR396 expression patterns under the various monochromatic light conditions have not been reported for barley. However, for other plant species, the impact of light stress on miRNA profile has been described. In *Zea mays* [103], *Populus tremula* [104], and *Prunus persica* [105], changes in miRNA profile were observed after UV-B application. Similarly, changes in the miRNA profile of *Dendrocalamus latiflorus* seedlings after exposure to white light [106] were documented. FR-responsive miRNAs were described in *Glycine max* [107] targeting genes related to PheC metabolism. This indicates that spectral quality induced changes in miRNA profiles can affect PheC related genes and further strengthens our hypothesis about the monochromatic light-responsive miRNAs outlined in Figure 10.

Ultimately, we propose that several miRNAs can affect GE of PheC related genes (mainly the "late genes"), but to confirm this hypothesis, additional experiments focused on sequencing small RNAs in the same experimental conditions are needed. The validity of our statements with regards to the influence of different irradiances of monochromatic light on levels of miRNAs in spring barley should be confirmed or refuted in subsequent studies, bearing in mind that library preparation for RNA-seq analysis, as well as the total RNA isolation procedure itself, can affect the acquired data. Deeper research should also include comparative analysis of miRNAs under various monochromatic light conditions in barley, and it should further search for the possible miRNA targets (mRNAs). Both wet-lab and in silico approaches should be considered in the future to confirm current and also to search for novel miRNA targets in spring barley and shed light on the mysterious and overlooked level of GE regulation of LMWAs, including PheCs.

## 4. Materials and Methods

### 4.1. Cultivation of Plant Material

Seeds of spring barley *Hordeum vulgare* L. cv Bojos were sown into square pots (a = 13 cm, V = 2200 cm<sup>3</sup>) containing a mixture (1:1 v/v) for house plants and gardening substrate (Agro CS, Česká Skalice, Czech Republic). Substrate was kept well-watered without additional fertilizers. Plants were cultivated in the growth chamber Phytoscope FS130 (PSI, Drásov, Czech Republic) with a 16-hour light period at 22 °C followed by an 8-hour dark period at 20 °C. Air humidity was approx. 60%. To ensure normal development of plants during germination, barley was grown for one week under low irradiation white light (RGB 1:1:1; total irradiance 100 μmol m<sup>-2</sup> s<sup>-1</sup>). Subsequently, plants were acclimated to various combinations of irradiances (L—low 100, M—medium 200, or H—high 400 μmol m<sup>-2</sup> s<sup>-1</sup>) and spectral qualities (R—red, G—green, B—blue, or W—white containing R:G:B in a ratio of 1:1:1) for 7 days. Table 2 summarizes spectral conditions and designation of treatments. The LED spectral properties used in the experiment are shown in Supplementary Figure S6. Samples of barley secondary leaves (central segments) were collected on day 14. Sampling procedure and sample preparation is further specified in the following sections. The samples were immediately frozen in liquid nitrogen and stored at –80 °C till analysis.

### 4.2. Epidermal UV-A Shielding

In vivo measurement of epidermal UV-A shielding was performed after 14 days of growth using DUALEX<sup>®</sup> Leaf Analyser (ForceA, Orsay, France). Epidermal UV-A shielding was measured at the central part of barley secondary leaves (12 samples per light treatment) approximately 1 h before the start of the light phase. After the measurement, leaves were used for the extraction of soluble PheCs (see below).

**Table 2.** Specification of light treatments (i.e., irradiance and spectral quality) used during the 7-day acclimation period of spring barley plants (*Hordeum vulgare* L. cv Bojos). W (white light), B (blue light), R (red light), G (green light), L (low irradiance,  $100 \mu\text{mol m}^{-2} \text{s}^{-1}$ ), M (medium irradiance,  $200 \mu\text{mol m}^{-2} \text{s}^{-1}$ ), and H (high irradiance,  $400 \mu\text{mol m}^{-2} \text{s}^{-1}$ ).

PAR Irradiance [ $\mu\text{mol m}^{-2} \text{s}^{-1}$ ]	Spectrum in PAR Region	Group ID
100	R	RL
200	R	RM
400	R	RH
100	G	GL
200	G	GM
400	G	GH
100	B	BL
200	B	BM
400	B	BH
100	W	WL
200	W	WM
400	W	WH

#### 4.3. Extraction of Soluble Phenolic Compounds

Plant extracts of soluble PheCs were prepared from central segments of *Hordeum vulgare* secondary leaves ( $100 \pm 5$  mg of fresh weight (FW), approximately 2 segments). Six samples per treatment were collected from dark-acclimated plants one hour before the light phase. Samples were homogenized using mortar and pestle in 3 mL of 40% methanol ( $\text{CH}_4\text{O}$ ,  $\geq 99.9\%$ ,  $M_r = 32.04 \text{ g}\cdot\text{mol}^{-1}$ , Sigma-Aldrich, Schnellendorf, Germany) with a small amount of sea sand (Penta, Prague, Czech Republic). The homogenate was ultrasonified for 5 min (K-51E, Krainetek Czech s.r.o., Hradec Králové, Czech Republic) and centrifuged (EBA 20, Hettich Zentrifugen, Tuttlingen, Germany) at 6000 rpm for 3 min. The supernatant was made up to 3 mL with 40% methanol in a volumetric tube and filtered into amber vials using a syringe with a Spartan filter (13/0.2 RC, Whatman, Dassel, Germany). Prepared extracts of PheCs were stored at  $-22^\circ\text{C}$  till analysis.

#### 4.4. HPLC-DAD Based Quantification of Soluble Phenolic Compounds

The semiquantitative analysis of soluble PheCs (extracted in 40% methanol as described above) was performed on an Agilent 1200 HPLC system (Agilent Technologies, Santa Clara, CA, USA) equipped with a UV-VIS absorption diode array detector (DAD; G1315D; Agilent Technologies, Santa Clara, CA, USA). PheCs were separated using Hypersil Gold chromatographic column (C18,  $50 \text{ mm} \times 2.1 \text{ mm}$ ,  $1.9 \mu\text{m}$ , Thermo Scientific, Waltham, NJ, USA). The column was tempered at  $30^\circ\text{C}$  during the whole separation process. Two acidified acetonitrile–water solutions were used as the mobile phases (m.p. A—5% ACN; m.p. B—80% ACN;  $\text{C}_2\text{H}_3\text{N}$ ,  $\geq 99.9\%$ ,  $M_r = 41.05 \text{ g}\cdot\text{mol}^{-1}$ , Sigma-Aldrich, Schnellendorf, Germany). The mobile phase was acidified by formic acid ( $\text{CH}_2\text{O}_2$ ,  $M_r = 46.03 \text{ g}\cdot\text{mol}^{-1}$ , Sigma-Aldrich, Schnellendorf, Germany) in a ratio of 999:1, *v/v*. The flow of mobile phases was set to  $0.3 \text{ mL}/\text{min}^{-1}$ . The gradient of mobile phases is shown in Table 3.

Samples were injected in a volume of  $10 \mu\text{L}$ . The relative quantity of PheCs was determined by manual integration of peaks detected at 314 nm. The peak area was further adjusted to the FW of the sample). Retention times and UV-Vis absorption spectra were acquired to facilitate compound identification and alignment with HPLC-DAD-MS data, which were primarily used for compound identification (Table 3). The total content of soluble PheCs for each chromatogram was evaluated as the sum of peak areas adjusted to the FW of each sample.

**Table 3.** Gradient of mobile phases used for HPLC based PheC separation.

Time [min]	A: 5% ACN [%]	B: 80% ACN [%]
0	100	0
2	95	5
10	80	20
15	60	40
18	20	80
22	0	100
24	0	100

#### 4.5. The Identification of Soluble Phenolic Compounds

The qualitative analysis of PheCs present in spring barely secondary leaves was performed using a UHPLC-DAD system (UltiMate 3000, Dionex, Sunnyvale, CA, USA) in tandem with a (Q-TOF) mass spectrometer micrOTOF-QII (Bruker Daltonics, Bremen, Germany). For the separation of PheCs, the same procedure as HPLC-DAD quantitative analysis was applied. The mass spectrometry analysis was conducted in negative ion mode—the electrospray was used as the ion source (end plate offset = 500 V, capillary voltage = 2900 V, nebulizer pressure 3.5 Bar, dry gas flow = 10 L min<sup>-1</sup>, temperature = 200 °C). The mass spectra were acquired in the range of 50 to 1500 *m/z*. Furthermore, collision-induced dissociation of detected compounds (at 35 eV) was performed to obtain MS (fragmentation) spectra. The tentative identification of PheCs was conducted based on the assessment of their retention behavior and by comparison of their UV-Vis absorption spectra, exact *m/z*, and fragmentation patterns with the literature [108–110], as well as with corresponding commercially available standards (saponarin; Extrasynthèse, FR) or similar compounds (such as homoorientin, isovitexin, luteolin, apigenin, and ferulic acid; Extrasynthèse, Genay, France) (Supplementary Section S1: The identification of soluble phenolic compounds).

#### 4.6. Antioxidant Activity Assay

The antioxidant activity of PheC extracts was determined by colorimetric assay using the stable DPPH• radical (2,2-Diphenyl-1-picrylhydrazyl, Sigma-Aldrich, Schnellendorf, Germany, Cat No. 1898-66-4). The DPPH solution used for measurement (and calibration) was prepared by the dissolution of 0.01875 g of DPPH• in 250 mL of 100% methanol. The method was calibrated using the antioxidant Trolox ((±)-6-Hydroxy-2,5,7,8-tetramethylchromane-2-carboxylic acid, Calbiochem, Cat No. 53188-07-1). The set of calibration solutions was prepared by the dilution of Trolox stock solution (1 mM; 0.0125 g in 50 mL of 100% methanol) to final concentrations of 0, 25, 50, 100, 200 and 300 µM. For the measurement of antioxidant activity, 2 mL of DPPH solution was mixed with 0.5 mL of Trolox solution (calibration samples), 0.5 mL of methanol (blank samples), or 0.5 mL of PheC-containing plant extracts. The mixture was incubated for 10 min in the dark before the spectrophotometrical analysis. The relative change of sample absorbance at 515 nm (compared to the blank) was recorded using a double-beam absorption spectrophotometer (Specord 250, Analytik Jena, Jena, Germany) with a monochromator width slit set to 0.5 nm. The resulting values were expressed as Trolox-equivalent antioxidant capacity (TEAC) based on established calibration curves and further adjusted to the FW of samples.

#### 4.7. RNA Isolation, DNase Treatment and Reverse Transcription

Central leaf segments (approx. 50 mg) were sampled (three biological replicates per treatment) and immediately frozen in liquid nitrogen. Frozen plant tissue was homogenized by mortar and pestle, washed with 0.5 mL of TRIzol (Sigma-Aldrich, St. Louis, MO, USA, Cat No. T9424) in a fresh Eppendorf tube, and stored in the freezer at −80 °C until RNA isolation. Total RNA extraction was performed according to the manufacturer's instructions. TURBO DNA-free protocol was used (Ambion, Austin, TX, USA, Cat No. AM 1907) to remove DNA traces in samples. The quality and quantity of RNA were assessed using a

NanoPhotometer (Implen, Westlake Village, CA, USA). For a random subset of samples, the RNA integrity was also determined by 1.5%-denaturing agarose gel electrophoresis. An amount of 1 µg of total RNA per sample was taken for the reverse transcription using a First Strand cDNA kit (Thermo Scientific, Waltham, NJ, USA, Cat No. K1612).

#### 4.8. qPCR

Primer sequences (Supplementary Table S3, Thermo Fisher Scientific, Waltham, NJ, USA) were selected based on the literature [111–116], supplied by the Thermo Fisher Scientific, and diluted according to the manufacturer's instructions using nuclease free water. For each qPCR reaction, 5 µL of EliZymeGreen MIX AddROX (Elisabeth Pharmacon, Brno, Czech Republic, Cat No. EZ4614), 1 µL of diluted forward, 1 µL of diluted reverse primers (to adjust a final concentration of oligonucleotides in the reaction mixture to 250 nM), and 2 µL of nuclease-free water were used. Diluted cDNA (1 µL; 20 µL cDNA:20 µL nuclease-free water) was added to the mixture. qPCR conditions for all listed primer pairs were the same: 1 min of initial denaturation (95 °C) followed by 35 cycles of 95 °C for 15 s, 57 °C for 15 s, and 72 °C for 15 s in 96-well optical reaction plates. Subsequently, a melting curve analysis was performed. All qPCR reactions were performed at Roche LC480<sup>®</sup> Instrument (Roche Diagnostics GmbH, Mannheim, Germany) in 3 technical replicates. RT-qPCR data were processed and normalized as described in Livak and Schmittgen (2001) [117]. Alpha tubulin was chosen as a reference gene. Differential expression was calculated relative to WM (white light medium irradiance).

#### 4.9. RNA Sequencing and Transcriptome Analysis

Total RNA for transcriptome sequencing was isolated and DNase treated as described above (Section 4.7). Purified RNA from 3 biological replicates was measured with a NanoPhotometer (Implen, Westlake Village, CA, USA) and pooled together in the same amount (approximately 6 µg from each sample per treatment). After preparation, samples were frozen in liquid nitrogen, and transported on dry ice to the Novogene company (Stockton, Sacramento, CA, USA). A quality check via bioanalyzer followed (all samples had RNA integrity number/RIN/above 6) and sequencing was performed using the Illumina HiSeq platform. Raw sequencing data were uploaded to Galaxy webserver [118] and trimmed and processed using the Kallisto quant tool (Freiburg, Germany, tool version 0.46.0, *Hordeum vulgare* IBC PGSB v2 built in transcriptome was applied as a reference accessed on 20 April 2020). The resulting tables of transcript abundances were exported and merged to a .txt file and processed using edgeR workflow (Supplementary Section S2: EdgeR workflow code) [119]. Genes with significantly different expression rates (DEGs) with false discovery rates (FDR) below 0.1 were uploaded to PLAZA Monocots 4.0 portal ([https://bioinformatics.psb.ugent.be/plaza/versions/plaza\\_v4\\_monocots/](https://bioinformatics.psb.ugent.be/plaza/versions/plaza_v4_monocots/), accessed on 11 June 2021) [120] and gene IDs were exported and processed using STRINGdb (<https://string-db.org/>, accessed on 6 October 2021) with parameters set as follows: minimum required interaction score of 0.400, 10 maximum interactions to show, disabled structure previews in bubbles, hidden disconnected nodes, shown input protein names and k-means clustering. All genes annotated at STRINGdb related to PheC biosynthesis were exported for further processing, including their abundances. Results focused on PheC related metabolism are listed in Figure 8.

#### 4.10. Data Visualisation and Statistical Analysis

Statistical testing and data visualization were performed in GraphPad Prism (v9.1.2.226, GraphPad Software, San Diego, CA, USA) and RStudio (v1.3.1093, RStudio Inc., Boston, MA, USA). Homoskedasticity and data normality for further analysis by parametric tests were verified by residuals vs. fitted plot and QQ plot followed by Leven and Shapiro-Wilk test. After verifying the variance and normal distribution, a two-way ANOVA (analysis of variance) was used to assess the effect of spectral quality, irradiation, their interaction



on PheC content, related sample parameters (epidermal UV-A shielding, AOX, etc.), and qPCR data. For multiple group comparisons, Tukey's post hoc test was applied.

Further cluster analysis and heatmaps illustrating the differences in the relative content of PheCs across treatments differing in spectral compositions and irradiance were created (RStudio, Supplementary Section S3). The relative contents of each PheC per treatment were averaged ( $n = 5-6$ ) and subsequently normalized to the maximum value among all light treatments. Cluster analysis was performed on normalized PheC quantitative data based on average linkage. Distance between rows (spectral conditions) and columns (PheCs) was determined by the Euclidean distance.

## 5. Conclusions

We present evidence that the blue spectral component of HI is essential for the accumulation of PheCs and activation of enzymatic ROS scavenging machinery (such as SOD, APX) in secondary leaves of *Hordeum vulgare*. Intriguingly, the changes in PheC metabolic profile (their relative content and quantity) enhanced the AOX of leaf extracts considerably more than the UV-A shielding properties of leaves. Specifically, it could be attributed to pronounced biosynthesis of dihydroxylated PheCs (homoorientin derivatives), which are at least partially caused by GE of F3'H under high blue light irradiance. Such responses were not induced by other spectral treatments, regardless of the examined irradiance range (100, 200, or 400  $\mu\text{mol m}^{-2} \text{s}^{-1}$ ). Our data also suggests that spectral quality could affect miRNAs involved in the PTGS of PheC-related genes. Three miRNAs (156, 828, and 396) seem to mediate the degradation of MBW complex transcripts, which could explain the different responsiveness between the expression of "early genes" and "late genes" in barley under different light treatments. On the other hand, more experiments focused on the barley epigenome under monochromatic light conditions are needed to explain the extent to which miRNAs affect PheC biosynthesis and to completely understand the complex epigenetic regulatory mechanisms leading to PheC biosynthesis, apart from miRNAs.

**Supplementary Materials:** The following supporting information can be downloaded at: <https://www.mdpi.com/article/10.3390/ijms23126533/s1>.

**Author Contributions:** V.Š. and J.N. conceived the study. HPLC analysis, epidermal UV-A shielding, and antioxidant capacity including data curation and visualization were performed by R.P. and supervised by J.N. Transcriptome analysis and qPCR including data curation and visualization were performed by A.V.; P.P., J.Č. and M.B. contribute to the transcriptomic analysis and supervised interpretation and processing of bioinformatic data. The article was written by R.P., A.V. and J.N., with all authors contributing to the writing. V.Š., J.N. and L.H. reviewed and edited the article. All authors have read and agreed to the published version of the manuscript.

**Funding:** This research was funded by the Czech Science Foundation (GACR 21-18532S to V.Š., J.N., R.P. and A.V.), the University of Ostrava (SGS11/PrF/2022 to R.P., A.V. and J.N.; SGS10/PrF/2022 to P.P.), and the Moravian-Silesian Region (RRC/10/2021 to R.P.). Participation of V.Š. was also supported by the Ministry of Education, Youth and Sports of the Czech Republic, project "SustES—Adaptation strategies for sustainable ecosystem services and food security under adverse environmental conditions" (CZ.02.1.01/0.0/0.0/16\_019/0000797). J.Č., P.P. and M.B. were supported by the National Agency for Agricultural Research (NAZV) of the Czech Republic grant no. QK1810391 "Utilization of genomic and transcriptomic approaches to create genetic resources and breeding materials of poppy with specific traits".

**Institutional Review Board Statement:** Not applicable.

**Informed Consent Statement:** Not applicable.

**Data Availability Statement:** Processed and derived data are available from the corresponding authors V.Š. and J.N. on request.

**Acknowledgments:** The authors would like to thank Běla Piskořová for her invaluable assistance during plant cultivation and analyses; further, also Martin Navrátil for the measurement of LED

spectra. We would like to also express our gratitude to Novogene (USA, Sacramento) for provided services during the RNA sequencing process.

**Conflicts of Interest:** The authors declare no conflict of interest. The funders had no role in the design of the study; in the collection, analyses, or interpretation of data; in the writing of the manuscript; or in the decision to publish the results.

## References

- Yeom, M.; Kim, H.; Lim, J.; Shin, A.-Y.; Hong, S.; Kim, J.-I.; Gil Nam, H. How Do Phytochromes Transmit the Light Quality Information to the Circadian Clock in *Arabidopsis*? *Mol. Plant* **2014**, *7*, 1701–1704. [[CrossRef](#)] [[PubMed](#)]
- Halaban, R. Effects of Light Quality on the Circadian Rhythm of Leaf Movement of a Short-Day-Plant. *Plant Physiol.* **1969**, *44*, 973–977. [[CrossRef](#)] [[PubMed](#)]
- Holmes, M.G.; Smith, H. The function of phytochrome in the natural environment—II. The influence of vegetation canopies on the spectral energy distribution of natural daylight. *Photochem. Photobiol.* **1977**, *25*, 539–545. [[CrossRef](#)]
- Xu, Y.; Wang, C.; Zhang, R.; Ma, C.; Dong, S.; Gong, Z. The relationship between internode elongation of soybean stems and spectral distribution of light in the canopy under different plant densities. *Plant Prod. Sci.* **2021**, *24*, 326–338. [[CrossRef](#)]
- Kotilainen, T.; Aphalo, P.J.; Brelford, C.; Böök, H.; Devraj, S.; Heikkilä, A.; Hernández, R.; Kylling, A.; Lindfors, A.; Robson, T. Patterns in the spectral composition of sunlight and biologically meaningful spectral photon ratios as affected by atmospheric factors. *Agric. For. Meteorol.* **2020**, *291*, 108041. [[CrossRef](#)]
- Swanson, S.; Gilroy, S. ROS in plant development. *Physiol. Plant.* **2010**, *138*, 384–392. [[CrossRef](#)]
- Ma, X.; Bai, L. Elevated CO<sub>2</sub> and Reactive Oxygen Species in Stomatal Closure. *Plants* **2021**, *10*, 410. [[CrossRef](#)]
- Sharma, P.; Jha, A.B.; Dubey, R.S.; Pessarakli, M. Reactive Oxygen Species, Oxidative Damage, and Antioxidative Defense Mechanism in Plants under Stressful Conditions. *J. Bot.* **2012**, *2012*, 217037. [[CrossRef](#)]
- You, J.; Chan, Z. ROS Regulation during Abiotic Stress Responses in Crop Plants. *Front. Plant Sci.* **2015**, *6*, 1092. [[CrossRef](#)]
- Kollist, H.; Zandalinas, S.I.; Sengupta, S.; Nuhkat, M.; Kangasjärvi, J.; Mittler, R. Rapid Responses to Abiotic Stress: Priming the Landscape for the Signal Transduction Network. *Trends Plant Sci.* **2019**, *24*, 25–37. [[CrossRef](#)]
- Kakuszi, A.; Sárvári, É.; Solti, Á.; Czégény, G.; Hideg, É.; Hunyadi-Gulyás, É.; Bóka, K.; Böddi, B. Light piping driven photosynthesis in the soil: Low-light adapted active photosynthetic apparatus in the under-soil hypocotyl segments of bean (*Phaseolus vulgaris*). *J. Photochem. Photobiol. B Biol.* **2016**, *161*, 422–429. [[CrossRef](#)] [[PubMed](#)]
- Takahashi, S.; Badger, M.R. Photoprotection in plants: A new light on photosystem II damage. *Trends Plant Sci.* **2011**, *16*, 53–60. [[CrossRef](#)]
- Tuteja, N.; Ahmad, P.; Panda, B.B.; Tuteja, R. Genotoxic stress in plants: Shedding light on DNA damage, repair and DNA repair helicases. *Mutat. Res./Rev. Mutat. Res.* **2009**, *681*, 134–149. [[CrossRef](#)] [[PubMed](#)]
- Yamamoto, Y. Quality Control of Photosystem II: The Mechanisms for Avoidance and Tolerance of Light and Heat Stresses are Closely Linked to Membrane Fluidity of the Thylakoids. *Front. Plant Sci.* **2016**, *7*, 1136. [[CrossRef](#)]
- Buettner, G.R. Superoxide Dismutase in Redox Biology: The Roles of Superoxide and Hydrogen Peroxide. *Anti-Cancer Agents Med. Chem.* **2011**, *11*, 341–346. [[CrossRef](#)] [[PubMed](#)]
- Kumar, S.; Abedin, M.M.; Singh, A.K.; Das, S. Role of Phenolic Compounds in Plant-Defensive Mechanisms. In *Plant Phenolics in Sustainable Agriculture*; Lone, R., Shuab, R., Kamili, A.N., Eds.; Springer: Singapore, 2020; pp. 517–532. [[CrossRef](#)]
- Kaspar, S.; Matros, A.; Mock, H.-P. Proteome and Flavonoid Analysis Reveals Distinct Responses of Epidermal Tissue and Whole Leaves upon UV–B Radiation of Barley (*Hordeum vulgare* L.) Seedlings. *J. Proteome Res.* **2010**, *9*, 2402–2411. [[CrossRef](#)]
- Hunt, L.; Klem, K.; Lhotáková, Z.; Vosolsobě, S.; Oravec, M.; Urban, O.; Špunda, V.; Albrechtová, J. Light and CO<sub>2</sub> Modulate the Accumulation and Localization of Phenolic Compounds in Barley Leaves. *Antioxidants* **2021**, *10*, 385. [[CrossRef](#)] [[PubMed](#)]
- Csepregi, K.; Hideg, É. Phenolic Compound Diversity Explored in the Context of Photo-Oxidative Stress Protection. *Phytochem. Anal.* **2018**, *29*, 129–136. [[CrossRef](#)]
- Kumar, S.; Pandey, A.K. Chemistry and Biological Activities of Flavonoids: An Overview. *Sci. World J.* **2013**, *2013*, 162750. [[CrossRef](#)]
- Panche, A.N.; Diwan, A.D.; Chandra, S.R. Flavonoids: An overview. *J. Nutr. Sci.* **2016**, *5*, e47. [[CrossRef](#)]
- Sharma, A.; Shahzad, B.; Rehman, A.; Bhardwaj, R.; Landi, M.; Zheng, B. Response of Phenylpropanoid Pathway and the Role of Polyphenols in Plants under Abiotic Stress. *Molecules* **2019**, *24*, 2452. [[CrossRef](#)] [[PubMed](#)]
- Casal, J.J. Photoreceptor Signaling Networks in Plant Responses to Shade. *Annu. Rev. Plant Biol.* **2013**, *64*, 403–427. [[CrossRef](#)] [[PubMed](#)]
- Rai, N.; Morales, L.O.; Aphalo, P.J. Perception of solar UV radiation by plants: Photoreceptors and mechanisms. *Plant Physiol.* **2021**, *186*, 1382–1396. [[CrossRef](#)] [[PubMed](#)]
- Klem, K.; Holub, P.; Štroch, M.; Nezval, J.; Špunda, V.; Tříška, J.; Jansen, M.; Robson, T.M.; Urban, O. Ultraviolet and photosynthetically active radiation can both induce photoprotective capacity allowing barley to overcome high radiation stress. *Plant Physiol. Biochem.* **2015**, *93*, 74–83. [[CrossRef](#)] [[PubMed](#)]

26. Brelsford, C.C.; Morales, L.O.; Nezval, J.; Kotilainen, T.K.; Hartikainen, S.M.; Aphalo, P.J.; Robson, T.M. Do UV-A radiation and blue light during growth prime leaves to cope with acute high light in photoreceptor mutants of *Arabidopsis thaliana*? *Physiol. Plant.* **2019**, *165*, 537–554. [[CrossRef](#)]
27. Rai, N.; Neugart, S.; Yan, Y.; Wang, F.; Siipola, S.M.; Lindfors, A.V.; Winkler, J.B.; Albert, A.; Brosché, M.; Lehto, T.; et al. How do cryptochromes and UVR8 interact in natural and simulated sunlight? *J. Exp. Bot.* **2019**, *70*, 4975–4990. [[CrossRef](#)]
28. Pham, V.N.; Kathare, P.K.; Huq, E. Phytochromes and Phytochrome Interacting Factors. *Plant Physiol.* **2018**, *176*, 1025–1038. [[CrossRef](#)]
29. Bilodeau, S.E.; Wu, B.-S.; Rufyikiri, A.-S.; MacPherson, S.; Lefsrud, M. An Update on Plant Photobiology and Implications for Cannabis Production. *Front. Plant Sci.* **2019**, *10*, 296. [[CrossRef](#)]
30. Battle, M.W.; Vegliani, F.; Jones, M.A. Shades of green: Untying the knots of green photoperception. *J. Exp. Bot.* **2020**, *71*, 5764–5770. [[CrossRef](#)]
31. Pedmale, U.V.; Huang, S.-S.C.; Zander, M.; Cole, B.J.; Hetzel, J.; Ljung, K.; Reis, P.A.; Sridevi, P.; Nito, K.; Nery, J.R.; et al. Cryptochromes Interact Directly with PIFs to Control Plant Growth in Limiting Blue Light. *Cell* **2016**, *164*, 233–245. [[CrossRef](#)]
32. Shin, J.; Park, E.; Choi, G. PIF3 regulates anthocyanin biosynthesis in an HY5-dependent manner with both factors directly binding anthocyanin biosynthetic gene promoters in *Arabidopsis*. *Plant J.* **2007**, *49*, 981–994. [[CrossRef](#)] [[PubMed](#)]
33. Nguyen, N.H. HY5, an integrator of light and temperature signals in the regulation of anthocyanins biosynthesis in *Arabidopsis*. *AIMS Mol. Sci.* **2020**, *7*, 70–81. [[CrossRef](#)]
34. Lee, S.; Wang, W.; Huq, E. Spatial regulation of thermomorphogenesis by HY5 and PIF4 in *Arabidopsis*. *Nat. Commun.* **2021**, *12*, 3656. [[CrossRef](#)] [[PubMed](#)]
35. Xiao, Y.; Chu, L.; Zhang, Y.; Bian, Y.; Xiao, J.; Xu, D. HY5: A Pivotal Regulator of Light-Dependent Development in Higher Plants. *Front. Plant Sci.* **2022**, *12*, 800989. [[CrossRef](#)] [[PubMed](#)]
36. Gangappa, S.N.; Botto, J.F. The Multifaceted Roles of HY5 in Plant Growth and Development. *Mol. Plant* **2016**, *9*, 1353–1365. [[CrossRef](#)]
37. Podolec, R.; Ulm, R. Photoreceptor-mediated regulation of the COP1/SPA E3 ubiquitin ligase. *Curr. Opin. Plant Biol.* **2018**, *45*, 18–25. [[CrossRef](#)]
38. Stracke, R.; Werber, M.; Weisshaar, B. The R2R3-MYB gene family in *Arabidopsis thaliana*. *Curr. Opin. Plant Biol.* **2001**, *4*, 447–456. [[CrossRef](#)]
39. Shin, D.H.; Choi, M.; Kim, K.; Bang, G.; Cho, M.; Choi, S.-B.; Choi, G.; Park, Y.-I. HY5 regulates anthocyanin biosynthesis by inducing the transcriptional activation of the MYB75/PAP1 transcription factor in *Arabidopsis*. *FEBS Lett.* **2013**, *587*, 1543–1547. [[CrossRef](#)]
40. Nguyen, N.H.; Jeong, C.Y.; Kang, G.; Yoo, S.; Hong, S.; Lee, H. MYBD employed by HY 5 increases anthocyanin accumulation via repression of MYBL 2 in *Arabidopsis*. *Plant J.* **2015**, *84*, 1192–1205. [[CrossRef](#)]
41. Wang, Y.; Wang, Y.; Song, Z.; Zhang, H. Repression of MYBL2 by Both microRNA858a and HY5 Leads to the Activation of Anthocyanin Biosynthetic Pathway in *Arabidopsis*. *Mol. Plant* **2016**, *9*, 1395–1405. [[CrossRef](#)]
42. Borgio, J.F. RNA interference (RNAi) technology: A promising tool for medicinal plant research. *J. Med. Plants Res.* **2010**, *3*, 1176–1183.
43. Sharma, D.; Tiwari, M.; Pandey, A.; Bhatia, C.; Sharma, A.; Trivedi, P.K. MicroRNA858 Is a Potential Regulator of Phenylpropanoid Pathway and Plant Development. *Plant Physiol.* **2016**, *171*, 944–959. [[CrossRef](#)] [[PubMed](#)]
44. Sharma, A.; Badola, P.K.; Bhatia, C.; Sharma, D.; Trivedi, P.K. Primary transcript of miR858 encodes regulatory peptide and controls flavonoid biosynthesis and development in *Arabidopsis*. *Nat. Plants* **2020**, *6*, 1262–1274. [[CrossRef](#)] [[PubMed](#)]
45. James, M.; Poret, M.; Masclaux-Daubresse, C.; Marmagne, A.; Coquet, L.; Jouenne, T.; Chan, P.; Trouverie, J.; Etienne, P. SAG12, a Major Cysteine Protease Involved in Nitrogen Allocation during Senescence for Seed Production in *Arabidopsis thaliana*. *Plant Cell Physiol.* **2018**, *59*, 2052–2063. [[CrossRef](#)]
46. Gregersen, P.; Culetic, A.; Boschian, L.; Krupinska, K. Plant senescence and crop productivity. *Plant Mol. Biol.* **2013**, *82*, 603–622. [[CrossRef](#)]
47. Roberts, I.N.; Veliz, C.G.; Criado, M.V.; Signorini, A.M.; Simonetti, E.; Caputo, C. Identification and expression analysis of 11 subtilase genes during natural and induced senescence of barley plants. *J. Plant Physiol.* **2017**, *211*, 70–80. [[CrossRef](#)]
48. Zmienko, A.; Samelak-Czajka, A.; Goralski, M.; Sobieszczuk-Nowicka, E.; Kozłowski, P.; Figlerowicz, M. Selection of Reference Genes for qPCR- and ddPCR-Based Analyses of Gene Expression in Senescing Barley Leaves. *PLoS ONE* **2015**, *10*, e0118226. [[CrossRef](#)]
49. Klem, K.; Gargallo-Garriga, A.; Rattanapichai, W.; Oravec, M.; Holub, P.; Veselá, B.; Sardans, J.; Peñuelas, J.; Urban, O. Distinct Morphological, Physiological, and Biochemical Responses to Light Quality in Barley Leaves and Roots. *Front. Plant Sci.* **2019**, *10*, 1026. [[CrossRef](#)]
50. Son, K.-H.; Oh, M.-M. Leaf Shape, Growth, and Antioxidant Phenolic Compounds of Two Lettuce Cultivars Grown under Various Combinations of Blue and Red Light-emitting Diodes. *HortScience* **2013**, *48*, 988–995. [[CrossRef](#)]
51. Ouzounis, T.; Parjikolaei, B.R.; Fretté, X.; Rosenqvist, E.; Ottosen, C.-O. Predawn and high intensity application of supplemental blue light decreases the quantum yield of PSII and enhances the amount of phenolic acids, flavonoids, and pigments in *Lactuca sativa*. *Front. Plant Sci.* **2015**, *6*, 19. [[CrossRef](#)]










52. Ouzounis, T.; Fretté, X.; Rosenqvist, E.; Ottosen, C.-O. Spectral effects of supplementary lighting on the secondary metabolites in roses, chrysanthemums, and campanulas. *J. Plant Physiol.* **2014**, *171*, 1491–1499. [[CrossRef](#)]
53. Siipola, S.M.; Kotilainen, T.; Sipari, N.; Morales, L.O.; Lindfors, A.V.; Robson, T.M.; Aphalo, P.J. Epidermal UV-A absorbance and whole-leaf flavonoid composition in pea respond more to solar blue light than to solar UV radiation. *Plant Cell Environ.* **2015**, *38*, 941–952. [[CrossRef](#)] [[PubMed](#)]
54. Ahmad, N.; Rab, A.; Ahmad, N. Light-induced biochemical variations in secondary metabolite production and antioxidant activity in callus cultures of *Stevia rebaudiana* (Bert). *J. Photochem. Photobiol. B Biol.* **2016**, *154*, 51–56. [[CrossRef](#)] [[PubMed](#)]
55. Taulavuori, K.; Pyysalo, A.; Julkunen-Tiitto, R. Responses of phenolic acid and flavonoid synthesis to blue and blue-violet light depends on plant species. *Environ. Exp. Bot.* **2018**, *150*, 183–187. [[CrossRef](#)]
56. Palma, C.F.F.; Castro-Alves, V.; Rosenqvist, E.; Ottosen, C.; Strid, Å.; Morales, L.O. Effects of UV radiation on transcript and metabolite accumulation are dependent on monochromatic light background in cucumber. *Physiol. Plant.* **2021**, *173*, 750–761. [[CrossRef](#)] [[PubMed](#)]
57. Khudyakova, A.Y.; Kreslavski, V.D.; Shmarev, A.N.; Lyubimov, V.Y.; Shirshikova, G.N.; Pashkovskiy, P.P.; Kuznetsov, V.V.; Allakhverdiev, S.I. Impact of UV-B radiation on the photosystem II activity, pro-/antioxidant balance and expression of light-activated genes in *Arabidopsis thaliana* hy4 mutants grown under light of different spectral composition. *J. Photochem. Photobiol. B Biol.* **2019**, *194*, 14–20. [[CrossRef](#)]
58. Løvdal, T.; Olsen, K.M.; Slimestad, R.; Verheul, M.; Lillo, C. Synergetic effects of nitrogen depletion, temperature, and light on the content of phenolic compounds and gene expression in leaves of tomato. *Phytochemistry* **2010**, *71*, 605–613. [[CrossRef](#)]
59. Wang, Q.; Lin, C. Mechanisms of Cryptochrome-Mediated Photoresponses in Plants. *Annu. Rev. Plant Biol.* **2020**, *71*, 103–129. [[CrossRef](#)]
60. Liu, B.; Yang, Z.; Gomez, A.; Liu, B.; Lin, C.; Oka, Y. Signaling mechanisms of plant cryptochromes in *Arabidopsis thaliana*. *J. Plant Res.* **2016**, *129*, 137–148. [[CrossRef](#)]
61. Folta, K.M.; Maruhnich, S.A. Green light: A signal to slow down or stop. *J. Exp. Bot.* **2007**, *58*, 3099–3111. [[CrossRef](#)]
62. Zhang, X.; Bian, Z.; Li, S.; Chen, X.; Lu, C. Comparative Analysis of Phenolic Compound Profiles, Antioxidant Capacities, and Expressions of Phenolic Biosynthesis-Related Genes in Soybean Microgreens Grown under Different Light Spectra. *J. Agric. Food Chem.* **2019**, *67*, 13577–13588. [[CrossRef](#)] [[PubMed](#)]
63. Nielsen, C.; Nørby, M.S.; Kongsted, J.; Solov'yov, I.A. Absorption Spectra of FAD Embedded in Cryptochromes. *J. Phys. Chem. Lett.* **2018**, *9*, 3618–3623. [[CrossRef](#)] [[PubMed](#)]
64. Terashima, I.; Fujita, T.; Inoue, T.; Chow, W.S.; Oguchi, R. Green Light Drives Leaf Photosynthesis More Efficiently than Red Light in Strong White Light: Revisiting the Enigmatic Question of Why Leaves are Green. *Plant Cell Physiol.* **2009**, *50*, 684–697. [[CrossRef](#)] [[PubMed](#)]
65. Smith, H.L.; McAusland, L.; Murchie, E. Don't ignore the green light: Exploring diverse roles in plant processes. *J. Exp. Bot.* **2017**, *68*, 2099–2110. [[CrossRef](#)] [[PubMed](#)]
66. Samuolienė, G.; Sirtautas, R.; Brazaitytė, A.; Duchovskis, P. LED lighting and seasonality effects antioxidant properties of baby leaf lettuce. *Food Chem.* **2012**, *134*, 1494–1499. [[CrossRef](#)]
67. Bian, Z.; Cheng, R.; Wang, Y.; Yang, Q.; Lu, C. Effect of green light on nitrate reduction and edible quality of hydroponically grown lettuce (*Lactuca sativa* L.) under short-term continuous light from red and blue light-emitting diodes. *Environ. Exp. Bot.* **2018**, *153*, 63–71. [[CrossRef](#)]
68. Zhang, X.; Bisbis, M.; Heuvelink, E.; Jiang, W.; Marcelis, L.F.M. Green light reduces elongation when partially replacing sole blue light independently from cryptochrome 1a. *Physiol. Plant.* **2021**, *173*, 1946–1955. [[CrossRef](#)]
69. Seikel, M.K.; Geissman, T. The flavonoid constituents of barley (*Hordeum vulgare*). I. Saponarin. *Arch. Biochem. Biophys.* **1957**, *71*, 17–30. [[CrossRef](#)]
70. Holub, P.; Nezval, J.; Štroch, M.; Špunda, V.; Urban, O.; Jansen, M.A.; Klem, K. Induction of phenolic compounds by UV and PAR is modulated by leaf ontogeny and barley genotype. *Plant Physiol. Biochem.* **2019**, *134*, 81–93. [[CrossRef](#)]
71. Tattini, M.; Galardi, C.; Pinelli, P.; Massai, R.; Remorini, D.; Agati, G. Differential accumulation of flavonoids and hydroxycinnamates in leaves of *Ligustrum vulgare* under excess light and drought stress. *New Phytol.* **2004**, *163*, 547–561. [[CrossRef](#)]
72. Yu, P.; McKinnon, J.J.; Christensen, D.A. Hydroxycinnamic acids and ferulic acid esterase in relation to biodegradation of complex plant cell walls. *Can. J. Anim. Sci.* **2005**, *85*, 255–267. [[CrossRef](#)]
73. Yang, J.-G.; Uchiyama, T. Hydroxycinnamic Acids and Their Dimers Involved in the Cessation of Cell Elongation in *Mentha* Suspension Culture. *Biosci. Biotechnol. Biochem.* **2000**, *64*, 1572–1579. [[CrossRef](#)] [[PubMed](#)]
74. Macoy, D.M.; Kim, W.-Y.; Lee, S.Y.; Kim, M.G. Biosynthesis, physiology, and functions of hydroxycinnamic acid amides in plants. *Plant Biotechnol. Rep.* **2015**, *9*, 269–278. [[CrossRef](#)]
75. Pannala, A.S.; Chan, T.S.; O'Brien, P.J.; Rice-Evans, C.A. Flavonoid B-Ring Chemistry and Antioxidant Activity: Fast Reaction Kinetics. *Biochem. Biophys. Res. Commun.* **2001**, *282*, 1161–1168. [[CrossRef](#)]
76. Agati, G.; Brunetti, C.; Fini, A.; Gori, A.; Guidi, L.; Landi, M.; Sebastiani, F.; Tattini, M. Are Flavonoids Effective Antioxidants in Plants? Twenty Years of Our Investigation. *Antioxidants* **2020**, *9*, 1098. [[CrossRef](#)] [[PubMed](#)]
77. Nezval, J.; Štroch, M.; Materová, Z.; Špunda, V.; Kalina, J. Phenolic compounds and carotenoids during acclimation of spring barley and its mutant Chlorina f2 from high to low irradiance. *Biol. Plant.* **2017**, *61*, 73–84. [[CrossRef](#)]

78. Del Valle, J.C.; Buide, M.L.; Whittall, J.B.; Valladares, F.; Narbona, E. UV radiation increases phenolic compound protection but decreases reproduction in *Silene littorea*. *PLoS ONE* **2020**, *15*, e0231611. [[CrossRef](#)] [[PubMed](#)]
79. Mathews, S. Phytochrome-mediated development in land plants: Red light sensing evolves to meet the challenges of changing light environments. *Mol. Ecol.* **2006**, *15*, 3483–3503. [[CrossRef](#)]
80. Tattini, M.; Gravano, E.; Pinelli, P.; Mulinacci, N.; Romani, A. Flavonoids accumulate in leaves and glandular trichomes of *Phillyrea latifolia* exposed to excess solar radiation. *New Phytol.* **2000**, *148*, 69–77. [[CrossRef](#)]
81. Agati, G.; Tattini, M. Multiple functional roles of flavonoids in photoprotection. *New Phytol.* **2010**, *186*, 786–793. [[CrossRef](#)]
82. Agati, G.; Brunetti, C.; Di Ferdinando, M.; Ferrini, F.; Pollastri, S.; Tattini, M. Functional roles of flavonoids in photoprotection: New evidence, lessons from the past. *Plant Physiol. Biochem.* **2013**, *72*, 35–45. [[CrossRef](#)] [[PubMed](#)]
83. Hunt, L.; Fuksa, M.; Klem, K.; Lhotáková, Z.; Oravec, M.; Urban, O.; Albrechtová, J. Barley Genotypes Vary in Stomatal Responsiveness to Light and CO<sub>2</sub> Conditions. *Plants* **2021**, *10*, 2533. [[CrossRef](#)] [[PubMed](#)]
84. Tohge, T.; Wendenburg, R.; Ishihara, H.; Nakabayashi, R.; Watanabe, M.; Sulpice, R.; Hoefgen, R.; Takayama, H.; Saito, K.; Stitt, M.; et al. Characterization of a recently evolved flavonol-phenylacyltransferase gene provides signatures of natural light selection in Brassicaceae. *Nat. Commun.* **2016**, *7*, 12399. [[CrossRef](#)] [[PubMed](#)]
85. Tohge, T.; de Souza, L.P.; Fernie, A.R. On the natural diversity of phenylacylated-flavonoid and their in planta function under conditions of stress. *Phytochem. Rev.* **2018**, *17*, 279–290. [[CrossRef](#)]
86. Hideg, É.; Barta, C.; Kálai, T.; Vass, I.; Hideg, K.; Asada, K. Detection of Singlet Oxygen and Superoxide with Fluorescent Sensors in Leaves Under Stress by Photoinhibition or UV Radiation. *Plant Cell Physiol.* **2002**, *43*, 1154–1164. [[CrossRef](#)]
87. Czégény, G.; Máta, A.; Hideg, É. UV-B effects on leaves—Oxidative stress and acclimation in controlled environments. *Plant Sci.* **2016**, *248*, 57–63. [[CrossRef](#)]
88. Agati, G.; Azzarello, E.; Pollastri, S.; Tattini, M. Flavonoids as antioxidants in plants: Location and functional significance. *Plant Sci.* **2012**, *196*, 67–76. [[CrossRef](#)] [[PubMed](#)]
89. Han, S.-H.; Park, Y.-J.; Park, C.-M. Light priming of thermotolerance development in plants. *Plant Signal. Behav.* **2019**, *14*, 1554469. [[CrossRef](#)]
90. Rehman, M.; Fahad, S.; Saleem, M.; Hafeez, M.; Rahman, M.; Liu, F.; Deng, G. Red light optimized physiological traits and enhanced the growth of ramie (*Boehmeria nivea* L.). *Photosynthetica* **2020**, *58*, 922–931. [[CrossRef](#)]
91. Bostancioglu, S.M.; Tombuloglu, G.; Tombuloglu, H. Genome-wide identification of barley MCs (metacaspases) and their possible roles in boron-induced programmed cell death. *Mol. Biol. Rep.* **2018**, *45*, 211–225. [[CrossRef](#)]
92. Sakuraba, Y. Light-Mediated Regulation of Leaf Senescence. *Int. J. Mol. Sci.* **2021**, *22*, 3291. [[CrossRef](#)] [[PubMed](#)]
93. Thwe, A.A.; Kim, Y.B.; Li, X.; Seo, J.M.; Kim, S.-J.; Suzuki, T.; Chung, S.-O.; Park, S.U. Effects of Light-Emitting Diodes on Expression of Phenylpropanoid Biosynthetic Genes and Accumulation of Phenylpropanoids in *Fagopyrum tataricum* Sprouts. *J. Agric. Food Chem.* **2014**, *62*, 4839–4845. [[CrossRef](#)] [[PubMed](#)]
94. Liu, Y.; Fang, S.; Yang, W.; Shang, X.; Fu, X. Light quality affects flavonoid production and related gene expression in *Cyclocarya paliurus*. *J. Photochem. Photobiol. B Biol.* **2018**, *179*, 66–73. [[CrossRef](#)] [[PubMed](#)]
95. Park, W.T.; Yeo, S.K.; Sathasivam, R.; Park, J.S.; Kim, J.K.; Park, S.U. Influence of light-emitting diodes on phenylpropanoid biosynthetic gene expression and phenylpropanoid accumulation in *Agastache rugosa*. *Appl. Biol. Chem.* **2020**, *63*, 25. [[CrossRef](#)]
96. Li, C.; Zhang, B. MicroRNAs in Control of Plant Development. *J. Cell. Physiol.* **2016**, *231*, 303–313. [[CrossRef](#)]
97. Kidner, C.A.; Martienssen, R.A. The developmental role of microRNA in plants. *Curr. Opin. Plant Biol.* **2005**, *8*, 38–44. [[CrossRef](#)]
98. Hsieh, L.-C.; Lin, S.-I.; Shih, A.C.-C.; Chen, J.-W.; Lin, W.-Y.; Tseng, C.-Y.; Li, W.-H.; Chiou, T.-J. Uncovering Small RNA-Mediated Responses to Phosphate Deficiency in *Arabidopsis* by Deep Sequencing. *Plant Physiol.* **2009**, *151*, 2120–2132. [[CrossRef](#)]
99. Luo, Q.-J.; Mittal, A.; Jia, F.; Rock, C.D. An autoregulatory feedback loop involving PAP1 and TAS4 in response to sugars in *Arabidopsis*. *Plant Mol. Biol.* **2012**, *80*, 117–129. [[CrossRef](#)]
100. Debernardi, J.; Rodriguez, R.; Mecchia, M.; Palatnik, J.F. Functional Specialization of the Plant miR396 Regulatory Network through Distinct MicroRNA–Target Interactions. *PLoS Genet.* **2012**, *8*, e1002419. [[CrossRef](#)]
101. Guo, X.-J.; Wang, J.-R. Global identification, structural analysis and expression characterization of bHLH transcription factors in wheat. *BMC Plant Biol.* **2017**, *17*, 90. [[CrossRef](#)]
102. Xie, Y.; Liu, Y.; Wang, H.; Ma, X.; Wang, B.; Wu, G.; Wang, H. Phytochrome-interacting factors directly suppress MIR156 expression to enhance shade-avoidance syndrome in *Arabidopsis*. *Nat. Commun.* **2017**, *8*, 348. [[CrossRef](#)] [[PubMed](#)]
103. Casati, P. Analysis of UV-B regulated miRNAs and their targets in maize leaves. *Plant Signal. Behav.* **2013**, *8*, e26758. [[CrossRef](#)] [[PubMed](#)]
104. Jia, X.; Ren, L.; Chen, Q.-J.; Li, R.; Tang, G. UV-B-responsive microRNAs in *Populus tremula*. *J. Plant Physiol.* **2009**, *166*, 2046–2057. [[CrossRef](#)] [[PubMed](#)]
105. Li, S.; Shao, Z.; Fu, X.; Xiao, W.; Li, L.; Chen, M.; Sun, M.; Li, D.; Gao, D. Identification and characterization of *Prunus persica* miRNAs in response to UVB radiation in greenhouse through high-throughput sequencing. *BMC Genom.* **2017**, *18*, 938. [[CrossRef](#)]
106. Zhao, H.; Chen, N.; Peng, Z.; Wang, L.; Gao, Z. Identification and Characterization of MicroRNAs in the Leaf of Ma Bamboo (*Dendrocalamus latiflorus*) by Deep Sequencing. *PLoS ONE* **2013**, *8*, e78755. [[CrossRef](#)]
107. Li, Y.; Varala, K.; Hudson, M.E. A survey of the small RNA population during far-red light-induced apical hook opening. *Front. Plant Sci.* **2014**, *5*, 156. [[CrossRef](#)]

108. Ferreres, F.; Andrade, P.; Valentão, P.; Gil-Izquierdo, A. Further knowledge on barley (*Hordeum vulgare* L.) leaves O-glycosyl-C-glycosyl flavones by liquid chromatography-UV diode-array detection-electrospray ionisation mass spectrometry. *J. Chromatogr. A* **2008**, *1182*, 56–64. [[CrossRef](#)]
109. Kuhnert, N.; Jaiswal, R.; Matei, M.F.; Sovdat, T.; Deshpande, S. How to distinguish between feruloyl quinic acids and isoferuloyl quinic acids by liquid chromatography/tandem mass spectrometry. *Rapid Commun. Mass Spectrom.* **2010**, *24*, 1575–1582. [[CrossRef](#)]
110. Masike, K.; Mhlongo, M.; Mudau, S.P.; Nobela, O.; Ncube, E.N.; Tugizimana, F.; George, M.J.; Madala, N.E. Highlighting mass spectrometric fragmentation differences and similarities between hydroxycinnamoyl-quinic acids and hydroxycinnamoyl-isocitric acids. *Chem. Cent. J.* **2017**, *11*, 29. [[CrossRef](#)]
111. Han, S.; Li, D.; Trost, E.; Mayer, K.F.; Vlot, A.C.; Heller, W.; Schmid, M.; Hartmann, A.; Rothballer, M. Systemic Responses of Barley to the 3-hydroxy-decanoyl-homoserine Lactone Producing Plant Beneficial Endophyte *Acidovorax radidis* N35. *Front. Plant Sci.* **2016**, *7*, 1868. [[CrossRef](#)]
112. Ghannam, A.; Alek, H.; Doumani, S.; Mansour, D.; Arabi, M.I.E. Deciphering the transcriptional regulation and spatiotemporal distribution of immunity response in barley to *Pyrenophora graminea* fungal invasion. *BMC Genom.* **2016**, *17*, 256. [[CrossRef](#)] [[PubMed](#)]
113. Shoeva, O.Y.; Mock, H.-P.; Kukoeva, T.V.; Börner, A.; Khlestkina, E.K. Regulation of the Flavonoid Biosynthesis Pathway Genes in Purple and Black Grains of *Hordeum vulgare*. *PLoS ONE* **2016**, *11*, e0163782. [[CrossRef](#)] [[PubMed](#)]
114. Cai, J.; Li, P.; Luo, X.; Chang, T.; Li, J.; Zhao, Y.; Xu, Y. Selection of appropriate reference genes for the detection of rhythmic gene expression via quantitative real-time PCR in Tibetan hulless barley. *PLoS ONE* **2018**, *13*, e0190559. [[CrossRef](#)] [[PubMed](#)]
115. Shagimardanova, E.; Gusev, O.; Bingham, G.E.; Levinskikh, M.A.; Sychev, V.N.; Tiansu, Z.; Kihara, M.; Ito, K.; Sugimoto, M. Oxidative Stress and Antioxidant Capacity in Barley Grown under Space Environment. *Biosci. Biotechnol. Biochem.* **2010**, *74*, 1479–1482. [[CrossRef](#)] [[PubMed](#)]
116. Parrott, D.L.; Martin, J.M.; Fischer, A.M. Analysis of barley (*Hordeum vulgare*) leaf senescence and protease gene expression: A family C1A cysteine protease is specifically induced under conditions characterized by high carbohydrate, but low to moderate nitrogen levels. *New Phytol.* **2010**, *187*, 313–331. [[CrossRef](#)]
117. Livak, K.J.; Schmittgen, T.D. Analysis of relative gene expression data using real-time quantitative PCR and the  $2^{-\Delta\Delta CT}$  Method. *Methods* **2001**, *25*, 402–408. [[CrossRef](#)]
118. Afgan, E.; Baker, D.; Batut, B.; van den Beek, M.; Bouvier, D.; Čech, M.; Chilton, J.; Clements, D.; Coraor, N.; Grüning, B.A.; et al. The Galaxy platform for accessible, reproducible and collaborative biomedical analyses: 2018 update. *Nucleic Acids Res.* **2018**, *46*, W537–W544. [[CrossRef](#)]
119. Robinson, M.D.; McCarthy, D.J.; Smyth, G.K. EdgeR: A Bioconductor package for differential expression analysis of digital gene expression data. *Bioinformatics* **2010**, *26*, 139–140. [[CrossRef](#)]
120. Van Bel, M.; Diels, T.; Vancaester, E.; Kreft, L.; Botzki, A.; Van De Peer, Y.; Coppens, F.; Vandepoele, K. PLAZA 4.0: An integrative resource for functional, evolutionary and comparative plant genomics. *Nucleic Acids Res.* **2018**, *46*, D1190–D1196. [[CrossRef](#)]

## Article

# Leaf Functional Traits in Relation to Species Composition in an Arctic–Alpine Tundra Grassland

Lena Hunt <sup>1</sup>, Zuzana Lhotáková <sup>1</sup>, Eva Neuwirthová <sup>1</sup>, Karel Klem <sup>2</sup>, Michal Oravec <sup>2</sup>, Lucie Kupková <sup>3</sup>,  
Lucie Červená <sup>3</sup>, Howard E. Epstein <sup>4</sup>, Petya Campbell <sup>5,6</sup> and Jana Albrechtová <sup>1,\*</sup>

<sup>1</sup> Department of Experimental Plant Biology, Faculty of Science, Charles University, Viničná 5, 12844 Prague, Czech Republic

<sup>2</sup> Global Change Research Institute, Czech Academy of Sciences, Bělidla 4a, 60300 Brno, Czech Republic

<sup>3</sup> Department of Applied Geoinformatics and Cartography, Faculty of Science, Charles University, Albertov 6, 12800 Prague, Czech Republic

<sup>4</sup> Department of Environmental Sciences, University of Virginia, Charlottesville, VA 22904, USA

<sup>5</sup> Goddard Earth Science Technology and Research (GESTAR) II, University of Maryland Baltimore County, Baltimore, MD 21250, USA

<sup>6</sup> Biospheric Sciences Laboratory, Building 33, NASA Goddard Space Flight Center, Greenbelt, MD 20771, USA

\* Correspondence: albrecht@natur.cuni.cz

**Abstract:** The relict arctic–alpine tundra provides a natural laboratory to study the potential impacts of climate change and anthropogenic disturbance on tundra vegetation. The *Nardus stricta*-dominated relict tundra grasslands in the Krkonoše Mountains have experienced shifting species dynamics over the past few decades. Changes in species cover of the four competing grasses—*Nardus stricta*, *Calamagrostis villosa*, *Molinia caerulea*, and *Deschampsia cespitosa*—were successfully detected using orthophotos. Leaf functional traits (anatomy/morphology, element accumulation, leaf pigments, and phenolic compound profiles), were examined in combination with in situ chlorophyll fluorescence in order to shed light on their respective spatial expansions and retreats. Our results suggest a diverse phenolic profile in combination with early leaf expansion and pigment accumulation has aided the expansion of *C. villosa*, while microhabitats may drive the expansion and decline of *D. cespitosa* in different areas of the grassland. *N. stricta*—the dominant species—is retreating, while *M. caerulea* did not demonstrate significant changes in territory between 2012 and 2018. We propose that the seasonal dynamics of pigment accumulation and canopy formation are important factors when assessing potential “spreader” species and recommend that phenology be taken into account when monitoring grass species using remote sensing.

**Keywords:** canopy; flavonoids; grasslands; orthophotos; phenolic compounds; remote sensing; secondary metabolism; SLA; species cover analysis; tundra



**Citation:** Hunt, L.; Lhotáková, Z.; Neuwirthová, E.; Klem, K.; Oravec, M.; Kupková, L.; Červená, L.; Epstein, H.E.; Campbell, P.; Albrechtová, J. Leaf Functional Traits in Relation to Species Composition in an Arctic–Alpine Tundra Grassland. *Plants* **2023**, *12*, 1001. <https://doi.org/10.3390/plants12051001>

Academic Editors: Elena Ormeño and Silvano Fares

Received: 17 January 2023

Revised: 19 February 2023

Accepted: 20 February 2023

Published: 22 February 2023



**Copyright:** © 2023 by the authors. Licensee MDPI, Basel, Switzerland. This article is an open access article distributed under the terms and conditions of the Creative Commons Attribution (CC BY) license (<https://creativecommons.org/licenses/by/4.0/>).

## 1. Introduction

The Czech Republic possesses a unique grassland ecosystem in the Krkonoše (Giant) Mountains. Since 1963, the area has been protected as a national park, and it was designated a United Nations Educational, Scientific, and Cultural Organization (UNESCO) biosphere reserve in 1992. Displaying characteristics of both sub-arctic and mountainous regions, the area has been designated Europe’s southernmost relict arctic–alpine tundra [1]. This unique habitat is home to many endemic, glacial relict, and rare species of high conservation value [2,3]. Anthropogenic disturbance has strongly influenced the Krkonoše alpine grasslands, where land was used for grazing livestock from the 9th century until the beginning of the 19th century [4,5]. In the second half of the 20th century, airborne ammonium, nitrate, sulfate, and chloride from air pollution led to widespread acidification of the Krkonoše ecosystems, including the arctic–alpine tundra [6], altering nutrient availability

and impacting species composition [7]. Alpine grasslands in general are also experiencing an increasing abundance of shrubs as high-elevation temperatures increase [8,9].

The Krkonoše grasslands have traditionally been dominated by dense tussocks of *Nardus stricta* L.—a short, relatively unpalatable grass known to be present in low-nutrient grazing areas—and provide habitat for endangered invertebrates and ground-nesting birds [2,10]. In the 1970s and 1980s, dolomitic limestone used in paving roads throughout the area resulted in changes in nearby soil pH from 3–3.6 to up to 8 [11]. *Deschampsia cespitosa* (L.) P.Beauv., a species resistant to mechanical damage, began spreading along the edges of hiking paths and roads, where trampling, soil compaction, mineral nutrient content, and increased soil pH created a new microhabitat [12,13]. Additionally, the cessation of traditional grassland management practices (grazing/cutting), combined with pollution-induced soil changes, spruce die-back, increased nitrogen deposition, and warming temperatures, has resulted in the expansion of *Calamagrostis villosa* J.F.Gmel., overtaking *N. stricta* territory [14–16]. This tall, defoliation-sensitive grass contributes to losses in species diversity in regions where it becomes dominant [17,18]. Competition among four species (*C. villosa*, *D. cespitosa*, *Molinia caerulea* Moench, and *N. stricta*) is of particular interest, as the conservation value of *Nardus* grasslands has become more apparent in recent years [2,19,20].

The growing season in the Krkonoše arctic–alpine tundra grassland is short (snow covers the area 180 days out of the year), and it is characterized by low temperatures in combination with high PAR (photosynthetically active radiation) and UV (ultraviolet) irradiance. High PAR in combination with low temperatures can result in the overproduction of ROS (reactive oxygen species), as the absorbed light energy exceeds what is required to drive photochemistry [21]. At high levels, oxidative stress occurs, with ROS damaging proteins, lipids, and nucleic acids and potentially leading to cell death [22]. Maintaining an equilibrium between the production of ROS and their scavenging by antioxidants is essential to plant survival.

Plants have developed a number of morphological/anatomical, physiological, and biochemical traits as mechanisms to avoid or cope with oxidative stress. These traits represent trade-offs between environmental resource availability and plant growth, survival, and reproduction [23]. Plant functional traits are increasingly used to develop mechanistic models predicting how ecological communities will respond to abiotic and biotic perturbations and how species will affect ecosystem function and services [24]. These can include growth properties that minimize irradiance exposure or increase the boundary layer in order to insulate the plant from the cold and reduce excess transpiration. The contents of chlorophyll and carotenoids indicate the capacity of a plant to engage in photosynthesis and safely dissipate excess photons [25,26]. Phenolic compounds (PheCs)—including anthocyanins, flavonoids, and phenolic acids—function as antioxidants and shield sensitive photosynthetic tissue from UV radiation in order to prevent ROS formation [27,28]. Additionally, PheCs can increase plant tolerance to stressors such as high light, high temperature, drought, heavy metal contamination, herbivores, and pathogens [29–31]. The widespread occurrence of PheCs in *Poaceae* makes them valuable chemical markers, as species and even genotypes have been shown to differ in their phenolic profiles [32].

As the climate changes, and microhabitats are created and destroyed, and the adaptive value of certain plant functional traits may also change, leading to changes in species composition [33]. Changes in species cover over the Krkonoše tundra grassland can be monitored remotely using different remote sensing methods, e.g., combinations of airborne and satellite data [34] or via orthophotos [35]. Pigment content, especially chlorophyll, can easily be detected using remote sensing methods, and it can serve as a proxy for plant health [36].

In this study, we compare the morphological, phenological, and biochemical traits of the four competing grass species in Krkonoše. As our work is intended to serve as a pilot study for the monitoring of grasslands using remote sensing (RS), we focused on leaf functional traits easily monitored by RS methods, specifically variations in pigment content



among the grass species throughout the growing season and how these variations could influence competition.

The aim of this work was to examine whether the expansion and retreat of grass species could be detected via orthophotos and to determine whether physiological and functional traits correspond to the expansion or decline of these species. We show the varying phenolic profiles of the four main Krkonoše grasses during the vegetative season and show the differences in the accumulation and histochemical localization of PheCs in leaf cross-sections. Furthermore, we present data about the stress status of the different species in homogenous stands. We use chlorophyll fluorescence to evaluate stress and tolerance to tundra conditions, and we present leaf element analysis in order to discuss how some species may be exploiting specific niches. We hypothesize that interspecific differences in plant functional traits could help to explain the expansion and retreat of grass species in the Krkonoše arctic–alpine tundra.

## 2. Results

### 2.1. Orthophotos Classifications

The main results of the orthophoto classifications from the years 2012 and 2018 are summarized in Table 1. The first area, “U Luční boudy,” meaning, “near the field house Luční bouda,” is a relatively high-traffic area, intersected by tourist walking paths. This area contains *D. cespitosa*, *M. caerulea*, and *N. stricta*, but not *C. villosa*. Wetlands, peat bogs, and water bodies are also present in this area. The overall accuracies for “U Luční boudy” reached ~80% for both years. The second area, “Bílá louka,” meaning, “white meadow,” is more undisturbed, set back from the walking paths and on a slight slope. This area contains *C. villosa*, *D. cespitosa*, and *N. stricta*, but not *M. caerulea*. It also contains an additional grass species, *Avenella flexuosa* (L.) Drejer. (For more details on the study area, see Section 4.1) The overall accuracies for “Bílá louka” were 78% for 2012 and 85% for 2018 (the relative changes in abundance in each area can be seen in the Figure 1). For both areas, the lowest accuracies for the studied grass species were for *D. cespitosa* due to high variability—sporadic flowering altered the reflectance. Especially in the “Bílá louka” area, the results for *D. cespitosa* were affected by low user accuracy, i.e., the class was overestimated in both years, particularly in 2012, so the decrease in area is lower than 10%. For *C. villosa*, we can confirm that its area increased ~9% between 2012 and 2018, because the class has good accuracy for both producers and users. Producer accuracy is the ratio between the correctly classified pixels and the pixels used for testing of a given class, i.e., real features on the ground. User accuracy describes the probability that a pixel assigned to a class on the map actually represents that class on the ground [37].

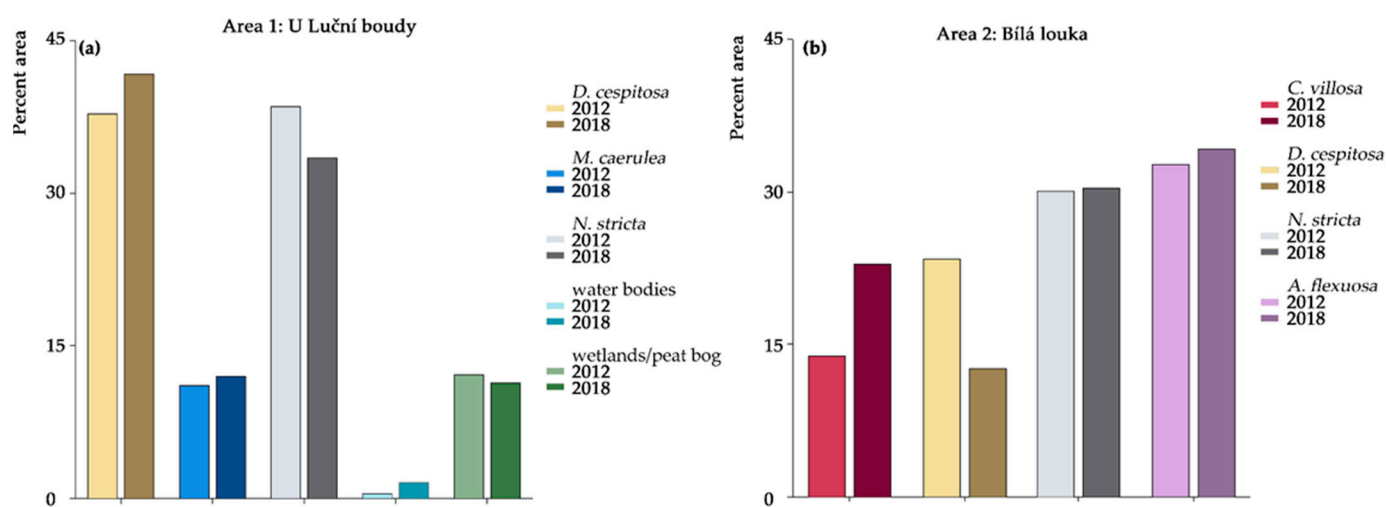
*N. stricta* decreased in the first area, “U Luční boudy,” although the decrease could be slightly overestimated, as the user accuracy in 2012 reached only ~78%. *N. stricta* remained stable in the second area, “Bílá louka” (similar accuracies for both years, lower producer accuracies between 75% and 80%). *M. caerulea* achieved good accuracies, apart from the producer accuracy for 2012 (68%), so it could be slightly underestimated in this year; overall we can say that this specie remained stable in the “U Luční boudy” area.

**Table 1.** Producer and user accuracies for classified species and the area of the species in 2012 and 2018 (PA = Producer accuracy, UA = user accuracy).

Area 1: U Luční Boudy						
class	Accuracies				Area in m <sup>2</sup>	
	2012		2018		2012	2018
	PA	UA	PA	UA		
<i>D. cespitosa</i>	79.05	90.84	75.12	85.89	4571.6	5042.9
<i>M. caerulea</i>	68.02	90.36	82.78	92.67	1341.9	1445.9
<i>N. stricta</i>	92.83	77.61	93.67	89.89	4660.8	4047.4
water bodies	93.44	64.77	70.59	34.53	58.1	183.4
wetlands and peat bogs	73.22	31.02	60.56	26.79	1466.0	1369.6

Area 2: Bílá Louka						
class	Accuracies				Area in m <sup>2</sup>	
	2012		2018		2012	2018
	PA	UA	PA	UA		
<i>C. villosa</i>	81.07	98.03	92.98	99.25	1628.3	2677.4
<i>D. cespitosa</i>	79.74	23.84	55.7	36.26	2751.9	1470.6
<i>N. stricta</i>	75.59	97.67	78.94	96.95	3529.0	3546.2
<i>A. flexuosa</i>	71.5	35.03	77.48	37.14	3845.2	4006.3

**Figure 1.** Relative area of the species in both studied areas in 2012 and 2018 based on the maximum likelihood classification of RGB orthophotos with a 25 cm pixel. Area 1: U Luční boudy (a); Area 2: Bílá louka (b).

## 2.2. Morphological Characteristics

The main aggressively spreading grass species—*C. villosa* and *M. caerulea* (which is also allegedly spreading [38], although it was not captured by our orthophotos from 2012–2018)—share similar anatomy and morphology. Both are tall grasses possessing flat or convolute leaves (Figure 2a,c, respectively). *C. villosa* has a pronounced midrib and pronounced adaxial segments, especially around larger vascular bundles (Figure 2a). *C. villosa* also notably has a layer of visible anthocyanins below the abaxial epidermis (Figure 2a,e). Details of the bulliform cells (bulbous epidermal cells found in most monocots that allow for leaf movement, i.e., curling of the leaf lamina inward around the midrib) of *C. villosa*, as well as abaxial anthocyanins can be seen in Figure 2f. *M. caerulea* has a smoother adaxial surface and sharper leaf margins than *C. villosa*. *M. caerulea* also has a less prominent midrib (it does not form a sharp point in cross-section as *C. villosa* does). Bulliform cells and small

protrusions in the epidermis, which contribute to an increased boundary layer, can be seen in Figure 2h.

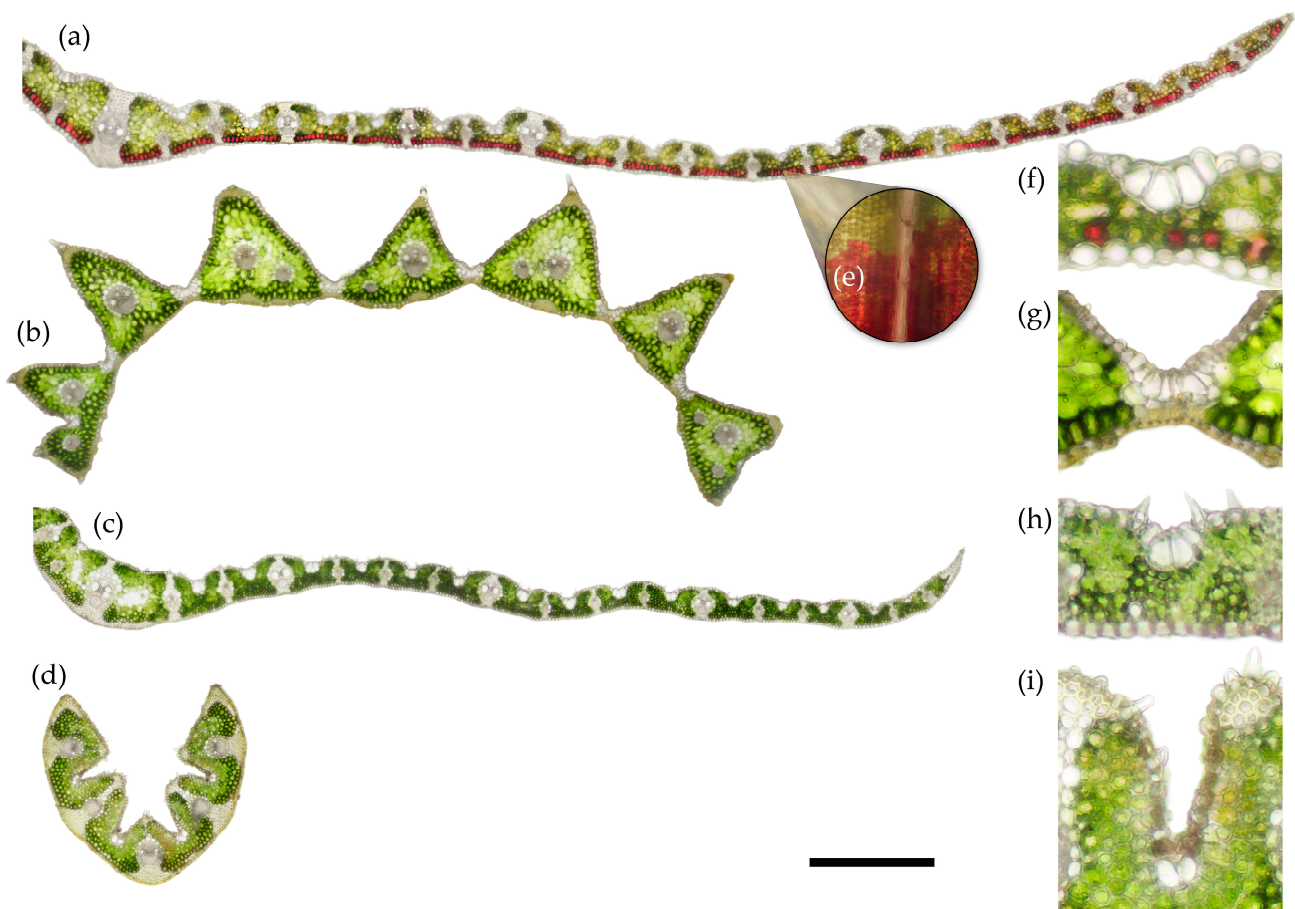


**Figure 2.** Representative unstained cross-sections of a fully developed leaf from each of the four competing grass species. The section was taken from the central part of the leaf blade in August 2020. Fresh hand sections, 70–80  $\mu\text{m}$  thick, imaged at 10 $\times$  magnification, bright field; the green color corresponds to mesophyll cells with chlorophyll, while the red color corresponds to vacuolar anthocyanins in mesophyll cells adjacent to abaxial epidermis. *Calamagrostis villosa* (half leaf) (a), *Deschampsia cespitosa* (b), *Molinia caerulea* (half leaf) (c), and *Nardus stricta* (d). The scale bar is equal to 0.5 mm. Detail of the anthocyanins in the abaxial mesophyll layer of *Calamagrostis villosa* shown in paradermal view at 10 $\times$  magnification (e). Bulliform cells of each species: *C. villosa* (f), *D. cespitosa* (g), *M. caerulea* (h), and *N. stricta* (i).

*D. cespitosa* appears to be a typical, flat-leaved grass when observed with the naked eye. Under the microscope, however, the structure of *D. cespitosa* is intermediary between the flat leaves of *C. villosa* and *M. caerulea* (Figure 2a,c) and the curled leaves of *N. stricta* (Figure 2d). The leaves of *D. cespitosa* lack an obvious midrib, and they are divided into triangular segments, each possessing 1–2 vascular bundles with the triangular tip on the adaxial side (Figure 2b). When unstressed, the leaves of *D. cespitosa* open flat or curl slightly outward towards the abaxial side (involute), however the bulliform cells enable the leaves to curl inwards in times of stress, thus lowering the incident radiation and transpirational water loss. Unlike the other species, the bulliform cells of *D. cespitosa* fully connect the adaxial and abaxial leaf surfaces, creating a hinge-like effect that allows for a wide range of motion (Figure 2g). The leaves of *D. cespitosa* are wider than those of *N. stricta*, but they are less than half the width of the other two grasses.

The morphology of *N. stricta* is distinct from the other grasses growing in the Krkonoše tundra grassland. The leaves are small and narrow, macroscopically needle-like, with margins rolled inward to the adaxial (upper) side of the leaf (Figure 1d). The leaves of *N. stricta* develop revolute, without the possibility of fully expanding. As the leaf develops from June to August, the adaxial side of the leaf expands, allowing for slight opening, however the leaves of *N. stricta* remain distinctly curled inward over the adaxial surface throughout their lifetime. Details of the bulliform cells and the abaxial epidermal protrusions are shown in Figure 2i.

Functional leaf traits were measured based on morphological/structural and physiological parameters during the vegetative season in 2020. *C. villosa* has the highest specific leaf area (SLA) of the four species, followed by *M. caerulea*. Both species displayed dynamic changes in SLA over the growing season (Figure 3). The SLA of *C. villosa* decreased at the end of the season (August), while *M. caerulea* reached peak SLA in July and August (Figure 3b). Both *N. stricta* and *D. cespitosa* have low SLA (statistically insignificant from each other), with no discernable variation throughout the growing season (Figure 3).

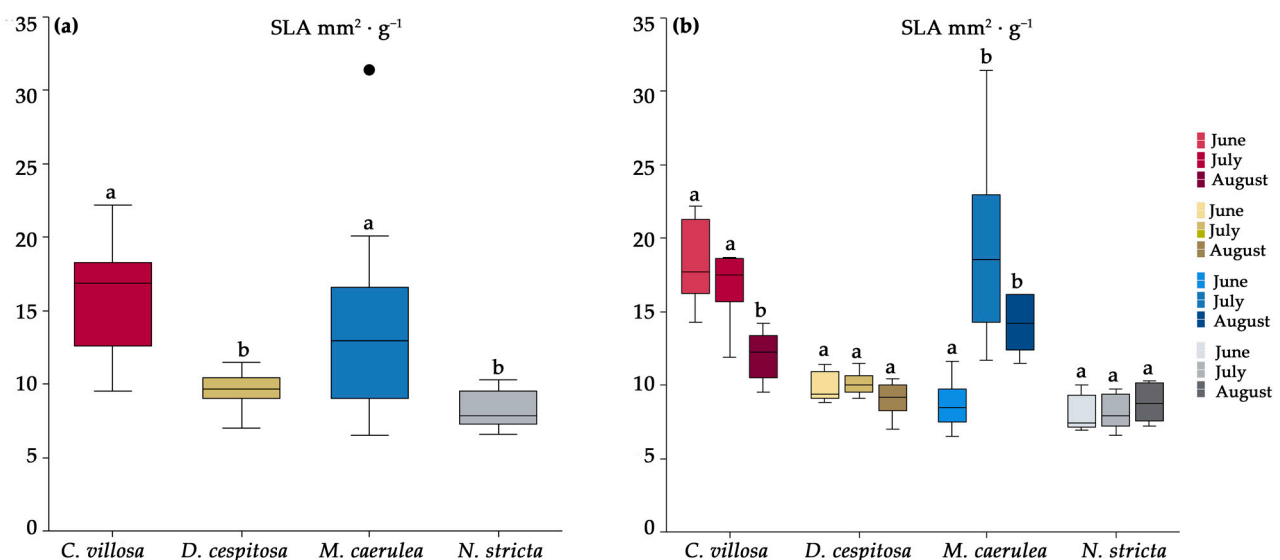


**Figure 3.** The specific leaf area (SLA) for *Calamagrostis villosa* (red boxes), *Deschampsia cespitosa* (yellow boxes), *Molinia caerulea* (blue boxes), and *Nardus stricta* (grey boxes), measured in 2020 and averaged over the growing season (a) and by month (b);  $n = 6$  per species per month. Medians (central line); 25 and 75 percentiles (boxes); 1.5 interquartile range (error bars); and outliers (dots) are indicated. Different letters denote significance  $\alpha = 0.05$  (one-way ANOVA and Tukey–Kramer post-hoc test).

The percentages of mesophyll tissue (see the green tissue with chloroplasts in Figure 2) and epidermis and vascular bundles (including sclerenchyma as non-photosynthetic structural tissue) were assessed on leaf cross sections of the studied species. *N. stricta* and *D. cespitosa*, with low SLA and rather curled leaves, contained more photosynthetic tissue (mesophyll) on cross-sections than *M. caerulea* and *C. villosa* (Table 2).

**Table 2.** The percentage of mesophyll, epidermis and vascular bundles including sclerenchyma on the leaf cross section. Mean and standard deviation (in brackets); different letters denote significant difference at  $\alpha = 0.05$  according to one-way ANOVA and Tukey–Kramer test. N = 6 for *C. villosa*, *D. cespitosa*, and *N. stricta*; n = 5 for *M. caerulea*.

Species	Mesophyll %	Epidermis %	Vascular Bundles Including Sclerenchyma %
<i>C. villosa</i>	46.6 (7.6) b	35.0 (4.9) a	17.9 (4.4) a
<i>D. cespitosa</i>	62.0 (4.3) a	30.8 (3.5) a	7.0 (0.6) b
<i>M. caerulea</i>	44.0 (3.9) b	33.6 (1.1) a	22.2 (3.3) a
<i>N. stricta</i>	60.0 (2.7) a	22.2 (2.2) b	17.5 (1.4) a

### 2.3. Histochemistry

Even without histochemical staining, it was possible to observe the presence of anthocyanins in *C. villosa* on both intact leaves and in cross sections (Figure 2a,e). The visible anthocyanins were localized in the layer of mesophyll cells adjacent to the abaxial epidermis. The distribution of abaxial anthocyanins was not consistent but rather occurred in patches, with clusters of mesophyll cells displaying mainly green chlorophyll in chloroplasts, and other clusters displaying red anthocyanins in vacuoles (see the paradermal view, Figure 2e). Although anthocyanins were detected biochemically in all of the sampled grass leaves (see Section 2.4), only *C. villosa* displayed a concentrated localization of anthocyanins in the leaf, visible to the naked eye as a patchy purple coloration of leaves, and observable as a layer of red-colored mesophyll cells via brightfield microscopy.

Lignin was detected as a pink coloration only in the vascular bundles via phloroglucinol-HCl in all species (Figure 4a,e,i,m); it can also be observed as blue fluorescence in cell walls under UV light (Figure 4c,g,k,o). *C. villosa* showed lignified sclerenchyma supporting minor vascular bundles (Figure 4a); however, lignin only occurred in the vascular bundles (xylem) in the other species (Figure 4e,i,m). The structural tissues present are therefore unlignified sclerenchyma in *D. cespitosa*, *M. caerulea*, *N. stricta*. Condensed tannins, which should appear red when treated with vanillin-HCl, were not found in any species (Figure 4b,f,j,n). The distribution of PheCs is visible as yellow fluorescence when treated with diphenylboric acid 2-amino ethyl ester (DPBA). In *C. villosa* and *M. caerulea*, the PheC distribution was homogenous throughout the mesophyll (Figure 4c,k), and it was more spatially variable in *D. cespitosa* and *N. stricta*. For *D. cespitosa*, there was a stronger adaxial (top) localization of PheC fluorescence; the brightest fluorescence occurred on the tips and sides of the triangular leaf segments that comprise the *D. cespitosa* leaf (Figure 4g,h). By contrast, the abaxial side tended to have stronger fluorescence in *N. stricta*, likely because the adaxial side was curled inwards, so the abaxial (bottom) side receives more exposure to irradiation (Figure 4o,p).

### 2.4. Biochemical Profiles

The total content of anthocyanins, carotenoids, phenolics, and chlorophyll a + b was analyzed using biochemical and spectrophotometrical techniques (see Section 4.3). Significant differences were found for chlorophyll and total anthocyanins, while the total carotenoids and total phenolics did not differ among the species (Figure 5). *N. stricta* accumulated significantly less chlorophyll per leaf dry mass than *D. cespitosa* and *M. caerulea* and fewer total anthocyanins than *D. cespitosa* (Figure 5b). This low chlorophyll content could contribute to the lower palatability of *N. stricta* leaves.

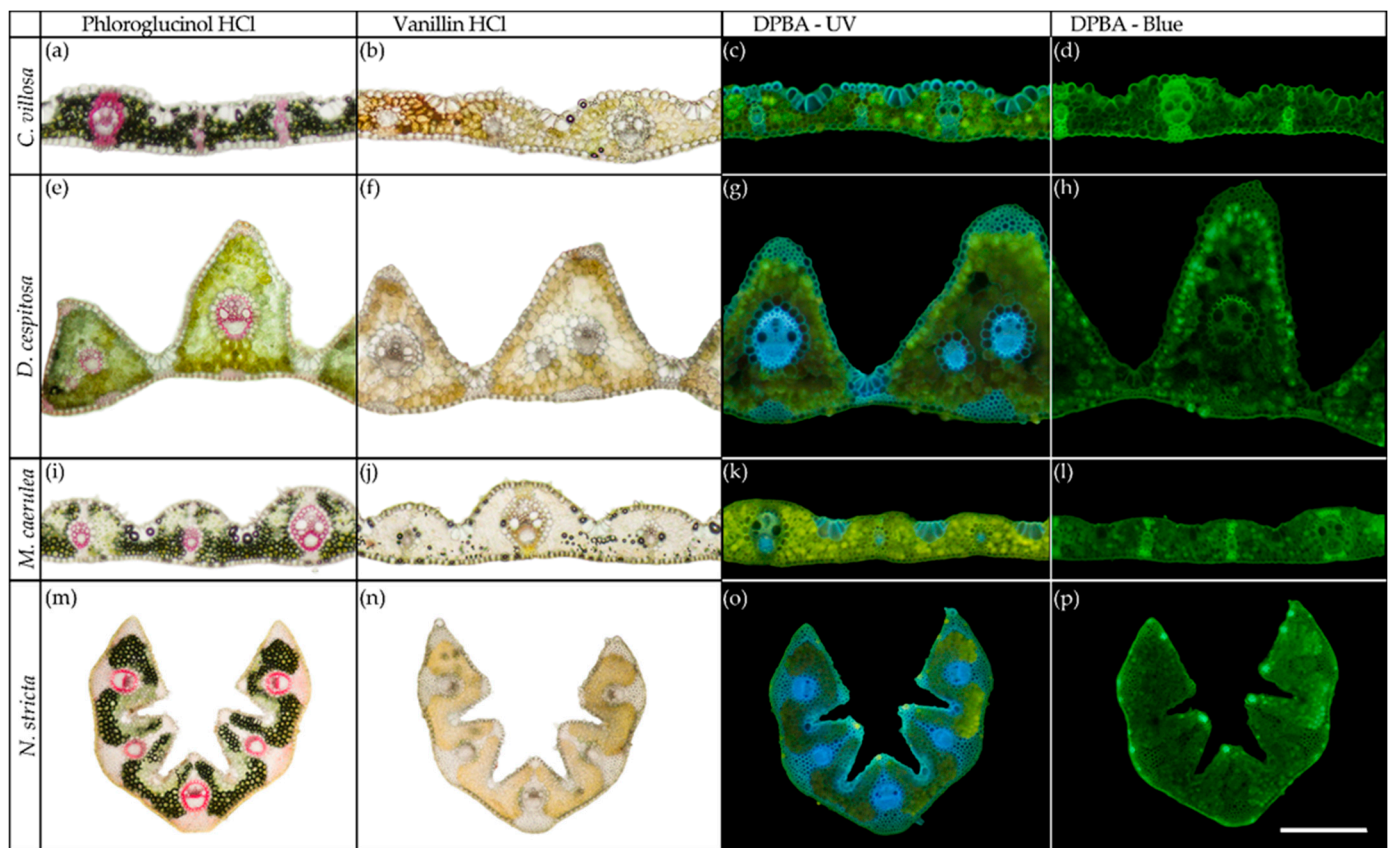


**Figure 4.** Representative cross-sections of fully developed leaves (August 2020) from the four competing grass species: *Calamagrostis villosa* [first row: (a–d)], *Deschampsia cespitosa* [second row: (e–h)], *Molinia caerulea* [third row: (i–l)], and *Nardus stricta* [fourth row: (m–p)]. The sections were taken from the central part of the leaf blades in August 2020. Histochemical tests: Phloroglucinol-HCl (first column: a,e,i,m) stains lignified cell walls pink, vanillin-HCl (second column: b,f,j,n) stains condensed tannins red, Naturstoff reagent A (DPBA) enhances yellow autofluorescence of flavonoids and blue autofluorescence of lignins and cell-wall-bound ferulic acid in UV light (third column: c,g,k,o) and (fourth column: d,h,l,p) enhances the yellow and green fluorescence of phenolic compounds in blue light excitation. The scale bar is equal to 0.5 mm.

The total contents of anthocyanins, carotenoids, phenolics, and chlorophyll a + b were also evaluated throughout the vegetative season (June–August) in 2020 in order to make observations of the dynamics of accumulation. In *C. villosa*, carotenoids (Figure 6a) and chlorophyll (Figure 6b) showed decreasing concentrations from the start of the season to the end of the season. The total anthocyanins were undynamic (Figure 6c), however, the total phenolics for *C. villosa* significantly increased between June and July, and they remained elevated in August. *C. villosa* was the only species to demonstrate a significant increase in total phenolics; the others maintained relatively fixed concentrations throughout the growing season (Figure 6d). *D. cespitosa* did not show any significant changes in pigment content over the growing season (Figure 6). *M. caerulea* displayed the opposite trend to *C. villosa*, significantly increasing carotenoids (Figure 6a), chlorophyll (Figure 6b), and total anthocyanins (Figure 6c) mid-season. *N. stricta* showed no seasonal dynamics in pigment content (Figure 6).

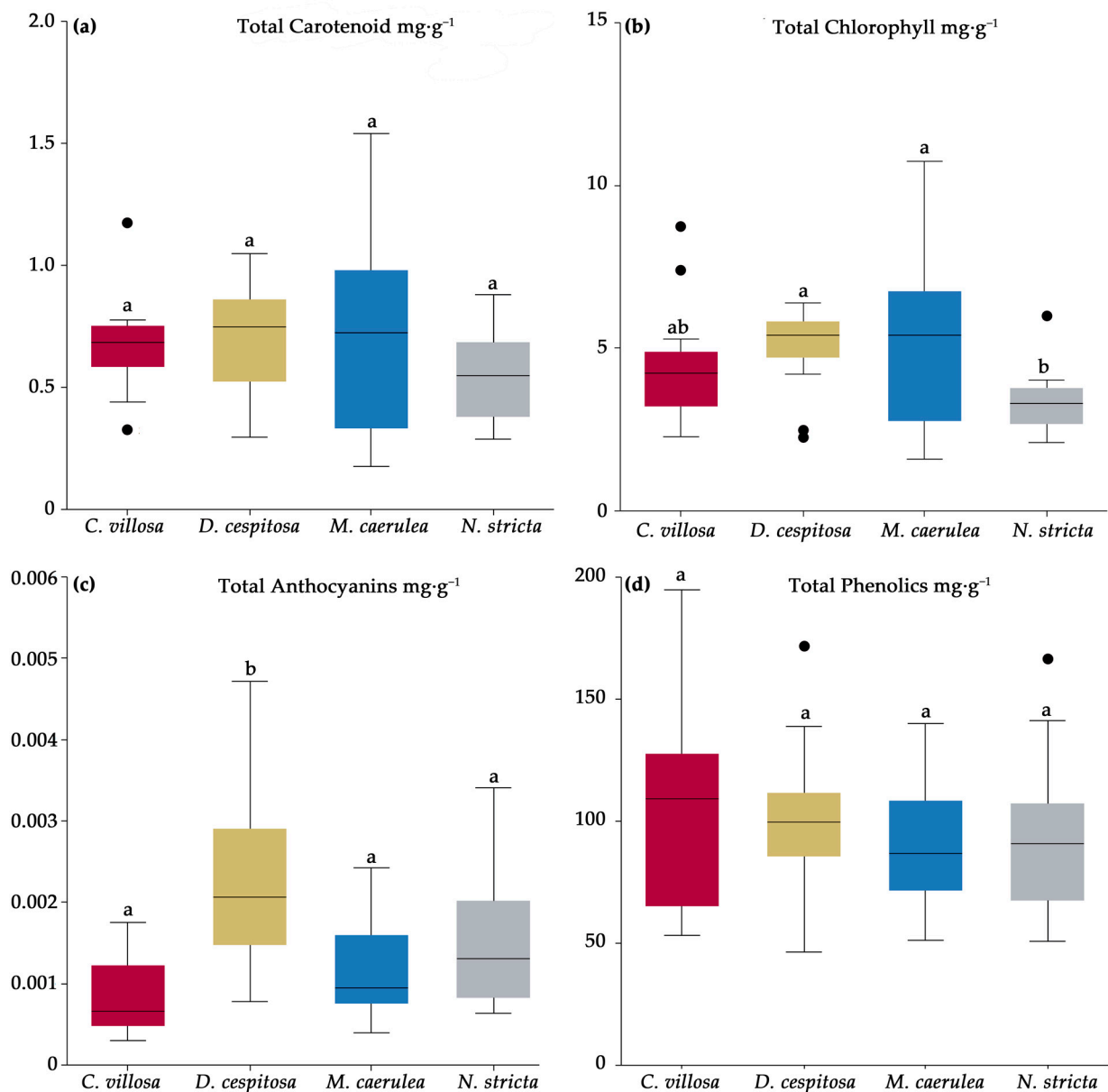


**Figure 5.** Total pigments of carotenoids (a), chlorophylls (b), anthocyanins (c), and phenolics (d) for *Calamagrostis villosa* (red boxes), *Deschampsia cespitosa* (yellow boxes), *Molinia caerulea* (blue boxes), and *Nardus stricta* (grey boxes), measured in 2020 and averaged over the growing season;  $n = 18$  per species. Medians (central line); 25 and 75 percentiles (boxes); 1.5 interquartile range (error bars); and outliers (dots) are indicated. Different letters denote significance,  $\alpha = 0.05$  (One-way ANOVA and Tukey–Kramer post-hoc test).

HPLC-HRMS (high-performance liquid chromatography–high-resolution mass spectroscopy) was used to detect the specific PheCs occurring in the four grasses studied. Fifteen PheCs were consistently found in all samples. Of the main PheCs, five were hydroxycinnamic acids (chlorogenic acid, ferulic acid, caffeic acid, sinapic acid, and 3-coumaric acid), five were hydroxybenzoic acids (3-hydroxybenzoic acid, vanillic acid, syringic acid, protocatechuic acid, and gallic acid), and five were flavonoids (saponarin, luteolin, isovitexin, homoorientin, and apigenin). Due to technical constraints, individual anthocyanins were not identified. *C. villosa* showed high levels of all of the hydroxycinnamic acids tested, except for sinapic acid. *C. villosa* was significantly higher in chlorogenic and caffeic acid levels compared to all other species (Figure 7a,d). For several compounds, *C. villosa* was higher

than the other species except *M. caerulea*: ferulic acid, protocatechuic acid, homoorientin, luteolin, and apigenin (Figure 7c,g,h,j,l). *M. caerulea* had significantly higher isovitexin levels compared to the other species (Figure 7b). *M. caerulea* also showed higher sinapic acid levels compared to the other species, except *D. cespitosa* (Figure 7f), but an otherwise low accumulation of phenolic acids. *D. cespitosa* accumulated mainly hydroxybenzoic acids and had higher levels of syringic and gallic acids compared to *N. stricta* and *M. caerulea* (Figure 7k,m) and higher levels of vanillic acid compared to *N. stricta* (Figure 7i). In all cases, *C. villosa* and *D. cespitosa* did not significantly differ in terms of hydroxybenzoic acid accumulation (Figure 7j,k,m). *N. stricta* did not differ from other species in the amount of any tested phenolic compound. While *N. stricta* did show a higher mean saponarin level, due to variability, it did not differ significantly from the other species (Figure 7e). The compounds saponarin, 3-hydroxybenzoic acid, and 3-coumaric acid were accumulated in all species and without significant differences (Figure 7e,n,o).

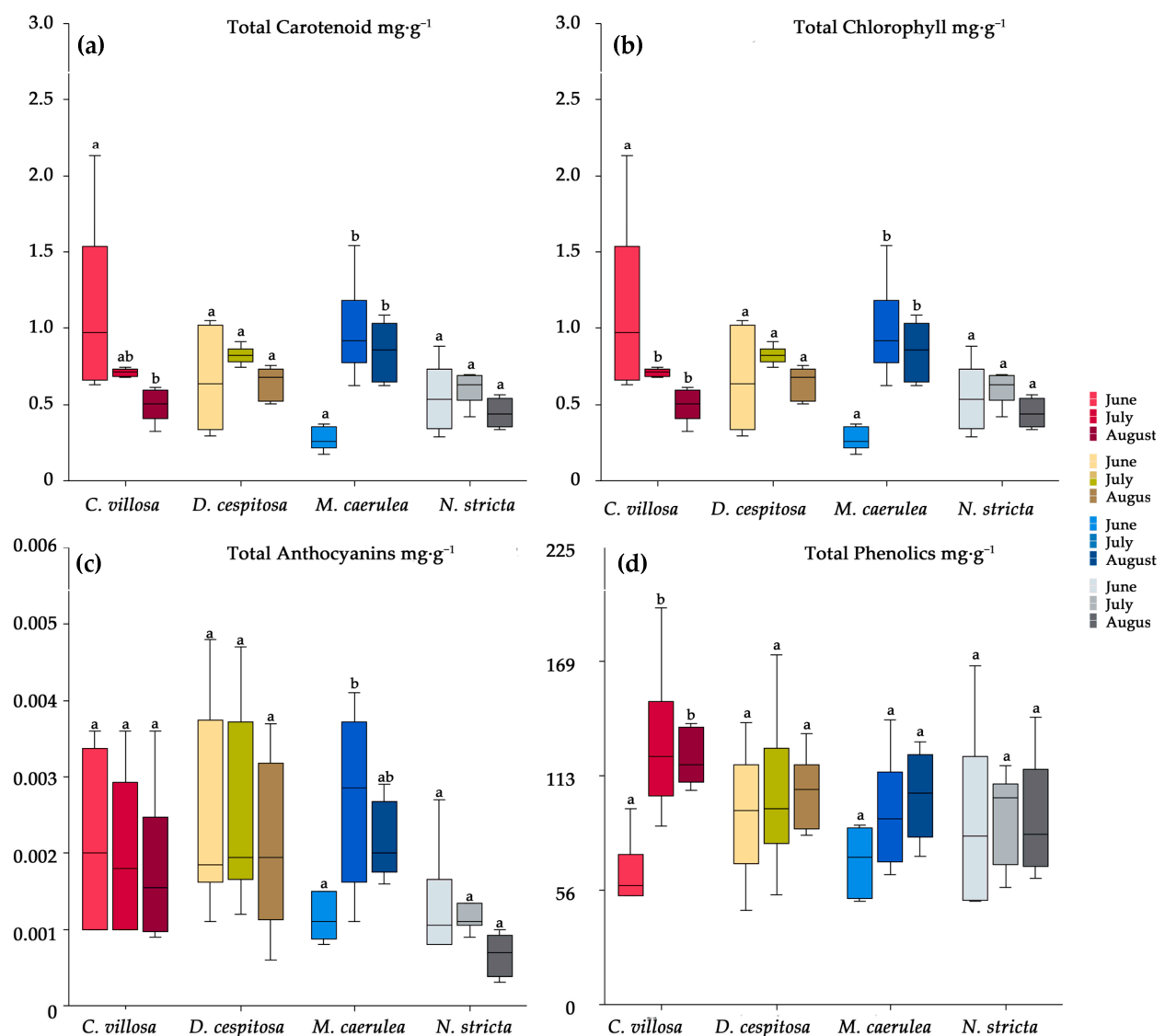


**Figure 6.** The seasonal dynamics of total carotenoids (a), chlorophyll (b), anthocyanins (c), and phenolics (d) for *Calamagrostis villosa* (red boxes), *Deschampsia cespitosa* (yellow boxes), *Molinia caerulea* (blue boxes), and *Nardus stricta* (grey boxes) measured in 2020;  $n = 6$  per species per month. Medians (central line); 25 and 75 percentiles (boxes); 1.5 interquartile range (error bars). Different letters denote significance according to the Kruskal–Wallis multiple-comparison Z-value test ( $\alpha = 0.05$ ) across species.



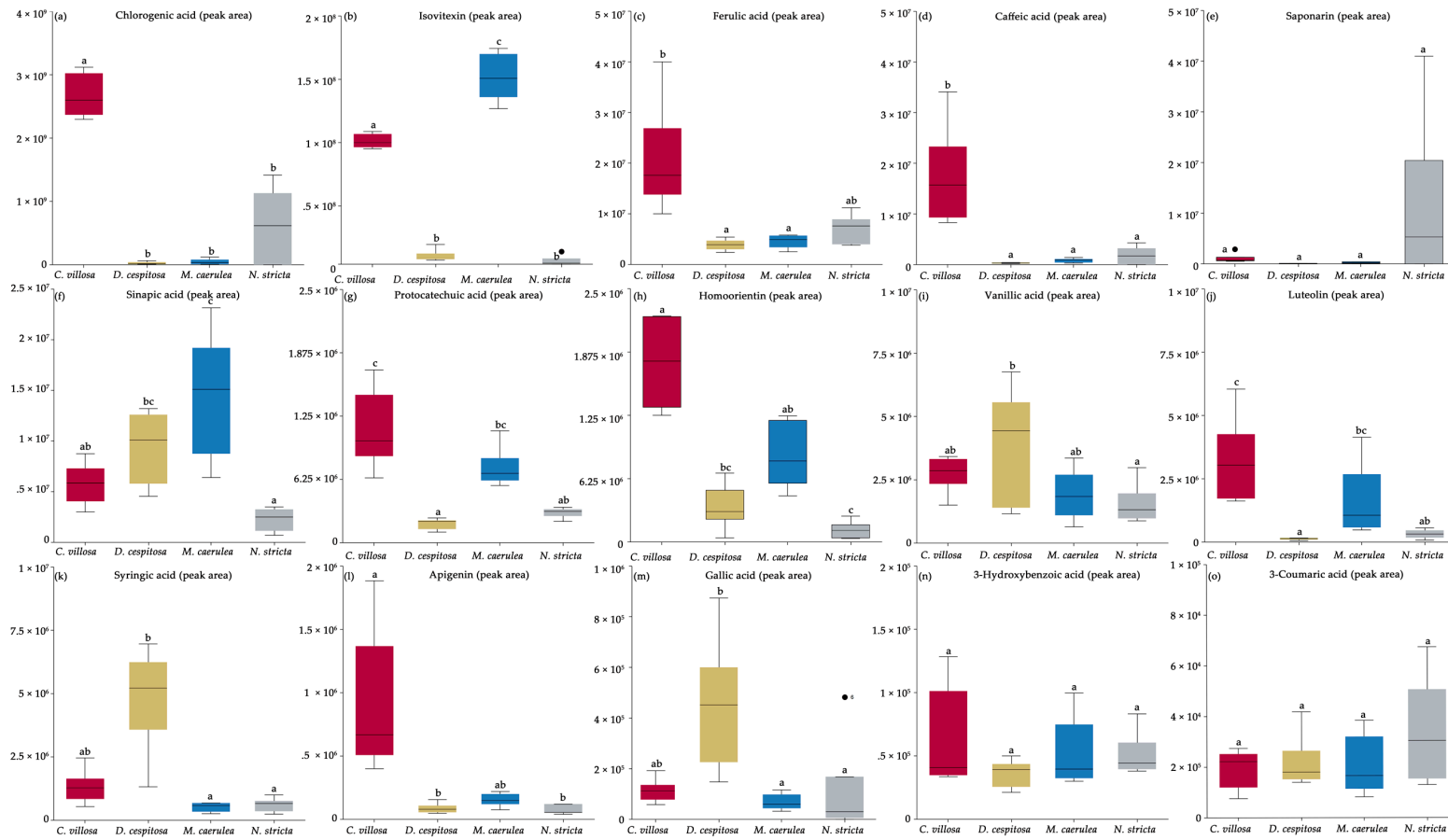


**Figure 7.** The accumulation of the most abundant phenolics in the four competing grass species from this study: *Calamagrostis villosa* (red boxes), *Deschampsia cespitosa* (yellow boxes), *Molinia caerulea* (blue boxes), and *Nardus stricta* (grey boxes). The PheC levels are expressed as the peak area corresponding to each PheC normalized based on the peak area of respective standard. Chlorogenic acid (a), Isovitexin (b), Ferulic acid (c), Caffeic acid (d), Saponarin (e), Sinapic acid (f), Protocatechuic acid (g), Homoorientin (h), Vanillic acid (i), Luteolin (j), Syringic acid (k), Apigenin (l), Gallic acid (m), 3-Hydroxybenzoic acid (n), 3-Coumaric acid (o). The means are presented ( $n = 6$  per species). Different letters of the identical color above boxes indicate statistically significant differences between means (among species) tested by Kruskal–Wallis multiple-comparison Z-value test ( $\alpha = 0.05$ ) across species.

Principal component analysis was applied to phenolic compounds present in all of the studied species. The results show (Figure 8) that PheCs profiles are species-specific, as the scores clustered according to species. PC1 explained 39% of PheCs variability and was mainly driven by the contents of chlorogenic acid, isovitexin, ferulic, protocatechuic and caffeic acids, luteolin, homoorientin, and apigenin (all positively correlated). The abundance of these compounds is also closely associated with the species *C. villosa*, which separated remarkably from the rest of the species along PC1. PC2 explained an additional 17% of the PheC variability and was driven mainly by the contents of 3-coumaric acid and saponarin (positively correlated) and gallic, syringic, vanillic, and sinapic acids (negatively correlated). *N. stricta* formed a distinct cluster characterized by high contents of p-coumaric acid and saponarin. The 3-hydroxybenzoic acid content contributed to both PC1 and PC2 almost equally. *M. caerulea* scores occupied the position in the center of the coordinate system.

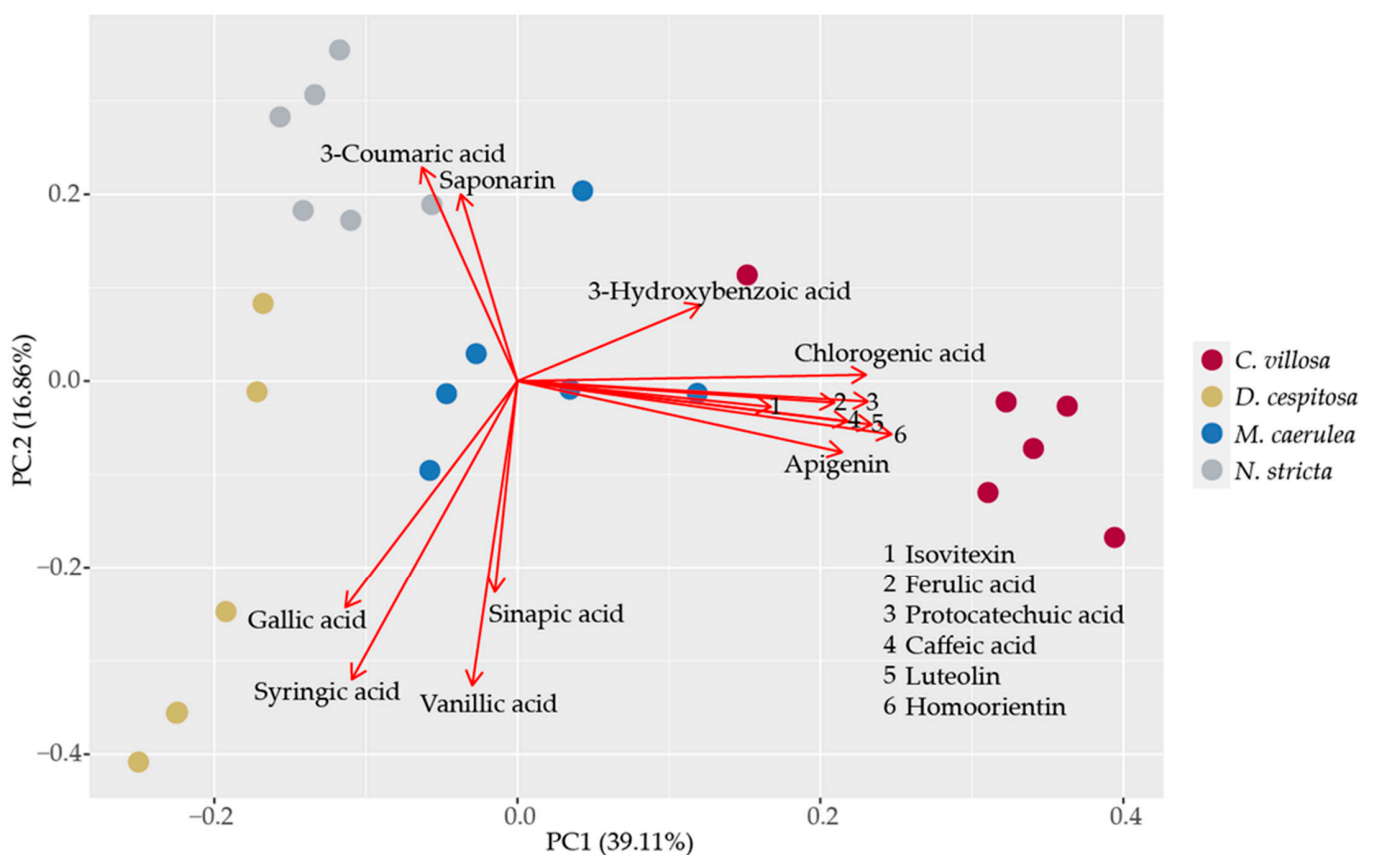


**Figure 8.** Principal component analysis of the most abundant phenolic compounds in all of the studied species. The points correspond to sample scores and are color-coded by species: *Calamagrostis villosa* (red dots), *Deschampsia cespitosa* (yellow dots), *Molinia caerulea* (blue dots), and *Nardus stricta* (grey dots). Red arrows correspond to PCA loadings for individual PheCs. Data from August 2021 were included in the analysis.

### 2.5. Leaf Element Composition

The leaf element composition averaged for June, July, and August 2020 is presented in Table S1. The principal component analysis was applied to the element composition of grass leaves in order to reveal whether their nutrition demands contributed to their mutual competition (Figure 9). The first two components explained 74.0% of the variability: PC1 and PC2, 50.6% and 23.4%, respectively. The phosphorus and nitrogen contents and C:N and N:P ratios mainly contributed to PC1. The carbon and calcium contents drove PC2. The potassium and magnesium contents contributed equally to both PC1 and PC2. The

species' separation was not so obvious; however, we still can find some patterns: Mg, C, Ca, N, P, and their ratio (N:P) are the main separators of *D. cespitosa* and *N. stricta*. *D. cespitosa* separated from the other species mainly due to higher Mg and P contents and low N:P ratio. *N. stricta* scores are located exactly on the opposite side of the PC1–PC2 space, showing low Mg and Ca contents, a high N:P ratio and a rather high C:N ratio. This pattern corresponds to the roles of *N. stricta* and *D. cespitosa* as coexisting but not necessarily competing species. The distribution may be dependent upon microhabitats for *D. cespitosa* (higher Mg and pH demands), as was mentioned in the introduction. The scores for *M. caerulea* and *C. villosa* share the common space, the latter also overlapping with *N. stricta*. This pattern in leaf element composition may indicate that *M. caerulea* and *C. villosa* compete for most nutrients, while for N and P, *C. villosa* competes more with *N. stricta* than *M. caerulea*.

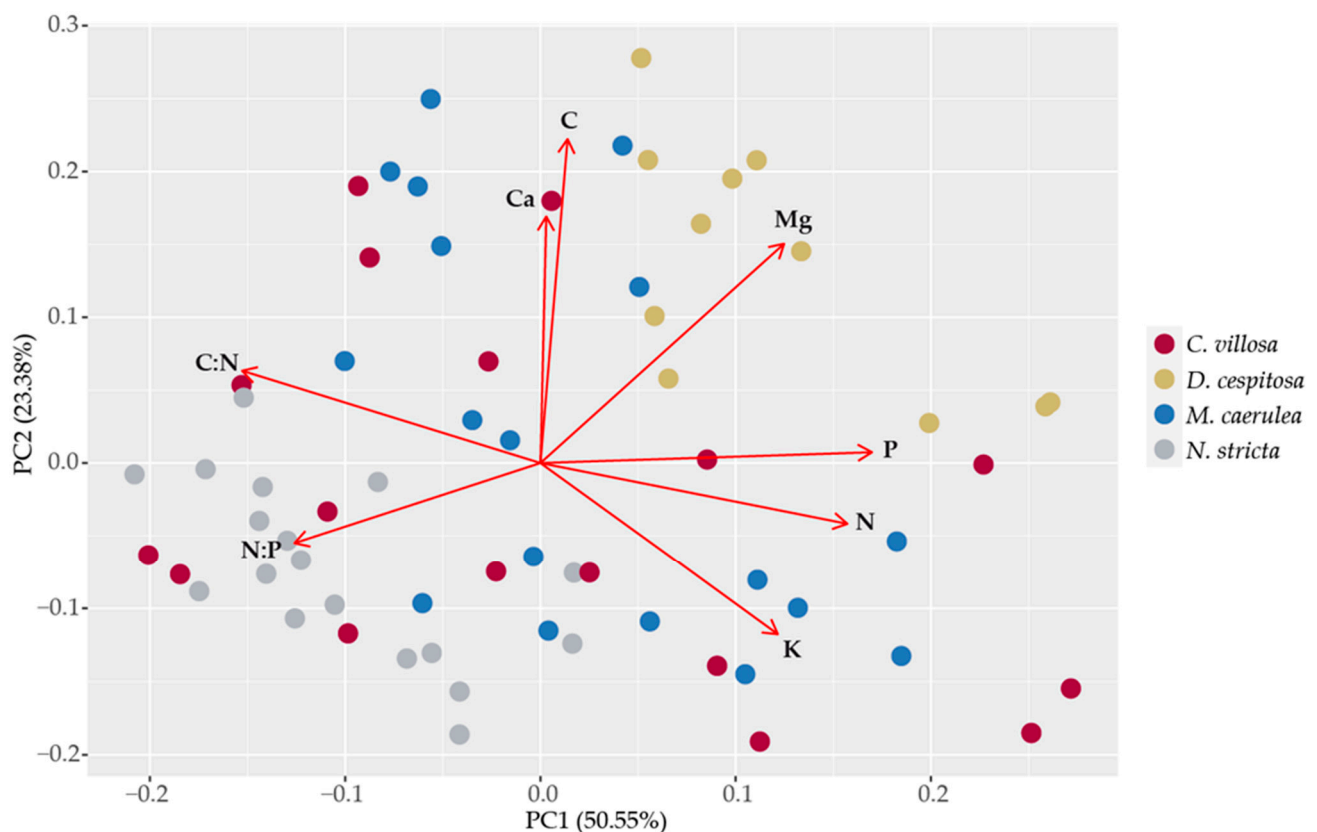


**Figure 9.** Principal component analysis of the leaf element composition. The points correspond to sample scores and are color-coded by species: *Calamagrostis villosa* (red dots), *Deschampsia cespitosa* (yellow dots), *Molinia caerulea* (blue dots), and *Nardus stricta* (grey dots). Red arrows correspond to PCA loadings for individual PheCs. Data from all vegetative seasons in 2020 were included in the analysis.

## 2.6. Chlorophyll Fluorescence

The chlorophyll fluorescence parameters  $F_v/F_m$  and  $\Delta V_{ip}$  are shown in Figure 10. The parameter  $F_v/F_m$  correlates to the maximum quantum yield of photosystem (PS) II photochemistry. It is calculated by dividing variable fluorescence by maximum fluorescence.  $F_v/F_m$  has a consistent value of  $\sim 0.83$  in non-photoinhibited, non-stressed leaves [38–41]. While all four grass species showed signs of photoinhibition and stress, *N. stricta* had the highest value at 0.73, significantly higher than *D. cespitosa* and *M. caerulea* (Figure 10a). *C. villosa*, *D. cespitosa*, and *M. caerulea* had values of 0.69, 0.67, and 0.67, respectively. The  $F_v/F_m$  values were constant over the season for all species except *D. cespitosa*, which had a significant increase in August. The data indicate that *N. stricta* was the least stressed, while *D. cespitosa* and *M. caerulea* were the most stressed.

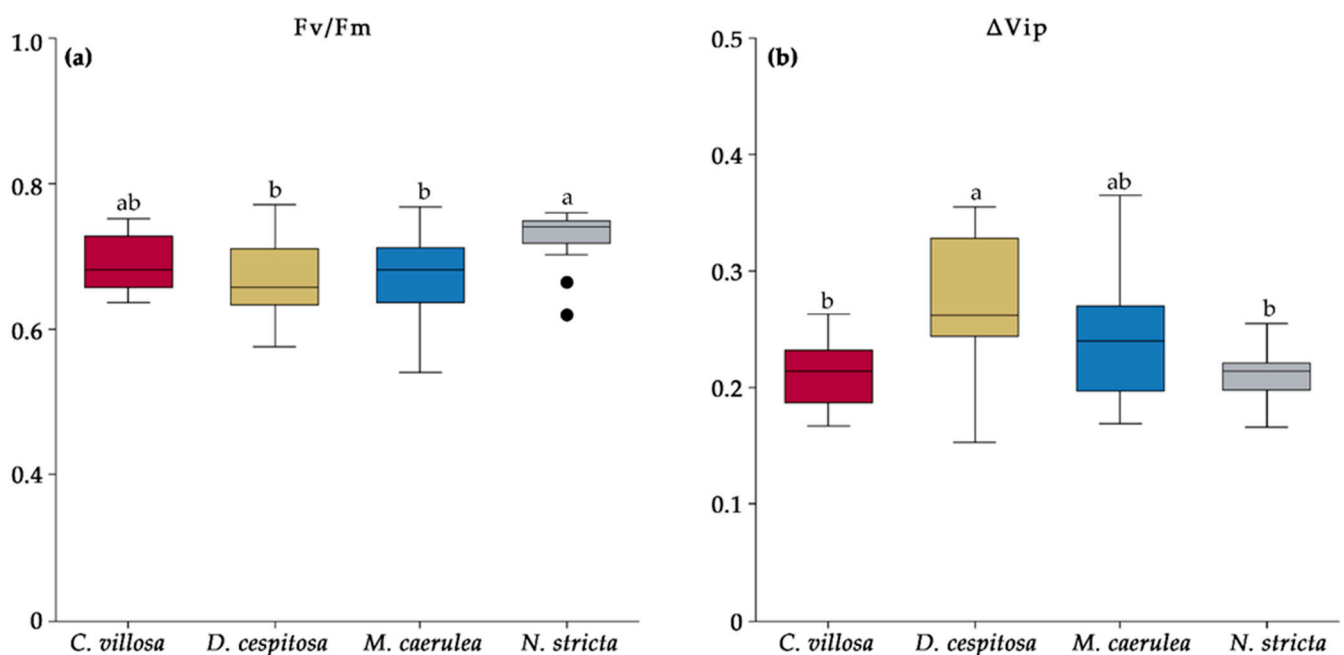


**Figure 10.** The chlorophyll fluorescence parameters Fv/Fm (a) and  $\Delta V_{ip}$  (b) measured in the four competing grass species from this study—*Calamagrostis villosa* (red boxes), *Deschampsia cespitosa* (yellow boxes), *Molinia caerulea* (blue boxes), and *Nardus stricta* (grey boxes)—as measured in 2020 and averaged over the growing season;  $n = 18$  (i.e., 6 measurements per species per month—June, July, and August). Medians (central line); 25 and 75 percentiles (boxes); 1.5 interquartile range (error bars); and outliers (dots) are indicated. Different letters denote significance  $\alpha = 0.05$  (one-way ANOVA and Tukey–Kramer post-hoc test).

Another parameter,  $\Delta V_{ip}$ , represents the relative increase in fluorescence between the I and P steps (the thermal phase) in the OJIP curve, correlates with the efficiency of electron flow to photosystem I (PSI) [42], and is higher in samples with greater PSI levels [43]. Elevated  $\Delta V_{ip}$  is associated with environmental stressors, such as salinity [44], drought [45], UV [46], and nutrient deficiencies [43], and it was the highest for *D. cespitosa*. The  $\Delta V_{ip}$  was significantly lower for *C. villosa* and *N. stricta* compared to *D. cespitosa*, while *M. caerulea* did not differ from the other species (Figure 10b), a similar trend to the Fv/Fm. The  $\Delta V_{ip}$  remained constant throughout the season for all of the species except *N. stricta*, which had an insignificant increase in July over June and a significant decrease in August (i.e., stress peaked in July for *N. stricta*).

### 3. Discussion

Species-rich, *N. stricta*-dominated grasslands occur widely throughout Europe and provide essential habitat for rare and endemic species [2]. Long-term pastoral traditions initiated these semi-natural habitats, with grazing animals selectively avoiding the low palatability of *N. stricta* leaves [47]. Recently, changes in land-use [2], land abandonment [48], and increased nutrient availability [49] and soil pH [48], alongside warming temperatures, have threatened the stability of *N. stricta*-dominated grasslands. Data from orthophotos (Figure 1) indicate the retreat of *N. stricta* and the spread of *C. villosa*. They show that *N. stricta* has decreased in total coverage in the highly trafficked U Luční boudy area (although it has not visibly decreased since 2012 in the more remote Bílá louka area). This supports the idea that anthropogenic disturbance plays a partial role in the decline of *N. stricta*. Our data also show an increase in *C. villosa* in Bílá louka (Figure 1). When utilizing remote sensing, results can be influenced by seasonal dynamics. In order to avoid potential phenological changes which might alter classification results, the dates of image acquisition were kept similar (8 July 2012 and 5 July 2018). The final areas of classified

species are further influenced by classification accuracies. As Table 1 shows, there are differences in the producer and user accuracies of individual species. The accuracy is influenced by the total area and species' separability. Since high accuracies were reached for all species (except for *D. cespitosa* in the Bílá louka area), we can reliably confirm the expansion of *C. villosa* and the retreat of *N. stricta*, as was observed by other studies [15,19].

Plant functional traits, such as stem and leaf shape, carbon and nutrient assimilation, chemical defenses, and canopy architecture, all play essential roles in the dynamics of terrestrial vegetation [24,33,49–51]. *N. stricta* presents a classically conservative growth form: narrow, erect leaves that reduce exposure to strong irradiance and limit water loss. The bygone selective pressure for efficient nutrient use and leaf durability is compounded by the fact that *N. stricta* is a clonal species with low genetic diversity [52]. *N. stricta*'s strategy of low productivity and long leaf lifespan is seen in its low and non-dynamic SLA (Figure 2). The percentages of structural and photosynthetic tissues in the studied species (Table 2) correspond to differences in SLA; flat and thin leaves, even with higher quantities of structural non-photosynthetic tissues (e.g., for *C. villosa* and *M. caerulea*), may be more effective at light capture in dense continuous canopies [53]. In contrast, low SLA is a trait associated with selective avoidance by some herbivores [54], and the erect leaves reduce high radiative loading and stress [55]. The localization of PheCs on the externally facing leaf side (abaxial in the case of *N. stricta*) is protective against oxidative stress resulting from high PAR and UV irradiation (Figure 4o). PheCs are known to accumulate after exposure to light [55–58], so the relative lack of PheCs observed on the adaxial side of *N. stricta* leaves may indicate effective structural avoidance of irradiation. By contrast, the flat leaves on *C. villosa* and *M. caerulea* have strong PheC fluorescence throughout the mesophyll, indicating steady exposure to high irradiation (Figure 4c,d,k,l).

Tall grasses, particularly *C. villosa* and *M. caerulea*, were previously suppressed by grazing and mowing [15,59,60]. Compared to *N. stricta*, which grows in dense tussocks with erect leaves 25–60 cm high, all three competing grasses have much taller growth forms, capable of overshadowing the shade-intolerant *N. stricta*—*C. villosa* has culms of 15–150 cm, *M. caerulea* of 15–120 cm, and *D. cespitosa* of 20–200 cm [61]. Whether *N. stricta* would have become so dominant without the selective pressure of grazing is uncertain. However, in grasslands where species are mown or cut (a practice which does not discriminate among species), *N. stricta*'s low rate of leaf expansion is uncompetitive [62]. The phenological delay in *M. caerulea* leaf expansion (Figure 3b) may partially explain why this tall species has not spread more (Figure 1a). This is in direct contrast to the early leaf expansion observed for *C. villosa*, which allows it to form a continuous canopy in the absence of mowing/grazing. While many grass species increase tiller density after defoliation, *N. stricta* (in addition to *M. caerulea*) shows a negative relationship between defoliation and tiller density [63]. Mowing slows the spread of *M. caerulea* and *C. villosa*, but it also hinders *N. stricta*. By contrast, *D. cespitosa* was found to expand in grasslands with both sheep grazing [64] and mowing regimes [65].

We were particularly interested in the way biochemical leaf traits may be influencing the dynamics of grass competition in the Krkonoše. Pigments contribute to non-photochemical quenching under high-irradiance conditions (carotenoids [66]) and act as antioxidants (anthocyanins and PheCs [27,30,56]). Chlorophyll, in particular, can be detected remotely and can be used as a proxy for the physiological status of plants [36]. While we did not find any total differences among species in terms of carotenoids or phenolics (Figure 5a,c), chlorophyll content was the highest for *D. cespitosa* and *M. caerulea* and was the lowest for *N. stricta* (Figure 5b). This is clearly reflected for *D. cespitosa* and *N. stricta* in terms of their positions relative to Mg content in the element analysis PCA (Figure 9). This lower concentration is further compounded by *N. stricta*'s higher percentage of photosynthetic tissue per leaf area compared to all other species (Table 2). By contrast, *C. villosa* and *M. caerulea* had the lowest ratio of photosynthetic to non-photosynthetic (structural) tissue (Table 2), i.e., their pigment contents were more concentrated in the leaf mesophyll. In general, “fast carbon acquisition traits,” such as higher SLA and greater chlorophyll

content (as in the case of *M. caerulea*), positively correlate with digestibility by ungulate herbivores [67,68].

Regarding anthocyanins, only *D. cespitosa* showed significantly elevated accumulation (Figure 5c). However, the distinct abaxial localization of anthocyanins in *C. villosa* (Figure 2d–f) is a curious feature. Abaxial anthocyanin localization is classically associated with low-light environments and the now-debunked “back-scatter” hypothesis—a theory that abaxial anthocyanins reflected red-photons that had been transmitted through the mesophyll and increased light-capture [69,70]. Adaxial anthocyanins attenuate light, and recent evidence suggests that abaxial anthocyanins function in the same way, preventing photoinhibition, particularly for shade-adapted plants exposed to short, high-intensity light such as transient sun-flecks [30,70,71]. Leaves with adaxial anthocyanins attenuate more light and have reduced photosynthesis at saturating light intensity as compared to those with abaxial anthocyanins [70]. In the case of non-shade plants, abaxial anthocyanins may be a function of leaf orientation: the abaxial side may be more frequently exposed to high irradiance and more sensitive than the adaxial side [72].

Currently, there is no information on how (or if) disperse anthocyanins (i.e., those that cannot be seen in cross sections but can still be detected biochemically, as is the case with *N. stricta*, *D. cespitosa*, and *M. caerulea* [Figures 5 and 6]) affect photoinhibition compared to anthocyanins that localize in a particular cell layer, as with *C. villosa* (Figure 1). Beyond light attenuation and the prevention of photoinhibition, anthocyanin accumulation can also correlate with nutrient stress (P and N deficiencies) [73], particularly when accumulating on the abaxial leaf surface [73,74], and help plants acclimate to cold temperatures [71,75]. Despite having the highest anthocyanin content, *D. cespitosa* simultaneously showed the highest N and P contents among the studied species (Table S1). However, being a highly plastic species with rather higher nutrient demands [76], we cannot exclude the idea that anthocyanins were accumulated as a response to lower N and P availability.

Throughout the season, pigment concentrations did not significantly vary for *D. cespitosa* and *N. stricta*, while *C. villosa* and *M. caerulea* showed opposite trends. *C. villosa* started the season with a higher SLA (Figure 3b) which decreased over the season alongside carotenoids (Figure 6a) and chlorophyll (Figure 6b), while increasing the concentration of PheCs (Figure 6d). This could potentially enable *C. villosa* to grow quickly and expand early in the season before prioritizing PheC biosynthesis in order to protect its leaves from high irradiation and cold stress for the remainder of the season. *M. caerulea*, by contrast, showed a slight developmental delay compared to the other species. In June, its SLA was still low, increasing significantly by July (Figure 3b) alongside its contents of carotenoids, chlorophyll, and anthocyanins (Figure 6). While individual plants tend to increase their photoprotective pigments after high light exposure, it is interesting that such diverse patterns of pigment accumulation were observed among species over the growing season.

While many PheCs occur across species, specific profiles of PheCs can be indicative of botanical and evolutionary relationships in *Poaceae* [32]. We found distinct clusters of PheCs in the PCA analysis for three of the four species investigated in this study (Figure 8). The profiles of specific PheCs may be more useful than the total phenolics, as the species did not significantly differ in terms of total phenolics (Figure 5d). *C. villosa*, which is expanding its territory in the Bílá louka area (Figure 1), was associated with a diverse range of PheCs: chlorogenic acid, ferulic acid, protocatechuic acid, caffeic acid, luteolin, homoorientin, and apigenin (Figure 8). This wide range of PheCs may protect *C. villosa* from a broader range of environmental stressors than species accumulating only one type of compound. In particular, the dihydroxy B-ring-substituted flavonoids, such as luteolin and apigenin, represent effective antioxidants located within or in the proximity of the centers of ROS generation (in mesophyll cells) in severely stressed plants [57]. Higher diversity of PheCs also ensures the employment of multiple protective mechanisms, which in turn can mean generally higher stability in highly variable environments. *C. villosa* also accumulated high levels of hydroxycinnamic acids (chlorogenic, ferulic, and caffeic acids), which are more efficient antioxidants compared to hydroxybenzoic acids due to their

structure [77,78]. By contrast, *D. cespitosa* predominantly accumulated hydroxybenzoic acids—gallic, syringic, and vanillic—at higher levels than the other grasses (Figure 7i,k,m and Figure 8). Grasses accumulating mainly hydroxybenzoic acids may be more responsive to environmental stimuli (ROS also function as signaling molecules) [78], although they may simultaneously be more prone to oxidative stress (this corresponds to our findings with chlorophyll fluorescence, see next paragraph). *N. stricta* was the most associated with a hydroxycinnamic acid (coumaric acid) and a flavonoid (saponarin) (Figure 8), although, due to high variability in *N. stricta* samples, the accumulations of these compounds were not significantly different from the other species (Figure 7e,o). *M. caerulea* did not correlate with a particular group of PheCs according to the PCA (Figure 8), however, it did accumulate significantly more isovitexin than all of the other species (Figure 5b) and significantly more sinapic acid than all of the other species except *D. cespitosa* (Figure 5f). In one comparative study of flavonoids, isovitexin was found to better rescue cells from ROS-induced apoptosis due to its low cytotoxicity, high antioxidative activity, and xanthine oxidase inhibition compared to apigenin, kaempferol, quercetin, myricetin, and genistein [79]. Thus, although not accumulating a wide range of PheCs, *M. caerulea* selectively accumulates an especially protective compound—isoovitexin—for the prevention of oxidative stress.

Chlorophyll fluorescence has emerged as a quick, non-invasive technique to evaluate stress in plants [80]. PSII frequently limits photochemistry in response to abiotic stress, especially light. The parameter  $F_v/F_m$  corresponds to the maximum efficiency with which light absorbed by PSII is used to reduce  $Q_A$  (the primary quinone electron acceptor of PSII), and it is frequently decreased when plants are stressed [81]. In general, decreases in  $F_v/F_m$  correlate with the stress-induced loss of chlorophyll [80,82]. However, we found the highest  $F_v/F_m$  in *N. stricta* (0.73) (Figure 10a), which concurrently had the lowest total chlorophyll content per gram of leaf mass (Figure 5b).  $F_v/F_m$  is generally measured to be ~0.83 in non-photoinhibited leaves [39]. Exposure to low temperatures initially induces some photoinhibition, which can also be reversed, as mechanisms such as antioxidant accumulation and xanthophyll cycle activity are increased [83]. The measured values of 0.73 (*N. stricta*), 0.69 (*C. villosa*), and 0.67 (*D. cespitosa* and *M. caerulea*) are in-line with the values observed for cold-hardened plants dealing with stress exposure, and none of these show signs of potentially lethal PSII damage (below 0.4) [83]. The lowest  $F_v/F_m$  was measured in *D. cespitosa*, which mainly accumulated PheCs with lower antioxidative capacity (hydroxybenzoic acids) (Figure 8); this supports the findings of other studies that antioxidant capacity is a significant contributor to oxidative damage protection [84]. *D. cespitosa* also showed the highest  $\Delta V_{ip}$  (Figure 10), which is the relative increase between the I and P step of an OJIP curve and is related to electron transfer to PSI end acceptors [42]. A depression of the IP-phase indicates a blockage of the acceptor side of PSI, such as by inactive ferredoxin-NADP<sup>+</sup>-reductase [85], or lower PSI content [43]. An increase in the PSII:PSI ratio could be created by growing plants hydroponically in a Mg<sup>2+</sup>-deficient solution [43]. It is interesting that Mg content was a main separator of *D. cespitosa* from other species during the PCA of leaves' elemental compositions (Figure 9). This may indicate higher Mg demands for *D. cespitosa* compared to the other species, resulting in a nutrient-limited inhibition of PSI [86].

*D. cespitosa* was shown to be increasing in abundance in the U Luční boudy area and decreasing in the Bílá louka area, although the accuracies for this measurement were not as high for *D. cespitosa* as for the other species (Table 1). The sampled area neighboring the Luční Bouda chalet was mown and fertilized regularly for at least 250 years until the 1960s, when the area was converted into a strictly protected nature reserve, and almost no direct human management was practiced in the tundra zone. At the same time, tourist pressure intensified, severely disturbing tundra vegetation. This area became known as the “grass garden.” In contrast to the surrounding grassland, the domination of *N. stricta*, *D. cespitosa*, and *Avenella flexuosa* prevailed in the grass garden [87]. The element analysis shows distinct correlation between *D. cespitosa* and Mg content and partly also N and P content (Figure 9). This could be due to the limestone (i.e., calcium magnesium carbonate)

used in paving roads in the area creating a distinct microhabitat and the long-term organic fertilization mentioned above, and would negatively influence *N. stricta*, which cannot tolerate calcareous soil [88]. Our results showing different element compositions in *N. stricta* and *D. cespitosa* confirm their contrasting nutrient demands, and, thus, their potential co-existence in localities with heterogeneous nutrient availability [89], although *N. stricta* is better able to tolerate nutrient-poor soils. *D. cespitosa* was also shown to effectively use P in forms of lower biological availability [90], which helps it to coexist with other species in low-nutrient stands. Fertilization significantly increases *D. cespitosa* height, but not that of *N. stricta* [88,91]. In fact, recreating nutrient-poor soil conditions is a recommended practice for restoring *N. stricta*-dominated grasslands [92]. *N. stricta* also prefers drier soil, while *D. cespitosa* thrives under low drainage [93], which may be an additional factor in the decline in *N. stricta* within the moister U Luční boudy area (Figure 1). The value of conservation of species-rich Nardetum communities also includes soil carbon storage, which was higher in Nardetum grasslands with lower P and Ca availability and high herb-species diversity [94].

Leaf phenolic compounds certainly play a role in leaf decomposition and influence nutrient turnover and thus their availability [95]. Phenolic-rich decomposing leaf biomass acts as an allelopathic agent inhibiting competing plant growth and also stimulating microbial activity [96] and N immobilization in microbial biomass [95]. We are aware that the focus on leaf functional traits for disentangling the relationships among grass species is limited without the consideration of belowground processes. However, we preferentially focused on aboveground traits, as this study was conducted as part of a project aimed at interpreting the RS data of different ecosystems. RS methods are crucial for mapping the effects of unprecedented warming on arctic tundra ecosystems [97–99]. RS methods are also frequently used for intense vegetation mapping in alpine tundra, since fast changes in vegetation cover occur there as well [99]. Changes in alpine meadow grasslands can be successfully monitored based on multi-source satellite data [100], as we previously showed for the Krkonoše tundra grassland [34,101]. We believe our study will contribute to the RS-based monitoring of ecosystem functioning via the phenological mapping of leaf functional traits in the Krkonoše alpine tundra grasses, as seasonal monitoring of chlorophyll content in the grassland community there has already begun [101]. Further investigations examining the interspecific differences in leaf biochemical traits in relation to leaf chlorophyll fluorescence and canopy solar-induced fluorescence are needed in order to confirm our findings for other species and locations using in-field and remote aerial UAV (unmanned aircraft system) observations.

## 4. Materials and Methods

### 4.1. Study Area

Sampling took place in the relict alpine–arctic tundra grassland of the Giant Mts (50.734 N, 15.696 E, Figure 11) over the years 2020 and 2021. The study area lies 1435 m above sea level. Six plots with a homogeneous canopy were sampled for each of the four species under investigation (24 total). The species' identities were confirmed by the botanist from the Krkonoše Mountains National Park Administration. Plots were marked with an orientational stake at specified GPS locations. The locations of the plots were detected at the start of each sampling using a Trimble R10 GNSS (global navigation satellite system) device (Westminster, CO, USA). In 2020, chlorophyll fluorescence measurements were taken on-site, and then leaf samples were collected for morphological, biochemical, and element analysis three times per vegetation season in early June, July, and August. The samples for histochemical analyses were taken from fully developed leaves in August 2020. Additionally, the leaf samples for the HPLC-HRMS analysis of individual PheCs were sampled from the identical georeferenced plots in August 2021 in order to extend the insight into PheCs, as the Folin–Ciocalteu assay for soluble phenolic compounds appeared to be too general.



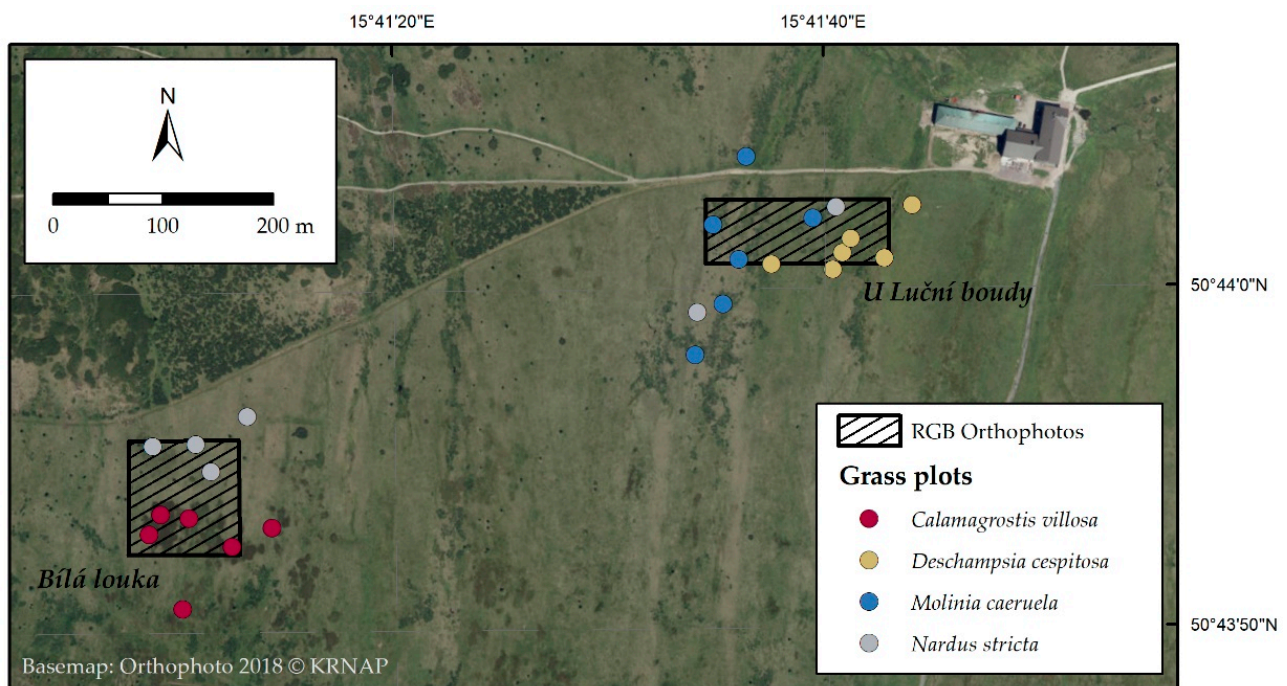


**Figure 11.** A map of studied area showing the location of sampling plots and two areas where the RGB orthophotos were classified (adapted from Červená et al., 2022 [101]).

#### 4.2. Morphology and Biochemical Analysis

Biomass was collected from two  $10 \times 10$  cm subplots within the main plot. In the laboratory, the collected biomass was divided into fresh biomass and necromass. A subsample of fresh biomass was scanned and then dried in an oven for at least 24 h at  $60^\circ$  and weighed. ImageJ software was used to determine the leaf area from the scans. The dry weight and leaf area of the sample were used to determine SLA (specific leaf area—leaf area related to the unit weight of the dry matter of the leaf) [102]. Many morphological, chemical, and physiological indicators have been proposed for evaluation of the conditions of plants in ecological systems. We selected leaf traits that are connected to photosynthetic capacity (chlorophyll content and chlorophyll fluorescence), protection against PAR and UV (carotenoids, anthocyanins, and PheCs contents) related to the specific conditions of the mountainous site, and SLA related to adaptation to radiative loading and stress. Most of these leaf traits also determine the optical properties of the canopy and are therefore detectable by remote sensing [103–105].

The analysis of the prompt fluorescence (PF) of chlorophyll is considered a powerful tool that combines richness of achievable information with operational quickness. This technique is especially suitable for large ecological surveys where it is necessary to screen many samples in a brief span of time. PF analysis allows for evaluation of the photochemical properties and functionalities of photosynthetic organisms utilizing a set of parameters—known as a ‘JIP-test’ and sometimes visualized as an ‘OJIP curve’. The distinct phases of the photochemical processes in terms of energy absorption, trapping, and electron transport can be described by these parameters. In this paper, we reanalyzed large PF datasets obtained from past research carried out under field conditions (forests, plantations, and pasture meadows) and within experimental setups (semi-controlled conditions). Our aim was to explore the relationships (redundancy and independence) among the JIP-test parameters and to select the most suitable ones to capture the variability of plant photosynthetic efficiency and their responses to environmental pressures. Principal component analysis (PCA) was applied to 43,987 measurements. The overall PCA results evidenced that the variability of the PF parameters was mainly explicated by two factors connected, respectively, to the processes of photon capture and primary photochemical events and to

the efficiency of the electron transport around Photosystem I. This result suggests that, in ecological studies, the photosynthetic functioning of the member of a population can be effectively described by two parameters representative of these two phases: the maximum quantum yield of the primary photochemistry of a dark-adapted sample (variable to maximal fluorescence intensity  $F_v/F_m$ ) and the amplitude of the I-P phase ( $\Delta VIP$ ).  $F_v/F_m$  and  $\Delta VIP$  were proven to be independent, and their correlation in various datasets may be either positive or negative in relation to the environmental factors considered. The physiological significance of the correlations between these parameters is discussed [106].

One sample was taken from each of the two subplots in order to determine the anthocyanin and phenolic contents. In order to determine chlorophyll and carotenoids, nine samples were taken per plot. These samples were immediately cooled and stored frozen until further processing. Anthocyanins were extracted in acidified methanol according to the method from reference [107], and they were converted into molar concentration using the Beer–Lambert equation with the universal molar extinction coefficient  $\epsilon = 30,000 \text{ L}\cdot\text{mol}^{-1}\cdot\text{cm}^{-1}$  [108] and related to leaf area. The SLA and molar weight of cyanidin 3-glucoside (one of the abundant anthocyanins in grasses, particularly *M. caerulea* [109]) was used in order to recalculate the quantity of anthocyanins per unit of dry mass into mg. The total content of soluble phenolic compounds was determined from dried and homogenized leaves. Soluble phenolic compounds were extracted in 80% methanol and determined spectrophotometrically using a Folin–Ciocalteu phenol reagent and gallic acid as a standard [110]; final phenol contents were related to dry mass. Chlorophyll and carotenoids were extracted by dimethylformamide [111] and assessed spectrophotometrically, and the contents were calculated according to the method from reference [112] and related to the unit of dry mass.

#### 4.3. Histochemistry and Anatomy

All of the samples used for histochemical and anatomical analyses were collected from fully developed leaves in August 2020. Cross sections of grass leaves were made at between 70–80  $\mu\text{m}$  thickness using a hand microtome (Leica RM 2255, Wetzlar, Germany). The cross sections were taken from the central part of the blade of fully developed leaves. Phloroglucinol-HCl was used to detect the presence of lignin [113], and vanillin-HCl was used to detect condensed tannins [114] with light microscopy; a 0.1% (*w/v*) Naturstoff reagent A solution used to detect flavonoids [115], [116] with fluorescent microscopy utilizing both blue- and UV-light excitation. The presence of anthocyanins was detectable without histochemical staining. All of the samples from all six plots per species were prepared for sections and staining, and the representative samples were presented.

The percentage of mesophyll, epidermis, and vascular bundles including sclerenchyma tissues was assessed using the point-counting method on Naturstoff reagent A-stained fluorescence images. The area of respective tissues on a cross section was related to the area of the whole cross section and was expressed as a percentage.

#### 4.4. Specific Phenolic Compounds Identified via HPLC-HRMS

Leaves from six samples of each of the four species (*C. villosa*, *D. cespitosa*, *M. caerulea*, and *N. stricta*) were collected during the 2021 sampling season and were transported back to the lab in plastic bags packed in coolers with ice. The leaves were then lyophilized and stored in vials in silica gel. The samples (0.12–0.27 g of dry mass) were homogenized using a mortar and pestle with liquid nitrogen and were then extracted using a methanol:chloroform:H<sub>2</sub>O solution (*v:v:v*, 1:2:2). An aliquot of the upper (polar) phase was used to analyze metabolites with an UltiMate 3000 high-performance liquid chromatograph (HPLC) (Thermo Fisher Scientific, US/Dionex RSLC, Dionex, Waltham, MA, USA) coupled with an LTQ Orbitrap XL high-resolution mass spectrometer (HRMS) (Thermo Fisher Scientific, Waltham, MA, USA) equipped with a heated electrospray ionization source. All of the samples were analyzed in the positive and negative polarity of Orbitrap, operated in full-scan mode over a range of *m/z* from 50 to 1000 (positive mode) and from

65 to 1000 (negative mode). The PheCs reported in the study were analyzed through non-target analysis, which aims to identify the maximum number of metabolites. PheCs were identified using a standard library and were confirmed by mass, retention time (RT),  $m/z$ , isotope ratios, by checking fragments that were formed during ionization, and also (at higher concentrations) by MS/MS data. During non-target analysis, it was not possible to perform quantification based on the concentration gradient of standards for each of the identified metabolites. Therefore, quantification was performed based on peak area analysis. This analysis allows for relative comparisons between species or variants but does not allow for the evaluation of absolute concentrations, e.g., in  $\mu\text{g}$  per g of dry or fresh weight. Over the course of the analyses, an injection of mixed standard (phenolic compounds and phthalates) was then used after analyzing each of the 25 samples. The following PheC groups were identified in all species: hydroxycinnamic acids (chlorogenic acid, ferulic acid, caffeic acid, sinapic acid, and 3-coumaric acid), five hydroxybenzoic acids (3-hydroxybenzoic acid, vanillic acid, syringic acid, protocatechuic acid, and gallic acid), and five flavonoids (saponarin, luteolin, isovitexin, homoorientin, and apigenin). Individual anthocyanins were not identified due to a lack of standards.

#### 4.5. Chlorophyll Fluorescence

In 2020, chlorophyll fluorescence was measured using a FluorPen FP 100/S (PSI, Drásov, Czech Republic). First, leaves were dark-acclimated by being wrapped in aluminum foil for 20 min prior to measurement. After the 20 min elapsed, a piece of black velvet cloth was placed over the sample area in order to prevent sunlight from reaching the leaves during measurement. Under the cloth, the aluminum was removed, and the sample was measured using the OJIP function. The OJIP function consists of a saturating pulse of blue light (455 nm, 3000  $\mu\text{mol m}^2/\text{s}$ ) being sent to the leaf. The measuring process took place during the interval from 10  $\mu\text{s}$  to 2 s, with a measurement taking place every 10  $\mu\text{s}$  until 600  $\mu\text{s}$ , then every 100  $\mu\text{s}$  until 14 ms, then every 1 ms until 90 ms, and finally every 10 ms until the end of the measurement at 2 s. Two parameters were derived from the measured values and were related to the efficiency of the plant photosynthetic apparatus:  $F_v/F_m$  and  $\Delta V_{ip}$  [106]. Five individual leaves were measured at each plot for *C. villosa*, *D. cespitosa*, and *M. caerulea*. The narrowness of the leaves of *N. stricta* necessitated several leaves (4–6) being measured together in order to cover the sensor, and the process was repeated for five tussocks.

#### 4.6. Element Analysis

Leaf element analysis was included because element composition and stoichiometry mirror species' ecological demands and are the subject of competition. Element analyses were conducted on green living biomass dried at 60 °C for 72 h. The analyses were carried out in the certified laboratories of the Research Institute for Soil and Water Conservation (<https://www.vumop.cz/en>, accessed on 11 November 2022). The samples were redried at 40 °C to constant weight and homogenized. For Ca, Mg, K, and P assessment, the samples were mineralized by  $\text{HNO}_3$  and  $\text{HClO}_4$ , and extracts were used for quantification by inductively coupled plasma optical emission spectrometry. The total N content was assessed spectrophotometrically and by Kjeldahl digestion. For total C content, the samples were oxidized with concentrated sulfuric acid and dichromate and finally assessed by titration using thiosulphate.

#### 4.7. Statistical Analyses

The differences between species were tested through one-way analysis of variance (ANOVA) at  $\alpha = 0.05$ . In the case of normal data distribution, the Tukey–Kramer test was used; otherwise, the Kruskal–Wallis test was used. The analyses were conducted in NCSS 9 software (NCSS 9 Statistical Software (2013). NCSS, LLC., Kaysville, UT, USA, [ncss.com/software/ncss](https://www.ncss.com/software/ncss)). Data for the principal component analysis were centered and

scaled using the `princomp` function from `ggfortify` package prior to analysis [117]. PCA was accomplished in R (4.1.2) [118].

#### 4.8. Analysis of Change in Grass Species Cover Using Remote Sensing

Two sets of RGB aerial data were used—RGB orthophoto from 2012 with a 25 cm pixel size provided by ČÚZK (Czech Office for Surveying, Mapping, and Cadaster) and RGB orthophoto from 2018 with a 12.5 cm pixel size provided by the Krkonoše Mountains National Park Administration. Both orthophotos were acquired at the beginning of July (8 July 2012 and 5 July 2018). Orthophotos from 2018 were resampled to a 25 cm pixel in order to ensure result comparability. Unfortunately, the younger dataset of orthophotos, which would be closer to the sampling dates, was not available. We supervised classification using the Maximum Likelihood algorithm. The training and validation data were collected by botanists in 2020 and were selected from the center of grass patches, so they are not affected by the change. For 2012 and 2018, all polygons were visually checked with the orthophoto and edited where necessary in order to ensure that all of the polygons reliably represented the predetermined categories. One third of the data was used for training and two thirds for validation.

## 5. Conclusions

Our hypothesis—that interspecific differences in plant functional traits could help explain the expansion and retreat of grass species in the Krkonoše arctic–alpine tundra—was upheld by the findings of this research. Despite the similarities between *C. villosa* and *M. caerulea* (i.e., similar leaf morphology, high ratio of structural to photosynthetic tissue, dynamically changing SLA, and high pigment content), only *C. villosa* has been expanding in area. The success of *C. villosa* may be partially explained by its rapid growth and accumulation of pigments early in the season combined its synthesis of a wide array of different phenolic compounds, while *M. caerulea* peaks later and accumulates a narrow field of phenolic compounds. Our findings further suggest that *D. cespitosa* is occupying an available niche (rather than outcompeting neighboring species) due to its accumulation of weaker antioxidants (hydroxybenzoic acids) and greater symptoms of stress (low Fv/Fm and high ΔVip, as well as high anthocyanin content, possibly due to nutrient deficiency). Our analysis of leaf traits reaffirmed *N. stricta*'s suitability in nutrient-poor soils, as it demonstrated low stress levels compared to the other three species. However, the slow growth rate and diminutive form of *N. stricta* present a disadvantage when competing for territory with taller, faster-growing species in the absence of grazing/mowing.

This work also confirmed that changes in grass species' dynamics can be detected remotely via orthophotos. This study was intended as a pilot study on the use of hyperspectral data acquired by UAVs. We emphasize that the phenology of pigments and morphology throughout the growing season should be taken into account with RS. We hope that hyperspectral data and derived vegetation indices, as well as remote chlorophyll fluorescence and canopy solar-induced fluorescence sensors on UAVs, will be useful in the future to monitor fragile grassland communities.

**Supplementary Materials:** The following supporting information can be downloaded at <https://www.mdpi.com/article/10.3390/plants12051001/s1>: Table S1, Element composition of green leaves for studied species.

**Author Contributions:** Conceptualization, J.A., L.H., Z.L., L.Č. and L.K.; methodology, L.H. and Z.L.; validation, L.H., Z.L., E.N. and L.Č.; formal analysis, L.H., Z.L., E.N. and L.Č.; investigation, L.H., Z.L., E.N., L.Č. and M.O.; resources, J.A., K.K. and L.K.; writing—original draft preparation, L.H.; writing—review and editing, L.H., J.A., Z.L., E.N., L.Č., L.K., K.K., P.C. and H.E.E.; visualization, L.H.; supervision, J.A.; project administration, J.A., Z.L. and L.K.; funding acquisition, J.A., L.K. and P.C. All authors have read and agreed to the published version of the manuscript.

**Funding:** This research was funded mainly by the Ministry of Education, Youth and Sports of the Czech Republic, scheme INTER-EXCELLENCE, INTERACTION, grant number LTAUSA18154, titled “Assessment of ecosystem function based on Earth observation of vegetation quantitative parameters retrieved from data with high spatial, spectral and temporal resolution”. This project is in collaboration with U.S. partners: P. Campbell and H. Epstein. Campbell’s contribution was supported by NASA, LCLUC Program, grant number 80NSSC18K0337, titled “Prototyping MuSLI canopy Chlorophyll Content for Assessment of Vegetation Function and Productivity”. Partial support for manuscript finalization and the analysis of phenolic compounds was funded through the Czech Science Foundation (GAČR grant number 21-18532S), titled “Light-induced protection mechanisms based on low-molecular-weight metabolites and their role in plant cross-tolerance to high temperature and drought”.

**Institutional Review Board Statement:** The research was carried out within the framework of long-term cooperation with the Krkonoše National Park Administration. For conducting research in the protected zone of the tundra, we had a research permit, number 89/2019, based on a research contract, which allowed entrance to the plots and the sampling of vegetation for research purposes.

**Data Availability Statement:** All data are contained within the article or Supplementary Materials.

**Acknowledgments:** We would like to thank the many students who assisted with field sampling and laboratory work, particularly Petr M. Mamula, who assisted extensively in both. We would also like to thank Miroslav Barták for his help with microscopy work and the preparation of graphics for this paper. We would also like to thank to Jana Müllerová from the Institute of Botany of the Czech Academy of Science for the collection of botanical training and validation samples for classification.

**Conflicts of Interest:** The authors declare no conflict of interest.

## References

1. Soukupová, L.; Krociánová, M.; Jeník, J.; Sekzra, J. Artic-alpine tundra in the Krkonoše, the Sudetes. *Opera Corcon.* **1995**, *32*, 5–88.
2. Galvánek, D.; Janák, M. Management of Natura 2000 Habitats. 6230 \*Species-Rich Nardus Grasslands; European Commission Natura 2000 Technical Report. 2008. Available online: [https://ec.europa.eu/environment/nature/natura2000/management/habitats/pdf/6230\\_Nardus\\_grasslands.pdf](https://ec.europa.eu/environment/nature/natura2000/management/habitats/pdf/6230_Nardus_grasslands.pdf) (accessed on 11 November 2022).
3. Štursa, J. Research and management of the giant mountains’ arctic-alpine tundra (Czech Republic). *AMBIO J. Hum. Environ.* **1998**, *27*, 358–360. Available online: <https://www.semanticscholar.org/paper/RESEARCH-AND-MANAGEMENT-OF-THE-GIANT-TUNDRA-%C5%A0tursa/9bb9e54762754b8f2002c7decdbd127fe27755443> (accessed on 16 January 2023).
4. Lokvenc, T. Analysis of anthropogenic changes of woody plant stands above the alpine timber line in the Krkonoše Mts. *Opera Corcon.* **1995**, *32*, 99–114.
5. Novák, J.; Petr, L.; Tremel, V. Late-Holocene human-induced changes to the extent of alpine areas in the East Sudetes, Central Europe. *Holocene* **2010**, *20*, 895–905. [[CrossRef](#)]
6. Brechtel, H.M. Impact of Acid Deposition Caused by Air Pollution in Central Europe. In *Responses of Forest Ecosystems to Environmental Changes*; Teller, A., Mathy, P., Jeffers, J.N.R., Eds.; Springer: Dordrecht, The Netherlands, 1992; pp. 594–595. ISBN 978-94-011-2866-7.
7. Rusek, J. Air-Pollution-Mediated Changes in Alpine Ecosystems and Ecotones. *Ecol. Appl.* **1993**, *3*, 409–416. [[CrossRef](#)]
8. Myers-Smith, I.H.; Forbes, B.C.; Wilmking, M.; Hallinger, M.; Lantz, T.; Blok, D.; Tape, K.D.; Macias-Fauria, M.; Sass-Klaassen, U.; Lévesque, E.; et al. Shrub expansion in tundra ecosystems: Dynamics, impacts and research priorities. *Environ. Res. Lett.* **2011**, *6*, 045509. [[CrossRef](#)]
9. Myers-Smith, I.H.; Hik, D.S. Climate warming as a driver of tundra shrubline advance. *J. Ecol.* **2018**, *106*, 547–560. [[CrossRef](#)]
10. Müllerová, J. Anthropogenous Vegetation Changes in Alpine Tundra, a Remote Sensing Study from the Krkonoše Mountains, Czech Republic. Preliminary Results. In *Proceedings of the EUROMAB-Symposium, Austrian Academy of Sciences, Vienna, Austria, 15–19 September 1999*; pp. 39–41.
11. Málková, J.; Kůlová, J. Impact of dolomitic limestone on changes of species diversity along roads of the eastern Krkonoše Mts. *Opera Corcon.* **1995**, *32*, 11–130.
12. Husáková, J. Subalpine turf communities with *Deschampsia cespitosa* along the tracks and paths in the Krkonoše (–Giant Mountains) National Park. *Preslia* **1986**, *58*, 231–246.
13. Müllerová, J.; Vítková, M. Long-term human impact on Alpine Tundra—25 years of changes assessed by aerial photography. *South-East. Eur. J. Earth Obs. Geomat.* **2014**, *3*, 483–487.
14. Harčarik, J. Management of the dwarf pine plantations on the naturally valuable localities in the Giant Mountains. *Opera Corcon.* **2007**, *36*, 363–369.
15. Hejčman, M.; Klauďisová, M.; Hejčmanová, P.; Pavlů, V.; Jones, M. Expansion of *Calamagrostis villosa* in sub-alpine *Nardus stricta* grassland: Cessation of cutting management or high nitrogen deposition? *Agric. Ecosyst. Environ.* **2009**, *129*, 91–96. [[CrossRef](#)]

16. Vacek, S.; Bastl, M.; Lepš, J. Vegetation changes in forests of the Krkonoše Mts. over a period of air pollution stress (1980–1995). *Plant Ecol.* **1999**, *143*, 1–11. [[CrossRef](#)]
17. Chambers, F.M.; Mauquoy, D.; Todd, P.A. Recent rise to dominance of *Molinia caerulea* in environmentally sensitive areas: New perspectives from palaeoecological data. *J. Appl. Ecol.* **1999**, *36*, 719–733. [[CrossRef](#)]
18. Pyšek, P. What do we know about *Calamagrostis villosa*?—A review of the species behaviour in secondary habitats. *Preslia* **1993**, *64*, 284–289.
19. Hejčman, M.; Pavlu, V.; Peterova, J.; Ricarova, P. The expansion of *Calamagrostis villosa* in the Giant Mountains—Preliminary results. *Acta Agrar. Et Silvestria Ser. Agrar.* **2003**. Available online: <https://www.infona.pl/resource/bwmeta1.element.ago-article-728d3f02-df5b-4b54-8b6d-25603886a947> (accessed on 16 November 2022).
20. Lokvenc, T.; Vacek, S.; Štursa, J. Vývoj zdravotního stavu a plodivosti kleče horské v Krkonoších. In *Výzkum a Management Ekosystémů na území KRNAP; VÚLHM: Opočno, Czech Republic*, 1996; pp. 224–228.
21. Nadarajah, K.K. ROS Homeostasis in Abiotic Stress Tolerance in Plants. *Int. J. Mol. Sci.* **2020**, *21*, 5208. [[CrossRef](#)]
22. Redza-Dutordoir, M.; Averill-Bates, D.A. Activation of apoptosis signalling pathways by reactive oxygen species. *Biochim. Biophys. Acta* **2016**, *1863*, 2977–2992. [[CrossRef](#)]
23. Díaz, S.; Kattge, J.; Cornelissen, J.H.C.; Wright, I.J.; Lavorel, S.; Dray, S.; Reu, B.; Kleyer, M.; Wirth, C.; Colin Prentice, I.; et al. The global spectrum of plant form and function. *Nature* **2016**, *529*, 167–171. [[CrossRef](#)]
24. Funk, J.L.; Larson, J.E.; Ames, G.M.; Butterfield, B.J.; Cavender-Bares, J.; Firn, J.; Laughlin, D.C.; Sutton-Grier, A.E.; Williams, L.; Wright, J. Revisiting the Holy Grail: Using plant functional traits to understand ecological processes. *Biol. Rev. Camb. Philos. Soc.* **2017**, *92*, 1156–1173. [[CrossRef](#)]
25. Palta, J.P. Leaf chlorophyll content. *Remote Sens. Rev.* **1990**, *5*, 207–213. [[CrossRef](#)]
26. Demmig-Adams, B.; Gilmore, A.M.; Iii, W.W.A. In vivo functions of carotenoids in higher plants. *FASEB J.* **1996**, *10*, 403–412. [[CrossRef](#)]
27. Grace, S. Phenolics as antioxidants. In *Antioxidants and Reactive Oxygen Species in Plants*; John Wiley & Sons: Hoboken, NJ, USA, 2008; ISBN 978-1-4051-7146-5.
28. Agati, G.; Tattini, M. Multiple functional roles of flavonoids in photoprotection. *New Phytol.* **2010**, *186*, 786–793. [[CrossRef](#)]
29. Dixon, R.; Paiva, N. Stress-Induced Phenylpropanoid Metabolism. *Plant Cell* **1995**, *7*, 1085–1097. [[CrossRef](#)]
30. Gould, K.S. Nature's Swiss Army Knife: The Diverse Protective Roles of Anthocyanins in Leaves. *J. Biomed. Biotechnol.* **2004**, *2004*, 314–320. [[CrossRef](#)]
31. Jansen, M.A.K.; Hectors, K.; O'Brien, N.M.; Guisez, Y.; Potters, G. Plant stress and human health: Do human consumers benefit from UV-B acclimated crops? *Plant Sci.* **2008**, *175*, 449–458. [[CrossRef](#)]
32. Míka, V.; Kubáň, V.; Klejdus, B.; Odstrčilová, V.; Nerušil, P. Phenolic compounds as chemical markers of low taxonomic levels in the family Poaceae. *Plant Soil Environ.* **2005**, *51*, 506. [[CrossRef](#)]
33. Venn, S.E.; Green, K.; Pickering, C.M.; Morgan, J.W. Using plant functional traits to explain community composition across a strong environmental filter in Australian alpine snowpatches. *Plant Ecol.* **2011**, *212*, 1491–1499. [[CrossRef](#)]
34. Kupková, L.; Červená, L.; Suchá, R.; Jakešová, L.; Zagajewski, B.; Březina, S.; Albrechtová, J. Classification of Tundra Vegetation in the Krkonoše Mts. National Park Using APEX, AISA Dual and Sentinel-2A Data. *Eur. J. Remote Sens.* **2017**, *50*, 29–46. [[CrossRef](#)]
35. Müllerová, J. Use of digital aerial photography for sub-alpine vegetation mapping: A case study from the Krkonoše Mts., Czech Republic. *Plant Ecol.* **2005**, *175*, 259–272. [[CrossRef](#)]
36. Gitelson, A.A.; Merzlyak, M.N. Remote estimation of chlorophyll content in higher plant leaves. *Int. J. Remote Sens.* **1997**, *18*, 2691–2697. [[CrossRef](#)]
37. Lillesand, T.M.; Kiefer, R.W.; Chipman, J. *Remote Sensing and Image Interpretation*, 6th ed.; John Wiley & Sons: Hoboken, NJ, USA, 2008; ISBN 978-0-470-05245-7.
38. Hejčman, M.; Češková, M.; Pavlů, V. Control of *Molinia caerulea* by cutting management on sub-alpine grassland. *Flora-Morphol. Distrib. Funct. Ecol. Plants* **2010**, *205*, 577–582. [[CrossRef](#)]
39. Björkman, O.; Demmig, B. Photon yield of O<sub>2</sub> evolution and chlorophyll fluorescence characteristics at 77 K among vascular plants of diverse origins | SpringerLink. *Planta* **1987**, *170*, 489–504. [[CrossRef](#)]
40. Johnson, G.N.; Young, A.J.; Scholes, J.D.; Horton, P. The dissipation of excess excitation energy in British plant species. *Plant Cell Environ.* **1993**, *16*, 673–679. [[CrossRef](#)]
41. Lawson, T.; Vialet-Chabrand, S. Chlorophyll Fluorescence Imaging. In *Photosynthesis*; Covshoff, S., Ed.; Methods in Molecular Biology; Humana Press: New York, NY, USA, 2018; Volume 1770, pp. 121–140. [[CrossRef](#)]
42. Bantis, F.; Früchtenicht, E.; Graap, J.; Ströll, S.; Reiningner, N.; Schäfer, L.; Pollastrini, M.; Holland, V.; Bussotti, F.; Radoglou, K.; et al. Special issue in honour of Prof. Reto J. Strasser—The JIP-test as a tool for forestry in times of climate change. *Photosynthetica* **2020**, *58*, 409–421. [[CrossRef](#)]
43. Ceppi, M.G.; Oukarroum, A.; Çiçek, N.; Strasser, R.J.; Schansker, G. The IP amplitude of the fluorescence rise OJIP is sensitive to changes in the photosystem I content of leaves: A study on plants exposed to magnesium and sulfate deficiencies, drought stress and salt stress. *Physiol. Plant.* **2012**, *144*, 277–288. [[CrossRef](#)]
44. Çiçek, N.; Oukarroum, A.; Strasser, R.; Schansker, G. Salt stress effects on the photosynthetic electron transport chain in two chickpea lines differing in their salt stress tolerance. *Photosynth. Res.* **2018**, *136*, 291–301. [[CrossRef](#)]

45. Oukarroum, A.; Schansker, G.; Strasser, R. Drought stress effects on photosystem I content and photosystem II thermotolerance analyzed using Chl a fluorescence kinetics in barley varieties differing in their drought tolerance. *Physiol. Plant.* **2009**, *137*, 188–199. [CrossRef]
46. Çiçek, N.; Kalaji, H.M.; Ekmekçi, Y. Probing the photosynthetic efficiency of some European and Anatolian Scots pine populations under UV-B radiation using polyphasic chlorophyll a fluorescence transient. *Photosynthetica* **2020**, *58*, 468–478. [CrossRef]
47. Armstrong, R.H.; Common, T.G.; Davies, G.J. The prediction of the in vivo digestibility of the diet of sheep and cattle grazing indigenous hill plant communities by in vitro digestion, faecal nitrogen concentration or indigestible acid-detergent fibre—ARMSTRONG—1989—Grass and Forage Science—Wiley Online Library. *Grass Forage Sci.* **1989**, *44*, 303–313.
48. Leuschner, C.; Ellenberg, H. *Ecology of Central European Non-Forest Vegetation: Coastal to Alpine, Natural to Man-Made Habitats: Vegetation Ecology of Central Europe, Volume II*; Springer: Berlin/Heidelberg, Germany, 2017; Volume 2, ISBN 978-3-319-43048-5.
49. Ceulemans, T.; Merckx, R.; Hens, M.; Honnay, O. Plant species loss from European semi-natural grasslands following nutrient enrichment—Is it nitrogen or is it phosphorus? *Glob. Ecol. Biogeogr.* **2013**, *22*, 73–82. [CrossRef]
50. CHAPIN, F.S. Effects of Plant Traits on Ecosystem and Regional Processes: A Conceptual Framework for Predicting the Consequences of Global Change. *Ann. Bot.* **2003**, *91*, 455–463. [CrossRef]
51. Jin, Y.; Lai, S.; Chen, Z.; Jian, C.; Zhou, J.; Niu, F.; Xu, B. Leaf Photosynthetic and Functional Traits of Grassland Dominant Species in Response to Nutrient Addition on the Chinese Loess Plateau. *Plants* **2022**, *11*, 2921. [CrossRef]
52. Zorić, N. Level and distribution of genetic diversity in the European species *Nardus stricta* L. (Poaceae) inferred from chloroplast DNA and nuclear amplified fragment length polymorphism markers. Master's Thesis, Norwegian University of Life Sciences, Ås, Norway, 2013. Available online: <https://nmbu.brage.unit.no/nmbu-xmlui/handle/11250/189603> (accessed on 10 November 2022).
53. Ehleringer, J.R.; Comstock, J. Leaf absorptance and leaf angle: Mechanisms for stress avoidance. In *Plant Response to Stress*; Tenhunen, J.D., Catarino, F.M., Lange, O.L., Oechel, W.C., Eds.; Springer: Berlin/Heidelberg, Germany, 1987; pp. 55–76.
54. Lloyd, K.M.; Pollock, M.L.; Mason, N.W.H.; Lee, W.G. Leaf trait-palatability relationships differ between ungulate species: Evidence from cafeteria experiments using naïve tussock grasses. *N. Z. J. Ecol.* **2010**, *34*, 219–226.
55. Smith, W.K.; Vogelmann, T.C.; DeLucia, E.H.; Bell, D.T.; Shepherd, K.A. Leaf Form and Photosynthesis. *BioScience* **1997**, *47*, 785–793. [CrossRef]
56. Hunt, L.; Klem, K.; Lhotáková, Z.; Vosolsobě, S.; Oravec, M.; Urban, O.; Špunda, V.; Albrechtová, J. Light and CO<sub>2</sub> Modulate the Accumulation and Localization of Phenolic Compounds in Barley Leaves. *Antioxidants* **2021**, *10*, 385. [CrossRef]
57. Agati, G.; Azzarello, E.; Pollastri, S.; Tattini, M. Flavonoids as antioxidants in plants: Location and functional significance. *Plant Sci. Int. J. Exp. Plant Biol.* **2012**, *196*, 67–76. [CrossRef]
58. Ryan, K.G.; Swinny, E.E.; Markham, K.R.; Winefield, C. Flavonoid gene expression and UV photoprotection in transgenic and mutant *Petunia* leaves. *Phytochemistry* **2002**, *59*, 23–32. [CrossRef]
59. Agati, G.; Stefano, G.; Biricolti, S.; Tattini, M. Mesophyll distribution of 'antioxidant' flavonoid glycosides in *Ligustrum vulgare* leaves under contrasting sunlight irradiance. *Ann. Bot.* **2009**, *104*, 853–861. [CrossRef]
60. Klimeš, L.; Klimešová, J. The effects of mowing and fertilization on carbohydrate reserves and regrowth of grasses: Do they promote plant coexistence in species-rich meadows? *Evol. Ecol.* **2002**, *15*, 363–382. [CrossRef]
61. Clayton, W.D.; Vorontsova, M.S.; Harman, K.T.; Williamson, H. GrassBase—The Online World Grass Flora. 2006. Available online: <http://www.kew.org/data/grasses-db.html> (accessed on 24 October 2022).
62. Grant, S.A.; Torvell, L.; Sim, E.M.; Small, J.L.; Armstrong, R.H. Controlled Grazing Studies on *Nardus* Grassland: Effects of Between-Tussock Sward Height and Species of Grazer on *Nardus* utilization and Floristic Composition in Two Fields in Scotland. *J. Appl. Ecol.* **1996**, *33*, 1053–1064. [CrossRef]
63. Jones, L.I. *Studies on Hill Land in Wales*; Welsh Plant Breeding Station: Aberystwyth, UK, 1967.
64. Krahulec, F.; Skálová, H.; Herben, T.; Hadincová, V.; Wildová, R.; Pecháčková, S. Vegetation changes following sheep grazing in abandoned mountain meadows. *Appl. Veg. Sci.* **2001**, *4*, 97–102. [CrossRef]
65. Mašková, Z.; Doležal, J.; Květ, J.; Zemek, F. Long-term functioning of a species-rich mountain meadow under different management regimes. *Agric. Ecosyst. Environ.* **2009**, *132*, 192–202. [CrossRef]
66. Ma, Y.-Z.; Holt, N.E.; Li, X.-P.; Niyogi, K.K.; Fleming, G.R. Evidence for direct carotenoid involvement in the regulation of photosynthetic light harvesting. *Proc. Natl. Acad. Sci. USA* **2003**, *100*, 4377–4382. [CrossRef]
67. Barrere, J.; Collet, C.; Saïd, S.; Bastianelli, D.; Verheyden, H.; Courtines, H.; Bonnet, A.; Segrestin, J.; Boulanger, V. Do trait responses to simulated browsing in *Quercus robur* saplings affect their attractiveness to *Capreolus capreolus* the following year? *Environ. Exp. Bot.* **2022**, *194*, 104743. [CrossRef]
68. Cornelissen, J.H.C.; Quested, H.M.; Gwynn-Jones, D.; Van Logtestijn, R.S.P.; De Beus, M.A.H.; Kondratchuk, A.; Callaghan, T.V.; Aerts, R. Leaf digestibility and litter decomposability are related in a wide range of subarctic plant species and types. *Funct. Ecol.* **2004**, *18*, 779–786. [CrossRef]
69. Lee, D.W.; Lowry, J.B.; Stone, B.C. Abaxial Anthocyanin Layer in Leaves of Tropical Rain Forest Plants: Enhancer of Light Capture in Deep Shade. *Biotropica* **1979**, *11*, 70–77. [CrossRef]
70. Hughes, N.M.; Vogelmann, T.C.; Smith, W.K. Optical effects of abaxial anthocyanin on absorption of red wavelengths by understory species: Revisiting the back-scatter hypothesis. *J. Exp. Bot.* **2008**, *59*, 3435–3442. [CrossRef]

71. Steyn, W.J.; Wand, S.J.E.; Holcroft, D.M.; Jacobs, G. Anthocyanins in vegetative tissues: A proposed unified function in photoprotection. *New Phytol.* **2002**, *155*, 349–361. [[CrossRef](#)]
72. Sun, J.; Nishio, J.N.; Vogelmann, T.C. High-light effects on CO<sub>2</sub> fixation gradients across leaves. *Plant Cell Environ.* **1996**, *19*, 1261–1271. [[CrossRef](#)]
73. Kovinich, N.; Kayanja, G.; Chanoca, A.; Otegui, M.S.; Grotewold, E. Abiotic stresses induce different localizations of anthocyanins in Arabidopsis. *Plant Signal. Behav.* **2015**, *10*, e1027850. [[CrossRef](#)]
74. Cobbina, J.; Miller, M.H. Purpling in Maize Hybrids as Influenced by Temperature and Soil Phosphorus. *Agron. J.* **1987**, *79*, 576–582. [[CrossRef](#)]
75. Chalker-Scott, L. Do Anthocyanins Function of Osmoregulators in Leaf Tissues? *Adv. Bot. Res.* **2002**, *37*, 103–127.
76. Veresoglou, D.S.; Fitter, A.H. Spatial and Temporal Patterns of Growth and Nutrient Uptake of Five Co-Existing Grasses. *J. Ecol.* **1984**, *72*, 259. [[CrossRef](#)]
77. Olszowy, M. What is responsible for antioxidant properties of polyphenolic compounds from plants? *Plant Physiol. Biochem.* **2019**, *144*, 135–143. [[CrossRef](#)]
78. Hunt, L.; Fuksa, M.; Klem, K.; Lhotáková, Z.; Oravec, M.; Urban, O.; Albrechtová, J. Barley Genotypes Vary in Stomatal Responsiveness to Light and CO<sub>2</sub> Conditions. *Plants* **2021**, *10*, 2533. [[CrossRef](#)]
79. Lin, C.-M.; Chen, C.-T.; Lee, H.-H.; Lin, J.-K. Prevention of Cellular ROS Damage by Isovitexin and Related Flavonoids. *Planta Med.* **2002**, *68*, 365–367. [[CrossRef](#)]
80. Ibaraki, Y.; Murakami, J. Distribution of chlorophyll fluorescence parameter *f<sub>v</sub>/f<sub>m</sub>* within individual plants under various stress conditions. *Acta Hortic.* **2007**, *761*, 255–260. [[CrossRef](#)]
81. Baker, N.R. Chlorophyll Fluorescence: A Probe of Photosynthesis In Vivo. *Annu. Rev. Plant Biol.* **2008**, *59*, 89–113. [[CrossRef](#)]
82. Sharma, D.K.; Andersen, S.B.; Ottosen, C.-O.; Rosenqvist, E. Wheat cultivars selected for high *F<sub>v</sub>/F<sub>m</sub>* under heat stress maintain high photosynthesis, total chlorophyll, stomatal conductance, transpiration and dry matter. *Physiol. Plant.* **2015**, *153*, 284–298. [[CrossRef](#)]
83. Rizza, F.; Pagani, D.; Stanca, A.M.; Cattivelli, L. Use of chlorophyll fluorescence to evaluate the cold acclimation and freezing tolerance of winter and spring oats. *Plant Breed.* **2001**, *120*, 389–396. [[CrossRef](#)]
84. Dias, M.C.; Correia, S.; Serôdio, J.; Silva, A.M.S.; Freitas, H.; Santos, C. Chlorophyll fluorescence and oxidative stress endpoints to discriminate olive cultivars tolerance to drought and heat episodes. *Sci. Hortic.* **2018**, *231*, 31–35. [[CrossRef](#)]
85. Schansker, G.; Tóth, S.Z.; Strasser, R.J. Methylviologen and dibromothymoquinone treatments of pea leaves reveal the role of photosystem I in the Chl *a* fluorescence rise OJIP. *Biochim. Biophys. Acta BBA-Bioenerg.* **2005**, *1706*, 250–261. [[CrossRef](#)]
86. Kalaji, H.M.; Oukarroum, A.; Alexandrov, V.; Kouzmanova, M.; Brestic, M.; Zivcak, M.; Samborska, I.A.; Cetner, M.D.; Al-lakhverdiev, S.I.; Goltsev, V. Identification of nutrient deficiency in maize and tomato plants by in vivo chlorophyll *a* fluorescence measurements. *Plant Physiol. Biochem.* **2014**, *81*, 16–25. [[CrossRef](#)]
87. Semelová, V.; Hejman, M.; Pavlů, V.; Vacek, S.; Podrázský, V. The Grass Garden in the Giant Mts. (Czech Republic): Residual effect of long-term fertilization after 62 years. *Agric. Ecosyst. Environ.* **2008**, *123*, 337–342. [[CrossRef](#)]
88. Chadwick, M.J. *Nardus stricta* L. *J. Ecol.* **1960**, *48*, 255–267. [[CrossRef](#)]
89. Peñuelas, J.; Fernández-Martínez, M.; Ciais, P.; Jou, D.; Piao, S.; Obersteiner, M.; Vicca, S.; Janssens, I.A.; Sardans, J. The bioelements, the elementome, and the biogeochemical niche. *Ecology* **2019**, *100*, e02652. [[CrossRef](#)]
90. Ahmad-Ramli, M.F.; Cornulier, T.; Johnson, D. Partitioning of soil phosphorus regulates competition between *Vaccinium vitis-idaea* and *Deschampsia cespitosa*. *Ecol. Evol.* **2013**, *3*, 4243–4252. [[CrossRef](#)]
91. Alonso, I.; Hartley, S.E.; Thurlow, M. Competition between heather and grasses on Scottish moorlands: Interacting effects of nutrient enrichment and grazing regime. *J. Veg. Sci.* **2001**, *12*, 249–260. [[CrossRef](#)]
92. Schelfhout, S.; Wasof, S.; Mertens, J.; Vanhellefont, M.; Demey, A.; Haegeman, A.; DeCock, E.; Moeneclaey, I.; Vangansbeke, P.; Viaene, N.; et al. Effects of bioavailable phosphorus and soil biota on typical *Nardus* grassland species in competition with fast-growing plant species. *Ecol. Indic.* **2021**, *120*, 106880. [[CrossRef](#)]
93. Lepš, J.J.P.; Grime, J.G. Hodgson and R. Hunt Comparative plant ecology. *Folia Geobot. Phytotaxon.* **1990**, *25*, 216. [[CrossRef](#)]
94. Sochorová, L.; Jansa, J.; Verbruggen, E.; Hejman, M.; Schellberg, J.; Kiers, E.T.; Johnson, N.C. Long-term agricultural management maximizing hay production can significantly reduce belowground C storage. *Agric. Ecosyst. Environ.* **2016**, *220*, 104–114. [[CrossRef](#)]
95. Clein, J.S.; Schimel, J.P. Nitrogen turnover and availability during succession from alder to poplar in Alaskan taiga forests. *Soil Biol. Biochem.* **1995**, *27*, 743–752. [[CrossRef](#)]
96. Meier, C.L.; Bowman, W.D. Phenolic-rich leaf carbon fractions differentially influence microbial respiration and plant growth. *Oecologia* **2008**, *158*, 95–107. [[CrossRef](#)]
97. Beamish, A.; Reynolds, M.K.; Epstein, H.; Frost, G.V.; Macander, M.J.; Bergstedt, H.; Bartsch, A.; Kruse, S.; Miles, V.; Tanis, C.M.; et al. Recent trends and remaining challenges for optical remote sensing of Arctic tundra vegetation: A review and outlook. *Remote Sens. Environ.* **2020**, *246*, 111872. [[CrossRef](#)]
98. Heijmans, M.M.P.D.; Magnússon, R.; Lara, M.J.; Frost, G.V.; Myers-Smith, I.H.; van Huissteden, J.; Jorgenson, M.T.; Fedorov, A.N.; Epstein, H.E.; Lawrence, D.M.; et al. Tundra vegetation change and impacts on permafrost. *Nat. Rev. Earth Environ.* **2022**, *3*, 68–84. [[CrossRef](#)]



99. Franke, A.K.; Feilhauer, H.; Bräuning, A.; Rautio, P.; Braun, M. Remotely sensed estimation of vegetation shifts in the polar and alpine tree-line ecotone in Finnish Lapland during the last three decades. *For. Ecol. Manag.* **2019**, *454*, 117668. [[CrossRef](#)]
100. Meng, B.; Ge, J.; Liang, T.; Yang, S.; Gao, J.; Feng, Q.; Cui, X.; Huang, X.; Xie, H. Evaluation of Remote Sensing Inversion Error for the Above-Ground Biomass of Alpine Meadow Grassland Based on Multi-Source Satellite Data. *Remote Sens.* **2017**, *9*, 372. [[CrossRef](#)]
101. Červená, L.; Pinlová, G.; Lhotáková, Z.; Neuwirthová, E.; Kupková, L.; Potůčková, M.; Lysák, J.; Campbell, P.; Albrechtová, J. Determination of Chlorophyll Content in Selected Grass Communities of Krkonoše Mts. Tundra Based on Laboratory Spectroscopy and Aerial Hyperspectral data. In Proceedings of the International Archives of the Photogrammetry, Remote Sensing and Spatial Information Sciences, Volume XLIII-B3-2022 XXIV ISPRS Congress (2022 edition), Nice, France, 6–11 June 2022; pp. 381–388.
102. Chen, J.M.; Black, T.A. Defining leaf area index for non-flat leaves. *Plant Cell Environ.* **1992**, *15*, 421–429. [[CrossRef](#)]
103. Ustin, S.L.; Gitelson, A.A.; Jacquemoud, S.; Schaepman, M.; Asner, G.P.; Gamon, J.A.; Zarco-Tejada, P. Retrieval of foliar information about plant pigment systems from high resolution spectroscopy. *Remote Sens. Environ.* **2009**, *113*, S67–S77. [[CrossRef](#)]
104. Gitelson, A.A.; Chivkunova, O.B.; Merzlyak, M.N. Nondestructive estimation of anthocyanins and chlorophylls in anthocyanic leaves. *Am. J. Bot.* **2009**, *96*, 1861–1868. [[CrossRef](#)]
105. Chlus, A.; Townsend, P.A. Characterizing seasonal variation in foliar biochemistry with airborne imaging spectroscopy. *Remote Sens. Environ.* **2022**, *275*, 113023. [[CrossRef](#)]
106. Bussotti, F.; Gerosa, G.; Digrado, A.; Pollastrini, M. Selection of chlorophyll fluorescence parameters as indicators of photosynthetic efficiency in large scale plant ecological studies. *Ecol. Indic.* **2020**, *108*, 105686. [[CrossRef](#)]
107. Mancinelli, A.L.; Yang, C.-P.H.; Lindquist, P.; Anderson, O.R.; Rabino, I. Photocontrol of Anthocyanin Synthesis: III. The Action of Streptomycin on the Synthesis of Chlorophyll and Anthocyanin 1. *Plant Physiol.* **1975**, *55*, 251–257. [[CrossRef](#)]
108. Merzlyak, M.N.; Chivkunova, O.B.; Solovchenko, A.E.; Naqvi, K.R. Light absorption by anthocyanins in juvenile, stressed, and senescing leaves. *J. Exp. Bot.* **2008**, *59*, 3903–3911. [[CrossRef](#)]
109. Fossen, T.; Slimestad, R.; Øvstedal, D.O.; Andersen, Ø.M. Anthocyanins of grasses. *Biochem. Syst. Ecol.* **2002**, *30*, 855. [[CrossRef](#)]
110. Singleton, V.L.; Rossi, J.A. Colorimetry of Total Phenolics with Phosphomolybdic-Phosphotungstic Acid Reagents. *Am. J. Enol. Vitic.* **1965**, *16*, 144–158.
111. Porra, R.; Thompson, W.; Kriedemann, P. Determination of Accurate Extinction Coefficients and Simultaneous-Equations for Assaying Chlorophyll-a and Chlorophyll-B Extracted with 4 Different Solvents—Verification of the Concentration. *Biochim. Biophys. Acta* **1989**, *975*, 384–394. [[CrossRef](#)]
112. Wellburn, A.R. The Spectral Determination of Chlorophylls a and b, as well as Total Carotenoids, Using Various Solvents with Spectrophotometers of Different Resolution. *J. Plant Physiol.* **1994**, *144*, 307–313. [[CrossRef](#)]
113. Brauns, F.E. *The Chemistry of Lignin*; Academic Press Inc.: New York, NY, USA, 1952.
114. Gardner, R.O. Vanillin-Hydrochloric Acid as a Histochemical Test for Tannin. *Stain Technol.* **1975**, *50*, 315–317. [[CrossRef](#)]
115. Hutzler, P.; Fischbach, R.; Heller, W.; Jungblut, T.P.; Reuber, S.; Schmitz, R.; Veit, M.; Weissenböck, G.; Schnitzler, J.-P. Tissue localization of phenolic compounds in plants by confocal laser scanning microscopy. *J. Exp. Bot.* **1998**, *49*, 953–965. [[CrossRef](#)]
116. Tattini, M.; Guidi, L.; Morassi-Bonzi, L.; Pinelli, P.; Remorini, D.; Degl’Innocenti, E.; Giordano, C.; Massai, R.; Agati, G. On the role of flavonoids in the integrated mechanisms of response of *Ligustrum vulgare* and *Phillyrea latifolia* to high solar radiation. *New Phytol.* **2005**, *167*, 457–470. [[CrossRef](#)]
117. Tang, Y.; Horikoshi, M.; Li, W. ggfortify: Unified Interface to Visualize Statistical Results of Popular R Packages. *R J.* **2016**, *8*, 474–485. [[CrossRef](#)]
118. R Core Team. R: A Language and Environment for Statistical Computing. R Foundation for Statistical Computing. 2021. Available online: <https://www.R-project.org/> (accessed on 11 November 2022).

**Disclaimer/Publisher’s Note:** The statements, opinions and data contained in all publications are solely those of the individual author(s) and contributor(s) and not of MDPI and/or the editor(s). MDPI and/or the editor(s) disclaim responsibility for any injury to people or property resulting from any ideas, methods, instructions or products referred to in the content.